NASA Tech Briefs

Transferring Technology to
American Industry
and Government

September 1989
Volume 13 Number 9

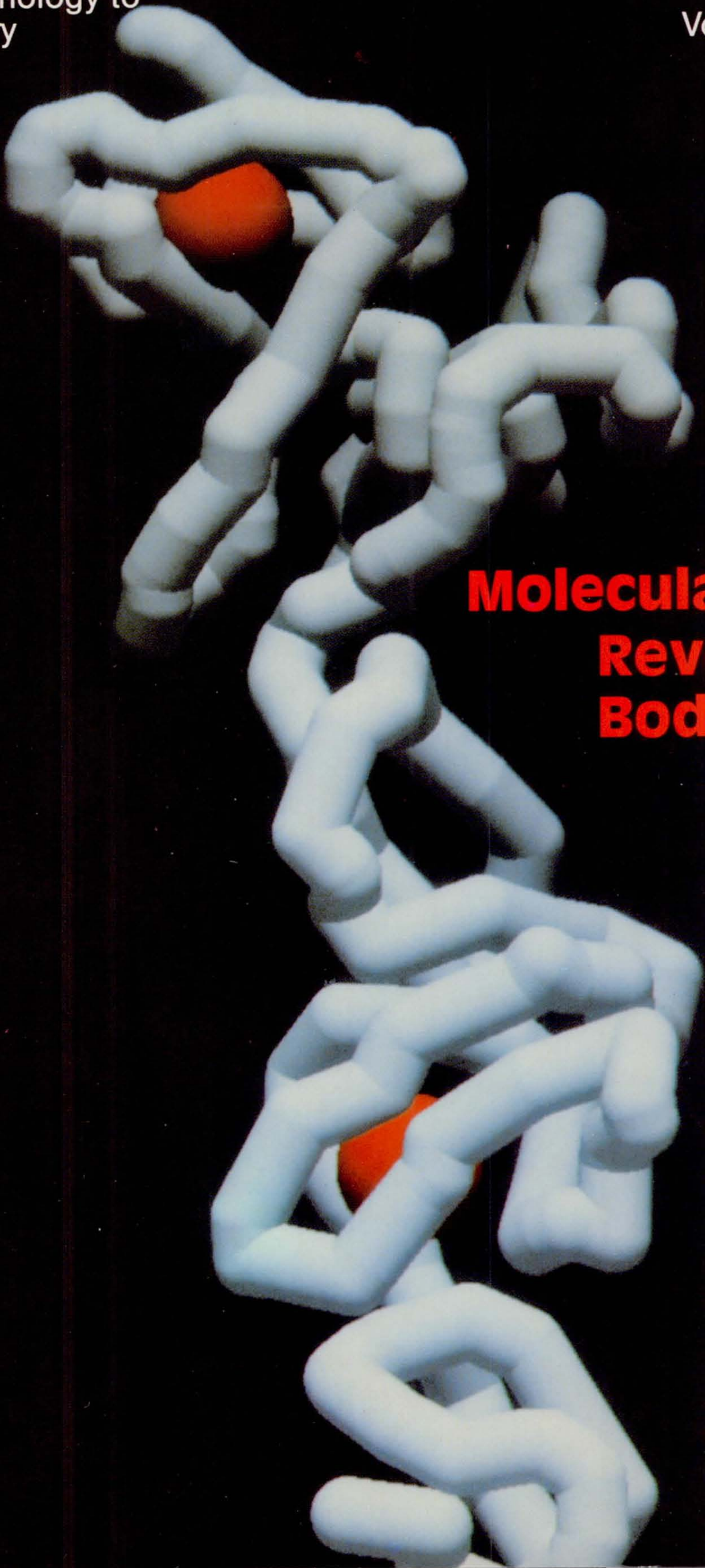

Molecular Mapping Reveals The Body's Secrets

In space: looking back to look forward.

What can the nature and origin of the universe tell us about the future of Earth? To help answer that question, we make craft and instruments for traveling billions of miles in space and seeing as far as 15 billion years back in time. Martin Marietta was the integrator and builder of two Viking landers, which sent back remarkable photos of the surface of Mars, examined soil samples, and studied Martian weather and seismic activity. For the Voyagers we provided instrumentation that reported on electromagnetic activity near Jupiter and Saturn—Voyager 2 went on to Uranus, some 2 billion miles from Earth. That was nine years after launch; next destination, Neptune, in 1989. These are but a few results of Martin Marietta's ability to create survivable, mystery-solving craft and their instruments—from concept through mission completion.

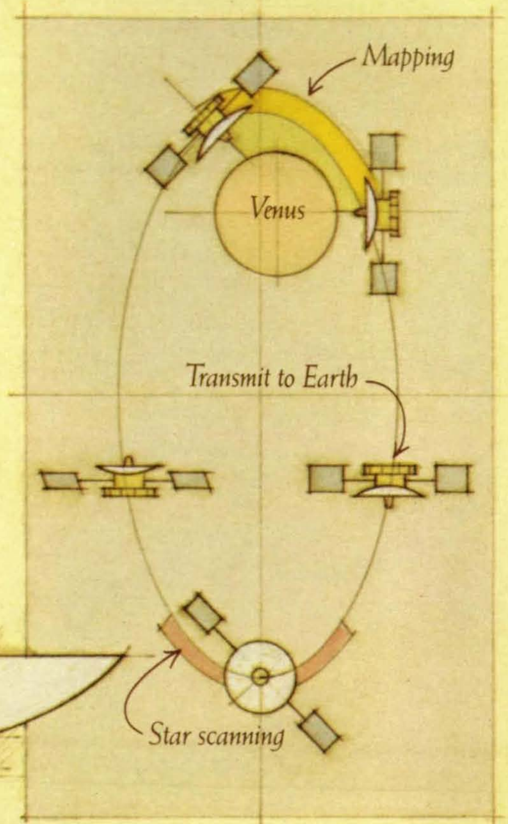

Orbit and orientation

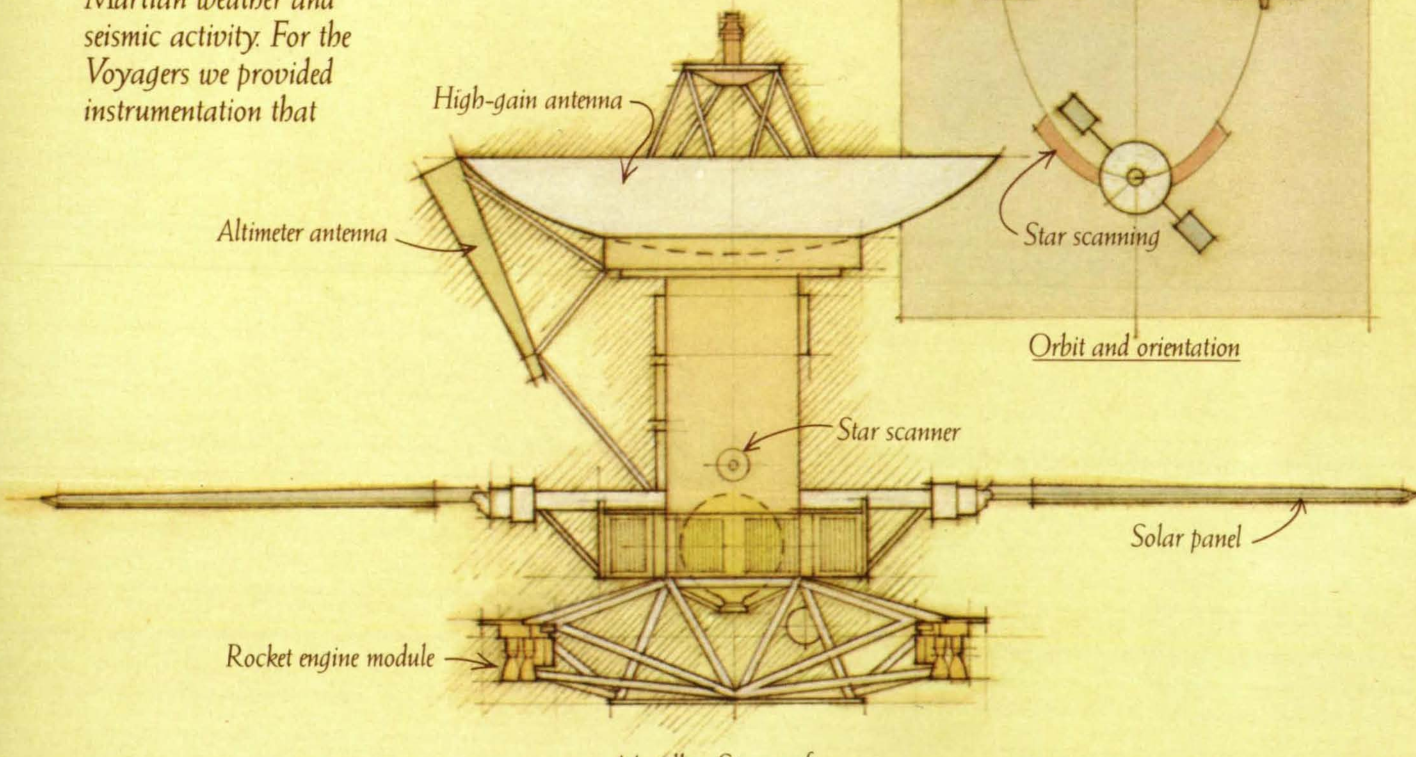

Magellan Spacecraft

Mission: map Venus.

From orbit, Magellan's radar will penetrate the planet's thick, gaseous cloud cover and send back photo-like images of nearly 90% of its surface. Our role: design, integrate, build and test the craft.

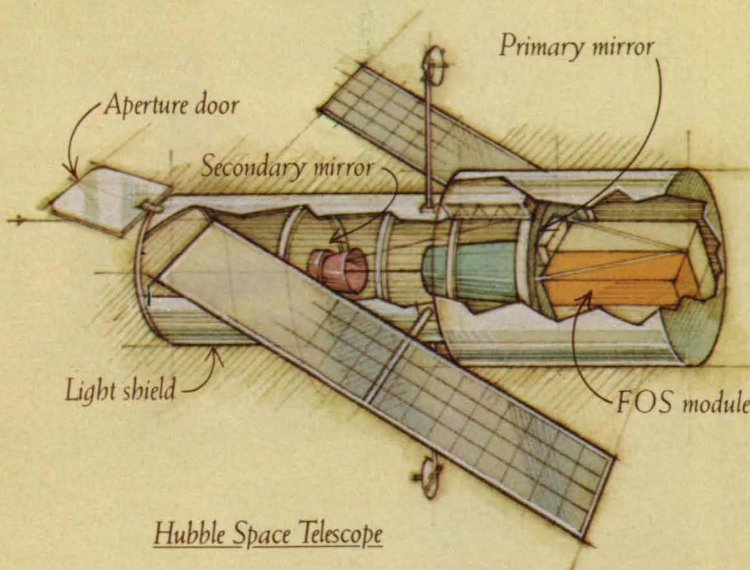

Hubble Space Telescope

Viewing the infant universe.

For the Hubble Space Telescope we are providing the Faint Object Spectrograph (FOS), which will see objects up to 15 billion light-years away. Since the universe is estimated to be 18-20 billion years old, astronomers will witness events close to its birth.

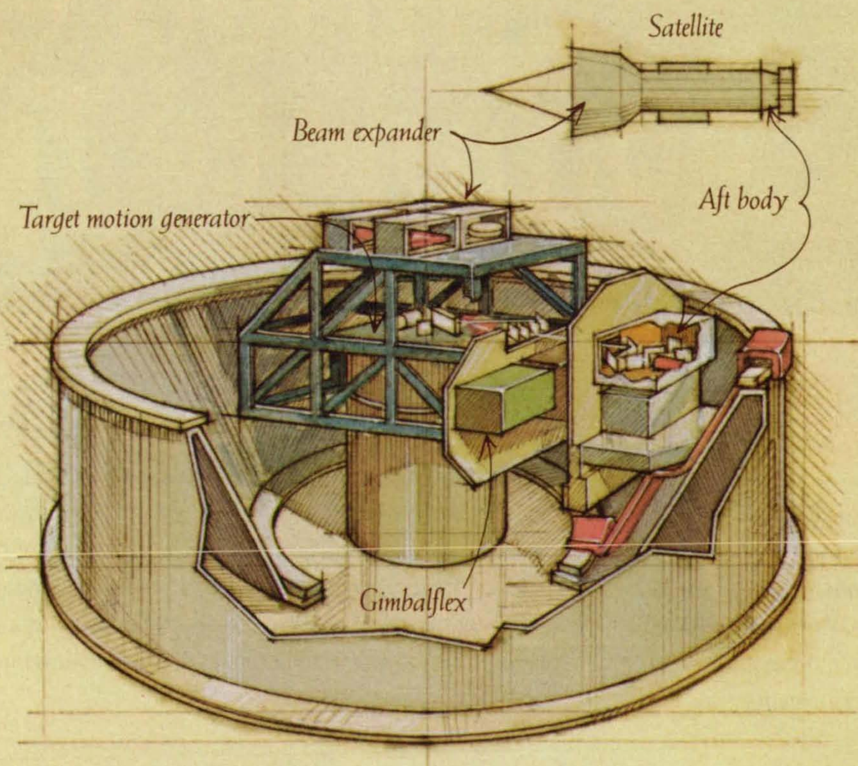

Fine Pointing Simulator

The fine points of fine pointing.

Precisely controlled, space-spanning energy delivery and collection systems create difficult pointing and retargeting challenges, which we can now simulate. This new lab is working toward the precision to zero in on a football-size object 3,000 miles away, in support of the Strategic Defense Initiative research program.

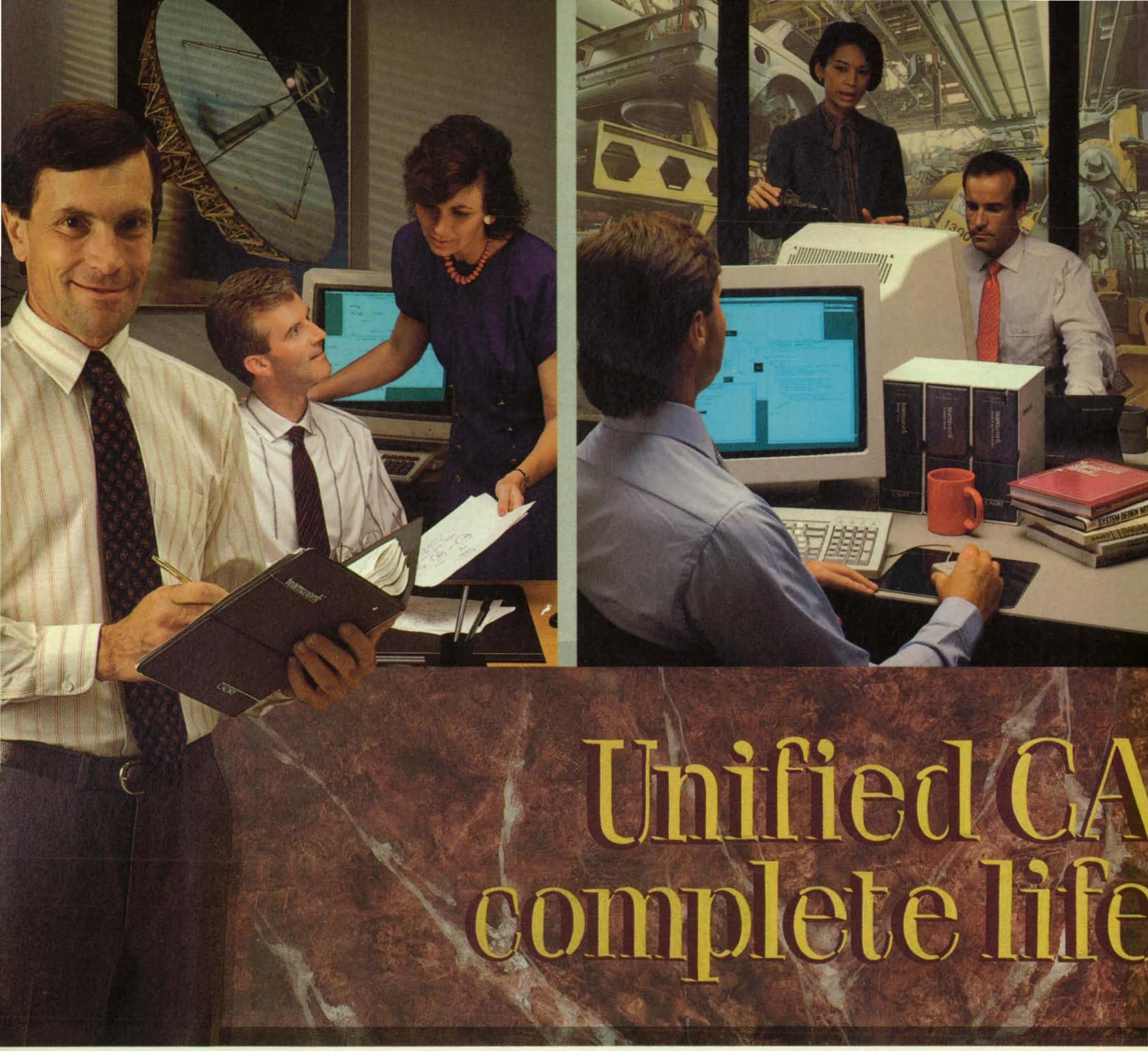

Requirements Analysis

Cadre's Unified CASE product family brings software design automation to the entire systems development lifecycle, from requirements analysis through to product test. Requirements analysis extracts product function and behavior from fundamental system requirements. Workstation-based Teamwork and ADAS describe system requirements and evaluate tradeoffs between cost and performance.

Design & Code

With requirements analysis completed, project teams implement software design and program logic using Teamwork. Design converts directly to code using Ada and C Source Builders, improving consistency and product maintainability. Cadre's networked Unified CASE environment moves design teams quickly through the product lifecycle to develop superior products.

teamwork®
Winning teams depend on it.

CADRE means

PathMap, PROBE, Software Analysis Workstation, Unified CASE, Ada Source Builder, and C Source Builder are trademarks of Cad

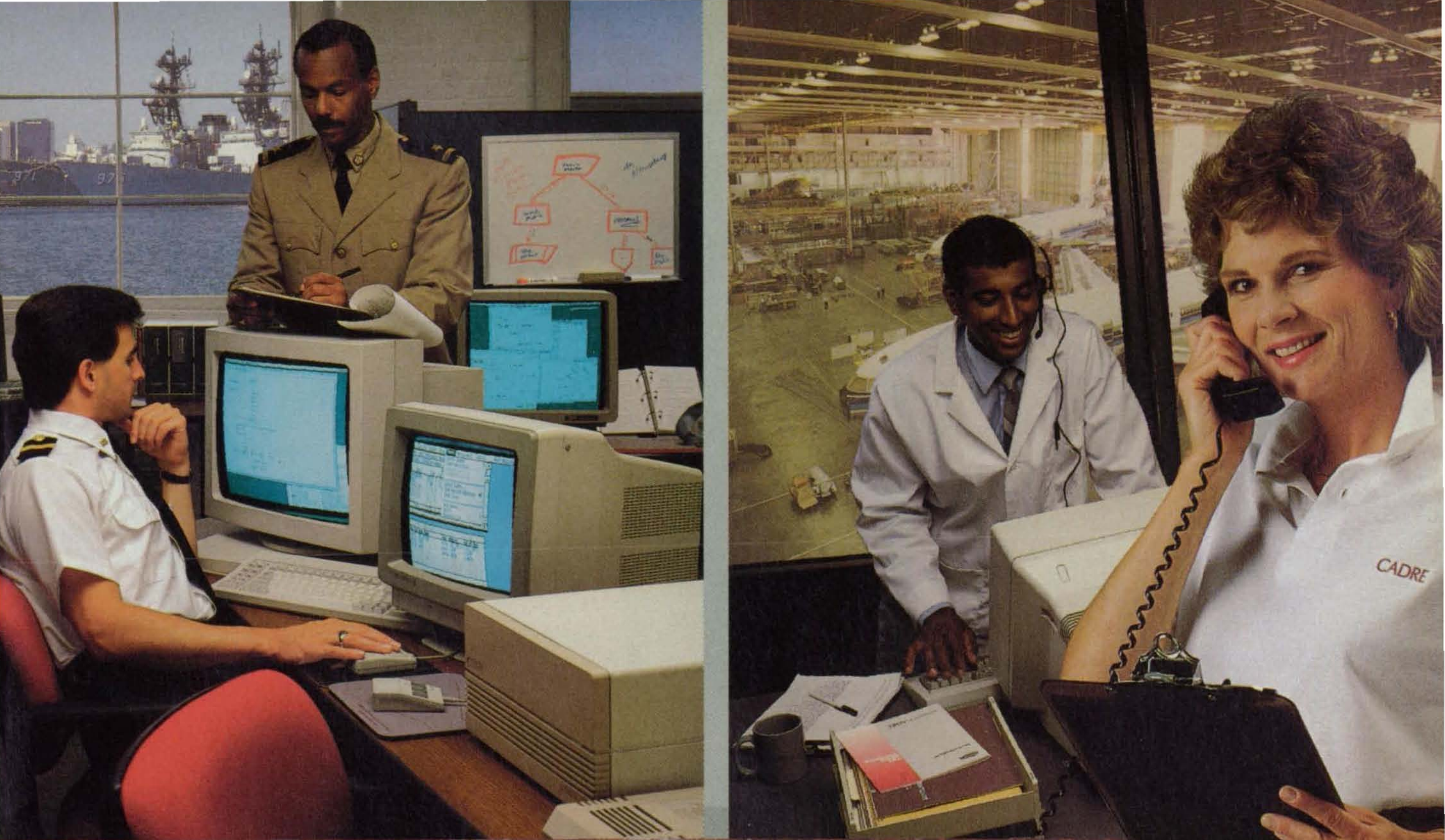

SE means
cycle support

Test & Integration

Cadre's Unified CASE test products debug and test embedded software directly in target hardware. Test data automatically annotates original design for complete traceability.
Cadre's Software Analysis Workstation, or SAW, measures execution and performance of embedded software. PathMap, Cadre's Run-time Reverse Engineering tool, creates design-level Structure Charts from actual code executing in target hardware. PROBE in-circuit emulators allow software engineers to operate from their own workstation platforms.

Ongoing Product Support

The Unified CASE product family includes Cadre's responsive customer service, specialized training programs, consulting services, and ongoing product enhancements. How can Unified CASE improve your products? To find out

Call (401) 351-CASE

When critical systems need to be developed, project leaders call for Unified CASE solutions. Available only from Cadre.

Jnified CASE

CADRE

Cadre Technologies Inc.
222 Richmond Street, Providence, RI
02903 U.S.A. (401) 351-2273

Winning teams depend on us.

Circle Reader Action No. 424

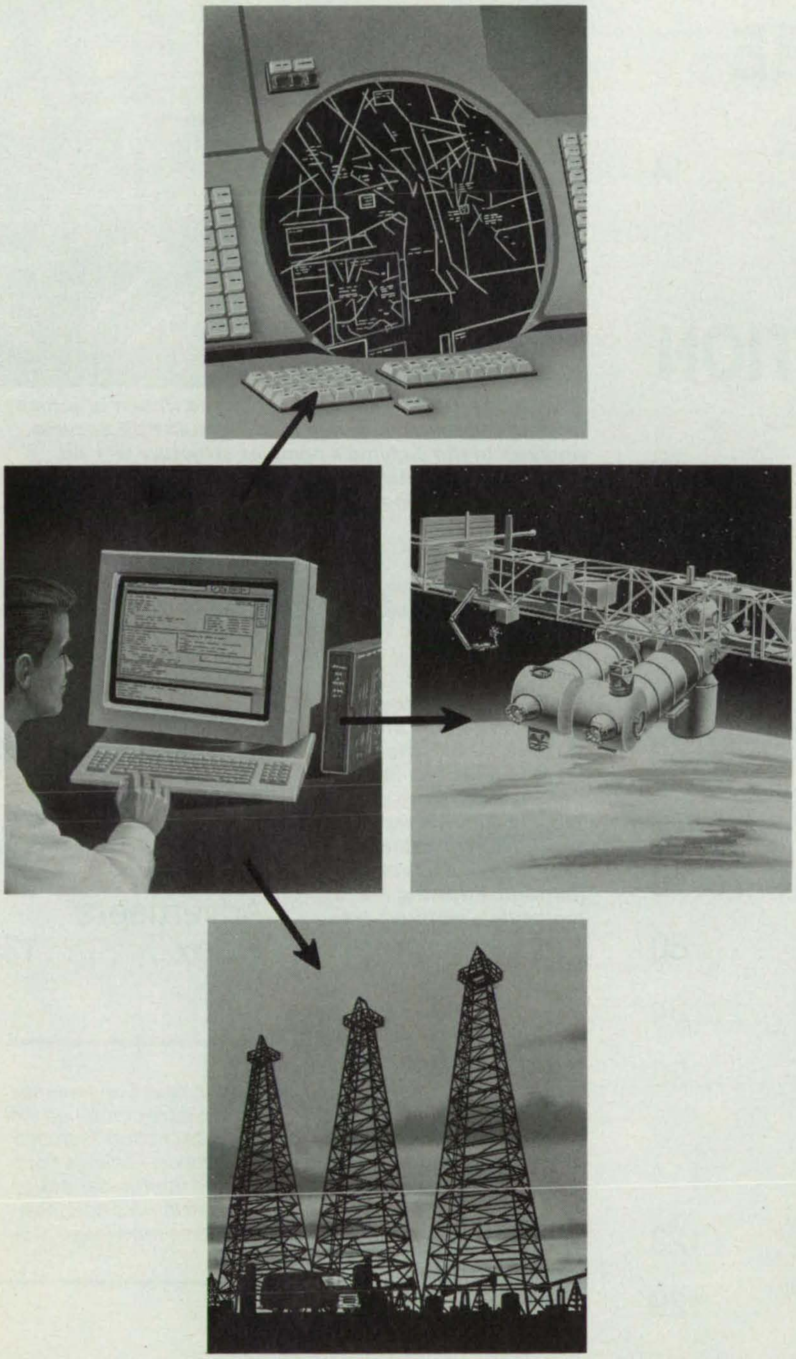

NASA Tech Briefs
Transferring Technology to
American Industry and Government

SEPTEMBER 1989
Volume 13 Number 9

SPECIAL FEATURE

TECHNICAL SECTION

Photo courtesy NASA

What looks like a batch of multicolored ribbon is actually a computer-generated model of the human PNP enzyme. Analysis of the enzyme's complex structure will aid researchers in creating anti-cancer agents. For more on molecular modeling, turn to page 14.

DEPARTMENTS

On The Cover: A computer simulation of the molecule serum albumin, the most abundant protein in the human circulatory system. The red spheres represent the binding locations of aspirin (top) and diazapine (bottom). Knowing the molecule's architecture may enable pharmaceutical companies to develop improved disease-fighting drugs. See page 14. (Photo courtesy NASA)

For Your Convenience
We have combined the Subscription/Technical Support Package Form and the Reader Action Card into a single, easy-to-use form (page 119).

ABP BPA

NASA Tech Briefs, ISSN 0145-319X, USPS 750-070, copyright © 1989 in U.S., is published monthly by Associated Business Publications Co., Ltd. 41 E. 42nd St., New York, NY 10017-5391. The copyrighted information does not include the individual Tech Briefs which are supplied by NASA. Editorial, sales, production and circulation offices at 41 E. 42nd Street, New York, NY 10017-5391. Subscriptions for non-qualified subscribers in the U.S., Panama Canal Zone, and Puerto Rico, $75.00 for 1 year; $125.00 for 2 years; $200 for 3 years. Single copies $10.00. Remit by check, draft, postal or express orders. Other remittances at sender's risk. Address all communications for subscriptions or circulation to NASA Tech Briefs, 41 E. 42nd Street, New York, NY 10017-5391. Second-class postage paid at New York, NY and additional mailing offices.

POSTMASTER: please send address changes to NASA Tech Briefs, 41 E. 42nd Street, Suite 921, New York, NY 10017-5391.

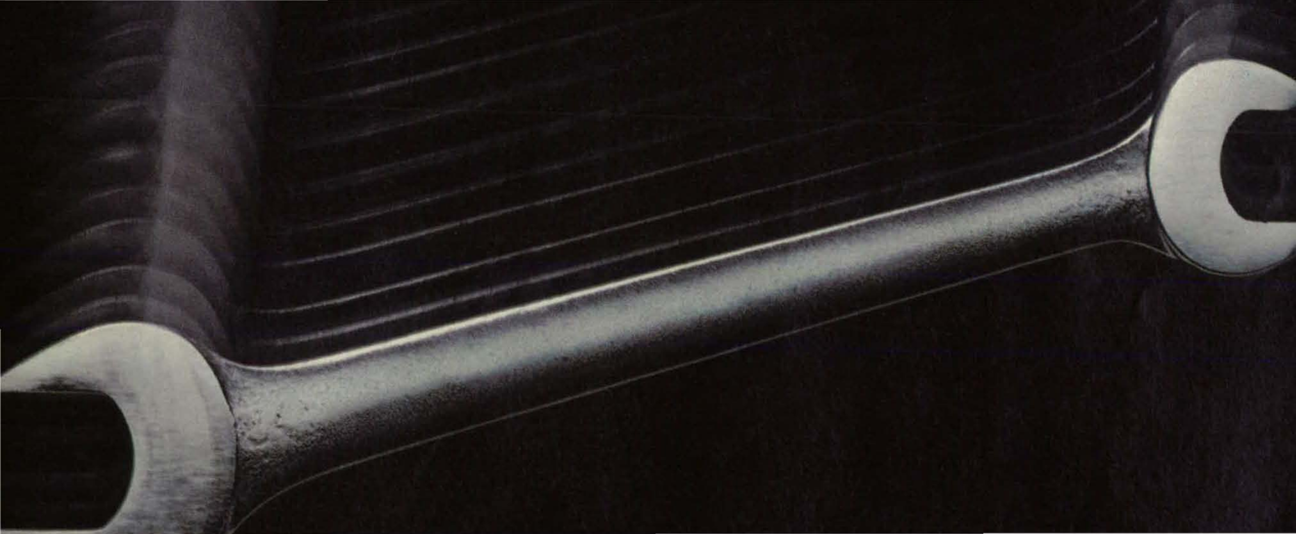

NASA Tech Briefs

National Aeronautics and Space Administration

ABP BPA

NASA Tech Briefs:

Published by .... **Associated Business Publications**
Editor-in-Chief/Publisher .... **Bill Schnirring**
Associate Publisher .... **Frank Nothaft**
Managing Editor .... **R. J. Laer**
Senior Editor .... **Joseph T. Pramberger**
Technical Advisor .... **Dr. Robert E. Waterman**
Production Manager .... **Rita Nothaft**
Traffic Manager .... **James E. Cobb**
Circulation Director .... **Anita Weissman**
Advertising Coordination Manager .... **Maya Falek**
Telecommunications Specialist .... **Evelyn Mars**
Reader Service Manager .... **Sylvia Ruiz**

Briefs & Supporting Literature:
Provided to National Aeronautics and Space Administration by **International Computers & Telecommunications, Inc.,** NY, NY with assistance from **Logical Technical Services,** NY, NY
Technical/Managing Editor .... **Ted Selinsky**
Art Director .... **Ernest Gillespie**
Administrator .... **Elizabeth Texeira**
Chief Copy Editor .... **Lorne Bullen**
Staff Writers/Editors .... **Dr. James Boyd, Dr. Larry Grunberger, Dr. Theron Cole, Jordan Randjelovich, George Watson, Oden Browne**
Graphics .... **Luis Martinez, Vernald Gillman, Charles Sammartano**
Editorial & Production **Bill Little, Ivonne Valdes, Frank Ponce, Susan Finelli**

NASA:
NASA Tech Briefs are provided by the National Aeronautics and Space Administration, Technology Utilization Division, Washington, DC:
Administrator .... **Richard H. Truly**
Assistant Administrator for Commercial Programs ..... **James T. Rose**
Deputy Assistant Administrator (Programs) .... **Henry J. Clarks**
Deputy Director TU Division (Publications Manager) ... **Leonard A. Ault**
Manager, Technology Utilization Office, NASA Scientific and Technology Information Facility .... **Walter M. Heiland**

Associated Business Publications
41 East 42nd Street, Suite 921, New York, NY 10017-5391
(212) 490-3999 FAX (212) 986-7864
President .... **Bill Schnirring**
Executive Vice President .... **Frank Nothaft**
Vice President .... **Domenic A. Mucchetti**
Operations Manager .... **Rita Nothaft**
Controller .... **Felecia Lahey**

Advertising:
New York Office: (212) 490-3999 FAX (212) 986-7864
National Sales Manager .... **James G. McGarry**
Regional Sales Manager (Mid-Atlantic) .... **Michelle Larsen**
Account Executive .... **Debby Crane** at (201) 967-9838
Account Executives (Midwest) ...... **Jack Cartwright** or **Paul Lesher** or **Michael Salberg** at (312) 501-4140
Account Executives (Eastern MA, NH, ME, RI) .... **Paul Gillespie** at (508) 429-8907; **Bill Doucette** at (617) 894-7931
Account Executive (Western MA, CT, VT) **George Watts** or **David Haggett** at (413) 253-9881
Account Executive (No. Calif., WA, OR) .... **Janice Richey King** at (415) 656-3613
Account Executives (So. Calif., AZ, NV, NM) for Area Codes 818/213/805 **Thomas Stillman** and for Area Codes 619/714—**Leslie Alley** at (213) 372-2744

NTBM-Research Center
Account Supervisor .... **Lourdes Del Valle**

Codonics brings you the first affordable graphics terminal without the jaggies

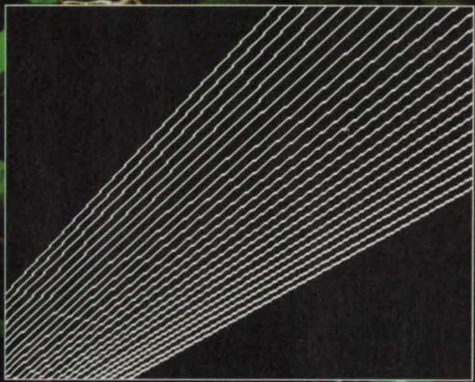

The competition's 1024 x 780 pixel display

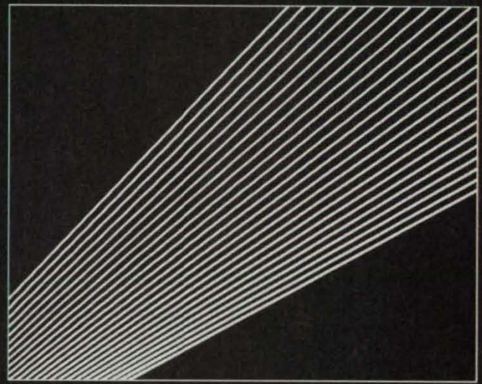

Codonics' true-line™ display

The Codonics 4096. Finally, a graphics terminal with Tektronix 4010/4014 emulation, DEC VT320/220/100 alphanumerics and no jaggies.

A few features:

- 16,000 x 12,000 effective resolution, utilizing Codonics' true-line™ beam geometry hardware
- True 4096 x 4096 sub-pixel addressability
- DEC VT320/220/100 emulation with high definition fonts
- Flawless Tektronix 4010/4014 emulation
- True pan and zoom with display list cache
- 73 Hz non-interlaced flickerless display
- Built in hardcopy support utilizing Codonics' true-line™ technology
- Mouse included as a standard feature

Our team of sales engineers are awaiting your call. 1-800-444-1198

CODONICS
We bring the Future into Focus

Computer Graphics Division
18001 Englewood Drive
Middleburg Hts., Ohio 44130
Telephone (216) 243-1198
Telex 650-292-8429


AND BEYOND.
8 GH
5 GHz
3 GHz

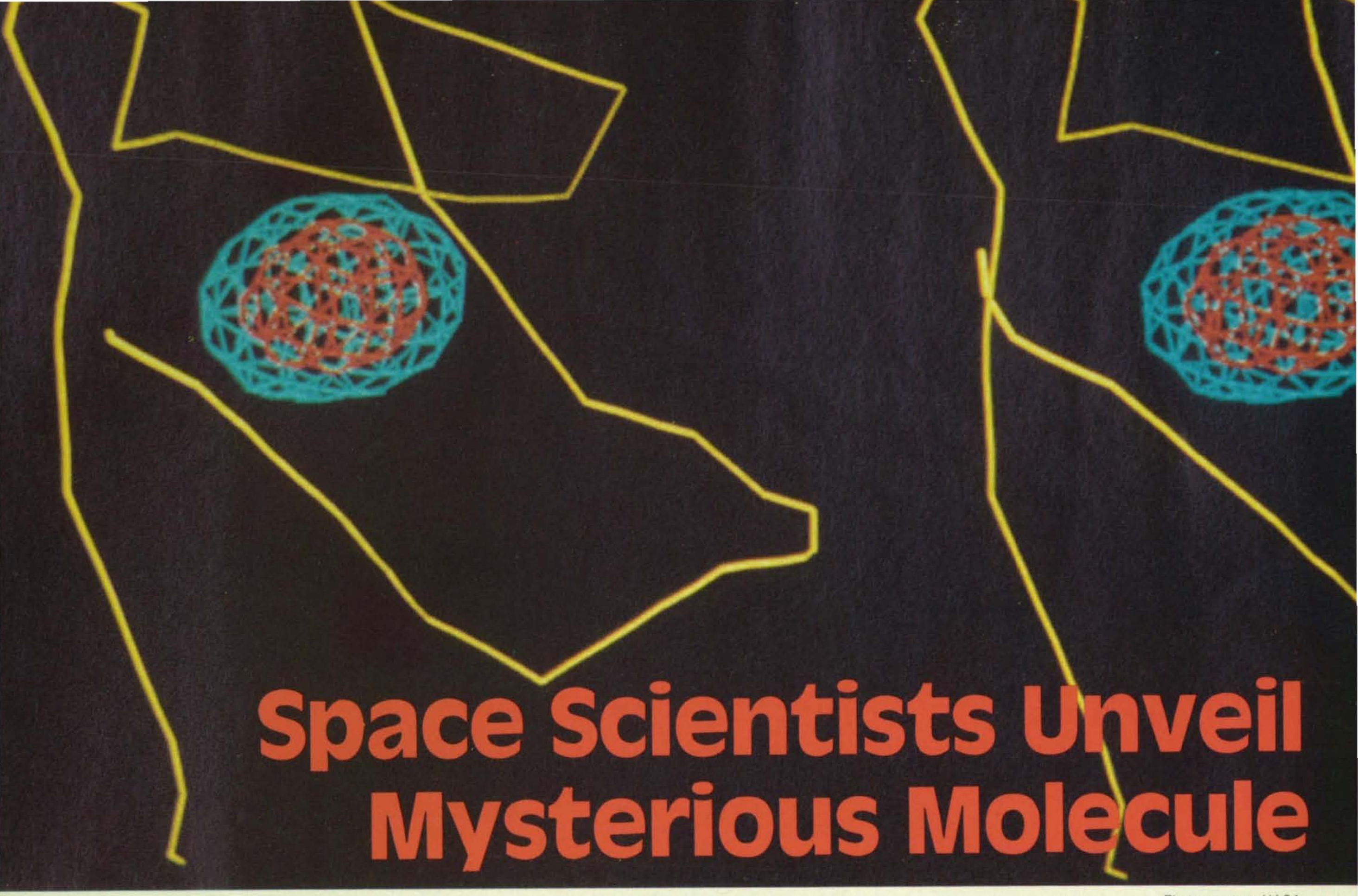

Space Scientists Unveil Mysterious Molecule

Photo courtesy NASA

NASA scientists have unraveled one of the human body's great mysteries. Using a technique called x-ray crystallography, researchers at NASA's Marshall Space Flight Center have uncovered the three-dimensional structure of human serum albumin, the principal protein of the blood plasma. Their discovery may lead to the development of novel drugs to combat cancer, sickle cell anemia, and a host of other diseases.

Compiling images from hundreds of individual x-ray diffraction experiments, Marshall researchers identified the protein as an ellipsoidal molecule containing six bundles of intertwining spirals of amino acids. The 3D model will help scientists to understand serum albumin's intricate workings. Besides regulating osmotic blood pressure, the protein binds and transports a variety of substrates in plasma, including calcium, copper, fatty and amino acids, hormones, and a wide spectrum of therapeutic drugs.

"People have traditionally thought of serum albumin as being a very sticky molecule that other substances just randomly adhere to," said crystallographer Dr. Daniel Carter, leader of the Marshall research team. "Our work has shown, however, that binding occurs only in discrete pockets within the molecule. Many compounds, including common aspirin, are transported inside just two of the molecule's bundles: the first and the fifth."

Knowing where and how substrates bind on the molecule will enable pharmaceutical companies to alter the metabolism of drugs so they may be more efficiently carried by serum albumin through the circulatory system. Many existing drugs are ineffective because their molecular structures either fail to bind or bind too tightly with the protein.

Examples of the latter include drugs designed to treat sickle cell anemia. Such drugs show promise in the test tube but cannot elude serum albumin's grasp, said Carter, who is working with Nobel prize-winning chemist Max Perutz to analyze the binding sites of these drugs to the protein.

The structural studies could also help in creating new blood substitutes, according to Carter. "Serum albumin is a very big molecule," he explained. "If you can determine its chemically active regions, you might be able to engineer a smaller, more stable synthetic version of the protein."

Crystal-Clear Images

To visualize serum albumin's molecular architecture, scientists placed single protein crystals in an x-ray beam and created diffraction patterns. Analysis of such a pattern is analogous to using a powerful microscope, except the image is developed with computers and graphics programs instead of lenses.

Past attempts at mapping the molecule were thwarted because researchers could not grow crystals pure or large enough for analysis. "It takes a good deal of trial and error, not to mention luck, to achieve high-quality crystals," said Carter. Slight changes in pH, ionic strength, temperature, buffer type, dielectric constant, and many other factors can hinder growth of the delicate crystals.

"Imperfect crystals—those with internal disorder—blur the images created from them," Carter said, "making it extremely difficult to obtain accurate coordinates."

Marshall scientists were able to produce batches of large, uniform crystals using a vapor diffusion process, in which droplets of protein containing concentrations of precipitant slightly below that needed to render the protein insoluable are placed over reservoirs with higher precipitant concentrations. The droplet then slowly equilibrates with the reservoir through the vapor phase. The process is typically

This stereo image shows the convoluted flow in one section of the serum albumin molecule. A binding site for salicylic acid (aspirin) is illustrated by the diamond shapes.

used for screening many different conditions by placing the protein droplets on siliconized coverslips, which are then inverted (to give hanging drops) and positioned over small reservoirs in multi-chamber plates.

The Next Step

Carter's group has successfully mapped the protein's structure to a resolution of six angstroms, providing an image with enough detail to extract information about individual molecules. Their next step will be to refine the resolution to three angstroms using highly pure crystals grown in space aboard the shuttle Discovery. The sharper images will help identify the chemical mechanisms at work in each molecular bundle, a process expected to take up to two years.

"Most of the hard work is behind us," Carter said. "Now that we know how to obtain this resolution, it's a matter of systematically refining the details. But scientists will be studying applications for the protein molecule for a long time." □

Growing Crystals In Space

Thousands of distinct proteins are present and essential in all forms of life. They enable biological organisms to form, grow, repair tissue, reproduce, and fight disease. Each protein is a specific arrangement of amino acids, and the work each performs is determined by its structure.

It is through sophisticated analysis of a protein in crystallized form that scientists are able to construct a model of its molecular architecture. The problem is that protein crystals grown on Earth are often small and flawed, making structural analysis difficult if not impossible. Crystal growth experiments flown on six Space Shuttle missions, including the March 1989 Discovery mission, have shown promising evidence that superior crystals can be obtained in the microgravity environment of space.

"Earth-grown protein crystals tend to sink to the bottom of the medium in which they are immersed," explained Dr. Charles Bugg, Director of the University of Alabama-Birmingham (UAB) Center for Macromolecular Crystallography. "This clumping prevents them from being bathed equally on all sides by the growth solution, and often the result is distorted or imperfect crystals. The zero-gravity of space eliminates this problem since the weightless crystals are suspended in drops of growth solution. In addition, zero-gravity controls solution turbulence that can interfere with uniform crystal growth."

Upon return to Earth, space-grown crystals are rushed in temperature-controlled housings to laboratories, where researchers use computer techniques to analyze their molecular structures and functions. This information can help scientists devise ways to influence protein functions and to create "designer" drugs for pharmaceutical and biochemical purposes.

Human serum albumin crystals have been grown twice in space, most recently during shuttle mission STS-26 last September. Other proteins produced aboard the shuttle include the enzyme reverse transcriptase, a chemical key to the replication of the AIDS virus; gamma interferon, a protein that stimulates the body's immune system to fight disease; renin, an enzyme produced by the kidneys that plays a major role in the chemical reac-

Photo courtesy NASA

Astronaut George Nelson photographs protein crystal growth experiments aboard the Space Shuttle Discovery in September, 1988.

tion controlling blood pressure; and phospholipase A2, a protein found in the venom of cottonmouth snakes that can help control pain and inflammation.

Several experiments have focused on proteins associated with the degradation of lung tissue in emphysema patients, and on enzymes that could lead to more potent fungicides for the treatment of crop diseases such as rice blasts.

Research is conducted under the auspices of UAB's Center for Macromolecular Crystallography—one of NASA's Centers for the Commercial Development of Space—in concert with the Marshall Space Flight Center and various pharmaceutical, biotechnology, and agrichemical companies. □

Computer-generated picture displays a cross-section of a serum albumin crystal. One side of each square is a molecule of the protein. The photo was taken by x-raying the crystal and recording a projection of its electron density. By stacking several photos, scientists can build a 3D model of the individual molecules.

Photo courtesy NASA

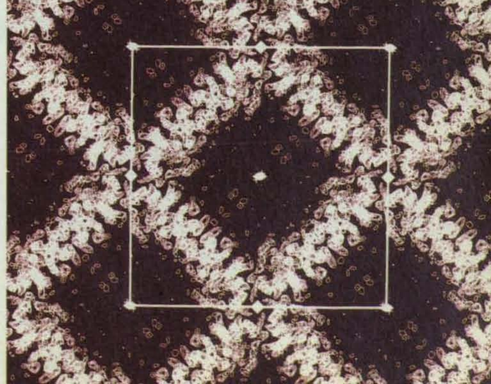

New Product Ideas

New Product Ideas are just a few of the many innovations described in this issue of *NASA Tech Briefs* and having promising commercial applications. Each is discussed further on the referenced page in the appropriate section in this issue. If you are interested in developing a product from these or other NASA innovations, you can receive further technical information by requesting the TSP referenced at the end of the full-length article or by writing the Technology Utilization Office of the sponsoring NASA center (see page 18). NASA's patent-licensing program to encourage commercial development is described on page 18.

Compact Apparatus Grows Protein Crystals

A laboratory apparatus provides a delicately balanced combination of materials and chemical conditions for the growth of protein crystals. The apparatus and the technique for growth are based on the hanging-drop method for the crystallization of macromolecules. (See 100).

Making Submicron $CoSi_2$ Structures on Silicon Substrates

An experimental fabrication process makes submicron-sized structures of single-crystal metallic $CoSi_2$ on silicon substrates. By the use of $CoSi_2$ structures as electron-beam resists, it may be possible to achieve dimensions smaller than those achievable by photoresist techniques. (See page 105).

Using Inorganic Crystals To Grow Protein Crystals

Tests with 50 inorganic substrates have shown that inorganic crystals can be used as nucleants or substrates for growing protein crystals. This process promises to make the growth of protein crystals more easily controllable, more reliable, and more reproducible. (See page 124).

Robotic Tool for Tightening and Cutting

A robot end effector is designed for tightening tube couplers and for cutting tubes. It can be used as a hand tool for assembling truss structures for buildings and oil rigs and in place of a pipe wrench in plumbing work. The tool is operable by simple movements. (See 98).

Paraboloidal Antenna Radiates Fan or Pencil Beams

Experiments have shown that the same paraboloidal antenna reflector can be used to radiate a pencil beam or fan beam, depending on the configuration of the feed. The far-field radiation pattern of a paraboloidal reflector illuminated by a linear-array feed antenna is wide in the one plane and narrow in a perpendicular plane. (See 24).

Test Structures for Bumpy Integrated Circuits

An improved combination of test structures built into an integrated circuit is used to evaluate design rules, fabrication processes, and the quality of interconnections. Electrical measurements of the test structures are processed by a computer. Both aluminum and polycrystalline silicon interconnections can be evaluated. (See 20).

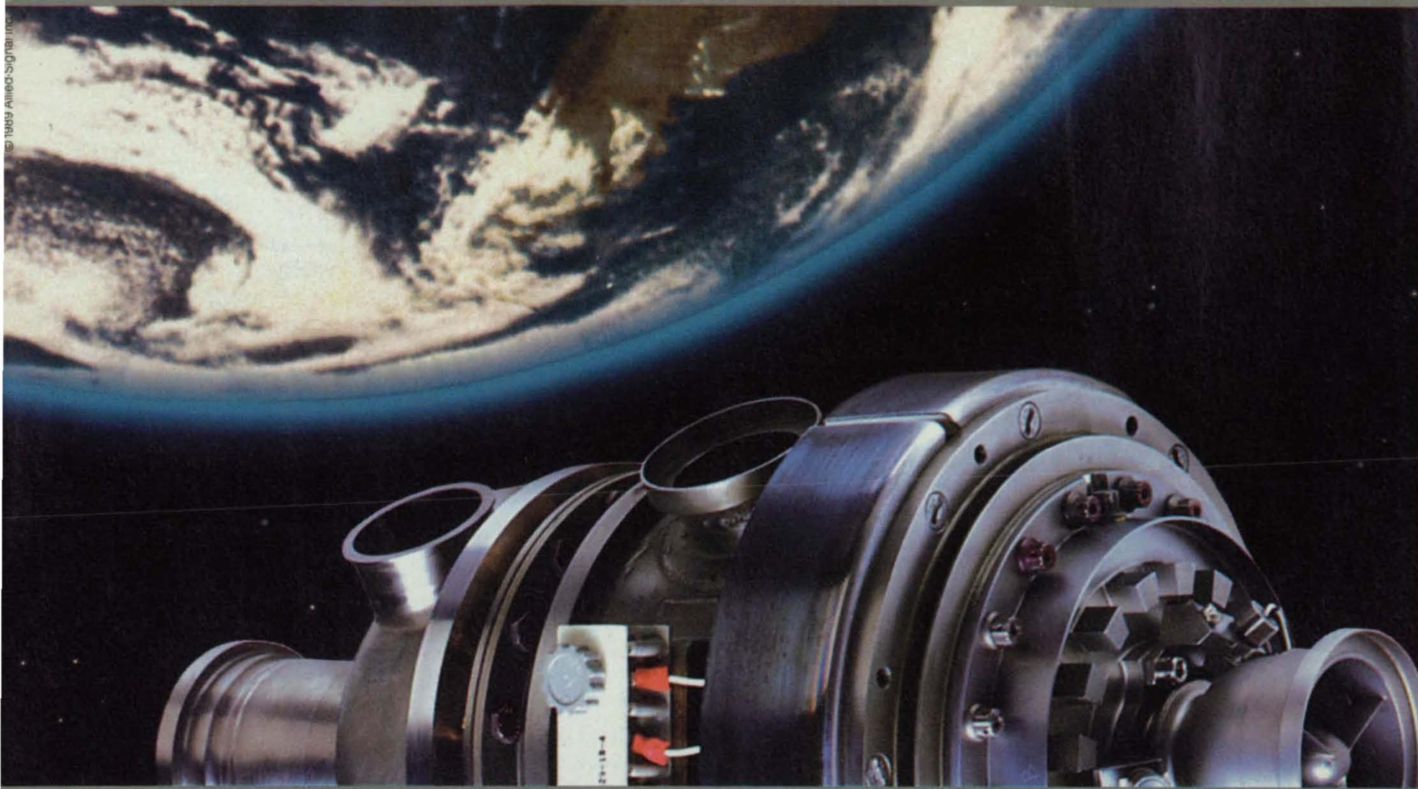

AFFORDABLE POWER FOR THE FINAL FRONTIER.

OVER THE 30-YEAR PLANNED GROWTH OF THE SPACE STATION, A SOLAR DYNAMIC POWER SYSTEM CAN SAVE OVER $3 BILLION, COMPARED TO CONVENTIONAL SYSTEMS.

TRANSLATION: AFFORDABLE POWER FOR A WIDE SPECTRUM OF MILITARY AND COMMERCIAL APPLICATIONS. DEVELOPED WITH NASA. A CLOSED BRAYTON CYCLE DESIGN SUPPORTED BY 220 MILLION HOURS OF TURBINE EXPERIENCE. UNAFFECTED BY ZERO GRAVITY OR THE COLD EMPTINESS OF SPACE. UNRIVALED FOR EFFICIENT ENERGY CONVERSION.

A LIGHTER PAYLOAD SPECIFIC WEIGHT AT LAUNCH, THE POTENTIAL FOR MORE KILOWATTS IN ORBIT. LESS SURFACE AREA FOR LESS DRAG AND RELIABILITY THAT EXCEEDS THE LIFE OF ANY SPACE STATION OR SPACE PLATFORM.

GARRETT FLUID SYSTEMS DIVISION 1300 WEST WARNER ROAD TEMPE AZ 85284 (602) 893-4421. WHERE THE ULTIMATE EFFICIENCY IS RELIABILITY.

Allied-Signal Aerospace Company

Circle Reader Action No. 415

Allied Signal

HOW YOU CAN BENEFIT FROM NASA's TECHNOLOGY UTILIZATION SERVICES

If you're a regular reader of TECH BRIEFS, then you're already making use of one of the low- and no-cost services provided by NASA's Technology Utilization (TU) Network. But a TECH BRIEFS subscription represents only a fraction of the technical information and applications/engineering services offered by the TU Network as a whole. In fact, when all of the components of NASA's Technology Utilization Network are considered, TECH BRIEFS represents the proverbial tip of the iceberg.

We've outlined below NASA's TU Network—named the participants, described their services, and listed the individuals you can contact for more information relating to your specific needs. We encourage you to make use of the information, access, and applications services offered by NASA's Technology Utilization Network.

How You Can Utilize **NASA's Industrial Applications Centers**—A nationwide network offering a broad range of technical services, including computerized access to over 100 million documents worldwide.

You can contact NASA's network of Industrial Applications Centers (IACs) for assistance in solving a specific technical problem or meeting your information needs. The "user friendly" IACs are staffed by technology transfer experts who provide computerized information retrieval from one of the world's largest banks of technical data. Nearly 500 computerized data bases, ranging from NASA's own data base to Chemical Abstracts and INSPEC, are accessible through the ten IACs located throughout the nation. The IACs also offer technical consultation services and/or linkage with other experts in the field. You can obtain more information about these services by calling or writing the nearest IAC. User fees are charged for IAC information services.

Aerospace Research Applications Center (ARAC)
Indianapolis Center for Advanced Research
611 N. Capitol Avenue
Indianapolis, IN 46204
Dr. F. Timothy Janis, Director
(317) 262-5036

Rural Enterprises, Inc. Central Industrial Applications Center/NASA (CIAC)
P.O. Box 1335
Durant, OK 74702
Steve R. Hardy, President
(405) 924-5094

North Carolina Science and Technology Research Center (NC/STRC)
Post Office Box 12235
Research Triangle Park, NC 27709
H. Lynn Reese, Director
(919) 549-0671

NASA Industrial Applications Ctr. 823 William Pitt Union
University of Pittsburgh
Pittsburgh, PA 15260
Dr. Paul A. McWilliams, Exec. Director
(412) 648-7000

NASA/Southern Technology Applications Center
Box 24
Progress Ctr., One Progress Blvd.
Alachua, FL 32615
J. Ronald Thornton, Director
(904) 462-3913
(800) 354-4832 (FL only)
(800) 225-0308 (toll-free US)

NASA/UK Technology Applications Program
University of Kentucky
109 Kinkead Hall
Lexington, KY 40506-0057
William R. Strong, Director
(606) 257-6322

NERAC, Inc.
One Technology Drive
Tolland, CT 06084
Dr. Daniel U. Wilde, President
(203) 872-7000

Technology Application Center (TAC)
University of New Mexico
Albuquerque, NM 87131
Dr. Stanley A. Morain, Director
(505) 277-3622

NASA Industrial Applications Center (WESRAC)
University of Southern California Research Annex
3716 South Hope Street, Room 200
Los Angeles, CA 90007-4344
Radford G. King, Exec. Director
(213) 743-8988
(800) 642-2872 (CA only)
(800) 872-7477 (toll-free US)

NASA/SU Industrial Applications Center
Southern University Department of Computer Science
P.O. Box 9737
Baton Rouge, LA 70813-9737
Dr. John Hubbell, Director
(504) 771-6272

If you represent a public sector organization with a particular need, you can contact NASA's Application Team for technology matching and problem solving assistance. Staffed by professional engineers from a variety of disciplines, the Application Team works with public sector organizations to identify and solve critical problems with existing NASA technology. **Technology Application Team, Research Triangle Institute, P.O. Box 12194, Research Triangle Park, NC 27709. *Doris Rouse, Director,* (919) 541-6980**

How You Can Access Technology Transfer Services At NASA Field Centers: **Technology Utilization Officers & Patent Counsels**—Each NASA Field Center has a Technology Utilization Officer (TUO) and a Patent Counsel to facilitate technology transfer between NASA and the private sector.

If you need further information about new technologies presented in *NASA Tech Briefs,* request the Technical Support Package (TSP). If a TSP is not available, you can contact the Technology Utilization Officer at the NASA Field Center that sponsored the research. He can arrange for assistance in applying the technology by putting you in touch with the people who developed it. If you want information about the patent status of a technology or are interested in licensing a NASA invention, contact the Patent Counsel at the NASA Field Center that sponsored the research. Refer to the NASA reference number at the end of the Tech Brief.

Ames Research Ctr.
Technology Utilization Officer: Laurance Milov
Mail Code 223-3
Moffett Field, CA 94035
(415) 694-4044
Patent Counsel: Darrell G. Brekke
Mail Code 200-11
Moffett Field, CA 94035
(415) 694-5104

Lewis Research Center
Technology Utilization Officer: Harvey Schwartz (acting)
Mail Stop 7-3
21000 Brookpark Road
Cleveland, OH 44135
(216) 433-5567
Patent Counsel: Gene E. Shook
Mail Code 301-6
21000 Brookpark Road
Cleveland, OH 44135
(216) 433-5753

John C. Stennis Space Center
Technology Utilization Officer: Robert M. Barlow
Code HA-32, Bldg.1103
Stennis Space Center, MS 39529
(601) 688-1929

John F. Kennedy Space Center
Technology Utilization Officer: Thomas M. Hammond
Mail Stop PT-PMO-A
Kennedy Space Center, FL 32899
(407) 867-3017
Patent Counsel: James O. Harrell
Mail Code PT-PAT
Kennedy Space Center, FL 32899
(407) 867-3017

Langley Research Ctr.
Technology Utilization Officer: John Samos
Mail Stop 139A
Hampton, VA 23665
(804) 864-2484
Patent Counsel: George F. Helfrich
Mail Code 279
Hampton, VA 23665
(804) 864-3523

Goddard Space Flight Center
Technology Utilization Officer: Donald S. Friedman
Mail Code 702.1
Greenbelt, MD 20771
(301) 286-6242
Patent Counsel: R. Dennis Marchant
Mail Code 204
Greenbelt, MD 20771
(301) 286-7351

Jet Propulsion Lab.
NASA Resident Office
Technology Utilization Officer: Gordon S. Chapman
Mail Stop 180-801
4800 Oak Grove Drive
Pasadena, CA 91109
(818) 354-4849
Patent Counsel: Paul F. McCaul
Mail Code 180-801
4800 Oak Grove Drive
Pasadena, CA 91109
(818) 354-2734
Technology Utilization Mgr. for JPL: Dr. Norman L. Chalfin
Mail Stop 156-211
4800 Oak Grove Drive
Pasadena, CA 91109
(818) 354-2240

George C. Marshall Space Flight Center
Technology Utilization Officer: Ismail Akbay
Code AT01
Marshall Space Flight Center, AL 35812
(205) 544-2223
FAX (205) 544-3151
Patent Counsel: Bill Sheehan
Mail Code CC01
Marshall Space Flight Center, AL 35812
(205) 544-0021

Lyndon B. Johnson Space Center
Technology Utilization Officer: Dean C. Glenn
Mail Code IC-4
Houston, TX 77058
(713) 483-3809
Patent Counsel: Edward K. Fein
Mail Code AL3
Houston, TX 77058
(713) 483-4871

NASA Headquarters
Technology Utilization Officer: Leonard A. Ault
Code CU
Washington, DC 20546
(202) 453-8377
Assistant General Counsel for Patent Matters: Robert F. Kempf, Code GP
Washington, DC 20546
(202) 453-2424

A Shortcut To Software: **COSMIC®**—For software developed with NASA funding, contact COSMIC, NASA's Computer Software Management and Information Center. New and updated programs are announced in the Computer Programs section. COSMIC publishes an annual software catalog. For more information call or write: **COSMIC®** 382 East Broad Street, Athens, GA 30602 *John A. Gibson, Dir.,* (404) 542-3265

If You Have a Question . . . **NASA Scientific & Technical Information Facility** can answer questions about NASA's Technology Utilization Network and its services and documents. The STI staff supplies documents and provides referrals. Call, write or use the feedback card in this issue to contact: **NASA Scientific and Technical Information Facility,** Technology Utilization Office, P.O. Box 8757, Baltimore, MD 21240-0757. *Walter M. Heiland, Manager,* (301) 859-5300, Ext. 242, 243

Test Structures for Bumpy Integrated Circuits

Cross-bridge resistors are added to comb and serpentine patterns.

NASA's Jet Propulsion Laboratory, Pasadena, California

An improved combination of test structures built into an integrated circuit is used to evaluate design rules, fabrication processes, and the quality of interconnections. Electrical measurements of the test structures are processed by a computer to determine whether interconnections thin excessively, break, or short-circuit as they pass over bumpy circuit elements on the surface of the integrated-circuit chip. Both aluminum and polycrystalline silicon interconnections can be evaluated.

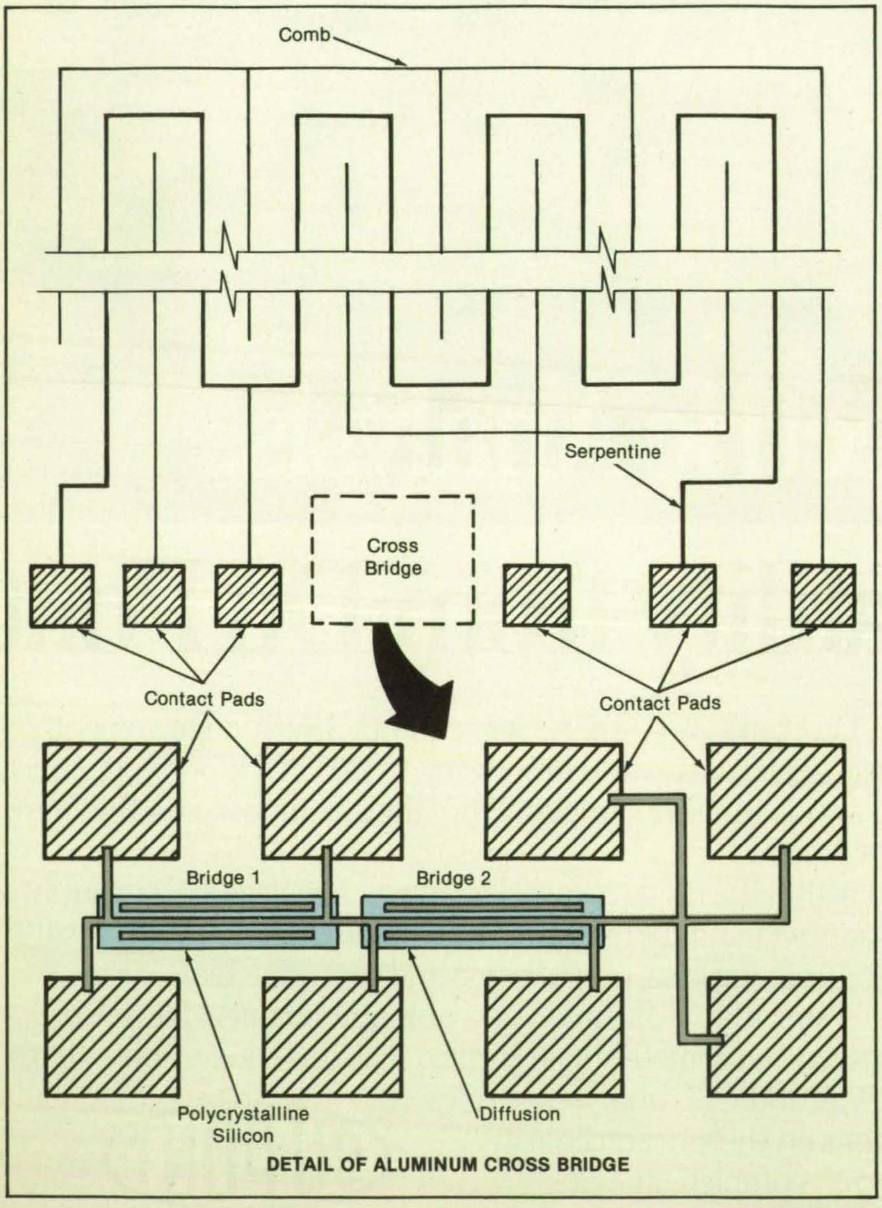

Figure 1. **Test Structures** consist of meshing serpentines and combs, and a cross bridge. These structures are used to make electrical measurements that reveal defects in the design or fabrication.

The combination of test structures includes three comb arrays, two serpentine arrays, and a cross bridge (see Figure 1). The test structures are made of aluminum or polycrystalline silicon, depending on the material in the integrated-circuit layers to be evaluated. Aluminum combs and serpentine arrays are deposited over steps made by the polycrystalline silicon and diffusion layers, while polycrystalline silicon versions of these structures are used to cross over steps made by the thick oxide layer (see Figure 2).

Measurements are taken by computer-controlled testing equipment that includes a current source, a differential voltmeter, and a power supply. Measurements taken on the cross bridge are used to determine the widths of the lines in the serpentine arrays. Previous optical and electrical measurements have shown that the width of a line tends to change where it crosses a step, and accurate values of width are needed to produce accurate evaluations. Measurements on the cross bridge are also used to determine the sheet resistance of the aluminum or polycrystalline silicon interconnection material.

To detect inadequate coverage of steps caused by the thinning of lines, the system forces a current along the serpentines — 500 μA for aluminum and 1 μA for polycrystalline silicon — and measures the voltage drop. From the known current and the measured voltage drop, the system calculates the resistance of the serpentine. From the calculated resistance and from the average width of the lines and the sheet resistance determined previously from measurements on the cross bridge, the system computes the effective length of the serpentine. If this length is more than 150 percent of the nominal length, the system considers the serpentine to have excessive resistance and labels the affected area of the circuit chip as having defective coverage of steps. Similarly, if a serpentine line is broken at any point, it carries no current, causing the system to detect an open circuit and to label the area as defective.

"Can we really replace all these boards with a single Toshiba

Megacell ASIC?"

"You bet! Toshiba's got the entire set of LSI, MSI, and SSI system components in their library."

"Are we also talking Z80® microprocessor, disk controller and 82CXX functions?"

"Yep. Into a single plastic flat pack."

"Do you realize what this means?"

"Yeah. We can have the smallest system footprint on the market."

"Fantastic! Let's get them in here today."

Through Toshiba's 1.2m Megacell ASIC technology, called Super Integration, an entire system can be put on a single chip. In fact, one or two Megacell ASICs are enough to create all the logic for an entire PC system.

Toshiba's patented Super Integration technology utilizes off-the-shelf LSI functions together with standard cell logic to form the most highly integrated megacell circuits. And each megacell is time-tested and benchmarked to meet compatibility requirements of complex LAN software and BIOS. These circuits can be extremely cost-effective since they can be delivered in any of a series of advanced surface mount flat packs ranging from 100 to 184 pins.

No other company today can match the level of integration available through Toshiba's Megacell ASIC technology, because Toshiba has the most extensive library: the Z80® family, the Intel® family, CRT controllers, LCD drivers, UARTs, analog circuits, RAM and ROM, and more. And Toshiba's experience in Megacell ASICs is unequalled in the industry. Toshiba has been delivering millions of Megacell ASICs since 1984, yielding the highest production maturity.

For complete information on how Toshiba's Megacell ASIC can help you clear your desk, call 1-800-888-0848 ext. 517 today. *Service is our key component.*

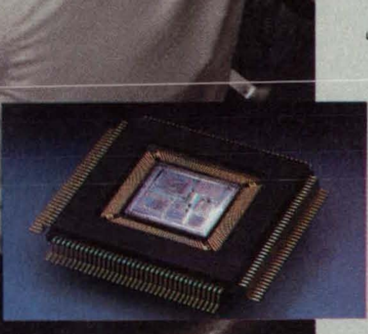

In Touch with Tomorrow

TOSHIBA

TOSHIBA AMERICA ELECTRONIC COMPONENTS, INC.

Circle Reader Action No. 635

CSM-88-003-2

MAINE, Datcom, Inc., (617) 891-4600; **MARYLAND,** D.G.R., Inc., (310) 583-1360; **MASSACHUSETTS,** Datcom, Inc., (617) 891-4600; **MICHIGAN,** Action Components Sales, (313) 349-3940; **MINNESOTA,** Electric Component Sales, (612) 933-2594; **MISSISSIPPI,** Montgomery Marketing, Inc., (205) 830-0498; **MISSOURI,** D.L.E. Electronics, (316) 744-1229, R.W. Kunz, (314) 966-4977; **MONTANA,** Components West, (206) 885-5880; **NEVADA,** Elrepco, Inc., (415) 962-0660; **NEW ENGLAND,** Datcom, Inc., (617) 891-4600; **NEW HAMPSHIRE,** Datcom, Inc., (617) 891-4600; **NEW JERSEY,** Nexus Technology, (201) 947-0151; **NEW MEXICO,** Summit Sales, (602) 998-4850; **NEW YORK,** Nexus Technology, (201) 947-0151; **NEW YORK** (Upstate), L.D. Allen, (315) 437-8387; **NORTH/SOUTH CAROLINA,** Montgomery Marketing, Inc., (919) 467-6319, (919) 851-0010; **NORTH/SOUTH DAKOTA,** Electric Component Sales, (612) 933-2594; **OHIO,** J.R. Thornberry, (216) 248-4995; **OHIO,** J.R. Thornberry, (214) 248-4995, (614) 792-5171; **OKLAHOMA,** MIL-Reps, (214) 644-6731; **OREGON,** Components West, (503) 684-1671; **PENNSYLVANIA,** Nexus Technology, (215) 675-9600, (Western), J.R. Thornberry, (216) 248-4995, (614) 792-5171; **RHODE ISLAND,** Datcom, Inc., (617) 891-4600; **TENNESSEE,** Montgomery Marketing, Inc., (205) 830-0498; **TEXAS,** MIL-Reps, (512) 346-6331, (713) 444-2557, (214) 644-6731; **UTAH,** Straube Associates Mountain States, Inc., (801) 263-2640; **VERMONT,** Datcom, Inc., (617) 891-4600; **VIRGINIA,** D.G.R., Inc., (301) 581-1360; **WASHINGTON,** Components West, (206) 885-5880, (509) 922-2412; **WEST VIRGINIA,** D.G.R., Inc., (301) 581-1360; **WISCONSIN,** Carlson Electronics, (414) 476-2790, Electric Component Sales, (612) 933-2594; **WYOMING,** Straube Associates Mountain States, Inc., (303) 426-0890; **CANADA, BRITISH COLUMBIA,** Electro Source, (204) 888-2412; **ONTARIO,** Electro Source, Inc., (416) 675-4490, (613) 592-3214; **QUEBEC,** Electro Source, Inc., (514) 630-7486.

To test for short circuits, the system supplies a constant 5 volts between the serpentine and the comb and measures the leakage current between them. If the leakage is greater than 10 nA, the layers are considered short-circuited, and the site is labeled as faulty.

The system presents its measurements in four ways:

1. It draws a map that shows the locations of defective test structures on the chip.
2. It generates a histogram of the effective lengths of the serpentines.
3. It prints out statistical information on the widths of the lines, the sheet resistances, and the resistances and effective lengths of the serpentines.
4. The characteristic number of elements per type of defect (short or open circuit) is calculated on the basis of Poisson distributions of defects and least-squares fits.

This work was done by Martin G. Buehler and Hoshyar R. Sayah of Caltech for **NASA's Jet Propulsion Laboratory**. *For further information, Circle 141 on the TSP Request Card.*

This invention is owned by NASA, and a patent application has been filed. Inquiries concerning nonexclusive or exclusive license for its commercial development should be addressed to the Patent Counsel, NASA Resident Office-JPL [see page 18]. Refer to NPO-17393.

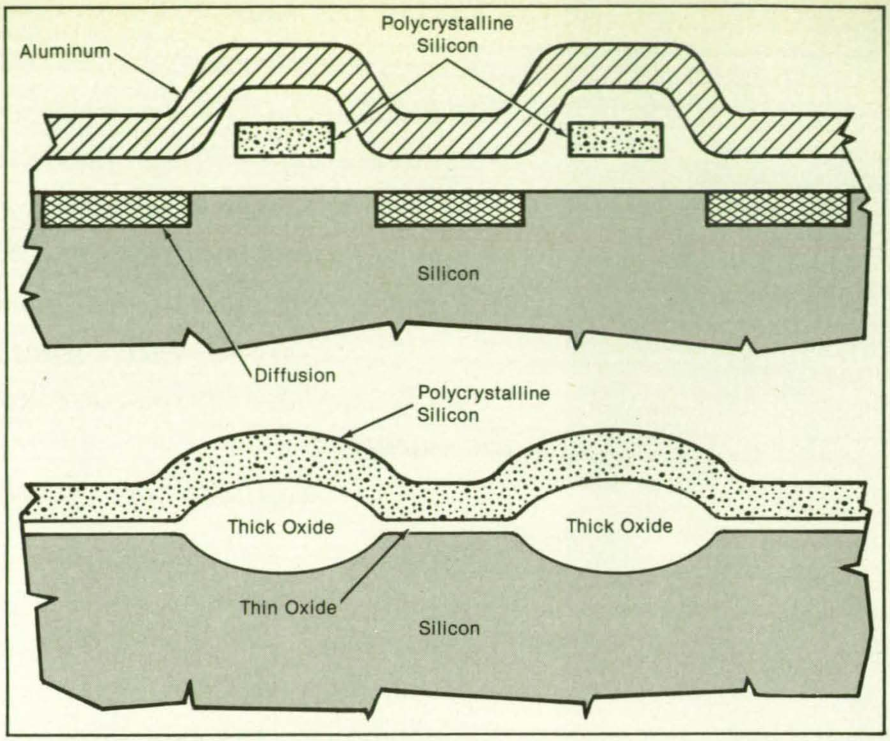

Figure 2. The **Test Structures** of Figure 1 are shown here in magnified cross-sectional views.

Paraboloidal Antenna Radiates Fan or Pencil Beams

The shape of the beam is determined by the type of feed.

NASA's Jet Propulsion Laboratory, Pasadena, California

Theory and experiments show that the same paraboloidal antenna reflector can be used to radiate a pencil beam or fan beam, depending on the configuration of the feed. Usually, a paraboloidal reflector is fed by a low-gain antenna or waveguide horn that acts as an approximate point source; such a feed illuminates the paraboloid fairly evenly, giving rise to a pencil-shaped (that is, circularly symmetrical about, and sharply pointed in, the forward direction) beam with side lobes.

Although a pencil-shaped beam is desirable in many applications, a fan-shaped beam is preferred in some scanning-radar and mapping-radar systems. One can use the approximate Fourier-transform relationship between the near-field pattern of the feed radiator and the far-field pattern of the overall antenna to make a preliminary selection of the feed pattern and, therefore, of the feed radiator that is likely to produce the desired fan-shaped far-field pattern. For example, a linear array of dipole radiators feeding a reflector would be expected to generate a far-field pattern that has approximately constant intensity over a wide angle in the plane of the array and a narrow pattern like that of a pencil beam in the plane perpendicular to the array (see figure).

An experiment was performed with a paraboloidal reflector that had a focal length of 48 in. (1. 22 m) and a diameter of 3.65 m. The reflector was illuminated at a frequency of 13.6 GHz, first by an 8-element microstrip linear array, the center of which was placed 13 in. (33 cm) off axis and 2.9 in. (7.4 cm) outward from the focal plane, then by a 16-element microstrip linear array, the center of which was placed 18.3 in. (46.5 cm) off axis and 4.7 in. (11.9 cm) outward from the focal plane. In the first case, the beam was turned ~15° off axis, ~3.5° wide in the plane of the array, and ~0.5° wide in the perpendicular plane. In the second case, the beam was turned ~21° off axis, ~5° wide in the plane of the array, and ~0.45° wide in the perpendicular plane.

The experiment showed that fan beams can be generated in this way and are not seriously distorted by the feed offsets tested. The experiments also showed that because the reflector is in the near field of the feed, the fan beam is not necessarily focused by placing the feed at the focal plane. Pending a more-complete theoretical analysis, it is necessary to find the optimum location for the feed by experimentation.

This work was done by John Huang of Caltech for **NASA's Jet Propulsion Laboratory**. *For further information, Circle 76 on the TSP Request Card.*
NPO-17503

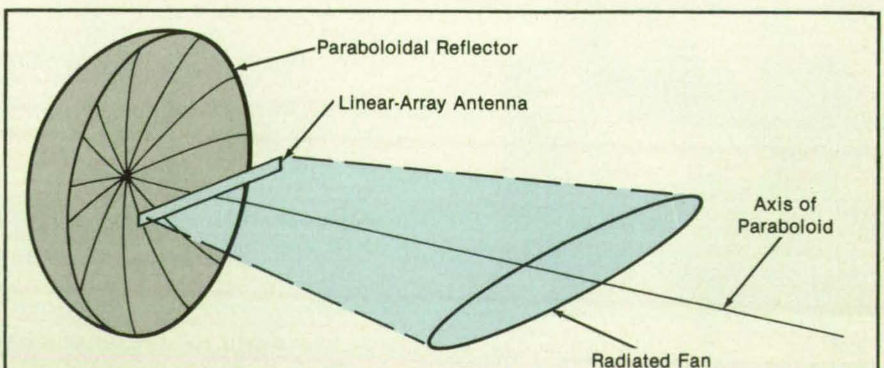

The **Far-Field** radiation pattern of a paraboloidal reflector illuminated by a linear-array feed antenna is wide in one plane and narrow in a perpendicular plane.

INTEL FROM HAMILTON/AVNET

For true, real-time computing that's
fordably priced, call Hamilton/Avnet
r a system on the cutting edge of
chnology—The Intel System 120.

The System 120 combines the power
nd speed of Intel's 32-bit, 386™ micro-
ocessor with iRMX®, a multi-tasking
perating system that provides guaran-
ed, real-time response to external
vents and interrupts.

The System 120 applications can also
e easily moved to Intel's MULTIBUS® I &
architectures, allowing for easy ex-
ansion as your computing needs grow.

And Hamilton/Avnet's Systems Engi-
eering Group can configure, install,
odify and test a System 120 to your
xact specifications.

Cut through the clutter and call
amilton/Avnet. For the location nearest
ou, call toll free, **1-800-442-6458**.

6 is a trademark of Intel Corporation.
MX and MULTIBUS are registered trademarks of Intel
rporation.

Hamilton/Avnet ELECTRONICS AN AVNET COMPANY

Circle 18

TEAR THROUGH REAL-TIME COMPUTING CONFUSION WITH INTEL'S SYSTEM 120

LET HAMILTON/AVNET SHOW YOU THE BENEFITS OF REAL-TIME COMPUTING

Send for free information and learn how Hamilton/Avnet's Systems Engineering Group can customize your Intel System 120.

These offers are good for a limited time only. Send in your coupon today!

Please check the following:

☐ Please send me Hamilton/Avnet's Systems Engineering Group/Intel brochure.

☐ Please send me the demo diskette on Intel's System 120.

NAME ______

TITLE ______

COMPANY ______

MSTOP ______

ADDRESS ______

CITY ______

STATE ______ ZIP ______

PHONE ______

APPLICATION ______

Mail to:

Mark Burnett
Advertising Services
10950 Washington Blvd.
Culver City, CA 90230

Coupon expires 9/30/89.

Circle Reader Action No. 668

SQUID With Integral Flux Concentrator

A slotted superconducting disk concentrates magnetic flux from an external coil.

Marshall Space Flight Center, Alabama

In an improved superconducting quantum interference device (SQUID), a change in the size and shape of the superconducting ring improves coupling to the external signal coil and eases coil-positioning tolerances. The new device is more rugged and easier to manufacture than are conventional SQUID's with comparable electrical characteristics. SQUID's can be used in magnetometers, ammeters, analog-to-digital converters, and related electronic applications in which high signal-to-noise ratios are required.

A radio-frequency SQUID comprises a low-inductance, strongly superconducting loop interrupted by a Josephson junction. The improved SQUID has a larger, washer-shaped, superconducting loop instead of the usual tiny ring-shaped loop (see figure). The small size of the central hole maintains the required low inductance. Currents induced in the superconductor by the magnetic field of the signal coil exclude the magnetic field of the coil from the superconductor (Meissner effect). Thus, the magnetic field becomes concentrated into the SQUID loop, and the coil and the SQUID are coupled tightly.

The position of the coil is not critical: the coil need only surround the central hole and lie entirely on the superconducting disk. Other coupling devices that were tried proved difficult to fabricate and align. These included integral, multiturn coils fabricated directly over the SQUID loop or slotted superconducting cylinders wound with the signal coil and shaped to concentrate the magnetic flux inside the SQUID loop.

The SQUID could be made with any of various types of Josephson junctions. The variable-thickness (notched) junction has been used successfully. However, a novel, single-step, single-material junction called the "step-function junction" has advantages over junctions that include very thin insulators or other dissimilar materials. The step-function junction is relatively easy to fabricate. It also provides an effective geometry for creating the short, narrow, junction region, the "weak link" that provides the phase shifting in the wave function of the supercurrent. It performs this function over a range of temperatures larger than that of other junctions. The step-function junction is quite rugged because it is less subject to electrical breakdown and galvanic corrosion than are other types of junctions.

This work was done by Palmer N. Peters and Robert C. Sisk of **Marshall Space Flight Center**. *For further information, Circle 18 on the TSP Request Card.*

This invention is owned by NASA, and a patent application has been filed. Inquiries concerning nonexclusive or exclusive license for its commercial development should be addressed to the Patent Counsel, Marshall Space Flight Center [see page 18]. Refer to MFS-28282.

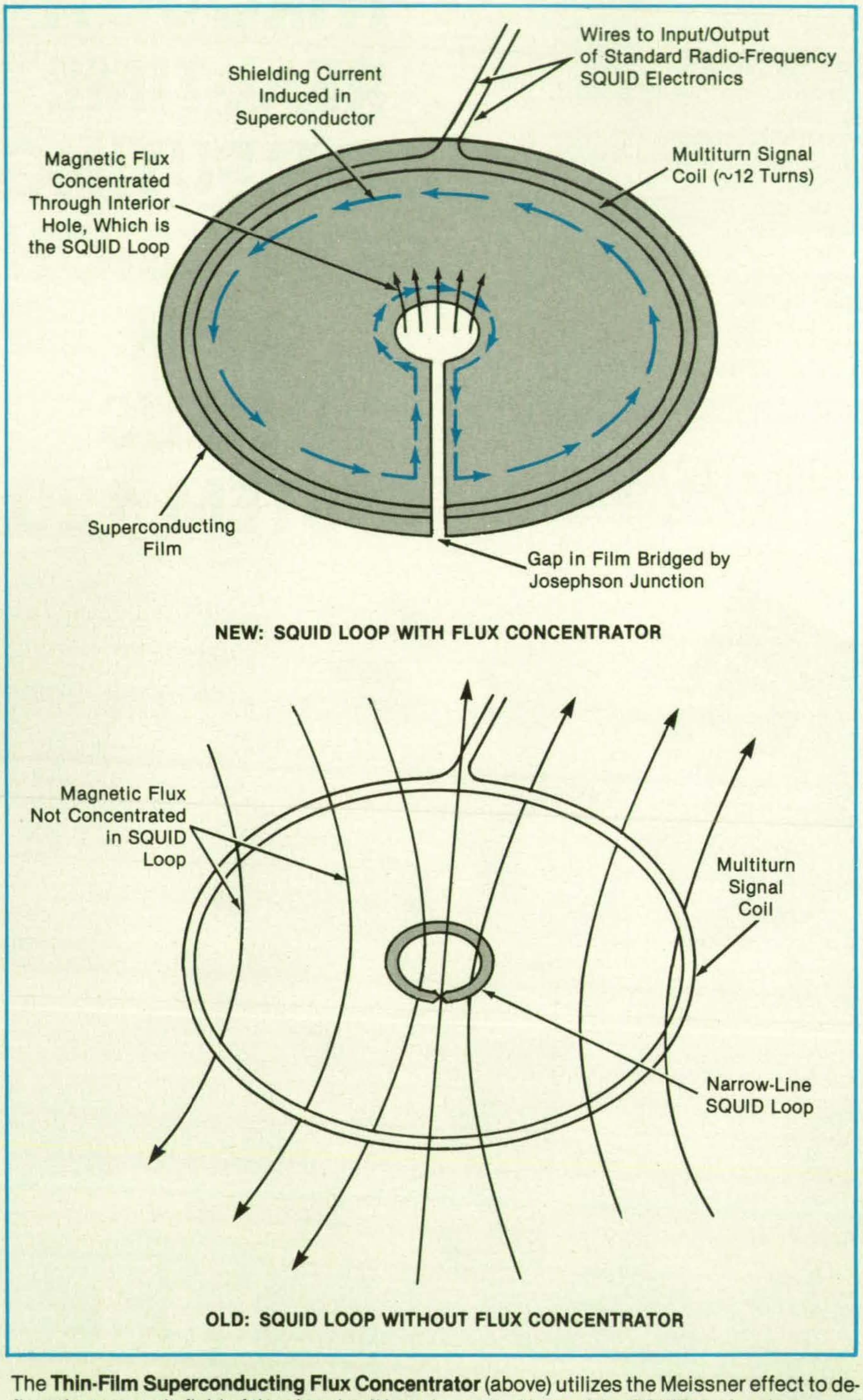

The **Thin-Film Superconducting Flux Concentrator** (above) utilizes the Meissner effect to deflect the magnetic field of the signal coil into the central hole of the SQUID. In the absence of a flux concentrator (below), coupling between the coil and SQUID would be weak because relatively little of the flux would be intercepted by the SQUID loop.

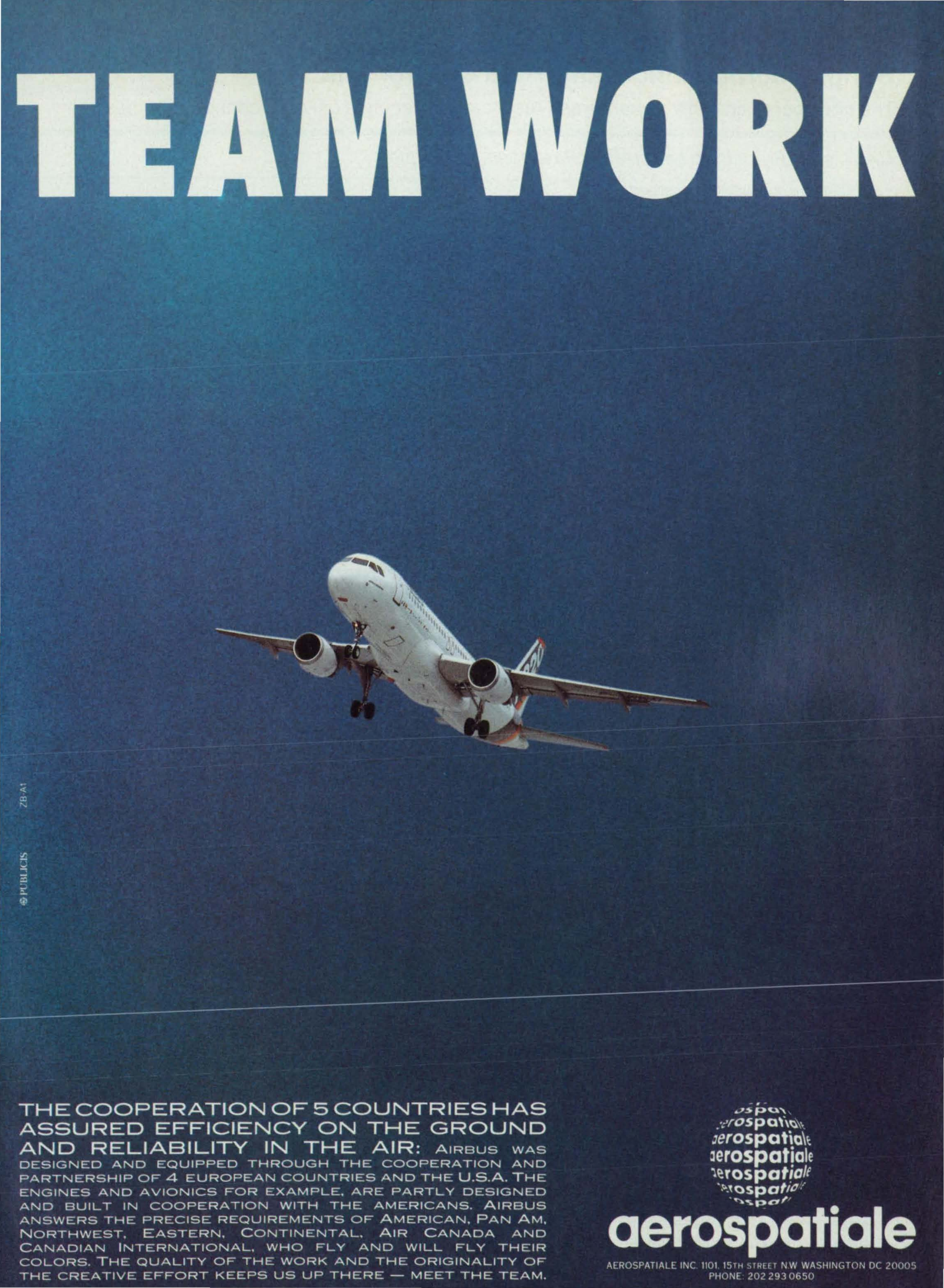
TEAM WORK
THE COOPERATION OF 5 COUNTRIES HAS ASSURED EFFICIENCY ON THE GROUND AND RELIABILITY IN THE AIR: AIRBUS WAS DESIGNED AND EQUIPPED THROUGH THE COOPERATION AND PARTNERSHIP OF 4 EUROPEAN COUNTRIES AND THE U.S.A. THE ENGINES AND AVIONICS FOR EXAMPLE, ARE PARTLY DESIGNED AND BUILT IN COOPERATION WITH THE AMERICANS. AIRBUS ANSWERS THE PRECISE REQUIREMENTS OF AMERICAN, PAN AM, NORTHWEST, EASTERN, CONTINENTAL, AIR CANADA AND CANADIAN INTERNATIONAL, WHO FLY AND WILL FLY THEIR COLORS. THE QUALITY OF THE WORK AND THE ORIGINALITY OF THE CREATIVE EFFORT KEEPS US UP THERE — MEET THE TEAM.
aerospatiale
AEROSPATIALE INC. 1101, 15TH STREET N.W WASHINGTON DC 20005
PHONE: 202 293 0650
© PUBLICIS ZB-A1

Simple Multiplexing Hand-Held Control Unit

The circuit contains only switches and resistors and requires only two connecting wires.

NASA's Jet Propulsion Laboratory, Pasadena, California

A simple analog multiplexing concept makes it possible to combine signals from a hand-held control unit so that they can be fed to a robot-control computer over a single pair of wires. The control unit contains no active electronic components.

The multiplexer consists of a series of resistors, each of which is shunted by a single-pole, single-throw switch (see figure). The user operates the switches by pressing buttons or squeezing triggers — for example, to control such robot functions as grasping, releasing, locking position, and emergency stopping. The value of each resistor is the double (or some other convenient multiple) of the value of its predecessor in the series.

A source supplies a constant current to the series of resistors. The voltage across the series varies according to the number of switches that are closed and their positions in the series. Each pattern of switch closures created by the operator produces a unique voltage at the terminal of an analog-to-digital converter to which the control unit is connected. The associated control computer interprets the output of the analog-to-digital converter in terms of the configuration of the switches.

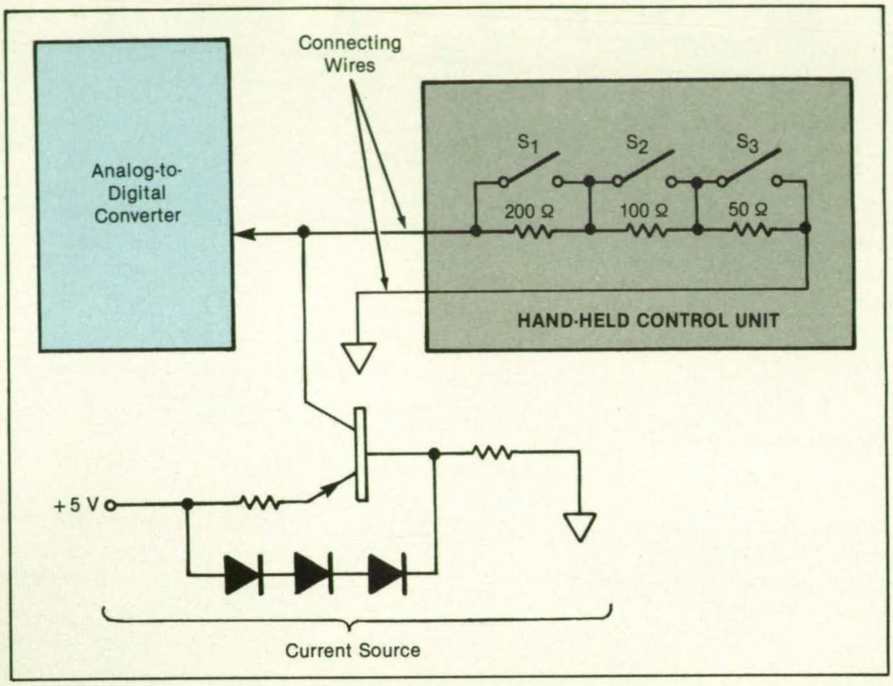

The **Voltage at the Input** of the analog-to-digital converter varies with the number and location of closed switches in the hand-held controller.

A prototype of the multiplexer that includes three switches has been operated successfully in over 200 hours of system operations. The number of switches that can be accommodated is determined by the signal-to-noise ratio of the current source, the noise induced in the control unit and cable, and the number of bits in the output of the analog-to-digital converter. Because many computer-controlled robots have extra analog-to-digital channels, such a multiplexer can be added at little extra cost.

This work was done by Blake Hannaford of Caltech for **NASA's Jet Propulsion Laboratory**. *For further information, Circle 124 on the TSP Request Card.*

In accordance with Public Law 96-517, the contractor has elected to retain title to this invention. Inquiries concerning rights for its commercial use should be addressed to

Edward Ansell
Director of Patents and Licensing
Mail Stop 301-6
California Institute of Technology
1201 East California Boulevard
Pasadena, CA 91125

Refer to NPO-17308, volume and number of this NASA Tech Briefs *issue, and the page number.*

Honeycomb-Fin Heat Sink

This strong, lightweight part increases the effectiveness of forced-air cooling.

NASA's Jet Propulsion Laboratory, Pasadena, California

An improved finned heat sink for electronic components is more lightweight, inexpensive, and efficient than conventional extruded-fin heat sinks. Designed for use with forced air, the heat sink can be easily scaled up to dissipate power up to a few hundred watts.

Although extrusion is an economical fabrication process, it yields fins that are thicker and more widely spaced than they should be for optimum transfer of heat. Extruded fins are about 10 times as heavy as optimized fins need be. An alternative to forced-air cooling with finned heat sinks is cooling by liquids flowing through internal channels in heat sinks. However, in comparison with forced-air systems, liquid cooling systems are more complicated, more expensive, and less reliable, and they need more maintenance.

In the new heat sink, the fins are the internal walls of an aluminum honeycomb structure (see figure). The honeycomb is made by an inexpensive process: sheets of aluminum are painted with stripes of adhesive, bonded together, and then expanded into hexagonal cells in the nonbonded sections. The process is a standard one that has been adapted to heat sinks by use of wider adhesive stripes, sheets that are thicker in proportion to the height of the cells, and a low ratio of width to height period of the cells (about 5 percent).

Instead of expanding bonded flat sheets of aluminum, the fins can be made by bonding corrugated sheets. Air flows easily through the channels created by the peaks and valleys of the corrugations, and, because of the large number of bonding points, the structure is strong.

Air flowing through the cells removes heat from the aluminum. The cells can be readily fabricated with dimensions in the optimum range for heat transfer: a sheet (or fin) thickness of 0.003 to 0.008 inch

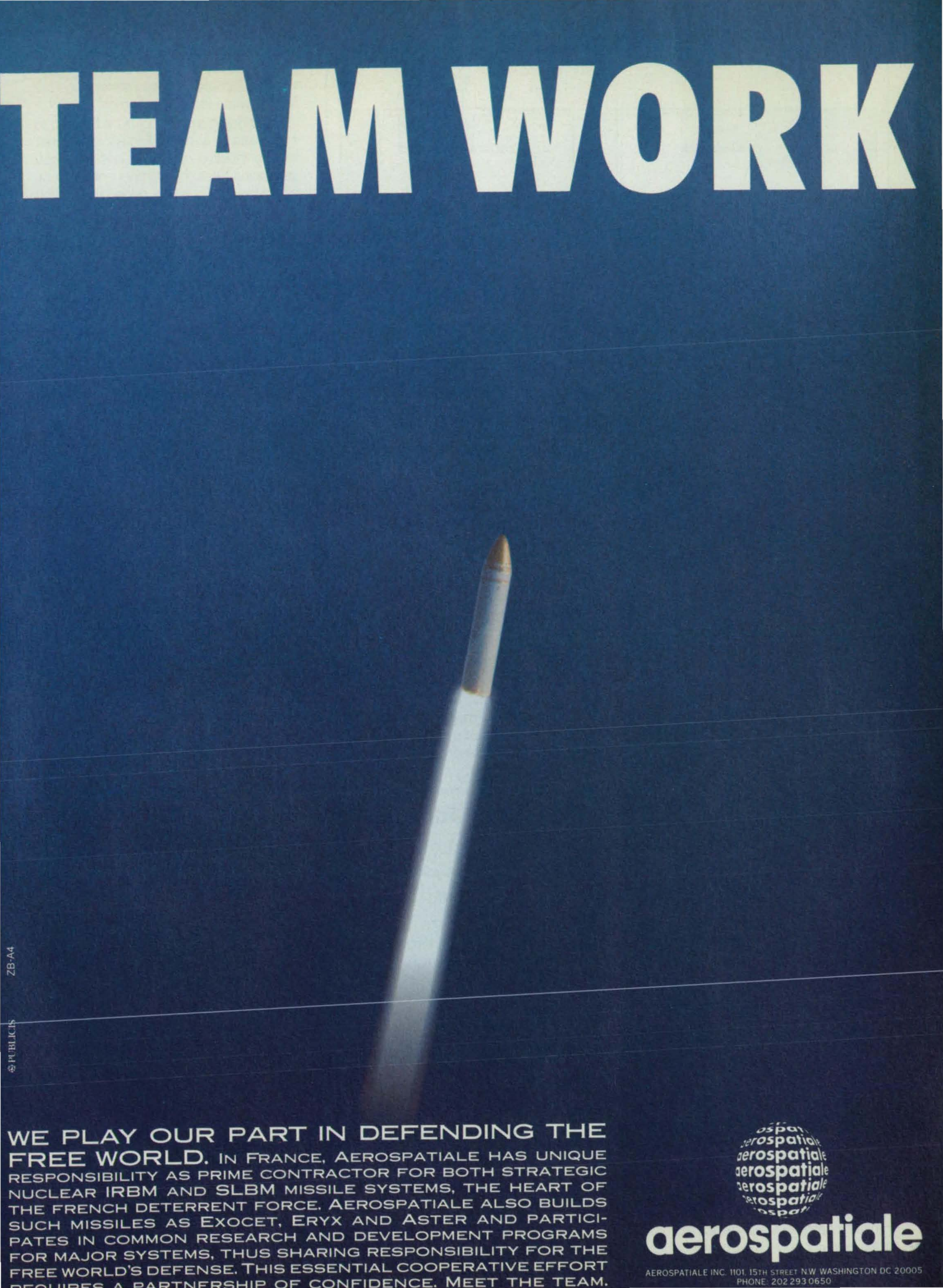
TEAM WORK
WE PLAY OUR PART IN DEFENDING THE FREE WORLD. IN FRANCE, AEROSPATIALE HAS UNIQUE RESPONSIBILITY AS PRIME CONTRACTOR FOR BOTH STRATEGIC NUCLEAR IRBM AND SLBM MISSILE SYSTEMS, THE HEART OF THE FRENCH DETERRENT FORCE. AEROSPATIALE ALSO BUILDS SUCH MISSILES AS EXOCET, ERYX AND ASTER AND PARTICIPATES IN COMMON RESEARCH AND DEVELOPMENT PROGRAMS FOR MAJOR SYSTEMS, THUS SHARING RESPONSIBILITY FOR THE FREE WORLD'S DEFENSE. THIS ESSENTIAL COOPERATIVE EFFORT REQUIRES A PARTNERSHIP OF CONFIDENCE. MEET THE TEAM.
aerospatiale
AEROSPATIALE INC. 1101, 15TH STREET N.W. WASHINGTON DC 20005
PHONE: 202 293 0650
© PUBLICIS ZB-A4

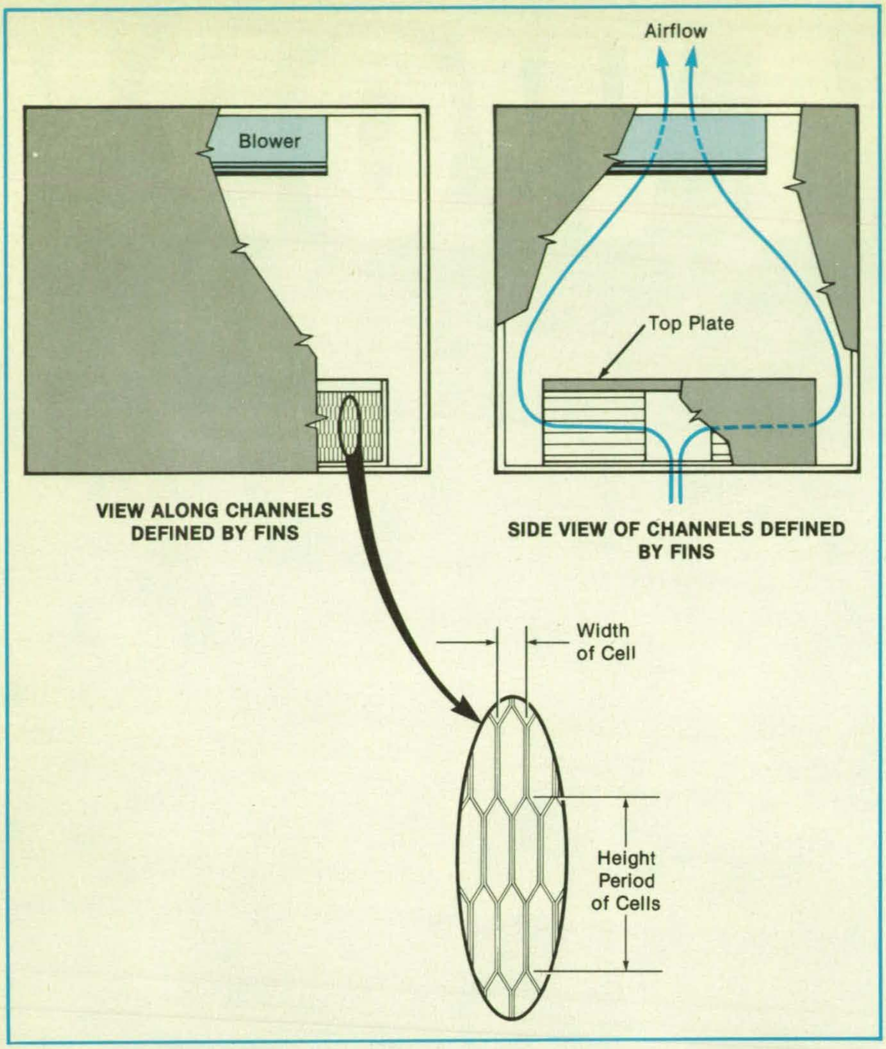

Honeycomb Cells Form Channels that guide air through a heat sink. The cell structure gives strength to the thin aluminum foil of which it is made. The length of the channels can be chosen for thermodynamic efficiency; columns of cells can be combined in any reasonable number because flowing air is distributed to all.

(0.076 to 0.203 millimeter) and a cell width (or fin spacing) of 0.020 to 0.050 inch (0.51 to 1.27 millimeters). These dimensions are far below the limits of extrusion.

The honeycomb structure is bonded to a top plate by a metal-filled epoxy or other heat-conductive adhesive, and the heat-generating electronic component is mounted on the top plate. For added rigidity and strength, the honeycomb may be placed in a slotted bottom plate.

A blower draws air through a port in the heat sink. The airflow divides in two after entering the port, passing through cells on both sides of the port. A single blower may be used for many heat sinks. The air flows nearly uniformly to all cells. The heat sink, therefore, cools nearly as effectively at its ends as it does near its center, no matter how many columns of cells are combined.

This work was done by Wally E. Rippel of Caltech for **NASA's Jet Propulsion Laboratory**. *For further information, Circle 62 on the TSP Request Card.*

In accordance with Public Law 96-517, the contractor has elected to retain title to this invention. Inquiries concerning rights for its commercial use should be addressed to

Edward Ansell
Director of Patents and Licensing
Mail Stop 301-6
California Institute of Technology
1201 East California Boulevard
Pasadena, CA 91125

Refer to NPO-17198, volume and number of this NASA Tech Briefs *issue, and the page number.*

Single Electrode Would Control Charge-Coupled Device

Space would be saved and interelectrode short circuits eliminated.

NASA's Jet Propulsion Laboratory, Pasadena, California

A proposed virtual-phase, interline-transfer, charge-coupled device would use a single gate electrode to control both the interline and intraline transfer of charge. The present version contains two control electrodes: one to transfer charge between the photosites and the shift register, another to transfer charge along the shift register. The contemplated changes in design would eliminate the vulnerability of the present version to electrical shorts between the control electrodes and increase the overall quantum efficiency of the device by eliminating the nonphotosensitive area required for the separation of the electrodes.

Figure 1 illustrates a portion of a buried-channel, linear, virtual-phase, interline-transfer, charge-coupled device according to the new concept. The control electrode includes gate-transfer (GT), charge-barrier (CB), and clocked-well (CW) regions that differ from each other in their concentrations of dopants. The portion of the shift register not in contact with the electrode also contains differentially-doped virtual-well (VW) and virtual-barrier (VB) regions.

Charge would be transferred along the shift register when the voltage on the con-

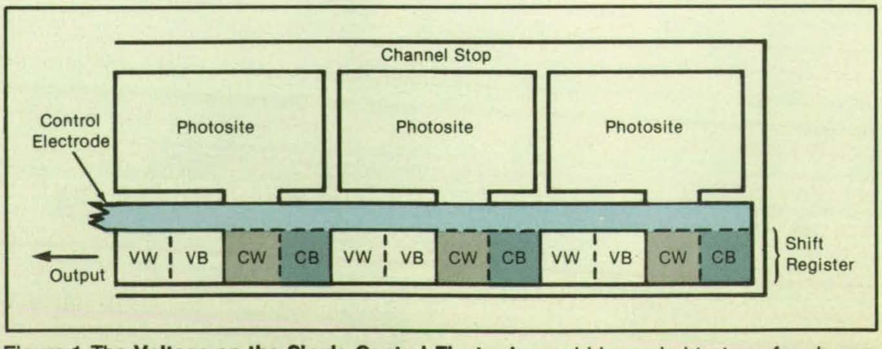

Figure 1. The **Voltage on the Single Control Electrode** would be varied to transfer charge from the photosites to the shift register, or else along the shift register. The two kinds of transfer would be independent of each other.

Our DCS750 is so user-friendly it enhances productivity right out of the box

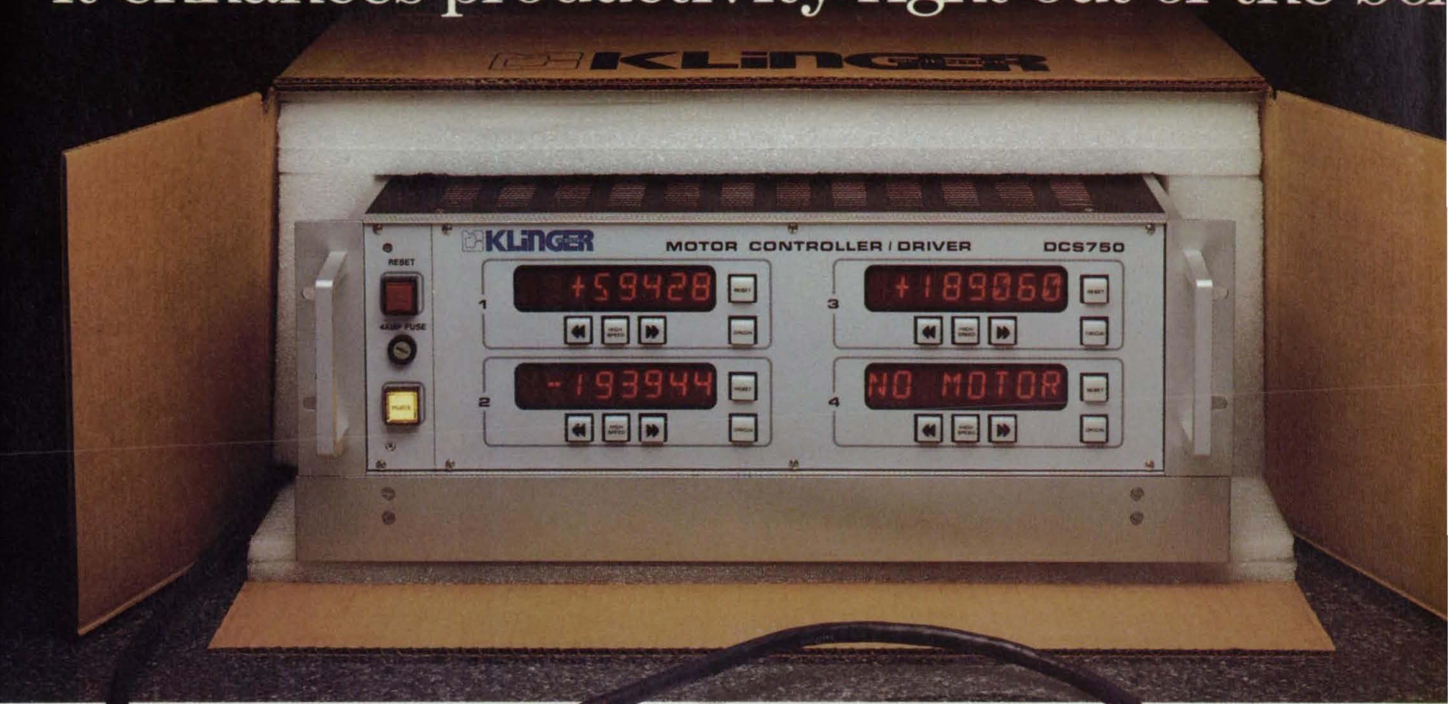

Set-up is simple. Plug in the cables and you're up and running. Klinger's DCS750 Motor Controller/Driver is completely integrated with controller modules, power supplies and amplifiers.

What's more, with its advanced programming power and ergonomic design, the DCS750 is a breeze to operate. It can simultaneously control up to four DC motor driven positioners in closed loop operation with pinpoint precision and minimal effort.

So when you want to step up the sophistication and performance of your application, the DCS750 steps up productivity as well. Right out of the box!

A NEW DIMENSION IN PERFORMANCE.

Equipped with both RS-232-C and IEEE-488 ports, the DCS750 interfaces with virtually any host computer or operates through its complete array of front panel controls to enhance performance. A command buffer relieves communication bottlenecks. And the system accepts and executes new commands on any axis from either interface, even while running a program.

The DCS750 allocates 16K bytes of non-volatile memory for program storage. All velocity, acceleration and PID parameters are programmable, preserved and automatically restored after power-up or reset.

THE VERY BEST IN PROGRAMMING.

The DCS750's instruction set includes 60 powerful commands that make programming easy.

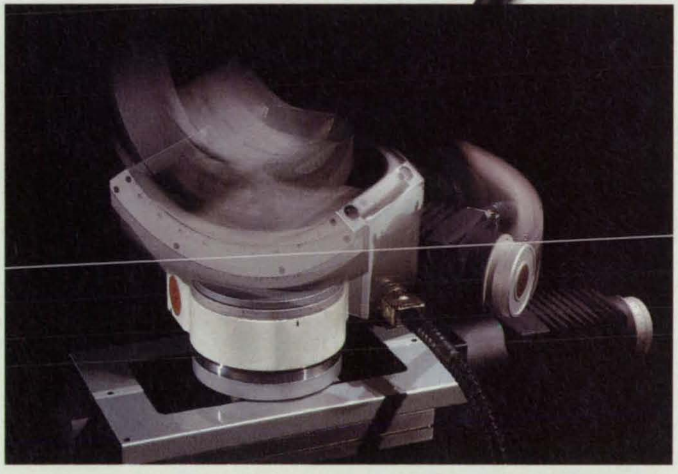

And an on-board editor and compiler reduces software development and debugging time.

In addition, the DCS750 can be programmed with "soft" travel limits for the positioner. Repeatability is assured by Klinger's unique home-seeking Origin Search function.

And the DCS750 works with most DC motors and over 1,000 Klinger micropositioners and mounts.

To learn more about the DCS750 and the thousands of other Klinger micropositioners and systems, write or call for our free micropositioning handbook and motor controller brochure. Klinger Scientific Corporation, 999 Stewart Avenue, Garden City, NY 11530. (516) 745-6800 FAX: (516) 745-6812.

KLINGER SCIENTIFIC

Building better positioning systems, piece by perfect piece.

U.S.A. Headquarters: 999 Stewart Avenue, Garden City, NY 11530 (516) 745-6800 Fax (516) 745-6812.
Regional Offices: Northern California (415) 969-0247; Southern California (714) 999-5088. **In Canada:** Longueuil, Quebec (514) 442-4666.
Worldwide distribution network: Contact Micro-Controle, Z.I. de St. Guenault, B.P. 144, 91005 Evry Cedex, France. Tel.33(1)64.97.98.98.
FAX 33(1)60.79.45.61.

Circle Reader Action No. 368

trol electrode is alternated between the gate potentials A and B shown in Figure 2. However, when the potential on the control electrode is raised to C, charge would not be transferred along the shift register; instead, charge would then be transferred from the photosites into the adjacent clocked-well portions of the shift register. Thus, the interline and intraline transfer of charge would be independent of each other, even though they would be controlled by the same electrode. This would be possible because the concentration of negative dopant in the gate-transfer region would be less than that of the surrounding regions.

The gate-transfer region would be made according to the following procedure:

1. Prepare slices according to the standard procedure for the fabrication of virtual-phase charge-coupled devices up to, but not including, the implantation of the buried channel.
2. Implant the buried channel at half the normal dose in all areas.
3. Mask the gate-transfer region and the photosites.
4. Implant the buried channel at half the normal dose.
5. Pattern and implant the clocked-well region according to the standard procedure.
6. Deposit polycrystalline silicon and pattern the control-electrode structure.
7. Mask the virtual-barrier and virtual-well regions.
8. Implant the buried channel at half the normal dose.
9. Continue the standard procedure to completion.

The proposed device could transfer charge from the photosites into the shift register and through to the output. It is also possible to make a device that would transfer charge into and through the shift register to storage at a photosite. This would be done by implanting at twice the standard dose in step 2 and compensating the excess negative dopant in steps 3 and 8.

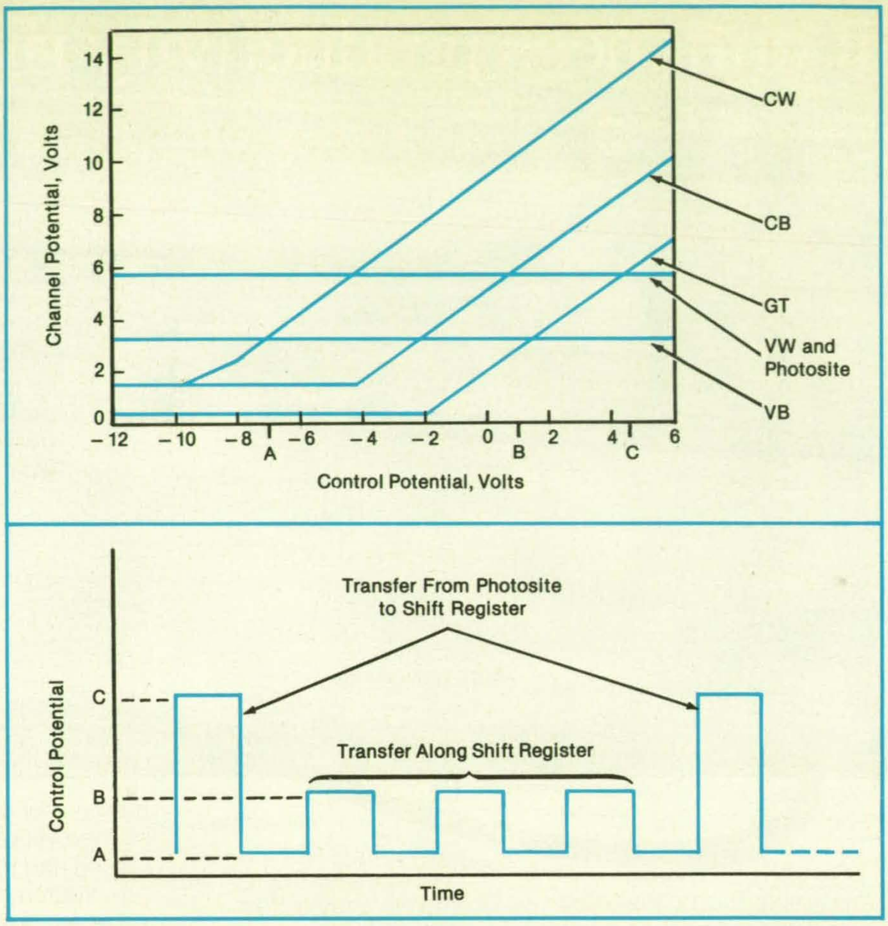

Figure 2. The **Maximums of the Electrostatic Potentials** in each region of the device are shown as functions of the voltage applied to the control electrode.

This work was done by Mark Wadsworth and Robert D. McGrath of Texas Instruments, Inc., for **NASA's Jet Propulsion Laboratory**. *For further information, Circle 21 on the TSP Request Card. NPO-17313*

Books and Reports

These reports, studies, handbooks are available from NASA as Technical Support Packages (TSP's) when a Request Card number is cited; otherwise they are available from the National Technical Information Service.

Radiation Damage in Advanced Bipolar Transistors

The degradation of current gain is measured.

A report describes measurements of the common-emitter current gains (h_{FE}) of advanced bipolar silicon transistors before, during, and after irradiation with 275-MeV bromine ions, 2.5-MeV electrons, and γ rays from cobalt-60 atoms. The decrease in h_{FE} is used as a measure of the radiation-induced damage. The nonionizing component involves the displacement of atoms from their sites in crystalline lattices. Displacement damage in the base region of a transistor can reduce the h_{FE}. Such damage in the oxide or on the surface (where it could increase surface recombination) may also play a role in the reduction of h_{FE}.

The specimens were commercial transistors made according to minimum-geometry design rules. The devices had n++ emitters, 2 μm^2 in area, inside p-type buffer bases. The devices were operated with a base current of 1 μA and a collector-to-emitter potential of 0.5 V. The collector currents ranged from a maximum of 76.5 μA before irradiation to a minimum of 35 μA after irradiation.

The total ionizing dose (TID), expressed in rad(Si), is a measure of the total of ionizing energy absorbed per unit mass of specimen. The data from the measurements indicate that the reduction in h_{FE} as a function of TID is different for the three different types of radiation. This is expected because equivalent TID does not imply equivalent nonionizing-energy dose, which is primarily responsible for the reduction in h_{FE} via a reduction in the lifetimes of minority charge carriers.

The bromine-ion data exhibit a linear variation in the change of $(1/h_{FE})$ with TID, suggesting that bulk displacement due to nonionizing dosage is the dominant mechanism of damage. Smaller changes in $(1/h_{FE})$ with TID are seen in the electron and γ-ray data. This was expected because a bombarding electron or a Compton electron produced by an incident γ-ray photon imparts much less energy to a lattice atom of Si than does a Br ion of equivalent kinetic energy.

This work was done by John A. Zoutendyk of Caltech, Charles A. Goben of Southern Illinois University, and Dale F. Berndt of Honeywell, Inc., for **NASA's Jet Propulsion Laboratory**. *To obtain a copy of the report, "Comparison of the Degradation Effects of Heavy Ion, Electron, and Cobalt-60 Irradiation on Advanced Bipolar Process," Circle 77 on the TSP Request Card.*
NPO-17570

Electronic Systems

Digital Signal Processor for GPS Receivers

Features include reliability and compactness.

NASA's Jet Propulsion Laboratory, Pasadena, California

Three innovative components have been combined to produce an all-digital signal processor with superior characteristics: outstanding accuracy, high-dynamics tracking, versatile integration times, lower loss-of-lock signal strengths, and infrequent cycle slips. The three components are a digital chip advancer, a digital carrier downconverter and code correlator, and a digital tracking processor. The all-digital signal processor is intended for use in receivers of the Global Positioning System (GPS) for geodesy, geodynamics, high-dynamics tracking, and ionospheric calibration.

The figure is a block diagram of the prototype GPS receiver. Using fixed-frequency local oscillators, the front end downconverts the GPS signals from radio frequency to baseband, where the signals are low-pass filtered and digitally sampled. Three digitally sampled signals are supplied: the P_1 and P_2 signals (e.g., each at 15.374 megasamples per second) and the C/A signal (e.g., at 1.5374 megasamples per second).

The sampling frequency should be essentially incommensurate with the fundamental chip rate (e.g., 15.374 MHz vs. 10.23 MHz) so that discrete sampling errors will be negligible. For stationary receivers on the Earth, the frequency offset of the local oscillators should be of the order of 10 kHz so that carrier downconversion in the baseband processor can work with high accuracy.

In an example of the operation of the system, the signals of all visible GPS satellites are simultaneously received by an omnidirectional antenna and are therefore all embedded in the baseband signal. In the digital baseband processor, a separate digital signal processor is provided to extract the signals from each satellite. A host microprocessor coordinates the digital signal processors and collects the output data. Even though this example shows each digital signal processor reducing the signal from only one satellite, more than one satellite could be processed by a digital signal processor by programming its microproc-

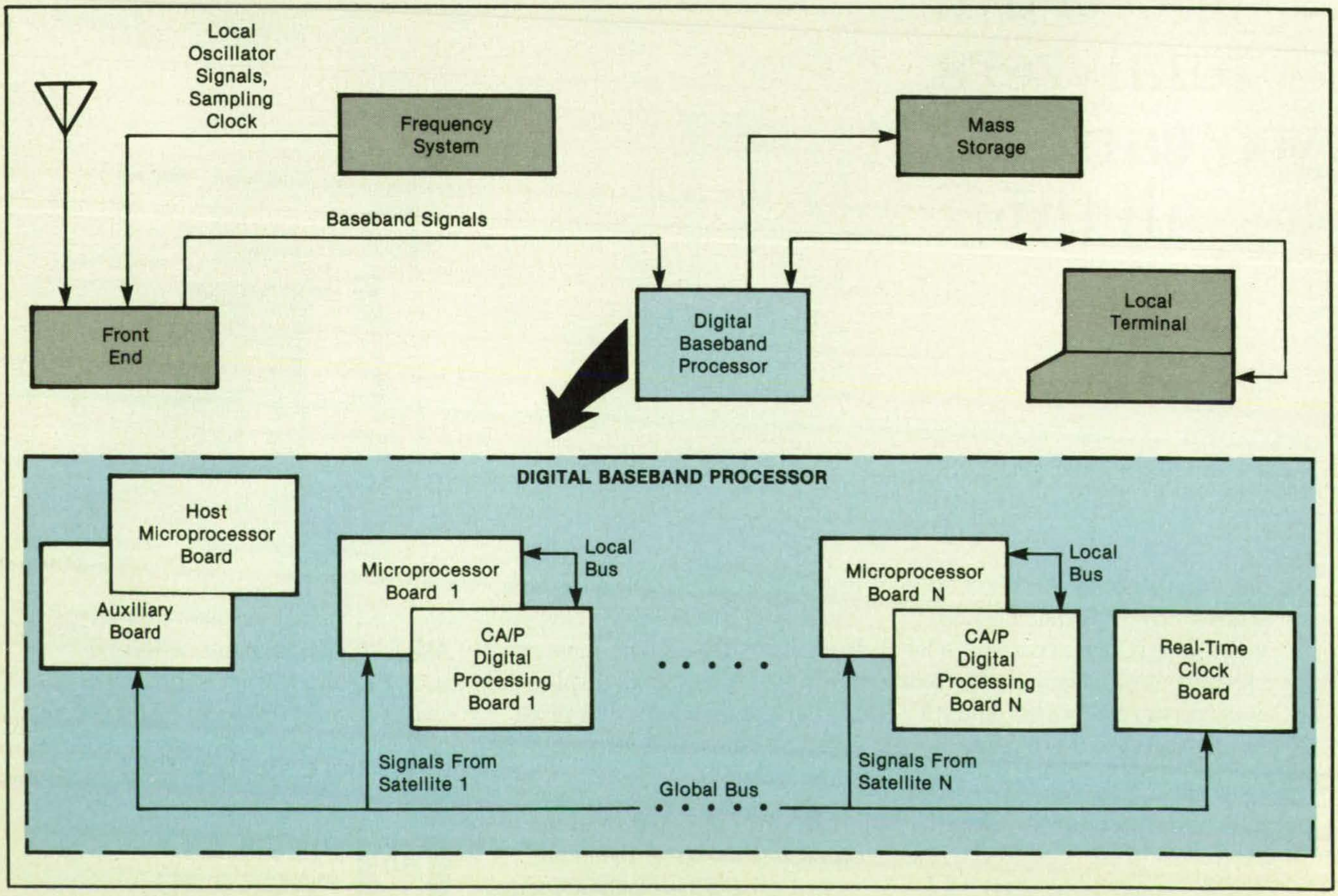

The **Prototype GPS Receiver** includes the digital signal processor, which operates on the baseband signal to extract the GPS data.

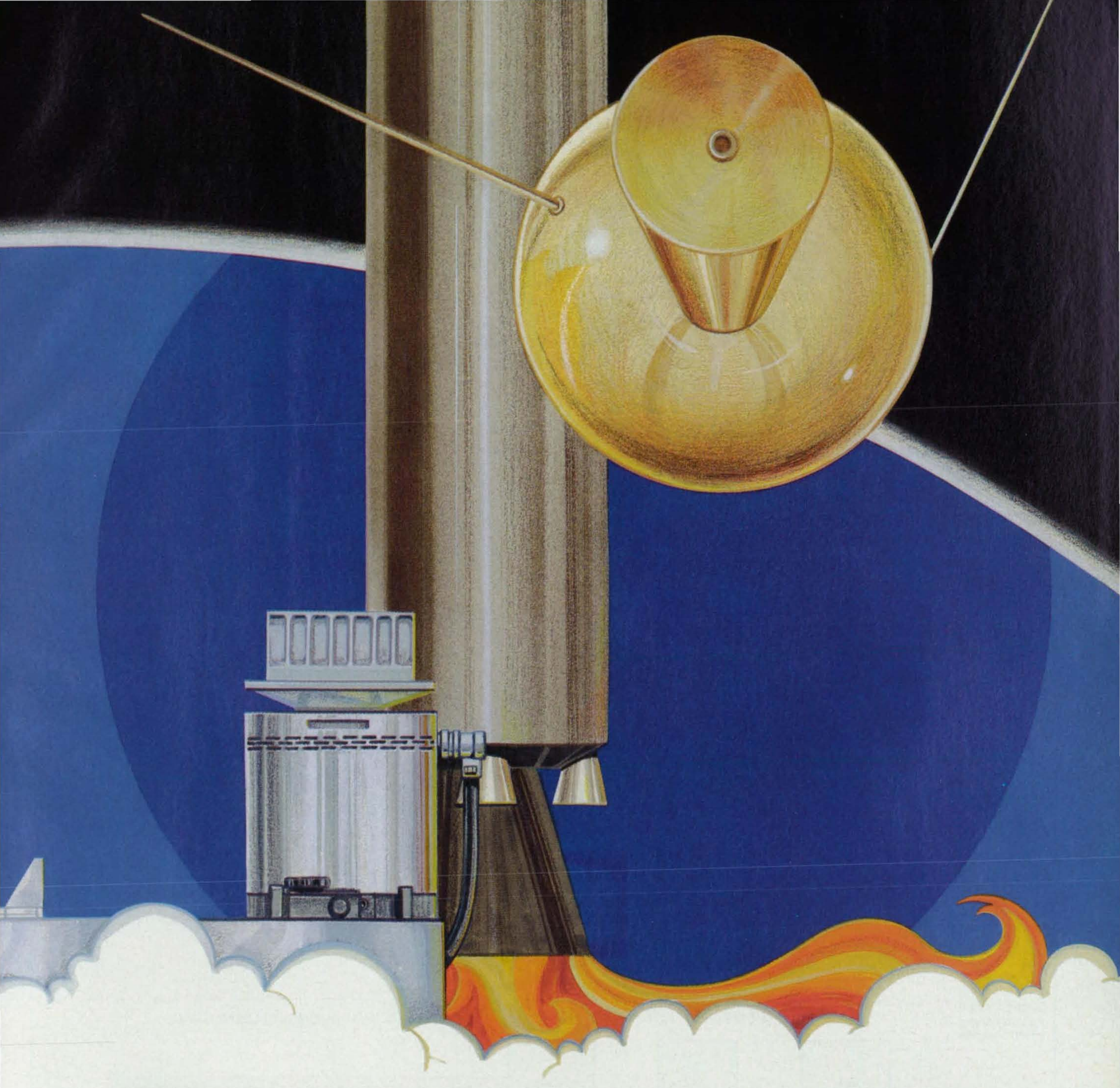

essor to time-multiplex its digital equipment between satellites.

In addition to the reliability and compactness that are usually characteristic of digital design, the design of the baseband processor offers the following advantages:

- The total delay and phase errors caused by the baseband processor are very small (less than 0.1 millichip and 1 millicycle, respectively).
- High-phase dynamics up to 1,000 Hz/s can be tracked with high accuracy.
- Signal strengths at which lock is lost are up to 4 to 6 dB lower than in other receivers.
- The rate of occurrence for cycle slips is extremely low for all channels.
- The design requires no special circuitry to count cycles or to maintain in-lock data-bit synchronization.
- Selectability of the fast-feedback interval (10 or 20 ms) provides valuable flexibility in making compromises between dynamics and the signal-to-noise ratio.
- Selectability of the output-point interval (1, 2, 3, ... 300 s) satisfies the requirements of a wide range of users. (If necessary, intervals between 20 and 1,000 ms could also be included in the design.) Subsequent data reduction is simplified for the user by forcing output timetags to fall on integer seconds that are synchronized with GPS time.
- Sample-rate and carrier-frequency offsets can be set within a wide range of values.
- The starting time and the integration interval can be set by the microprocessor, providing great flexibility in operation, including multiplexing between satellites.

This work was done by J. B. Thomas, T. K. Meehan, and J. M. Srinivasan of Caltech for **NASA's Jet Propulsion Laboratory**. *For further information, Circle 144 on the TSP Request Card.*

In accordance with Public Law 96-517, the contractor has elected to retain title to this invention. Inquiries concerning rights for its commercial use should be addressed to

Edward Ansell
Director of Patents and Licensing
Mail Stop 301-6
California Institute of Technology
1201 East California Boulevard
Pasadena, CA 91125

Refer to NPO-16997., volume and number of this NASA Tech Briefs *issue, and the page number.*

Adaptive Telemetry Multiplexer

Data-acquisition characteristics can be changed as conditions change.

Lyndon B. Johnson Space Center, Houston, Texas

A telemetry-data-acquisition unit can be adjusted remotely to produce changes in the sampling rate, sampling channels, measurement scale, and output-bias level. Its functional configuration can be adapted to changing conditions or new requirements by a distant operator over the telemetry link. The reconfiguration is done in real time, without removing the equipment from service.

The prototype unit (see figure) includes an intelligent bus-interface unit (BIU) and a low-rate adaptive multiplexer (LRAM). It accommodates up to 31 remote terminals, each with 56 analog sensors, 10 gain ranges, 32 bias levels, sensor-sampling rates ranging from less than 1 to 200 samples per second, and optional automatic gain rescaling. The telemetry unit acquires signals directly from the sensors and performs signal conditioning, multiplexed channel sampling, amplification, output-bias-level adjustment, and analog-to-digital conversion. It stores digitized raw data from each channel in a dual-port, random-access memory.

The remotely adjustable parameters are stored in an electronically programmable read-only memory (EPROM). The operator reprograms the EPROM chip

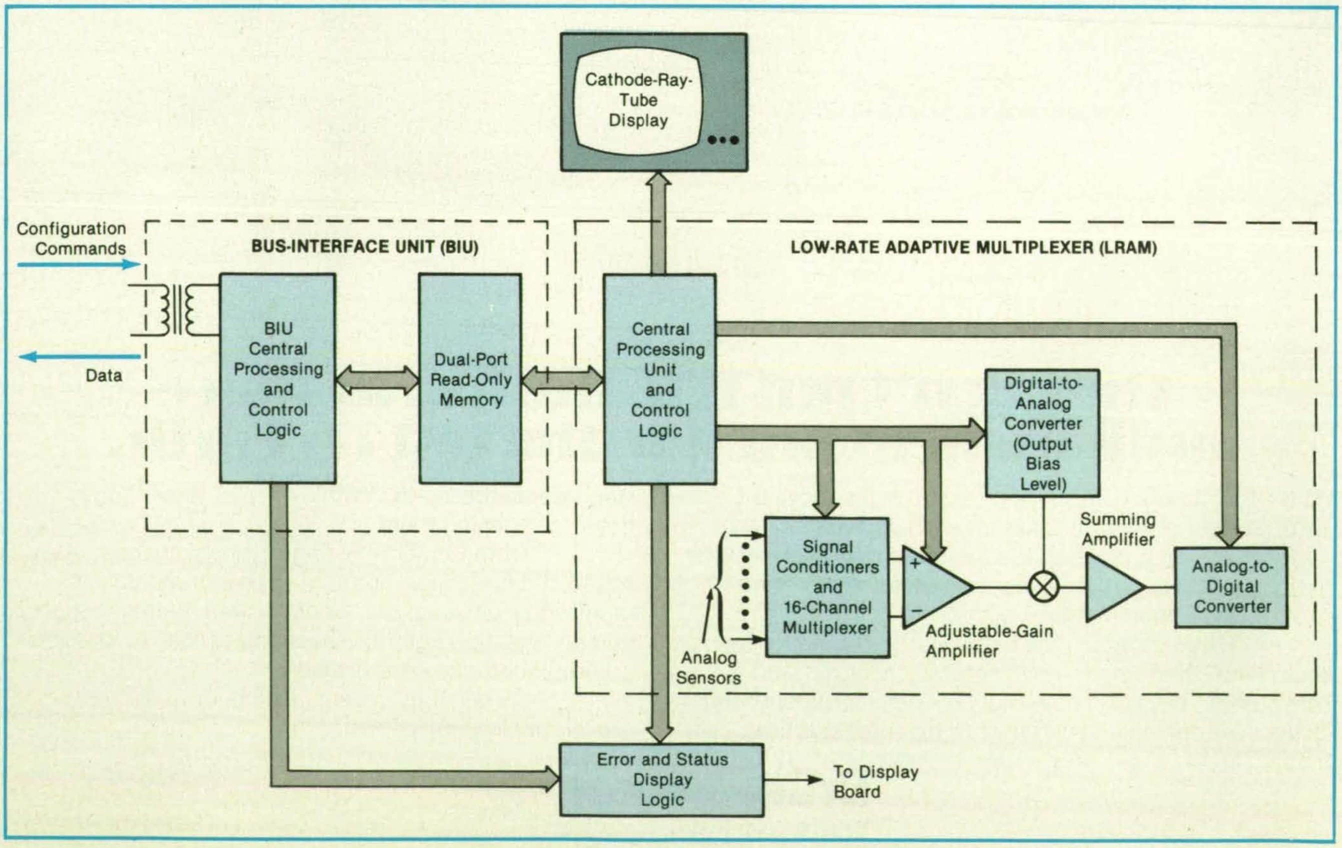

The **Bus-Interface Unit Accepts Reprogramming Commands** and translates them for the low-rate adaptive multiplexer. The reprogrammable equipment reduces the need for spare parts, since it is not necessary to stock a variety of hardware with fixed characteristics.

through the BIU for new channel selections, sampling rates, measurement scales, and output bias levels as they are needed.

The automatic-gain-rescaling feature changes the gain of a channel to the next higher (or lower) setting if the lower (or upper) data limits are exceeded on two consecutive samples. The data limits can be reprogrammed remotely.

The BIU recognizes the following nine commands from the remote operator:
1. Send data from all channels.
2. Send discrete word.
3. Send built-in-test-equipment word.
4. Send adaptive-status word.
5. Echo reprogrammed parameters.
6. Reprogram channel parameters as specified by the data words sent.
7. Start data acquisition.
8. Stop data acquisition.
9. Change to new sampling rate.

Commands 1 through 5 are transparent to the LRAM. Commands 6 through 9 must be translated by the BIU processor into commands recognized by the software of the LRAM.

In tests, the adaptive multiplexer performed well: amplitude errors were less than 0.5 percent, distortion was less than 0.25 percent, and crosstalk and common-mode rejection were indiscernible.

This work was done by R. L. Sinderson and G. A. Salazar of **Johnson Space Center**, *and C. M. Haddick, Jr., C. J. Spahn, and C. N. Venkatesh of Lockheed Corp. For further information, Circle 92 on the TSP Request Card.*

This invention is owned by NASA, and a patent application has been filed. Inquiries concerning nonexclusive or exclusive license for its commercial development should be addressed to the Patent Counsel, Johnson Space Center [see page 18]. Refer to MSC-21170.

Vector Adaptive/Predictive Encoding of Speech

Vector quantization enhances the quality of digitally transmitted speech.

NASA's Jet Propulsion Laboratory, Pasadena, California

The vector adaptive/predictive technique for the digital encoding of speech signals yields decoded speech of very good quality after transmission at a coding rate of 9.6 kb/s and of reasonably good quality at 4.8 kb/s. The vector adaptive/predictive technique requires 3 to 4 million multiplications and additions per second. It combines the advantages of adaptive/predictive coding, which performs very well but only at rates above 16 kb/s, and code-excited linear prediction, which yields speech of high quality but requires 600 million multiplications and additions per second at an encoding rate of 4.8 kb/s.

The basic idea of this technique is (1) to approximate each vector of speech samples for transmission by using each of the *N* code vectors stored in a vector quantization (VQ) "codebook" (actually an electronic memory that contains the code) and (2) to use the transmitted code vectors to excite a time-varying synthesis filter in the receiving decoder. In the encoder (see figure), the sampled speech waveform is first buffered and partitioned into frames, each of which contains several vectors of speech samples. Pitch-predictive analysis and linear-predictive-coding (LPC) analysis are then performed for each frame. The pitch period, the gain *G*, the pitch predictor, and the LPC predictor are determined in the analyses, and they are quantized and reset every frame. A perceptual-weighting filter based on the short-term spectral envelope of speech is used to help determine the code vector that minimizes the perceptual distortion between the coded speech and the original speech. The perceptual-weighting filter is also reset every frame, but it is not quantized because the decoder does not need it.

At the beginning of each frame, *N* zero-state response vectors are computed and stored in a zero-state-response codebook. These *N* zero-state response vectors are obtained by setting the memory of the en-

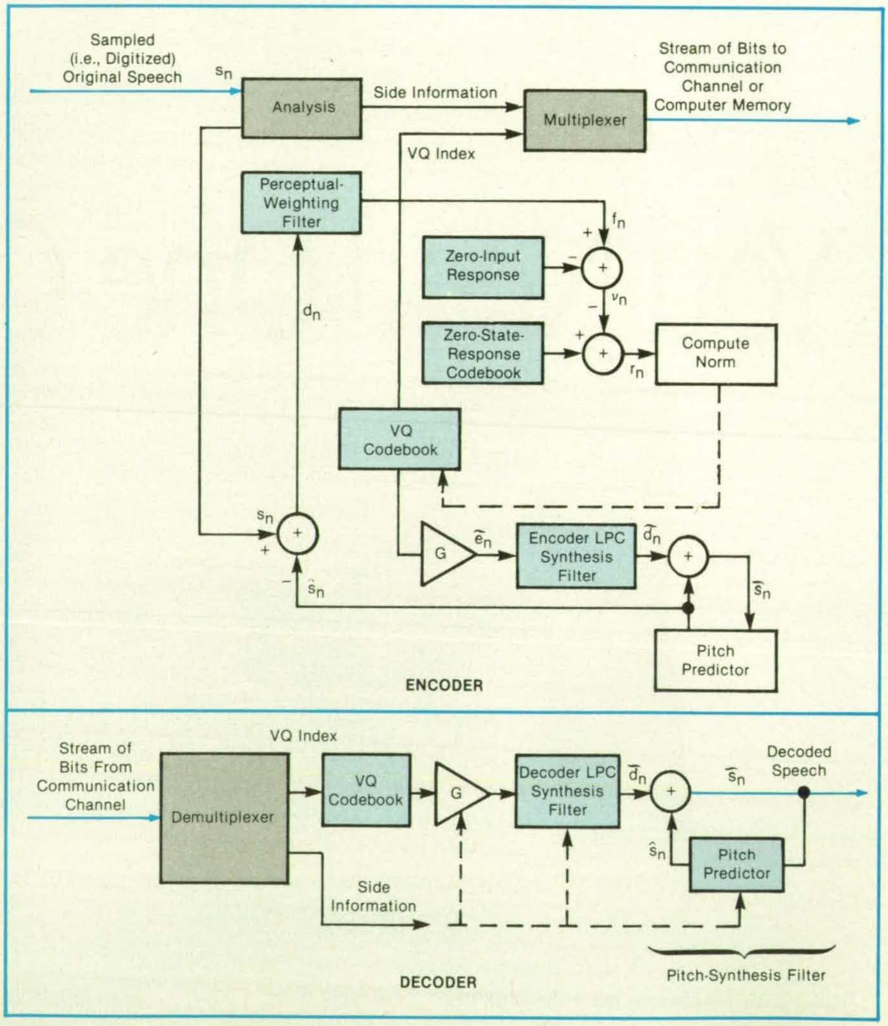

The **Vector Adaptive/Predictive Coding Technique** bridges the gaps in performance and complexity between adaptive/predictive coding and code-excited linear prediction.

coder LPC synthesis filter and the perceptual-weighting filter to zero and then exciting these cascaded filters by using one code vector at a time. In encoding each speech vector s_n within the frame, the zero-input response vector of the cascaded filter (the ringing from previous vectors) is first computed. Then, the pitch-predicted vector $\hat{s}_n$ is substracted from s_n, and the difference vector d_n is passed through the perceptual-weighting filter. The zero-input response vector is then subtracted from the filtered difference vector f_n, and the resulting vector v_n is compared with the *N* stored zero-state response vectors.

The index of the zero-state response

Genius should not go unrewarded.

CALL FOR PAPERS

THE 1989 IBM SUPERCOMPUTING COMPETITION

IBM invites you to submit your accomplishments. We seek to honor those individuals whose imagination has elevated the state of the art in analysis and modeling. Included are those who have contributed to creating new leading-edge uses of large-scale computers, innovative applications or algorithms and advances in numerically intensive computing.

The best papers on innovative uses of the IBM 3090 will be chosen in the following four divisions: physical sciences and mathematics; engineering; life and health sciences; social sciences, humanities and the fine arts. Each division will receive a first, second and third prize of $25,000, $15,000 and $10,000, respectively. In addition, a "PROCEEDINGS" of selected papers will be published.

Universities that provide substantial support to first prize papers will receive a $10,000 award as well.

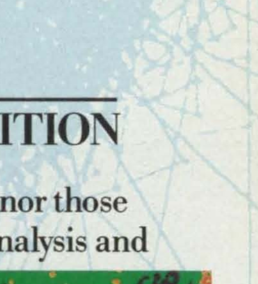

Contestants must register an abstract of their paper, according to specifications, by October 2, 1989. Those who have properly registered their abstracts will then be invited to forward their papers by January 15, 1990.

To select the winners, IBM will retain a panel of independent authorities in each division. Winners will be announced by March 1, 1990.

Simply put, IBM would like to acknowledge those individuals who share the same interest we do...the unrelenting pursuit of knowledge.

For more information contact your IBM marketing representative, or call (914) 686-6318; in Canada, (416) 758-4136.

To obtain the general information package and an entry form write to:

Competition Administrator
IBM Corporation, Dept. 72/BNG
44 South Broadway
White Plains, NY 10601

Name ____________________

Affiliation ____________________

Address ____________________

City ________ State ________ Zip ________ NTB

IBM®

vector that is closest to v_n identifies the best code vector in the VQ codebook. The best code vector is used to excite the LPC synthesis filter to generate $\tilde{d}_n$, which is used by the pitch predictor for following speech vectors. The index of the best code vector is combined with the side information (which specifies the pitch, the gain, and the two predictors) in the multiplexer. The resulting stream of bits is transmitted over a communication channel or stored in computer memory.

In the decoder, the stream of bits is first demultiplexed to separate the VQ index and side information. The VQ index is used to extract the corresponding code vector from the duplicated VQ codebook in the decoder, and the code vector is used to excite the decoder LPC synthesis filter and the pitch-synthesis filter. The output of the pitch-synthesis filter is the coded speech, which is perceptually close to the original speech.

This work was done by Juin-Hwey Chen and Allen Gersho of the University of California, Santa Barbara, for **NASA's Jet Propulsion Laboratory**. *For further information, Circle 65 on the TSP Request Card. NPO-17230*

Synchronizing Photography for High-Speed-Engine Research

Light flashes when a shaft reaches a predetermined angle.

Lewis Research Center, Cleveland, Ohio

A synchronization system facilitates the visualization of flow in high-speed internal-combustion engines. Designed for cinematography and holographic interferometry, the system synchronizes a camera and a light source with a predetermined rotational angle of an engine shaft. A 10-bit resolution of an absolute optical shaft encoder has been adapted, and 2^{10} combinations of

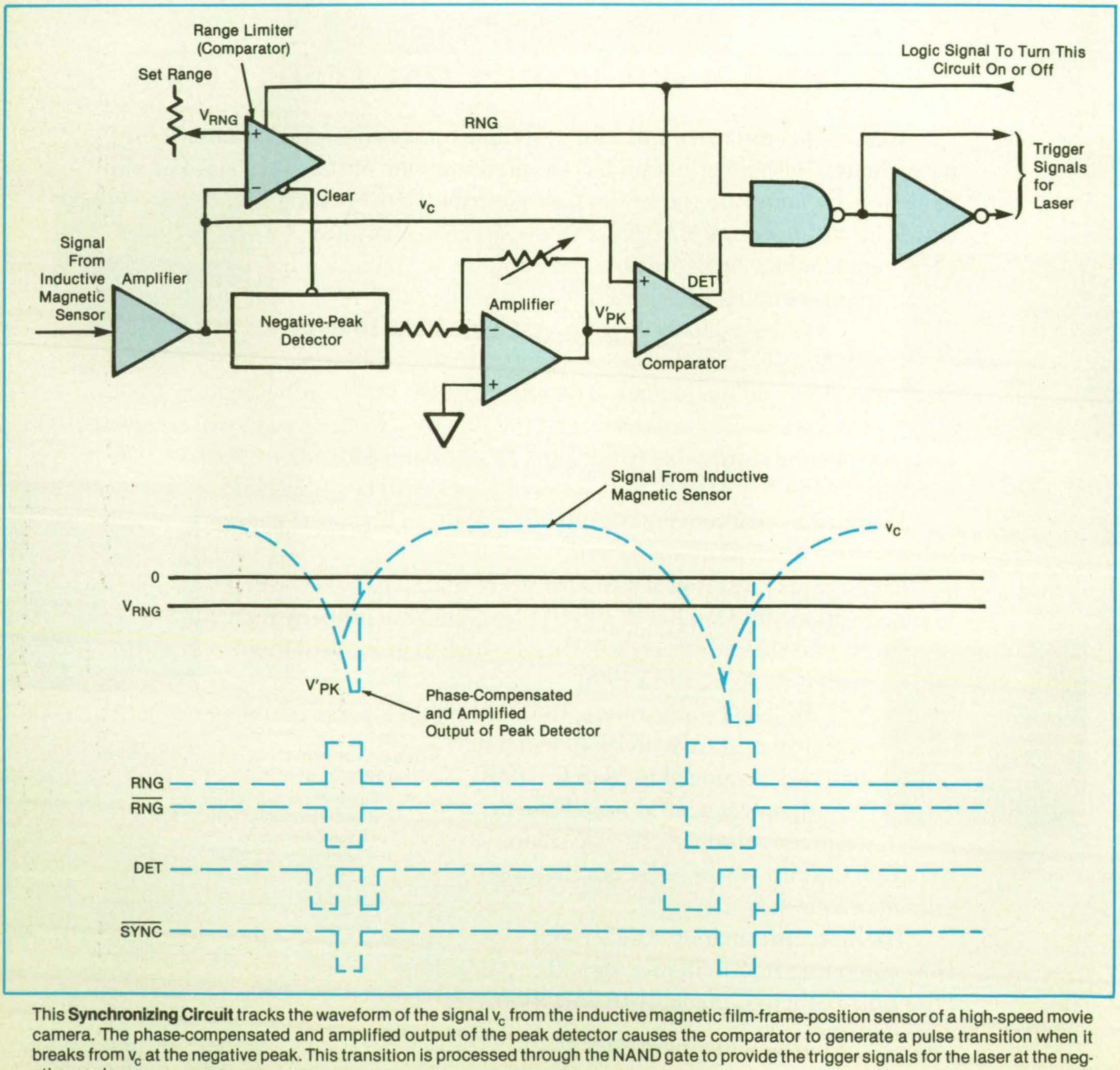

This **Synchronizing Circuit** tracks the waveform of the signal v_c from the inductive magnetic film-frame-position sensor of a high-speed movie camera. The phase-compensated and amplified output of the peak detector causes the comparator to generate a pulse transition when it breaks from v_c at the negative peak. This transition is processed through the NAND gate to provide the trigger signals for the laser at the negative peak.

Get a close look at the big picture.

With the new HI JetPro™ printer/plotter.

Select your drawing. Preview it on your monitor. Zoom in on the tightest detail. Clip it, scale it, mark a "window." Then press a key to get a high-quality hardcopy of the segment you want.

You can do all of this—*plus* high-speed draft and letter-quality printing—with one machine: the HI JetPro printer/plotter.

The flexible hardcopy control system

Whether it's an E-size drawing or a scanned data file, HI JetPro delivers the flexibility you need and the image you want. With HI's JetPro, you have a complete hardcopy control system that includes hardware and software for high-speed, high-resolution printing and plotting—in both vector and raster environments.

Convenient, quiet, and precise

HI JetPro produces your images on ordinary paper, in sizes up to 16.5 × 23.3 inches (DIN A2), with the incredibly sharp clarity of 360 dpi. And because it's a bubble-jet, it prints and plots quickly and quietly.

Simple to use and easy to maintain, the HI JetPro printer/plotter is fully backed by Houston Instrument's reputation for price-performance, quality, and support.

To get a closer look, call *1-800-444-3425* or 512-835-0900.

HOUSTON INSTRUMENT™
A DIVISION OF AMETEK

8500 Cameron Road, Austin, TX 78753

Houston Instrument and HI JetPro are trademarks of AMETEK, Inc.

Circle Reader Action No. 550

10-bit binary data have been computed to the corresponding angle values. The precomputed angle values are programmed into EPROM's (erasable programmable read-only memories) to use as an angle lookup table. It can resolve this shaft angle to within 0.35° at rotational speeds up to 73,240 revolutions per minute.

To achieve the required fast response, the system compares in-parallel bits put out by an optical shaft-angle encoder with the precoded 10-bit address data that point to an angle in the angle lookup table. When it finds a match, it decides that the shaft is in the proper position and generates a trigger pulse to activate the light source and the camera. The method eliminates on-line angle computation and numerical comparison processes that have been obstacles to high-speed capability.

To obtain instant ("snapshot") photographs with a low-speed movie camera, it is necessary to synchronize the light source with a shaft angle at which an event of interest is expected. The synchronizing system sends a trigger pulse to a laser each time the shaft passes the preset position (which is adjustable between 0° and 720°). The laser illuminates the transparent experimental combustion chamber. The film in the camera is thus exposed at a precise angle of the engine cycle.

The synchronizing system can also be used with a high-speed movie camera that makes a continuous record of combustion processes and does not have to be synchronized with the engine cycle. In this case, a negative peak voltage in the output of an inductive magnetic sensor indicates the alignment of the film frame with the aperture of the camera and serves as the raw timing signal for the laser.

Because the magnitude of the peaks varies with the running speed of the camera, the use of a fixed trigger level to detect a negative peak would give correct synchronization at only one running speed. To compensate for this effect, the system uses a dynamic peak-tracking method. A negative-peak detector tracks the output of the magnetic sensor and retains the peak value (see figure). The output of the sensor and the output of the detector remain superimposed until the peak is reached. Both signals are applied to a comparator, that produces a pulse transition at the negative peak. The output of another comparator also contains pulse transitions when the output of the sensor passes through a preset peak-track range threshold. The output of the peak-sensing comparator is applied to a NAND gate with the range threshold-passing pulses to extract the peak pulse, which is used to generate a laser-trigger pulse.

This work was done by K. S. Chun of **Lewis Research Center**. *Further information may be found in NASA TM-89902 [N87-23902], "Synchronizing Trigger Control System for Flow Visualization."*

Copies may be purchased [prepayment required] from the National Technical Information Service, Springfield, Virginia 22161, Telephone No. (703) 487-4650. Rush orders may be placed for an extra fee by calling (800) 336-4700.
LEW-14713

Hyperswitch Network for Hypercube Computer

Data-driven dynamic switching enables high speed data transfer.

NASA's Jet Propulsion Laboratory, Pasadena, California

The performance of a parallel algorithm depends mostly on the interconnection topology of the multicomputer system. A proposed hyperswitch network is based on mixed static and dynamic topologies. Here, available or fault-free paths need not be specified by a source because the routing header can be modified in response to congestion or faults encountered as a path is established. Static topology, such as the hypercube network, can meet this requirement if the nodes have switching elements that perform the necessary routing header revisions dynamically.

A multicomputer interconnection network may be judged by many different criteria, but network-link reliability and availability should be given the most emphasis. The proposed hypercube topology that is now being implemented with a switching

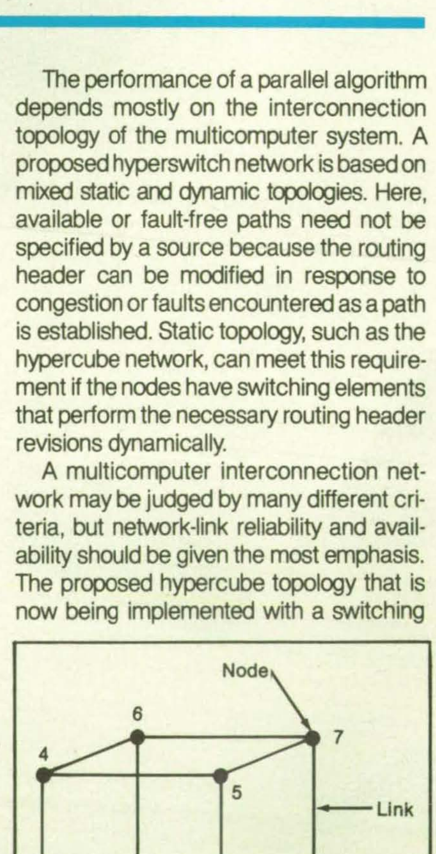

Figure 1. **Hypercube With Eight Computer Nodes** is shown in 3-dimensional hyperspace.

element in each computer node, as shown in Figure 1, is aimed at designing a very-richly-interconnected multicomputer system. This interconnection network connects a great number of small computer nodes, using the fixed hypercube topology, which is characterized by point-to-point links between the nodes.

As can be seen in Figure 1, any two computer nodes that are not connected directly by a link need to have their messages relayed by the intervening nodes. In contrast with the fixed hypercube topology, the proposed network has no fixed dedicated links between the nodes but rather establishes these links through explicit switching elements and message-routing control logic located in each node, using the adaptive-routing algorithm. Therefore, the multicomputer system can route messages dynamically by this routing control logic, setting each switching element so that the links are shareable among a number of node pairs.

The adaptive-routing algorithm, which has been developed and implemented in hardware for the hyperswitch network, utilizes network pruning to avoid known busy or bad links and thus to establish the shortest path setup-time. Then the untried network territories are systematically explored to select one of the many possible paths.

Once a complete path has been traced and reserved, the path sections are latched to form a complete path for message transmission from the originating node to the destination node. The complete path may span many nodes, and, since it is latched by the routing control logic before any data are sent, transmitted data need not enter any intervening node for interaction with that computer or memory during the data transmission. Once the link is established data may be pipelined at rates up to the hardware limits of the communication path.

This type of network has the advantages of both static and dynamic networks. The static network characteristics enable the hyperswitch network to maintain locality, increase the number of I/O links, and provide multiple paths between two communicating nodes. The dynamic network characteristics provide high permutability, short message latency, and the capability to explore other computational/problem-mapping models.

Detailed simulation results have shown that the hyperswitch network is consistently more efficient than fixed-path routing for large-message-traffic conditions. The simulation results, shown in Figure 2, also show that the hyperswitch network extends the application of parallel systems to problems that place heavy demand on the communication network for high bandwidth, low latency, and non-local communication.

This work was done by Edward Chow,

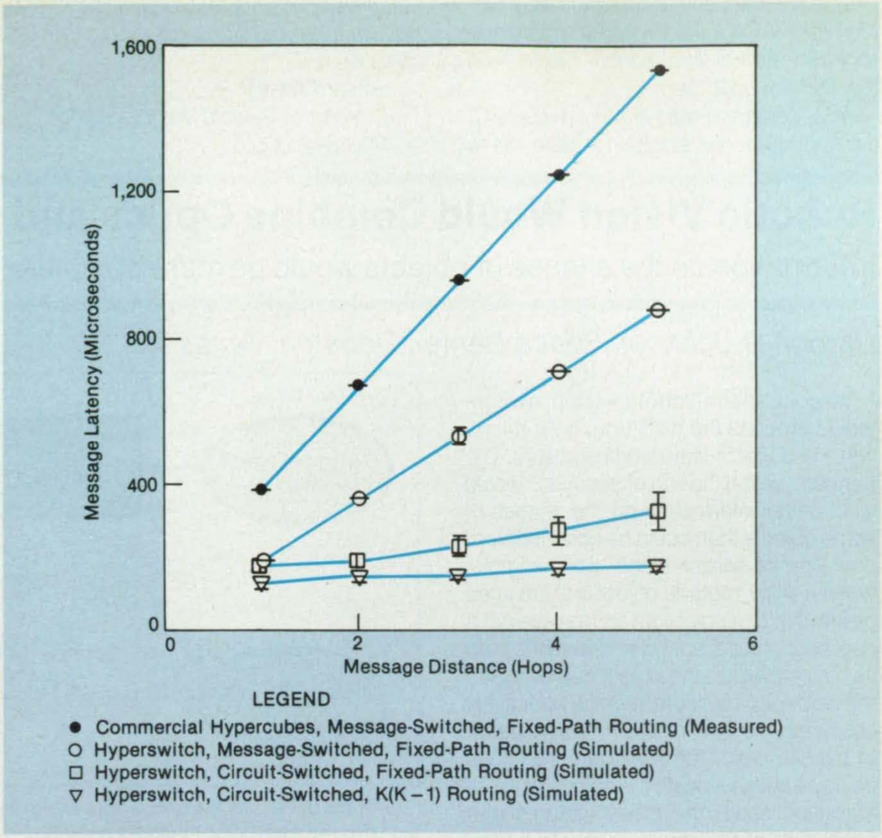

Figure 2. A **Comparison of Network Performance** shows the K(K – 1) routing scheme versus fixed-path routing schemes.

Herbert Madan, and John Peterson of Caltech for **NASA's Jet Propulsion Laboratory**. For further information, Circle 7 on the TSP Request Card.

In accordance with Public Law 96-517, the contractor has elected to retain title to this invention. Inquiries concerning rights for its commercial use should be addressed to

Edward Ansell
Director of Patents and Licensing
Mail Stop 305-6
California Institute of Technology
1201 East California Boulevard
Pasadena, CA 91125

Refer to NPO-16905, volume and number of this NASA Tech Briefs issue, and the page number.

Robotic Vision Would Combine Optics and Microwaves

Information on the shapes of objects would be more complete.

Lyndon B. Johnson Space Center, Houston, Texas

A conceptual robotic-vision system would process the data from both microwave and visible-wavelength sensors. The concept, called "fusion of sensors," would yield better information on the shapes of some objects than could be obtained from one type of sensor alone. For example, when a shiny, metallic object is illuminated by the Sun or a point light source against a dark background, specular reflections from points or lines on the object can overload the visible-light sensors, thereby effectively obscuring the view of less-reflective parts. In such a case, the specular reflections could be used to locate the object, while information about the gross features and orientation of the object might still be obtained by analyzing the scattering of microwaves from its surface.

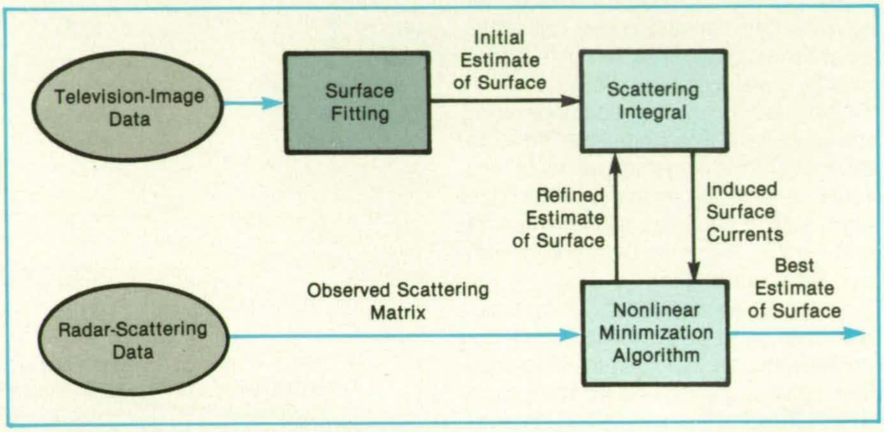

The **Robotic-Vision System** would integrate the information from television and radar images to reconstruct a three-dimensional image of the object.

The proposed robotic-vision system would fuse data from television images with polarized low-resolution radar-scattering cross sections. Using an iterative procedure, the system would generate successive approximations to the shape of the target by minimizing the differences be-

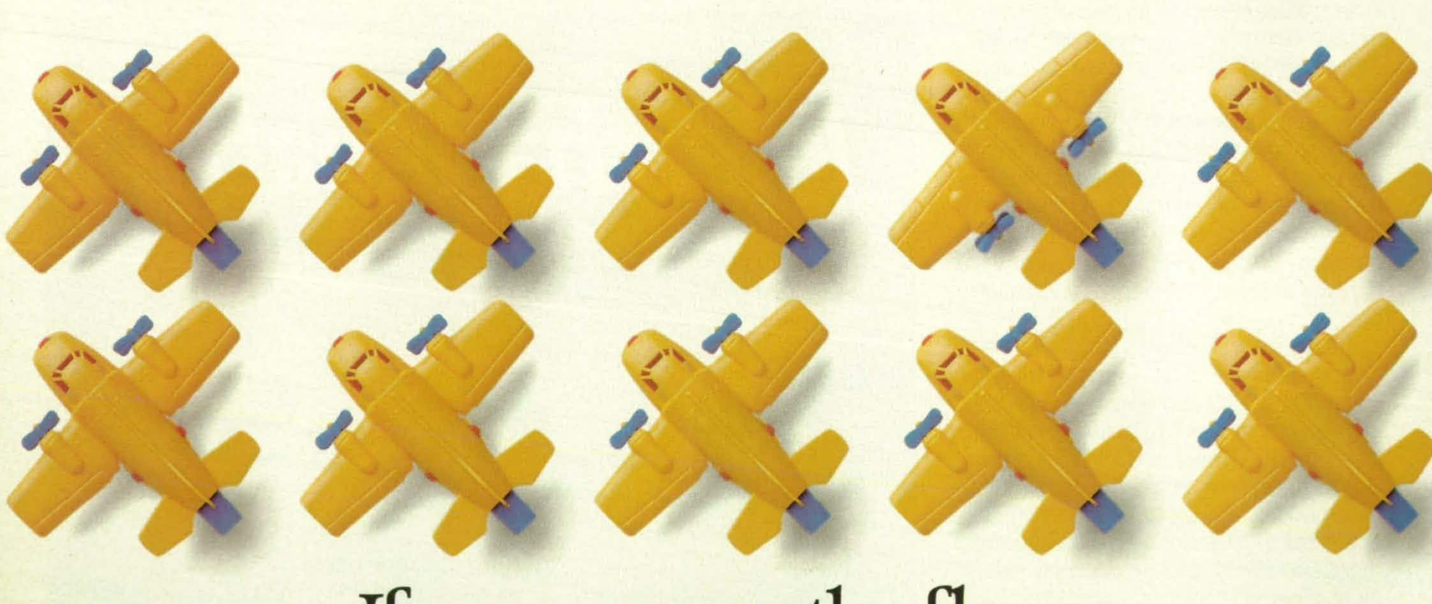

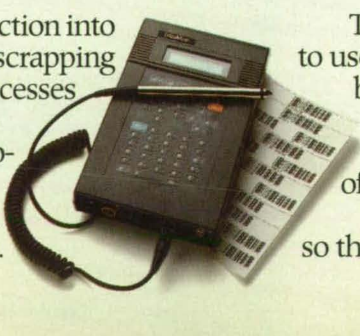

tween the observed radar returns and the radar returns that would be observed if the object were characterized by a computed scattering transfer matrix.

Assuming that the object is a perfect electrical conductor, the scattering of microwaves can be calculated by numerical integration of terms involving phased vector surface-current densities as functions of a set of parameters that describe the surface. In one version of the iterative procedure (see figure), the surface currents would be found from an initial estimate of the surface from visual data, then used to make an initial estimate of the radar scattering. The computed and actual scattering data would then be compared, and the differences would be used to refine the parameters of the surface from the initial estimate. The process would be repeated until the visible and microwave-derived estimates of the surface converged.

In a proposed test of the system, radar cross sections would be obtained from various surfaces at various frequencies and attitudes. Each surface should be smooth, contain at most one specular point, and be easy to model on a computer. The surface should be covered with a conductive material of thickness much greater than its skin depth at the microwave frequency of interest. Target shapes that lend themselves most readily to this type of investigation include spheres, ellipsoids, paraboloids, and hyperboloids.

This work was done by Kuma Krishen of **Johnson Space Center** *and Scott Shaw and Rui J. P. deFigueiredo of Rice University. For further information, Circle 122 on the TSP Request Card.*

This invention is owned by NASA, and a patent application has been filed. Inquiries concerning nonexclusive or exclusive license for its commercial development should be addressed to the Patent Counsel, Johnson Space Center [see page 18]. Refer to MSC-21334.

Digital 8-DPSK Modem for Trellis-Coded Communication

Signal-processing elements are realized largely in software.

NASA's Jet Propulsion Laboratory, Pasadena, California

A digital real-time modem processes octuple differential-phase-shift-keyed (8-DPSK) trellis-coded modulation. The modem is intended for use in communicating data at a rate up to 4.8 kb/s in a land-mobile satellite channel (Rician fading) of 5-kHz bandwidth at a carrier frequency of 1 to 2 GHz. Other communication systems that might benefit from this type of modem include land mobile (without satellites), paging, digitized voice, and frequency-modulation subcarrier data broadcasting.

The modem includes digital signal processors, each programmed to execute a different function. The flexibility afforded by basing the system largely on software enables both rapid realization of design and refinement via changes in algorithms. In keeping with this approach, the signal processors are constructed on general-purpose circuit boards, the central element of each of which is a commercially available digital signal-processing chip.

Each board has two 4K × 16-bit word spaces for program and data memory. In addition, the program memory is switchable between operation as a random-access memory for development and as an electrically programmable read-only memory for final placement of the algorithm. Ad-

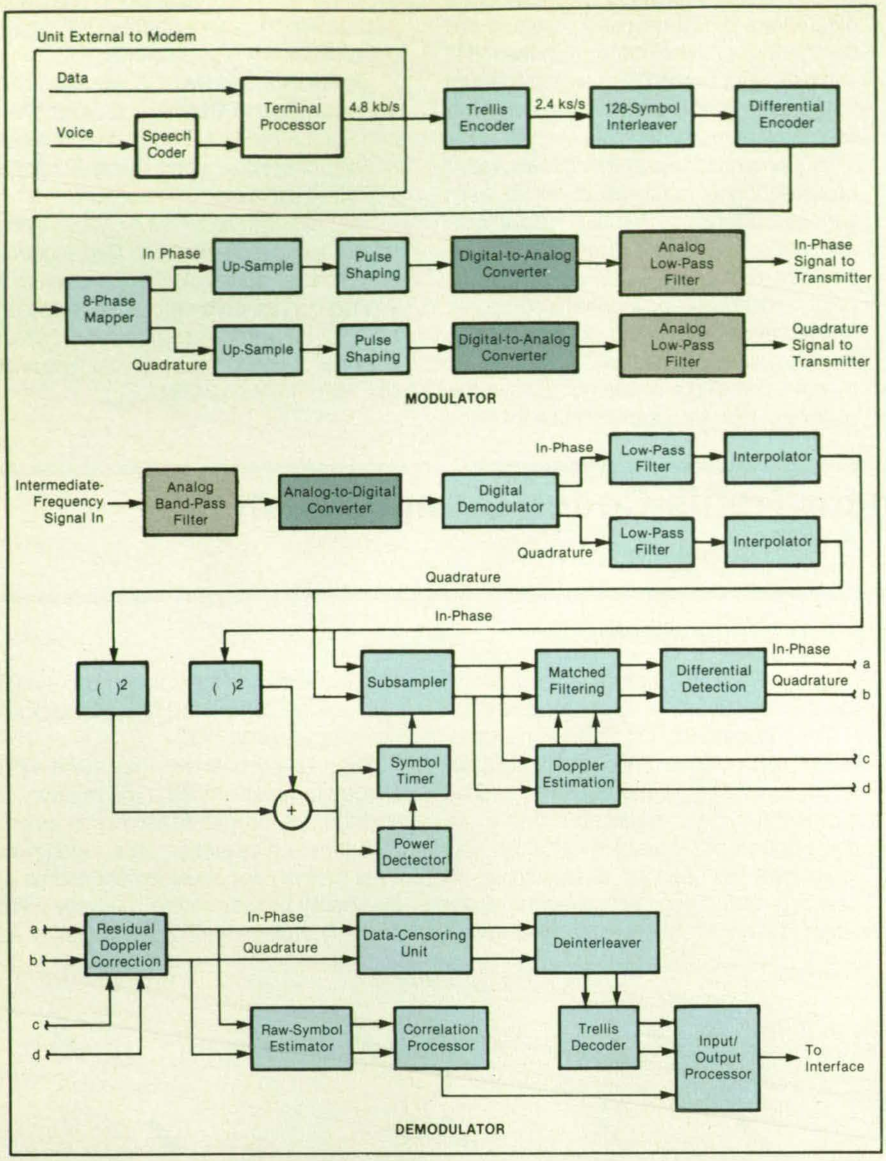

The **Modulator and Demodulator** contain digital signal processors that perform the modem functions. The design is flexible in that functions can be altered via software.

ditional circuitry supports five dedicated 16-bit parallel input/output ports (two input and three output). Three levels of hardware interruption are accessible.

The modulator and demodulator (see figure) are partitioned into two distinct systems under separate asynchronous control by an external controller. The multiprocessor design is greatly simplified by following a pipelined approach. Taken separately, the flow of signals for either the modulator or demodulator can essentially be viewed as feedforward for both control and data signals. This results in simple interfaces between boards and provides an effective architecture for mitigating the effects of the fading channel. Data are passed in parallel fashion sequentially from board to board on an interruption basis.

The modulator consists of a single circuit board, a clock unit (shared with the demodulator), and two digital-to-analog subsystems. The clock unit provides clock signals locked to frequencies of 4.8 and 28.8 kHz. The 4.8-kHz clock is used to transfer the raw data to be transmitted from the external terminal processor to the modulator, while the 28.8-kHz clock is used to transfer data from the modulator circuit board to the digital-to-analog subsystems. Each digital-to-analog subsystem consists of a 12-bit digital-to-analog converter and a 4-kHz low-pass filter.

The demodulator consists of an analog-to-digital subsystem, six circuit boards, and two clock units. The analog-to-digital subsystem consists of a 40-kHz-wide band-pass filter centered at 28.8 kHz, followed by a 12-bit analog-to-digital converter. The first clock unit (common with the modulator) provides a clock signal at 18.432 MHz, which is divided down by the analog-to-digital subsystem to the 115.2 kHz sampling frequency. The second clock unit, also run from the 18.432-MHz signal, is the 4.8-kHz jitter clock used to transfer data from the demodulator to the terminal processor. The phase of the jitter-clock signal can be advanced or retarded by the demodulator to the timing derived from the incoming data.

This power- and bandwidth-efficient modem incorporates many novel features. Among these features are the modulation scheme and the feedforward architecture that have been optimized to combat the effects of the fading channel. The 100-percent root raised cosine pulse shaping employed has the unique feature of two intersymbol interference-free points per symbol. These two points per symbol are utilized for a data-derived Doppler estimator and matched filtering and contribute to the robustness of the data-derived symbol timing, which has zero data-induced timing variance at these points. This modem has been successfully tested and evaluated in both laboratory and field experiments, including a recent full-scale satellite experiment. In all cases, the modem has perfomed within 1 dB of theory.

This work was done by T. C. Jedrey, N. E. Lay, and W. Rafferty of Caltech for **NASA's Jet Propulsion Laboratory**. *For further information, Circle 154 on the TSP Request Card.*

This invention is owned by NASA, and a patent application has been filed. Inquiries concerning nonexclusive or exclusive license for its commercial development should be addressed to the Patent Counsel, NASA's Resident Office-JPL [see page 18]. Refer to NPO-17578

Physical Sciences

Optical Measurement of Sound Pressure

A noninvasive technique does not disturb the field it measures.

NASA's Jet Propulsion Laboratory, Pasadena, California

An optical technique can be used to measure acoustic pressure without direct contact. The technique is especially valuable where it is necessary to measure in a remote, inaccessible, or hostile environment or to avoid perturbation of the measured region. In the original application, the technique was used to measure the acoustic pressure around a sphere acoustically levitated in a furnace. Because the measurements are almost instantaneous, the technique can be employed to generate feedback control signals for acoustic levitators, for example.

A laser beam is directed at the region of high acoustic pressure to be measured. The sound causes rapid alternations of density and, therefore, of the index of refraction, and the alternations in turn produce oscillatory deflections of the beam. The deflection is proportional to the acoustic pressure. The laser beam has a negligible influence on the acoustic field.

After passing through the region of interest, the beam is focused onto a knife edge, as in a schlieren system (see figure). The knife edge is adjusted to intercept all or part of the undeflected beam so that the portion that passes the edge and falls on a photodetector varies with the deflection. Thus, the greater the acoustic pressure and the deflection of the beam, the greater the intensity of the deflected beam and the amplitude of the output of the photodetector. A detailed map of the pressure field can be obtained by scanning the field in three orthogonal directions.

This work was done by Eugene H. Trinh, Mark Gaspar, and Emily W. Leung of Caltech for **NASA's Jet Propulsion Laboratory**. *For further information, Circle 135 on the TSP Request Card.* *NPO-17565*

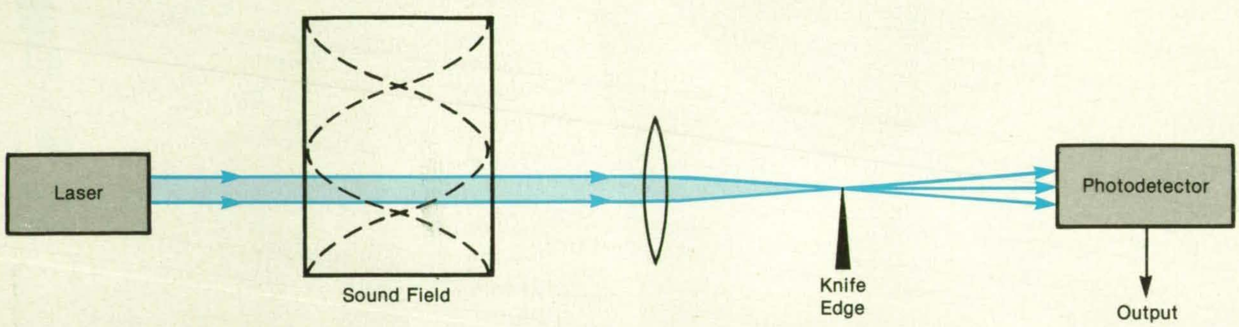

The **Sound Field Deflects** the laser beam proportionally to its amplitude. A knife edge intercepts the undeflected beam, allowing only the deflected beam to reach a photodetector. The apparatus is calibrated by comparing the output of the photodetector with that of a microphone.

ESR Measurement of Crystallinity in Semicrystalline Polymers

Photogenerated free radicals decay at different rates in crystalline and amorphous phases.

NASA's Jet Propulsion Laboratory, Pasadena, California

The degree of crystallinity in a polymer that has both crystalline and amorphous phases can be measured indirectly by a technique based in part on electron-spin-resonance (ESR) spectroscopy. The accuracy of crystallinity determined by the new technique equals or exceeds that of similar determinations by differential scanning calorimetry, wide-angle x-ray scattering, or measurement of density.

When a polymer matrix is illuminated with ultraviolet light, molecules in the matrix decompose partly into free radicals that act as spin probes. Immediately after illumination, the radicals are distributed uniformly throughout the crystalline and amorphous phases. At this time, the concentration of the radicals is measured by ESR.

Because of the relatively loose and random arrangement of polymer chains in the amorphous phase, the radicals there have higher mobility and, therefore, decay more rapidly after illumination than do the radicals in the crystalline phase, where the polymer chains are packed more tightly and, therefore, restrict the mobilities of the radicals more severely.

When molecules of a liquid that does not dissolve the polymer are introduced into the polymer, they penetrate the amorphous phase much faster than they penetrate the crystalline phase. The plasticizing effect of the liquid increases the mobility of the free radicals, and, because this effect reaches the amorphous phase first, the

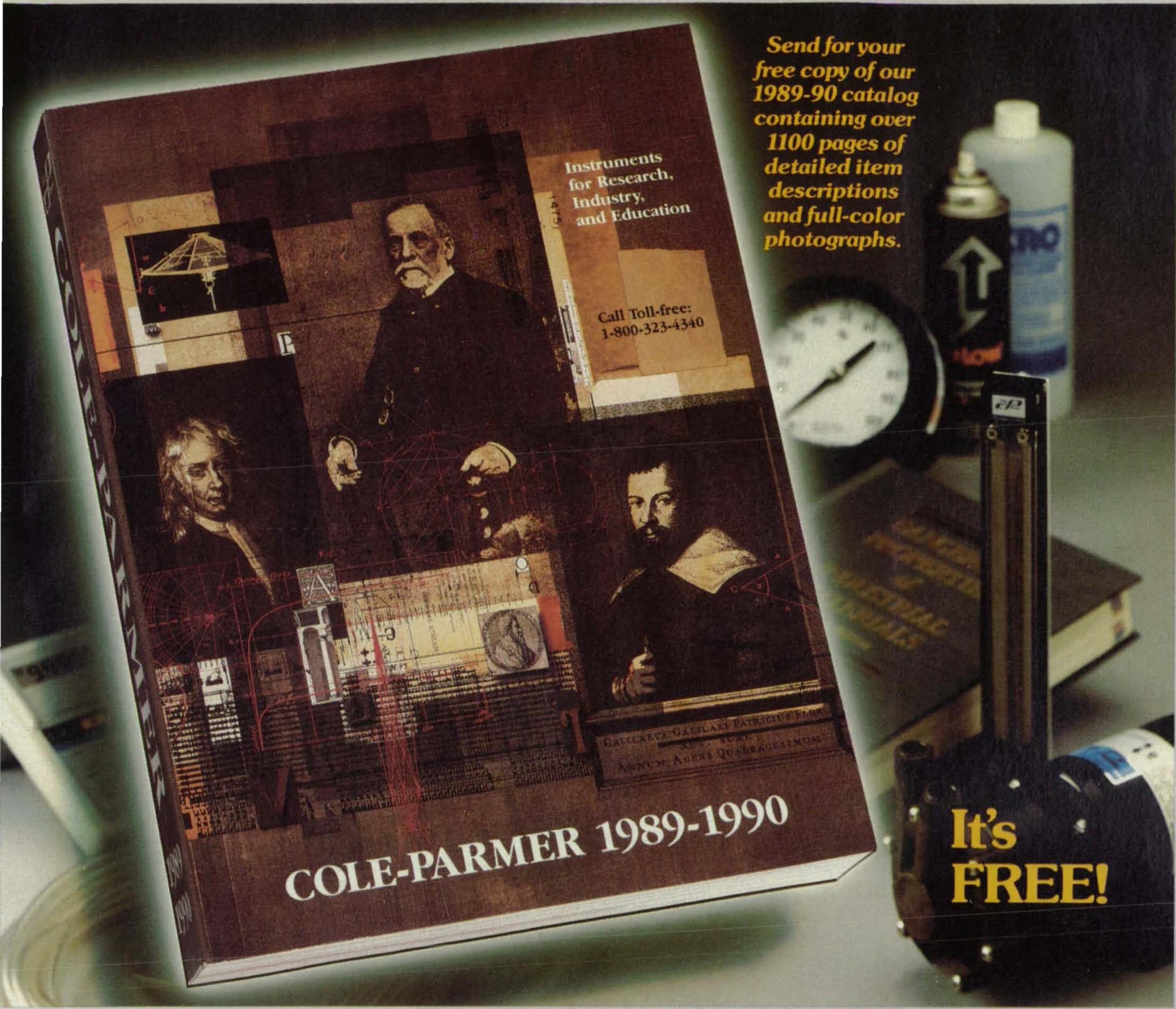

Cole-Parmer is...
industrial instruments *and more!*

Cole-Parmer offers a wide selection of instruments, transmitters, and supplies for use in today's industrial market— over 20,000 items.

And we go one step further with:

Skilled technical application support—Our network of technical and service specialists is available to assist you with your measurement and control applications.

Fast delivery—90% of all orders are shipped within 72 hours.

Responsive customer service—We're committed to your satisfaction.

Easy ordering—Our experienced sales staff stands ready to assist you with your product needs.

Our many product lines include:

• Books • Computer software • Conductivity • Data acquisition • Environmental testing equipment • Distributed process controllers • Temperature measurement and control • Flowmeters • Fluid handling equipment • Humidity measurement and control • Liquid level control • Mixers • Ovens and furnaces • pH measurement and control • Pressure monitors and controls • Pumps • Recorders • Tubing • Viscosity controls... and more.

Cole Parmer **Cole-Parmer Instrument Company** 7425 North Oak Park Avenue Chicago, Illinois 60648 1-800-323-4340

Circle Reader Action No. 638

free radicals there decay even more rapidly. (The decay occurs through the recombination of free radicals or the abstraction of hydrogen.)

After an appropriate interval that can range from minutes to days, most of the radicals in the amorphous phase have decayed, so that most of those that remain are in the crystalline phase. At this time, the concentration of radicals is again measured by ESR. Thus, the degree of crystallinity can be determined from the ratio of the remaining concentration to the original concentration of free radicals.

The technique was demonstrated with semicrystalline polymer, poly(vinylidene fluoride). The figure shows the ESR spectrum immediately after exposure to ultraviolet and a similar spectrum of about half the original intensity after 16 h of exposure to chlorobenzene. A third spectrum taken after 40 h of exposure to chlorobenzene shows no further decay. These spectra indicate a crystallinity of 50 percent, consistent with the crystallinity of 50 percent determined by differential scanning calorimetry.

This work was done by Soon Sam Kim and Fun-Dow Tsay of Caltech for **NASA's Jet Propulsion Laboratory**. *For further information, Circle 36 on the TSP Request Card.* *NPO-17369*

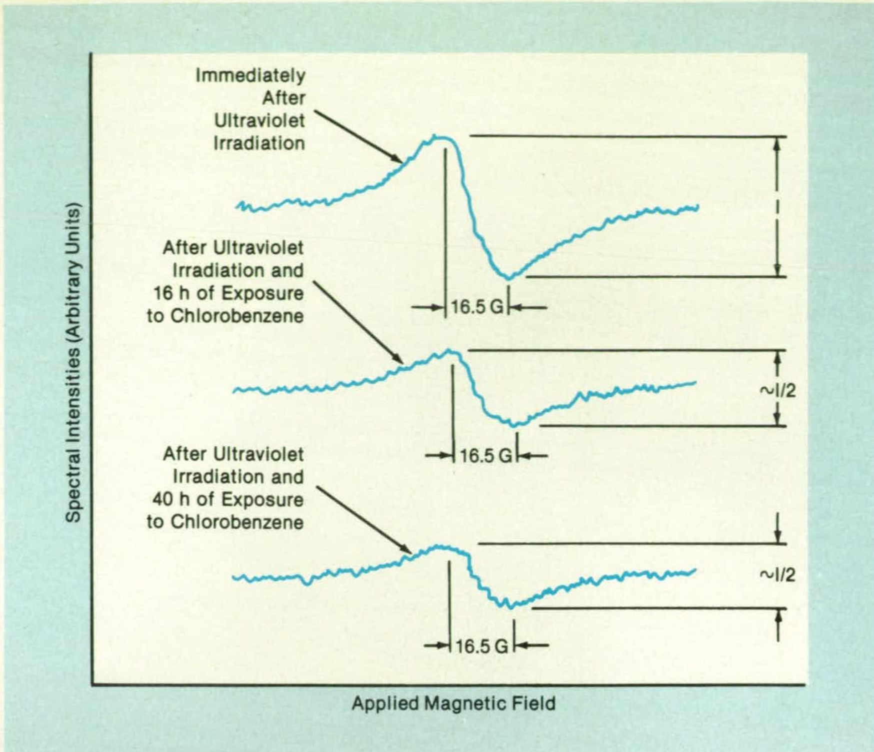

The **Intensity of the ESR Spectrum** after 16 and 40 h of exposure to chlorobenzene is about 50 percent of the intensity immediately after exposure to ultraviolet. This indicates about 50 percent crystallinity.

Speckle-Suppression Apparatus

Multiple delays reduce speckle in an unmodulated laser pulse.

Langley Research Center, Hampton, Virginia

A technique and apparatus have been developed to reduce speckle in unmodulated laser pulses, using a reduced number of optical fibers. The technique is expected to decrease the costs of bundles of optical fibers used to transmit unmodulated laser pulses.

Speckle can result from the interaction of spectrally narrow laser light with a reflecting or diffusing surface. This interaction causes a random-intensity distribution of light in the laser pulse that produces a granular, or speckled, pattern of light and dark spots when the pulse is reflected from a diffusing surface.

The new apparatus reduces speckle in an optically transmitted, unmodulated laser input pulse by introducing a number of independent delays into the pulse. The number of delays is equal to the shorter of the coherence length of the laser pulse source or the duration of the delayed laser output pulse. The reduction in the noise or variance generated by speckle is a function of the number of independent delays. The apparatus could include a number of optical fibers of different optical lengths, a single optical fiber in combination with one or more beam splitters, or a single circulator capable of generating a succession of delayed independent laser output pulses from a single laser input pulse.

The preferred configuration is illustrated in the figure. It includes a laser, which provides an initial unmodulated laser input pulse of known coherence length L_C. The pulse passes through a suitable diffuser or integrating sphere into a number of optical fibers of optical lengths L_O, $2L_O$, $3L_O$, and $4L_O$. The optical length L_O is chosen so that the optical fibers provide a series of four independent and delayed laser output pulses of equal duration. The delays between the pulses put out by the fibers may vary. All may equal or exceed the shorter of the coherence length L_C of the laser or the length L_P of the pulse.

The independent laser output pulses are transmitted through a conventional Fabry-Perot interferometer to a detector, where they are combined or added. Because the delays in the fibers scramble the phases of the output pulses, any noise or variance in the laser input pulse caused by speckle is reduced proportionally to the square root of the number of delays.

This work was done by Israel Taback of the Bionetics Corp. for **Langley Research Center**. *For further information, Circle 116 on the TSP Request Card.* *LAR-13771*

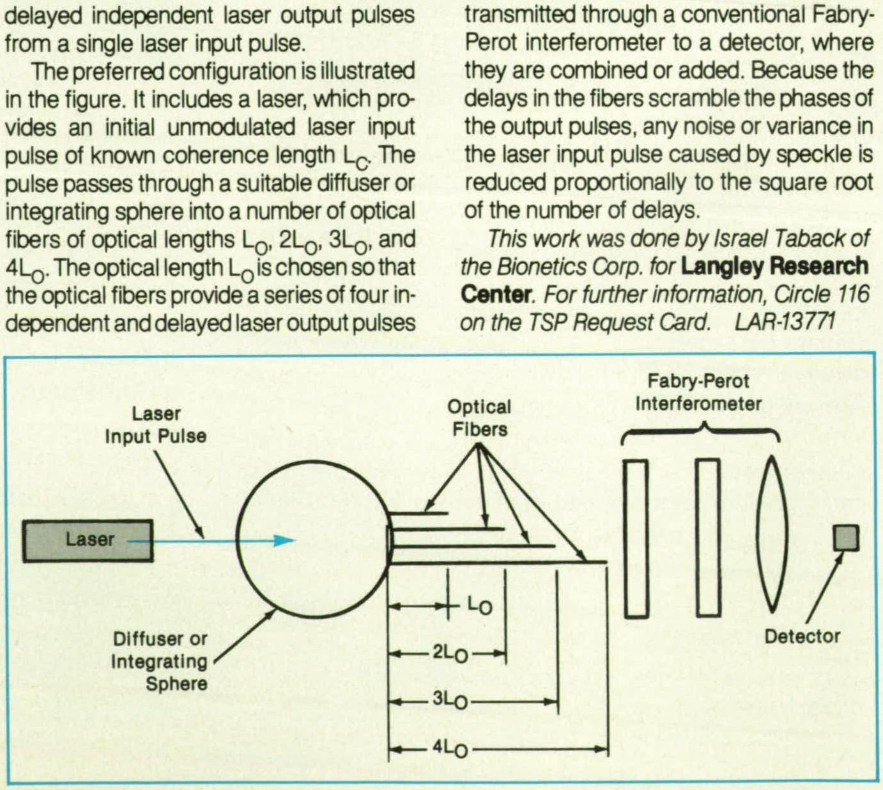

Optical Fibers of Different Length scramble the relative phases of the succession of laser output pulses.

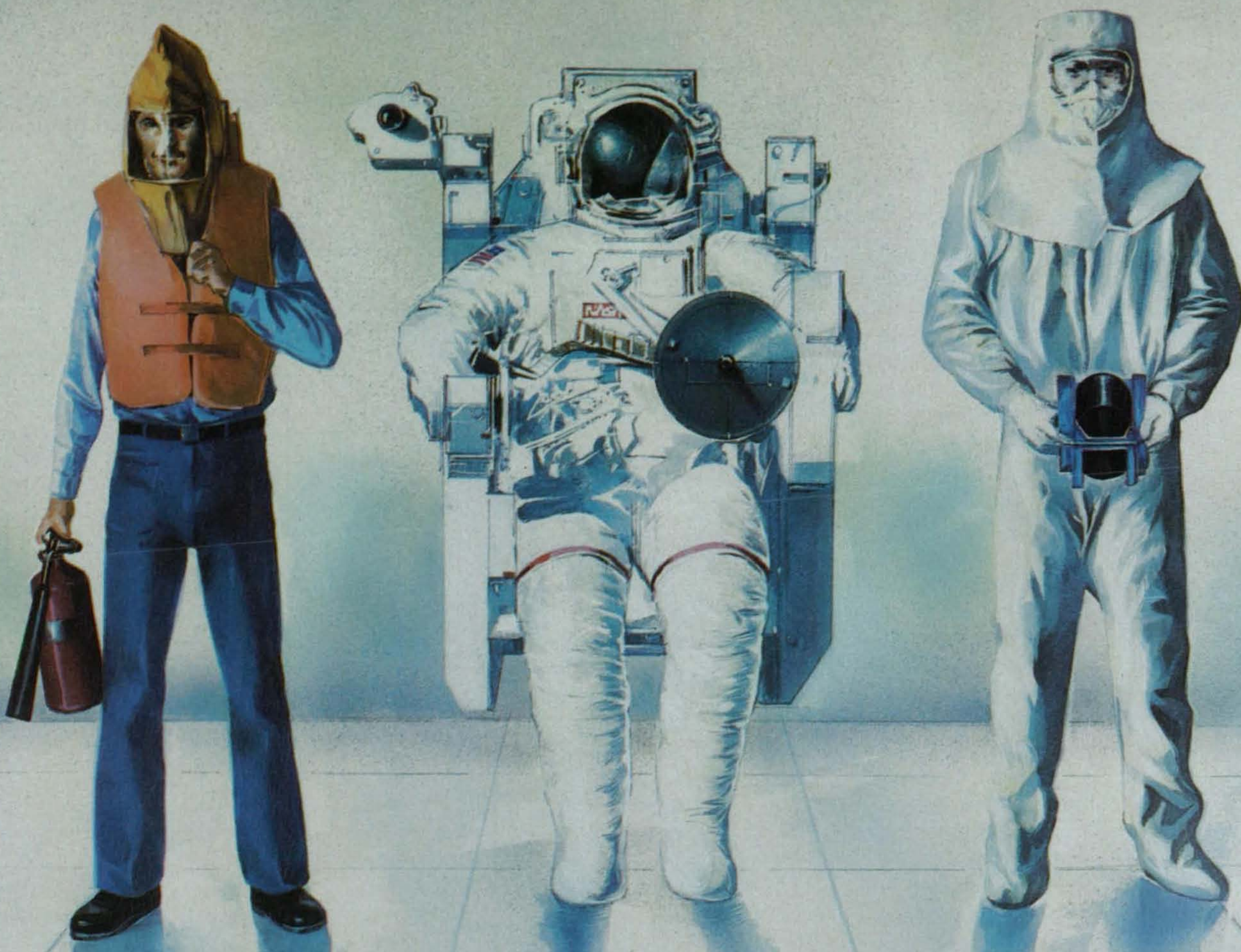

Probe Samples and Cools Hot Gas

The sampled gas enters an inner tube immersed in flowing coolant.

Lewis Research Center, Cleveland, Ohio

In many aeronautical applications, it has been found necessary to sample hot gas streams, the temperatures of which are well above the melting temperatures of nonreactive candidate probe materials. In addition, there is often a requirement to condition a gas sample to a particular temperature and pressure in a specified time.

A simple concentric-tube gas-sampling probe, illustrated in the figure, was developed for this type of application. The probe includes a straight outer tube and an inner tube, which is bent to be concentric to the outer tube at one end and tangent to the outer tube in the sampling region at the other end. The two tubes are brazed together along the sampling region and at the end to prevent the sampled gas and the cooling stream from mixing. The inner tube contains the sampled gas, and the space outside the inner tube but inside the outer tube is the path for the cooling stream.

In the sampling region, gas-sampling holes are drilled through the brazed walls to permit gas to flow into the inner tube. The braze fillet provides the seal between the two tubes. The cooling fluid drains through an orifice on the back side of the probe at the upper end. Thus, the coolant helps to cool the hot gas prior to expulsion up the stack. A flow-separating T is used to cap and separate the two fluid streams at the external (lower) end of the probe.

The probe is made of 304 stainless-steel tube 12.70 by 0.89 mm (0.5 by 0.035 in.) and 6.35 by 0.89 mm (0.25 by 0.035 in.) and is nickel-brazed. Noble metals are avoided to minimize catalytic reactions that could bias the results. For extended service life in severe environments, a thermal-barrier coat can be applied to the exterior of the probe.

Conditioning of gas samples is obtained by sizing the sampling holes to provide choked flow, varying the length of the cooling-fluid passage, and by varying the temperature and type of the cooling fluid. The choked sampling holes ensure a representative sample through each hole. The type and temperature of cooling fluid and the length of the probe are selected to adjust the temperature of the sample. It has been found that simple heat-transfer and pressure-drop calculations that take account of the type and temperature of the cooling fluid usually provide a usable probe design on the first design iteration.

This probe operated successfully for several years of intermittent use at temperatures of 400 to 1,920 K (260 to 3,000 °F) in a stream of hydrocarbon combustion gas

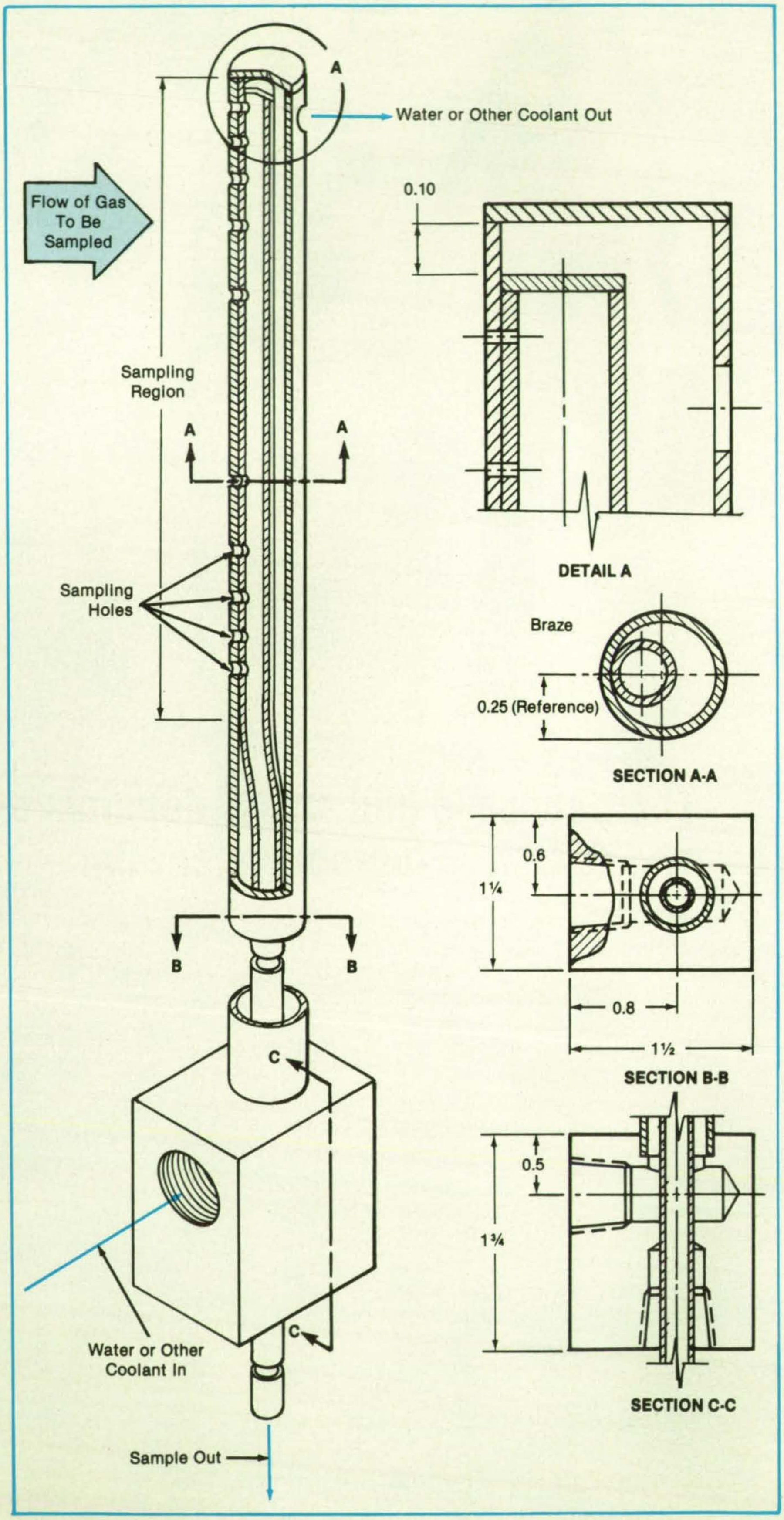

The **Sampling Probe** cools the sampled stream of hot gas before sending it on for analysis. Dimensions are in inches.

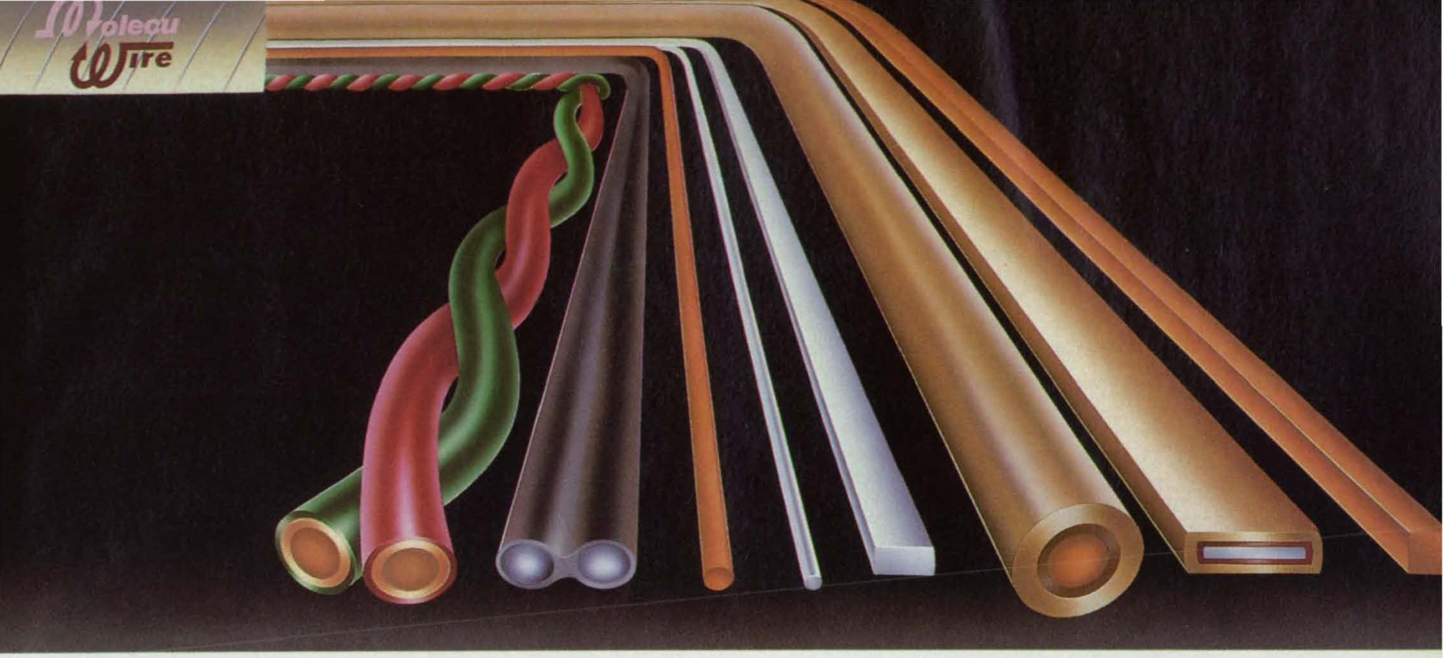

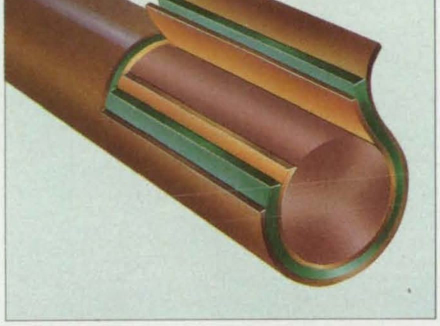

at pressures of 3 to 12 atm (0.3 to 1.2 MPa) with no leakage or significant deterioration, while being cooled with steam at a pressure of 8 atm (0.8 MPa) at the lower sampling pressures and temperatures and water at ambient temperature at the higher sampling temperatures and pressures. Other coolant fluids for consideration with this design are air or inert gases, depending on the temperature of the sampling stream, the desired temperature of the sample at the exit from the probe, and the combustion properties of the gas stream being sampled (for example, it may not be desirable to dump air into a hot gas stream rich in fuel).

This work was done by Donald F. Schultz of **Lewis Research Center**. *For further information, Circle 156 on the TSP Request Card.*
LEW-14856

Separating Isotopes With Laser and Electron Beams

The need for a second laser is eliminated.

NASA's Jet Propulsion Laboratory, Pasadena, California

In a scheme for the separation of isotopes, electrons of suitable kinetic energy ionize a specific isotope that has been excited by a laser beam in a magnetic field. In most other schemes, the excited isotopes are photoionized or photodissociated by second laser beams. Ionization by electron beams is cheap and efficient in comparison to ionization by laser beams, and it requires no special technical developments. The feasibility of the new scheme has been demonstrated in the selective ionization of Ba^{138}, making possible the separation of this isotope from the Ba isotopes of atomic weight 130, 132, 134, 135, 136, and 137.

The beam of atoms including mixed isotopes is projected through a vacuum perpendicular to an applied magnetic field. The beam of electrons is collimated by, and travels along, the magnetic field, striking the beam of atoms. The laser beam, which is perpendicular to both the magnetic field and the beam of atoms, illuminates the beam of atoms at the point of incidence of the electrons (see Figure 1).

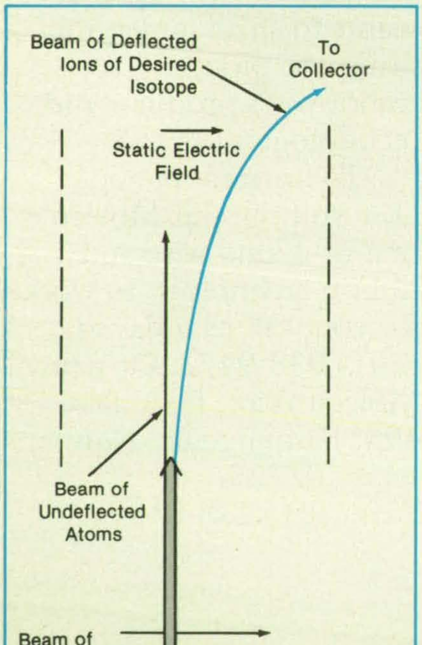

Figure 1. The **Desired Isotope Is Separated** from others in the same atomic species by a process of excitation and ionization followed by electrostatic deflection.

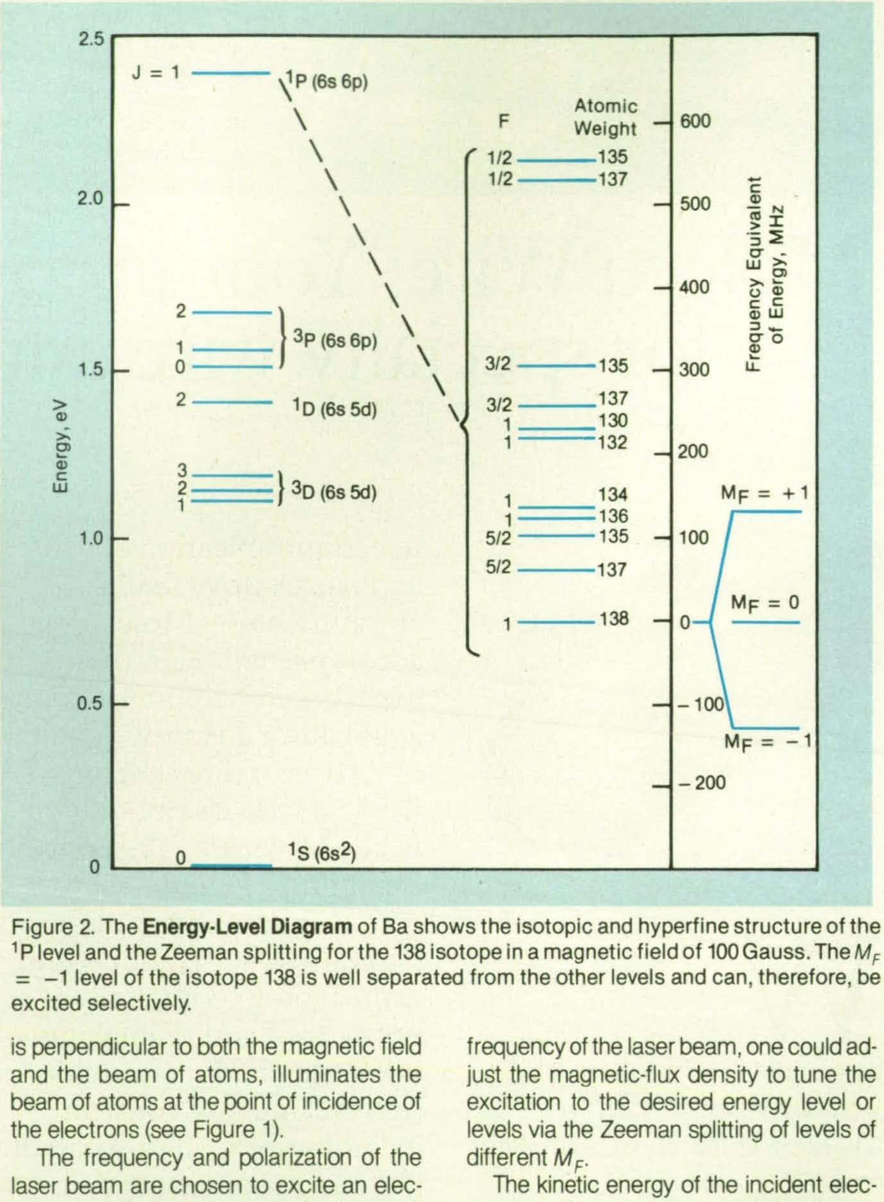

Figure 2. The **Energy-Level Diagram** of Ba shows the isotopic and hyperfine structure of the ^1P level and the Zeeman splitting for the 138 isotope in a magnetic field of 100 Gauss. The $M_F = -1$ level of the isotope 138 is well separated from the other levels and can, therefore, be excited selectively.

The frequency and polarization of the laser beam are chosen to excite an electronic energy level of the desired isotope that is well separated from the corresponding levels of the other isotopes. Typically, this would be the lowest magnetic sublevel of the desired isotope. In the case of Ba^{138}, it would be the $M_F = -1$ sublevel of the $F = 1$ level [where F and M_F are the quantum numbers of the total (nuclear plus electronic) angular momentum and the component of the total angular momentum along the magnetic field, respectively]. Alternatively or in addition to adjusting the frequency of the laser beam, one could adjust the magnetic-flux density to tune the excitation to the desired energy level or levels via the Zeeman splitting of levels of different M_F.

The kinetic energy of the incident electrons must be chosen so that they ionize the excited atoms (of the isotope to be selected), but not the atoms in the ground state (the other isotopes). Consequently, the energy must exceed the ionization energy of the desired species but be less than the ionization energy of the ground-state species. In the case of Ba^{138}, this means that the energy must lie between 2.97 and 5.21 eV. This requirement is easily satisfied with a magnetically collimated electron gun.

Request Card.

In accordance with Public Law 96-517, the contractor has elected to retain title to this invention. Inquiries concerning rights for its commercial use should be addressed to

Edward Ansell
Director of Patents and Licensing
Mail Stop 301-6
California Institute of Technology
1201 East California Boulevard
Pasadena, CA 91125

Refer to NPO-17362, volume and number of this NASA Tech Briefs *issue, and the page number.*

Eye-Safe Lidar

Experimental solid-state systems may find use in meteorology.

NASA's Jet Propulsion Laboratory, Pasadena, California

A laser infrared radar (lidar) undergoing development is harmless to human eyes, consists almost entirely of solid-state components, and offers high range resolution. The lidar operates at a wavelength of about 2 μm. If the radiation from such a device strikes an eye, it is almost completely absorbed by the cornea without causing damage (provided that the lidar is sufficiently distant and suitably low in power or pulse energy), even if aimed directly at the eye. The 2-μm lidar is intended for remote Doppler measurements of winds and differential-absorption measurements of concentrations of gases in the atmosphere.

The lidar includes a continuous-wave ring-laser oscillator pumped by a semiconductor laser diode. A multipass slab laser amplifier is pumped by a flashlamp, which is the only major non-solid-state component. Diodes cannot yet provide the intense light needed by a laser power amplifier. Even here, however, laser-diode pumping is likely to be feasible in the future. Laser-diode pumps have efficiencies of 35 to 40 percent. The use of laser-diode pumping offers high overall efficiency (approaching 15 percent) and long lifetime (approaching 20,000 h). Furthermore, the solid-state laser medium allows energy to be stored and radiation to be amplified in volumes large enough to generate 100 W average power.

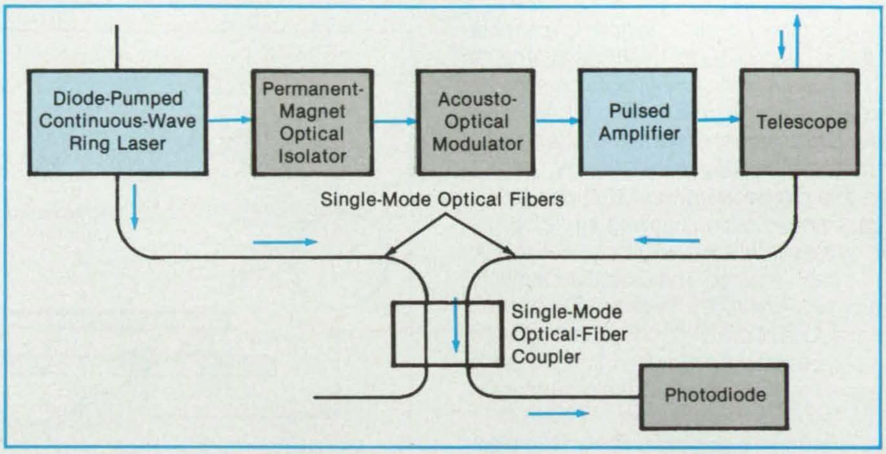

Continuous-Wave Light from a laser oscillator is amplified and modulated for transmission from a telescope. A small portion — about 1 mW — of the output of the oscillator is fed to a single-mode fiber coupler, where it mixes with return pulses.

The output of the oscillator passes through a permanent-magnet optical isolator. An acousto-optical device gates the continuous wave and imposes 40 MHz of frequency modulation (see figure). The power amplifier converts the gated, modulated signal into high-power pulses. A paraboloidal mirror in a telescope launches the pulses into space. The mirror collects reflected pulses, and a single-mode optical fiber carries them to a single-mode optical-fiber coupler, where the reflection signal is combined with the transmitter signal or the signal from another local oscillator. The output of the coupler is fed to a photodiode, which converts the output optical signal into an electrical signal for processing.

In experiments, an yttrium aluminum garnet (YAG) laser doped with thulium and holmium produced continuous-wave light at 2 μm. The Tm:Ho:YAG laser requires a minimum pump power of 4.4 mW at the diode-laser wavelength of 0.782 μm. The thulium ions absorb the pump radiation ef-

The excitation and ionization processes take place continuously in the beam of atoms. The desired isotope is finally selected by electrostatic deflection of the ions out of the beam.

This work was done by Sandor Trajmar of Caltech for **NASA's Jet Propulsion Laboratory**. *For further information, Circle 5 on the TSP Request Card.*

This invention is owned by NASA (U.S. Patent No. 4,704,197). Inquiries concerning nonexclusive or exclusive license for its commercial development should be addressed to the Patent Counsel, NASA's Resident Office-JPL [see page 18]. Refer to NPO-16907

Tunnel-Effect Displacement Sensor

This simple device is extremely sensitive to small displacements.

NASA's Jet Propulsion Laboratory, Pasadena, California

The tunnel position sensor is a simple device that measures small displacements or accelerations. Tunnel position sensors could be used to make compact, sensitive accelerometers or strain gauges or to measure the impacts of particles.

The device was inspired in part by recent advances in scanning tunneling microscopy, in which resolution as fine as 1 Å has been attained. The essential elements are two electrodes in proximity to each other. One of the electrodes is mounted on a piezoelectric cantilever, which is used to make fine adjustments of the gap between the electrodes (see figure).

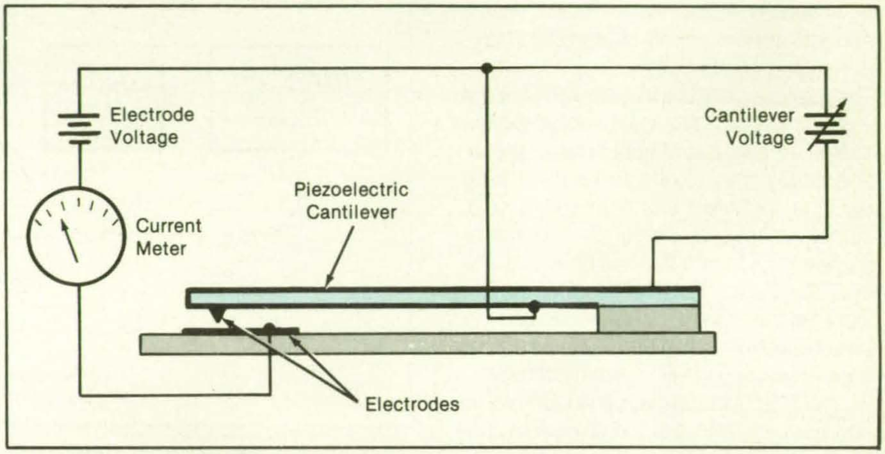

In the **Tunnel Position Sensor** (more precisely, a displacement sensor), the variation in distance between two electrodes is measured via the variation in tunneling current between them.

A voltage is applied between the electrodes. If the electrodes are so close that the electron probability-density waves in them overlap, then an electrical current flows between them by the quantum-mechanical tunneling effect. The magnitude of this tunneling current is extremely sensitive to the distance between the electrodes, and the variation of the current can therefore be used to measure small displacements of the electrodes relative to each other.

Tunnel current typically varies by one order-of-magnitude per Angstrom of electrode-separation change. The incorporation of electron tunneling into accelerometer technology provides a potential increase in sensitivity by several orders of magnitude. This improvement in sensitivity may be used to provide enhanced system sensitivity, dynamic range, or bandwidth. Devices based on tunnel position detection will have application as sensitive sensors for acceleration, force, and strain.

A proof-of-concept electron tunnel accelerometer has been fabricated for testing the basic principles of this new technology. The prototype device shows acceleration sensitivity of 10 micro-g/(Hz)$^{1/2}$ with a 3-kHz bandwidth. Fully integrated tunnel microsensors may be fabricated together with microelectronics in a monolithic Si package. Tunnel microsensors would provide versatility for application as accelerometers, force sensors, strain sensors, particle detectors, and other devices for space applications.

This work was done by William J. Kaiser and Steven B. Waltman of Caltech for **NASA's Jet Propulsion Laboratory**. *For further information, Circle 155 on the TSP*

Circle Reader Action No. 615

ficiently and transfer it to the holmium ions without radiation. This laser works at a slope efficiency (2-μm output divided by the excess of the 0.782-μm pump input over the threshold) of 19 percent. Work continues on the Tm:Ho:YAG laser in the effort to attain single-mode oscillation.

Meanwhile, the lidar system has been demonstrated with a neodymium-doped YAG laser as the continuous-wave oscillator. This device produces light at 1.064 μm — not an eye-safe wavelength. Nevertheless, the demonstration showed that the system can coherently detect scattered laser radiation from clouds and from atmospheric aerosols.

This work was done by Robert L. Byer of Stanford University for **NASA's Jet Propulsion Laboratory**. *For further information, Circle 58 on the TSP Request Card.* *NPO-17464*

Making Excited Oxygen Molecules and Atoms

Excited oxygen should enable oxidation of semiconductors and superconductors at relatively low temperatures.

NASA's Jet Propulsion Laboratory, Pasadena, California

The oxidation of semiconductors and high-temperature superconductors could be achieved at lower temperatures than in current fabrication processes by use of oxygen molecules or atoms that have been raised into specific excited states. The use of excited oxygen (or other species) is also of interest in research on the kinetics and mechanisms of chemical reactions.

The use of excited species reduces the thermal energy required for oxidation. Such a gaseous oxidizing species would have negligible nonthermal kinetic energy, unlike the ion beams or plasmas used in typical low-temperature processing methods, in which substrates undergoing treatment are degraded by sputtering, mixing, and the like. Unlike oxidation induced by beams of ions, electrons, or photons, excited-gas oxidation should be suitable for processing specimens that have large areas.

During the past decade, chemists have developed techniques for the controlled generation of specific excited species of oxygen in useful quantities. These methods include irradiation of oxygen gas with low-energy (< 4-eV) electrons, microwave discharges, and irradiation by lasers tuned to the frequencies of specific transitions in the energy levels of molecules. The most-promising molecular species is the first excited state ($a^1\Delta_g$) of molecular oxygen, which can be produced by laser light. This level lies 0.98 eV above the ground state ($X^3\Sigma_g^-$) and has a radiative half-life of 45 minutes, which is shortened to 9 minutes by nonradiative collisional processes.

Because the direct optical excitation of this state involves a doubly forbidden transition, a two-step process is required. First, the molecule is optically excited to the second excited state ($b^1\Sigma_g^+$), which is 1.63 eV above the ground state. It then undergoes collisional relaxation to the first excited state.

A laser tuned to about 7,610 Å would irradiate oxygen either in the processing chamber or in a separate gas holding chamber. The use of a separate chamber, combined with a delay to allow collisional relaxation to the $a^1\Delta_g$ state, would ensure that a single excited species was reacting with the substrate. This technique should also be of interest in fundamental studies of oxidation. It could be used in an ultrahigh-vacuum chamber that is also equipped for such surface-analytical techniques as x-ray photoelectron spectroscopy.

Another possibility would be to generate excited atomic species. Photons of energy greater than about 6 eV can excite oxygen from the ground state to the $B^3\Sigma_u^-$ state, creating two oxygen atoms in the ground ^3P state via a nonradiative transition. The 1,849-Å radiation from a mercury-arc lamp may be suitable. The oxygen pressure in the chamber should be kept below 10 torr (1.3 kPa) to suppress the formation of ozone. If ozone is desired, pressures greater than 0.5 atm (51 kPa) can be used. However, commercial ozone sources are available.

The dissociation of oxygen by photons of energy greater than about 7 eV results in one atom in the ground (^3P) state and one in the first excited (^1D) state. These two atomic species could also be obtained by the dissociation of ozone or N_2O.

This work was done by Richard P. Vasquez of Caltech for **NASA's Jet Propulsion Laboratory**. *For further information, Circle 8 on the TSP Request Card.*

This invention is owned by NASA, and a patent application has been filed. Inquiries concerning nonexclusive or exclusive license for its commercial development should be addressed to the Patent Counsel, NASA's Resident Office-JPL [see page 18]. Refer to NPO-17534

Unpressurized Container for Cryogenic Testing

Samples do not have to be sealed in the vessel.

Marshall Space Flight Center, Alabama

A nonpressurized cryostat makes the mechanical testing of materials at low temperatures more convenient. The cryostat maintains specimens at temperatures of −400 to −450 °F (33 to 5.4 K) without sealing them in a gastight, vacuum-insulated container. It is relatively easy to insert and remove specimens and to attach instrumentation wiring to them. In addition, because the cryostat vessel is covered only loosely, it vents vapor continuously. There is no danger of buildup of internal pressure from evaporating cryogenic liquid. Safety procedures, test equipment, and test facilities are therefore simpler than in older testing systems that depend on sealed and vented containers.

The cryostat includes two concentric chambers with stainless-steel walls and fiber insulation (see figure). The outer chamber holds liquid nitrogen. The inner chamber, which holds liquid helium and the test specimen, rests on spacers so that the liquid nitrogen extends under its bottom as well as along its sidewall. A stem that lies along the axis of the chambers applies mechanical loads to specimens.

A specimen is mounted in the inner chamber, and such instruments as extensometers and thermocouples are attached to it. To precool the apparatus, liquid nitrogen is poured into the inner chamber as well as the outer one. The nitrogen in the outer chamber is replenished as needed to keep it two-thirds to three-fourths full. The liquid nitrogen in the inner chamber is allowed to boil off until its surface drops below the level of the specimen holder.

A loose lid of polystyrene foam or other suitable material is placed over the vessel. A hole in the lid provides access for the stinger of a vacuum-insulated helium-transfer line and for the instrumentation of the specimen, which must extend above the top of the cryostat. The liquid helium is fed into the inner chamber until the specimen is submerged. The liquid nitrogen remaining in the inner chamber freezes, forming an insulating layer on the bottom. The test is conducted, and the specimen is removed.

When several tests are performed in quick succession, the precooling step has to be done only once. Smaller quantities of cryogenic liquids are therefore used than in a series of tests at long intervals.

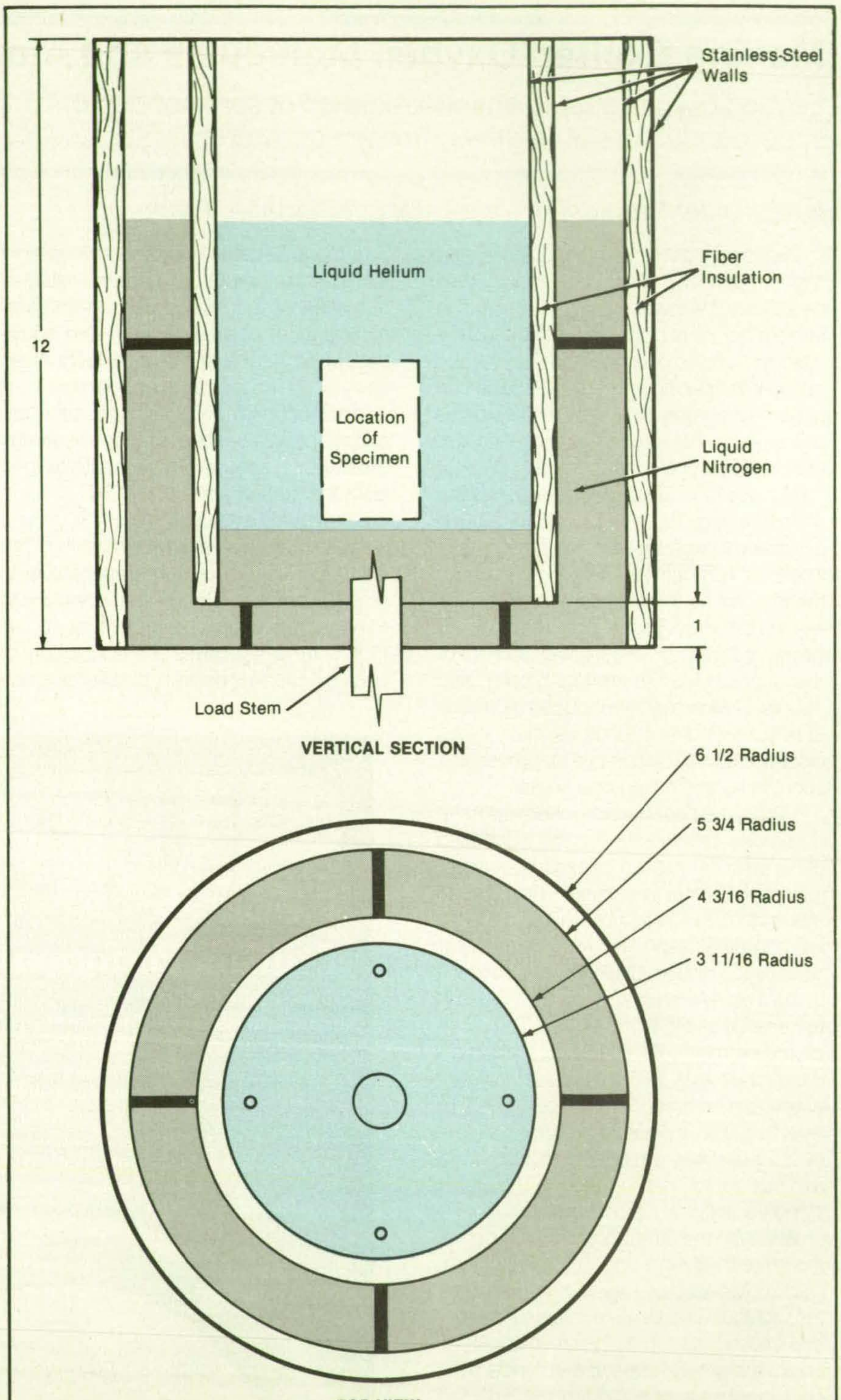

The **Outer Chamber Contains Liquid or Solid Nitrogen**, which surrounds the bottom and side of the inner chamber. Although fiber insulation is used, the spaces between the stainless-steel walls could be evacuated for more effective insulation, if necessary. Dimensions are in inches and are not critical.

This work was done by Susan B. Walker of United Technologies Corp. for **Marshall Space Flight Center**. *No further documentation is available.*

Inquiries concerning rights for the commercial use of this invention should be addressed to the Patent Counsel, Marshall Space Flight Center [see page 18]. Refer to MFS-28347

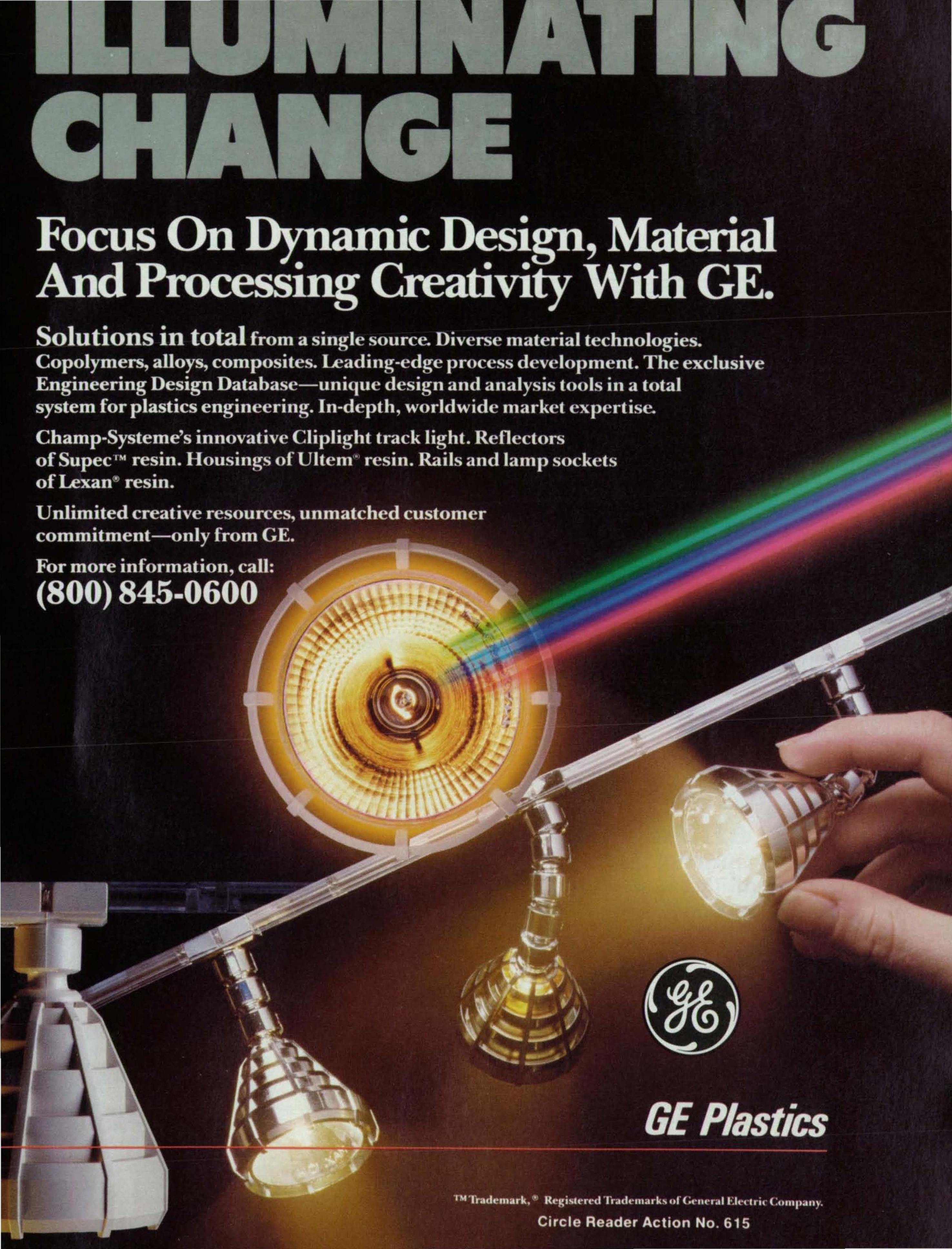

Convergent-Filament Nonmechanical Pump

The restrictions imposed by capillaries are avoided.

NASA's Jet Propulsion Laboratory, Pasadena, California

A simple device induces a small flow of liquid without the help of moving parts, in the presence or absence of gravity. Unlike other nonmechanical pumps based on wicks or capillary tubes, this one is not limited by internal absorption or restricted cross-sectional area. One important use is expected to be returning liquid condensate in heat pipes. Another might be the collection of samples from clouds or fog.

A prototype transports a slow but steady flow of isopropyl alcohol. The prototype includes 11 filaments on concentric rings in a conical structure (see figure). The filaments, which are ordinary polymeric fishing line, are spaced about 0.25 in. (0.6 cm) apart on the wide end. On the narrow end, the filaments are spaced as closely as

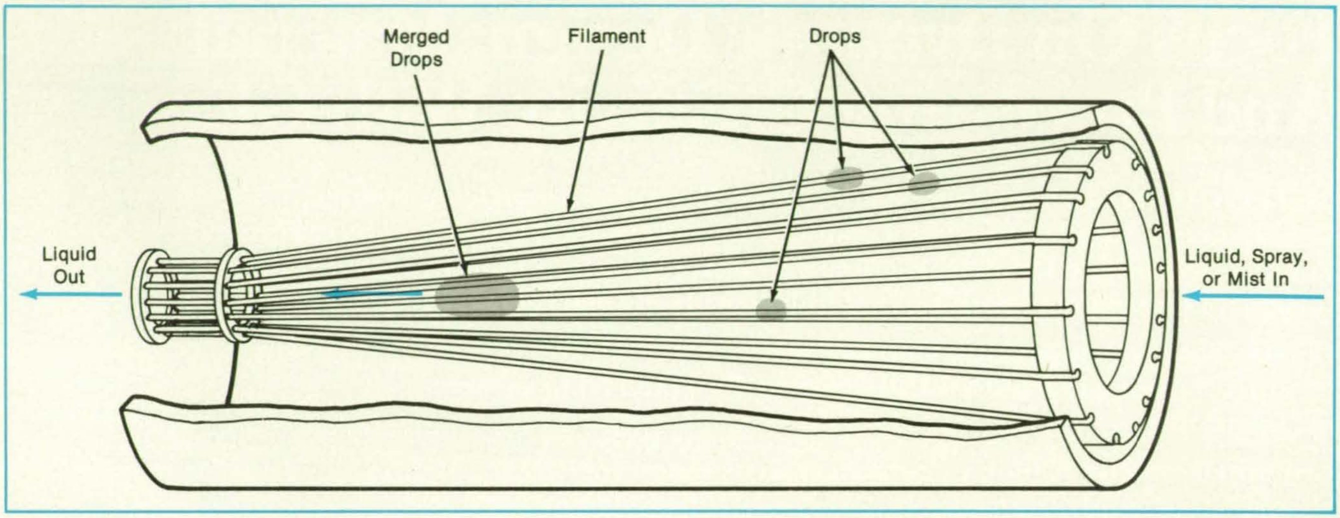

Drops of Liquid Move on filaments from the wide end of the cone to the narrow end. The drops gradually blend with drops on adjacent filaments to form large drops with menisci.

When your needs call for assistance from design through delivery,

call for Emcor®

When you work with Emcor, you'll get the right enclosure for your requirements, supplied just the way you want it and delivered when you need it.

LOCAL AND FACTORY SUPPORT

As a part of our commitment to total customer support, we have 41 field sales offices throughout the U.S. and Canada staffed with more than 100 factory trained representatives. Just call us and a field or factory representative will personally come to your site to consult with you concerning your enclosure requirements.

CUSTOM DESIGN

Emcor thrives on special challenges - from simple holes and cutouts to unique configurations, sizes, and shapes. Work with our experienced group of design engineers and you will be teamed up with industry experts using the latest in CAD/CAM technology. Emcor is dedicated to providing you with exactly what you want: a cabinet designed and manufactured to your specifications at a price you can afford.

QUALITY CONTROL

Emcor ensures conformance to high quality standards through the use of the most modern quality control equipment available on the marketplace today. Dimensional accuracy is closely controlled through the use of a Brown and Sharp coordinate measuring machine. Our ACS digital color computer guarantees a consistent color match of painted items every time. Emcor can also provide inspection systems capable of meeting the most exacting government requirements such as MIL-I-45208A.

CUSTOMER SERVICE

Emcor's factory staff is the best in the business. They will assist you in analyzing your enclosure needs and will coordinate their vast resources to fully support and fulfill your cabinetry requirements. Every step of the way, from your first quotation through order shipment, you will find no one better able to serve and support you. Your needs deserve Emcor's kind of attention.

Crenlo, Inc.
1600 - 4th Ave. N.W.
Rochester, MN 55901
Phone 507-289-3371
FAX # 507-287-3405

EMCOR®

Emcor is listed under GSA contract # GS-07F-17241.

Circle Reader Action No. 460

possible without touching. The filaments are about 4 in. (10 cm) long.

The liquid enters the pump at the large end of the cone. Drops of liquid move onto the filaments and merge with other drops, forming slugs of liquid held by pairs of filaments. Driven by what are believed to be unbalanced surface-tension forces, the slugs slide to the narrow end of the cone.

In practice, a larger array of filaments would probably be used. The array need not be conical; it might be planar or arranged in another three-dimensional configuration.

This work was done by Earl R. Collins, Jr., of Caltech for **NASA's Jet Propulsion Laboratory**. *For further information, Circle 52 on the TSP Request Card.*

This invention is owned by NASA, and a patent application has been filed. Inquiries concerning nonexclusive or exclusive license for its commercial development should be addressed to the Patent Counsel, NASA's Resident Office-JPL [see page 18]. Refer to NPO-17301

Polymeric Electrolytic Hygrometer for Harsh Environments

An improved design reduces vulnerability to organic vapors and dust.

NASA's Jet Propulsion Laboratory, Pasadena, California

The design of a polymeric electrolytic hygrometer has been improved to meet the need for reliable measurements of relative humidity in the harsh environments of pulpmills and papermills. The hygrometer can operate in the presence of organic vapors, dust, traces of sulfur dioxide, acidic vapors, and strong oxidizing agents. It tolerates temperatures near 65 °C and flows of air near 10 m/s easily. Its maximum temperature rating is much higher, near 130 °C.

The basic humidity-sensing element is a piece of Nafion* or similar polytetrafluoroethylene resin with persulfonic acid substitutions that has been treated with lithium hydroxide. The sensing element is sandwiched between noble metal or other relatively unreactive electrodes. Moisture absorbed from the air is ionized in the polymer. Both the H^+ and OH^- ions transport electrical charge. An alternating voltage is applied to the electrodes to measure the conductivity of the polymer, from which the humidity can be deduced.

A previous version of the sensor has contacts of gold plating at the ends of a small ribbon of the Nafion polymer. These tended to separate during use probably because of swelling of polymer. Gold appears not to adhere strongly to the polymer.

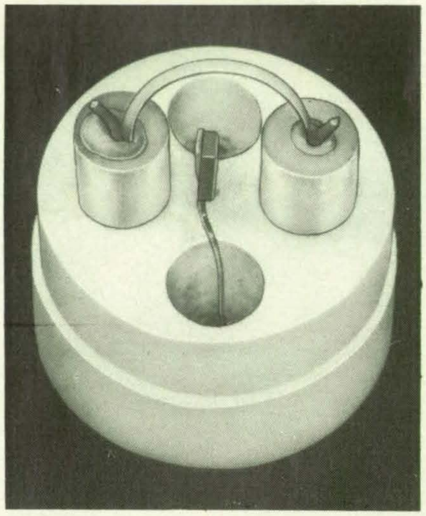

The **Redesigned Sensor Head** features a shorter, more-rigidly-held sensing element that is less vulnerable than the previous version was to swelling and loss of electrical contact.

The redesigned sensor (see figure) has a short length of sensing polymer and electrode wire. The sensing-polymer strip is mounted in an electrically-conductive silver epoxy, which is very rigid and adheres strongly to the sensing polymer. The sensing polymer and epoxy fill a glass capillary bonded to a polytetrafluoroethylene holder, which has gold-plated pins connecting to the measuring circuits via multicore cable. Contact between the gold-plated pins and the silver epoxy is established through a short platinum wire.

The improved sensor performed well in tests in papermills. It exhibited low hysteresis, rapidity of response, and sensitivity sufficient for use in controlling humidity in the manufacture of paper. It may also be useful for the control of batch dryers in the food and pharmaceutical industries.

This work was done by Daniel D. Lawson, Parthasarathy Shakkottai, and Shakkottai P. Venkateshan of Caltech for **NASA's Jet Propulsion Laboratory**. *For further information, Circle 100 on the TSP Request Card.*

**"Nafion" is a registered trademark of Du Pont, E. I., de Nemours & Co., Inc.*

NPO-17365

High-Resolution, Two-Wavelength Pyrometer

Optical and electronic parts of a commercial instrument are modified.

NASA's Jet Propulsion Laboratory, Pasadena, California

A modified two-color pyrometer measures the temperatures of objects with high spatial resolution. Like other two-color pyrometers, it determines the temperature by calculating the ratio of the intensity of radiation received in two different wavelength bands. Because the instrument uses a ratio, its accuracy is less sensitive to the intensity of radiation falling on its detectors than is that of a pyrometer that measures in one wavelength band only.

A conventional two-color pyrometer can resolve a target that subtends an angle of about 1/100 rad, but the modified pyrometer can resolve a target only 1/800 rad wide. Designed to measure the temperatures of objects in crystal-growing furnaces, the modified pyrometer has a dynamic range of 1,100 to 1,600 °C and a sensitivity of 5 mV/°C.

In a conventional two-color pyrometer, the image of the target is focused on the planar end of a bundle of optical fibers for transmission to the detectors. In the modified instrument, the image is focused on a hole 0.002 in. (0.05 mm) in diameter in a brass sheet near the end of the bundle, causing the image to be distributed so that the fibers are covered by defocused radiation from the target (see figure). The pinhole ensures that radiation from only a small part of the target scene reaches the detector, thus providing the required spatial resolution. Moreover, by spreading the radiation over the bundle, the pinhole ensures that the entire active area of the detectors is utilized.

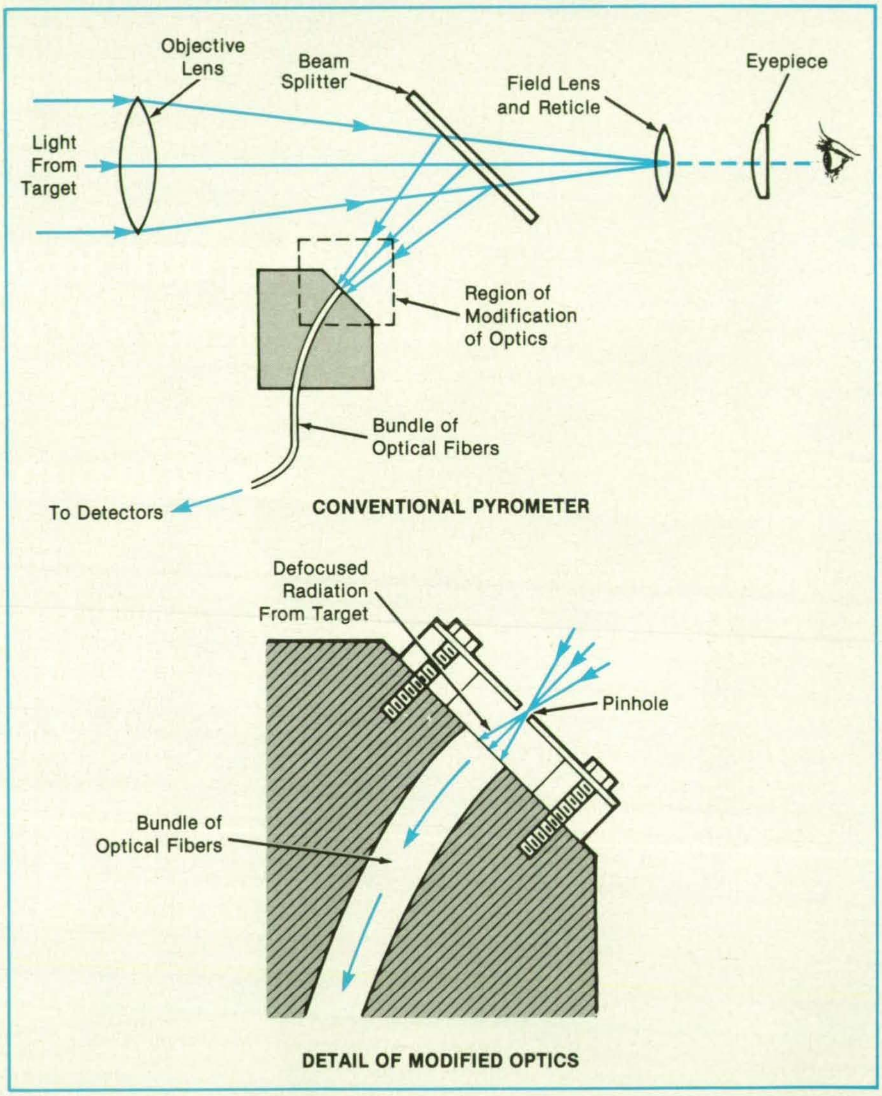

A **Pinhole in a Sheet** distributes light from a distant hot source over the flat end surface of a bundle of optical fibers. The plate lies 0.1 in. (2.54 mm) away from the bundle, which is 0.032 in. (0.81 mm) in diameter.

In the first version of the instrument, using the modified optics with the commercial signal-processing electronics, the signal output of the detectors was too low to drive the signal-processing circuitry. The fixed logarithmic gain characteristic of that circuitry responded to low input signals with low gain, yielding a poor signal-to-noise ratio.

Accordingly, an entirely-new signal-processing package was designed and installed. It uses high-gain, high-stability, chopper-stabilized operational amplifiers. It also uses resistive feedback, which gives a higher signal-to-noise ratio than does logarithmic feedback. As a result, the modified pyrometer produces a signal as quiet as that of conventional instruments but with only 1/64 the input radiation.

Each of the two channels from the detector — one for each color — feeds two stages of chopper-stabilized amplification. The stages consist of linear current-to-voltage converters and preamplifiers. The preamplified signals are connected through shielded cables to scaling amplifiers and a linear divider circuit. After filtering, the output of the divider goes to a panel meter and to a pair of output terminals. The output of the divider is calibrated internally by a pair of voltages fed to the input of the divider to simulate a known input from the detectors.

This work was done by Donald B.

IN CASE OF EXTREME TEMPERATURE AND HIGH LOADS...

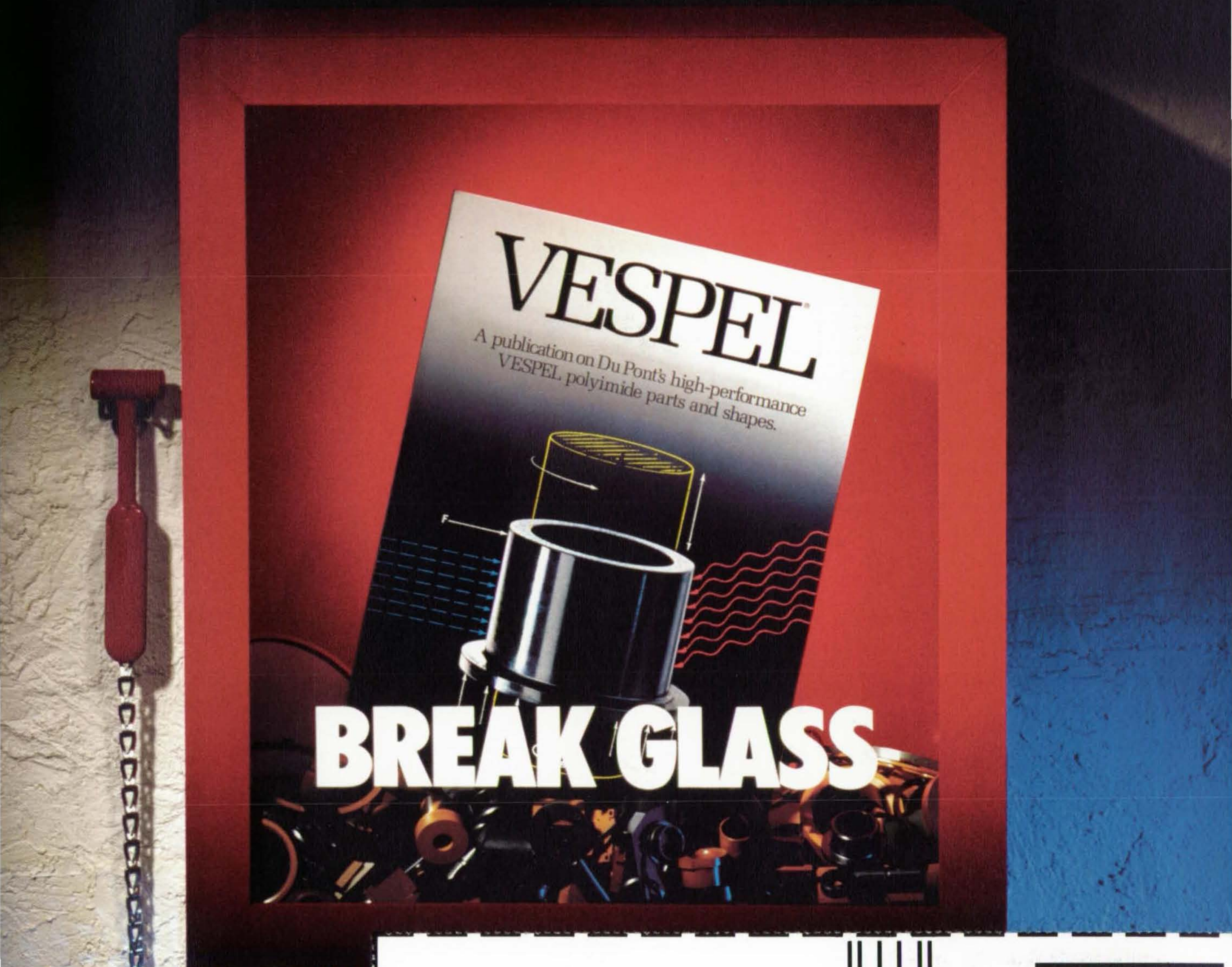

Get your own *free copy* of this informative brochure, "VESPEL," by completing the postpaid card at right and dropping it in the mail. **For more information, turn the page.**

NO POSTAGE
NECESSARY
IF MAILED
IN THE
UNITED STATES

BUSINESS REPLY MAIL

FIRST CLASS PERMIT NO. 4 BLOOMFIELD HILLS, MI

POSTAGE WILL BE PAID BY ADDRESSEE

Du Pont VESPEL® Product Information
P.O. Box 1138
Bloomfield Hills, Michigan 48303-1138

Bickler, Paul K. Henry, and D. Daniel LoGiurato of Caltech for **NASA's Jet Propulsion Laboratory**. For further information, Circle 87 on the TSP Request Card.

In accordance with Public Law 96-517, the contractor has elected to retain title to this invention. Inquiries concerning rights for its commercial use should be addressed to

Edward Ansell
Director of Patents and Licensing
Mail Stop 301-6
California Institute of Technology
1201 East California Boulevard
Pasadena, CA 91125

Refer to NPO-17287, volume and number of this NASA Tech Briefs *issue, and the page number.*

Books and Reports

These reports, studies, handbooks are available from NASA as Technical Support Packages (TSP's) when a Request Card number is cited; otherwise they are available from the National Technical Information Service.

Hydrodynamic Stability and Frames of Reference

Criteria of stability are different in different sets of coordinates.

A report discusses the dependence of the criteria of hydrodynamic instability upon the frame of reference used to analyze the motion of a fluid. This theoretical topic has practical implications since that instability is related to turbulence and is the source of noise, vibration, and other destructive effects in fluid machinery and structures immersed in fluids.

A flow is considered to be unstable if a small disturbance in the velocity, pressure, stream function, or other characteristic grows into a large disturbance. Mathematically, the problem is usually treated by a linear small-perturbation analysis. In the example of this study, a small two-dimensional disturbance velocity field is introduced into an inviscid, incompressible plane shear flow that is initially parallel to two walls that constitute the boundaries. The velocity field is expressed in both Eulerian (stationary — in this case, Cartesian) and Lagrangian (streamline) coordinates.

It is shown that, in general, the partial derivative of the stream function with respect to time is not the same in these two frames of reference. The Lagrangian equations of flow are linearized with respect to the unperturbed shear flow, and a specific shear velocity profile is selected. It is shown that analysis of stability for this profile based on the classical Orr-Sommerfeld equation in Eulerian coordinates yields the conclusion that the flow is stable, even though the analysis based on the stream function in Lagrangian coordinates shows the flow to be unstable.

Thus, the use of the stream function in a criterion for instability of the velocity field can lead to different conclusions in different frames of reference. The two conclusions do not necessarily contradict each other, provided that one has a way of determining which one is related to the onset of turbulence. The distinction can be important because the stability of streamlines is directly related, whereas the stability of the velocity field is only indirectly related, to the onset of turbulence.

This work was done by Michail A. Zak of Caltech for **NASA's Jet Propulsion Laboratory**. *To obtain a copy of the report, "Hydrodynamic Stability and Frames of Reference," Circle 82 on the TSP Request Card.*
NPO-17740

Temperature Dependence of Elastic Constants of Polymers

The theory of small elastic deformations of disordered solids at low temperatures is extended.

Two papers extend the theory of the elastic constants of disordered solids to finite temperatures below their glass-transition temperatures. These and related studies are part of the effort to understand the macroscopic mechanical properties of glassy polymers and similar materials on the basis of mathematical models of atoms arranged in lattices of unit cells, governed by the Lennard-Jones 6,12 potential

$$U(R) = -AR^{-6} + BR^{-12}$$

where A and B are constants and R represents the distance between atoms.

The first paper, entitled "Elastic Constants of Disordered Solids II: Temperature Dependence," applies to cryogenic temperatures. As in previous studies devoted to this theory, it begins by stating some relationships between the mathematical models and macroscopic thermodynamical properties. It retains the previous assumptions of anisotropic stress, strains small enough to remain within the linear elastic range, and central interparticle forces.

At sufficiently low temperatures, the motion of the reference particle (the atom in question when computing on the microscopic level) is treated by a quasi-harmonic approximation, in which the particle is restricted to excursions close to the center of its unit cell. Under this approximation, all potential-energy terms of order higher than quadratic in the displacement are negligibly small, and the motion of the reference particle at and near zero strain is that of an anisotropic harmonic oscillator, the frequency of which depends on the volume and the strains.

This approximation accounts for an initial linear increase of the Poisson ratio μ and a similar decrease of Young's modulus Y with increasing temperature. Numerical evaluation of the complete cell potential and of the free-volume integral shows that as temperature increases further, the increases in Y and μ level off to plateaus. The numerical evaluation also indicates a third, higher temperature region in which μ increases and Y decreases more rapidly. The bulk modulus is but weakly dependent on temperature in these regions.

The results for the third region require further examination, for upon a further increase in temperature, the model becomes invalid and predicts a reversal in the sign of the temperature coefficient of Y and impermissible values for μ. This is qualitatively similar to the performance of the cell theory in predicting the thermal expansivity of glasses at low temperatures. An examination of experimental results for some inorganic and organic glasses indicates the existence of the three temperature regions, or at least the last two.

The second paper, entitled "Theory of Thermoelastic Properties for Polymer Glasses," develops a unified treatment for static compressional and elongational properties at temperatures up to glass-transition temperatures. It derives equations for the extensional elastic moduli as functions of temperature and pressure by a generalization of the equation of state.

Whereas the previous paper confined itself to the low-temperature region, where the characteristic free-volume function is effectively frozen, this paper proceeds to higher temperatures, where the temperature and pressure dependence of this function play a decisive role. The static Young's and shear modulus and the Poisson ratio are computed, based solely on information derived from the equation of state. This is illustrated by applications to poly(vinyl acetate) glasses at low and elevated pressures and for different formation histories. Further comparisons with experimental results are presented for poly(methyl methacrylate).

This work was done by Robert Simha and Elisabeth Papazoglou of Case Western Reserve University for **NASA's Jet Propulsion Laboratory**. *To obtain a copy of the reports, "Elastic Constants of Disordered Solids II: Temperature Dependence," and "Theory of Thermoelastic Properties for Polymer Glasses," Circle 88 on the TSP Request Card.*
NPO-17762

Accelerated Testing of Photothermal Degradation of Polymers

Arrhenius plots reveal maximum safe temperatures.

NASA's Jet Propulsion Laboratory, Pasadena, California

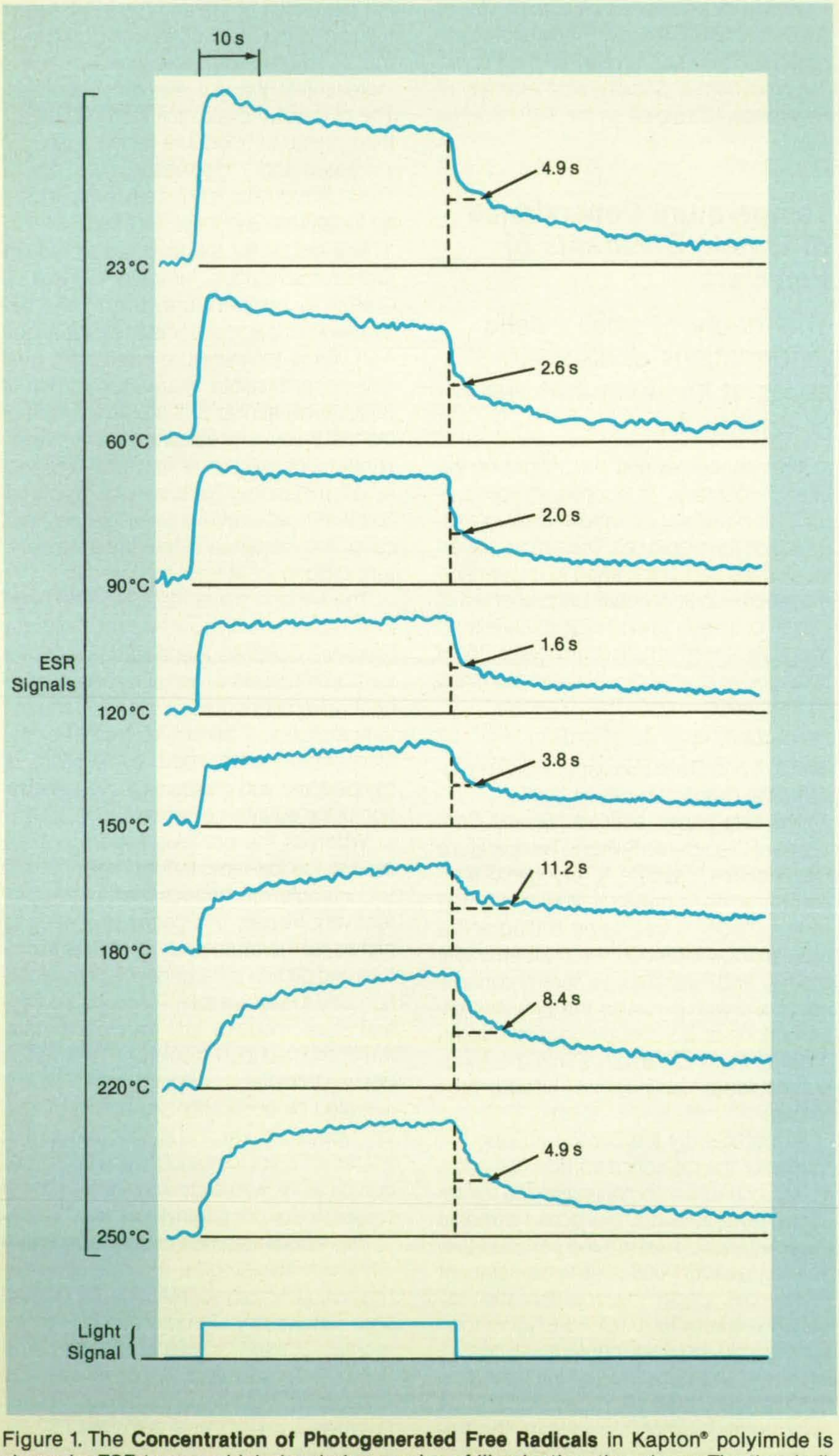

Figure 1. The **Concentration of Photogenerated Free Radicals** in Kapton® polyimide is shown by ESR traces, which rise during a pulse of illumination, then decay. The time indicated next to each decaying signal is the characteristic decay half life, $\tau_{1/2}$.

Electron-spin-resonance (ESR) spectroscopy and Arrhenius plots can be used to determine the maximum safe temperature for accelerated testing of photothermal degradation of polymers. Aging can be accelerated by increasing the illumination, the temperature, or both. The results of aging tests at temperatures higher than those encountered in normal use are valid as long as the mechanism of degradation is the same throughout the range of temperatures. A transition between different mechanisms at some temperature can be identified via a transition between activation energies, which manifests itself as a change in the slope of an Arrhenius plot at that temperature.

The photothermal degradation of a polymer involves the photogeneration of free radicals, which decay through recombination and cross-linking of polymer chains. The kinetics of formation and decay of free radicals can be monitored by ESR. Specifically, the polymer is illuminated with a pulse of light, after which the ESR signal decays. The kinetic parameter, k, is inversely proportional to the characteristic decay time of the ESR signal.

The kinetic parameter of a given polymer is calculated from ESR measurements at several temperatures, then plotted versus the reciprocal of absolute temperature to fit the data to the Arrhenius equation

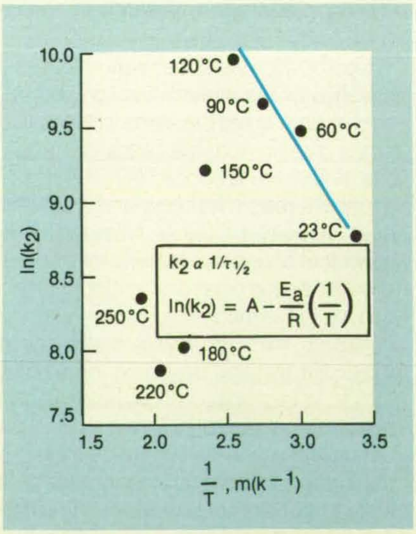

Figure 2. This **Arrhenius Plot** is obtained from the data of Figure 1. The abrupt change in slope at 120 °C indicates a transition between different mechanisms of degradation.

$$\ln(k) = A - E_a/RT$$

where A is a constant, E_a = the activation energy, R = the ideal-gas constant, and T = the absolute temperature. For example, Figure 1 shows ESR traces from photogenerated free radicals in Kapton® polyimide film at various temperatures, and Figure 2 shows the resulting Arrhenius plot of the second-order rate constant, k_2. The simple linear relationship of the Arrhenius plot breaks off as the temperature rises above 120 °C. Thus, one can safely study photothermal degradation by accelerated aging of this material at temperatures up to 120 °C.

This work was done by Soon Sam Kim, Ranty Hing Liang, and Fun-Dow Tsay of Caltech for **NASA's Jet Propulsion Laboratory**. *For further information, Circle 74 on the TSP Request Card.*
NPO-17454

Surrogate Seeds for Growth of Crystals

Larger crystals of higher quality can be grown.

NASA's Jet Propulsion Laboratory,
Pasadena, California

An alternative method for starting the growth of a crystal involves the use of a seed crystal of different material instead of the same material as that of the solution. The method is intended for growing single-crystal proteins for experiments but is applicable in general to the growth of crystals from solutions and may also be applicable to the growth of semiconductor or other crystals from melts.

The material for the surrogate seed must be insoluble in the solution and have a crystal lattice, the form and dimensions of which match those of the material being grown as closely as possible. Such a material could be selected from a computerized data bank of materials.

Because the seed material does not dissolve in the solution, the temperature of the solution can be raised substantially higher than if a seed of the material to be grown were used. At the higher temperature, potential crystal-nucleation sites are dissolved; with proper control of conditions, nucleation should occur only at the interface between the solution and the seed. As a result, a single large crystal with few, if any, imperfections can be grown.

This work was done by Paul J. Shlichta of Caltech for **NASA's Jet Propulsion Laboratory**. *For further information, Circle 128 on the TSP Request Card.*
NPO-17339

Books and Reports

These reports, studies, handbooks are available from NASA as Technical Support Packages (TSP's) when a Request Card number is cited; otherwise they are available from the National Technical Information Service.

The ACEE Program and Basic Research on Composites

Significant results in the technology of composites were achieved between 1975 and 1986.

A NASA reference publication describes research in composites conducted at the Langley Research Center between 1975 and 1986. The research includes Langley basic technology and the composite-primary-structures element of the NASA Aircraft Energy Efficiency (ACEE) Program. The basic technology documents cited in the bibliography are grouped according to the research activity; for example, design and analysis, fatigue and fracture, and tolerance to damage. The ACEE documents cover the development of composite structures for transport aircraft.

A crossroads event in the history of research on composites at the Langley Research Center occurred in 1975. Before 1975, the development of composites had proceeded from laboratory-scale experiments to limited applications. The Langley research was focused in accordance with a 1972 Air Force/NASA Long-Range Planning Study for Composites (RECAST). The event that caused a fundamental change was the formation of the ACEE Program. From 1976 until its termination in 1985, the ACEE Program was the central element in NASA research on composites.

Composite structures were one element of a comprehensive plan for the development of aeronautical fuel-conservation technology. The goal of the composite-primary-structures element of the ACEE Program was to accelerate the application of composites to primary structures in new civil transport aircraft by (1) development of design and manufacturing techniques for composite empennage, wing, and fuselage structures; (2) dissemination of technology throughout the transport industry; and (3) extensive flight-service evaluations.

ACEE research on composites was performed under contracts with the builders of transport aircraft and managed by a small project staff at Langley. An extensive base technology program in composite materials and structures was performed under the auspices of Langley Research Center. Together the ACEE and Langley base research programs produced results of major significance to the technology of composites in the United States.

This report summarizes the ACEE and base programs in composite materials and structures and presents an annotated bibliography of the many reports and documents on the subject produced during the 11 years from 1975 to 1986. The bibliography of over 600 publications, with their abstracts, is organized into subsections according to research disciplines or aircraft structural components. An index of the authors of these documents is also provided. This report deals only with resin/matrix composite materials.

This work was done by Marvin B. Dow of **Langley Research Center**. *Further information may be found in NASA RP-1177 [N87-29612], "The ACEE Program and Basic Composites Research at Langley Research Center (1975 to 1986) — Summary and Bibliography."*

Copies may be purchased [prepayment required] from the National Technical Information Service, Springfield, Virginia 22161, Telephone No. (703) 487-4650. Rush orders may be placed for an extra fee by calling (800) 336-4700.
LAR-14028

Computer Programs

COSMIC: Transferring NASA Software

COSMIC, NASA's Computer Software Management and Information Center, distributes software developed with NASA funding to industry, other government agencies and academia.

COSMIC's inventory is updated regularly; new programs are reported in *Tech Briefs*. For additional information on any of the programs described here, circle the appropriate TSP number.

If you don't find a program in this issue that meets your needs, call COSMIC directly for a free review of programs in your area of interest. You can also purchase the 1988 *COSMIC Software Catalog*, containing descriptions and ordering information for available software.

COSMIC is part of NASA's Technology Utilization Network.

COSMIC® — *John A. Gibson, Director*, (404) 542-3265
The University of Georgia, 382 East Broad Street, Athens, Georgia 30602

Computer Programs

These programs may be obtained at a very reasonable cost from COSMIC, a facility sponsored by NASA to make computer programs available to the public. For information on program price, size, and availability, circle the reference number on the TSP and COSMIC Request Card in this issue.

Mechanics

Calculating Transonic Flows About Airfoils

Small disturbances and aeroelastic effects can be simulated.

The XTRAN2L computer program is used to calculate two-dimensional transonic flows about airfoils. XTRAN2L uses a time-accurate, alternating-direction, implicit (ADI) finite-difference scheme to solve the two-dimensional complete unsteady transonic small-disturbance equation. Engquist-Osher monotone spatial differencing is used in the ADI solution algorithm to provide a robust and efficient program.

Airfoil-flow-tangency boundary conditions are defined to include the contour of the airfoil, the deformation of the chord, plunge displacement, pitch, and deflection of the trailing edge of the control surface. The wake is represented as a slit downstream of the trailing edge of the airfoil. Nonreflecting far-field boundary conditions are included to minimize reflections of disturbances of the flow field from the computational boundaries.

Three types of unsteady motion can be specified to define the plunge displacement, pitch, and deflection of the trailing edge of the control surface. These types of motion are as follows: (1) forced harmonic, (2) pulse, and (3) aeroelastic transient. The forced harmonic and pulse motions can be used to determine the real and imaginary components of the unsteady aerodynamic forces in the frequency domain.

The forced-harmonic-motion procedure uses analysis of the instantaneous forces calculated over the last cycle of motion to determine the harmonic components of force. The pulse-motion procedure (an alternate to the forced harmonic-motion procedure) calculates aerodynamic transients based upon causing the airfoil to undergo a small prescribed pulse in a specified mode of motion. Fourier analysis can then be applied to the aerodynamic-force-versus-time histories to determine the harmonic components of force.

The aeroelastic-transient capability enables the user to determine the history of motion of the airfoil at a given flow condition. The equations of motion of the structure are coupled with the procedure for solution of the equations of aerodynamic motion, and the two are integrated simultaneously to determine the history of motion.

XTRAN2L was developed on a CDC CYBER mainframe computer running under NOS 2.4. It is written in FORTRAN V and uses overlays to minimize storage requirements. The program requires 120K of memory in overlayed form. XTRAN2L was developed in 1987.

This program was written by David A. Seidel, John T. Batina, and Woodrow Whitlow, Jr., of **Langley Research Center**. *For further information, Circle 107 on the TSP Request Card. LAR-13899*

Calculating Trajectories and Orbits

Two programs calculate the motions of spacecraft and landers.

The Double Precision Trajectory Analysis Program, DPTRAJ, and the Orbit Determination Program, ODP, have been developed and improved over the years to provide the NASA Jet Propulsion Laboratory with a highly reliable and accurate navigation capability for their deep-space missions like the Voyager. DPTRAJ and ODP are

each collections of programs that work together to provide the desired computational results. DPTRAJ, ODP, and their supporting utility programs are capable of handling the massive amounts of data and performing the various numerical calculations required for solving the navigation problems associated with planetary fly-by and lander missions. They were used extensively in support of NASA's Voyager project.

DPTRAJ produces a spacecraft ephemeris by numerical integration of the equations of motion, which can be formulated using a full set of mathematical models of acceleration. For each particular trajectory case, the extent of the modeling employed and the precision of the integration process are controlled by specifications entered by the user. The equation of motion includes four types of terms. An acceleration term accounts for the basic conic motion of the spacecraft with respect to the central body. Terms that measure the attraction of the perturbing bodies on the spacecraft and terms that indirectly affect the motion as perturbations on the central body can be included. Terms are also provided to account for other gravitational and nongravitational effects on the motion.

The function of ODP is the processing of the observational data in order to compute precise estimates of the position-coordinate histories of the spacecraft or lander. This function is executed by processing the observational data and auxiliary calibration information. ODP also computes a spacecraft-state vector, or a lander-position vector, along with parameters that define the acceleration. The heart of the ODP process is a data-fitting subprocess in which validated, edited, and corrected observational data are transformed into a state-vector estimate. The derived state-vector estimate can then be used to generate an estimated trajectory. This trajectory contains the final product of the orbit-determination process, which is the time evolution of the estimated position coordinates of the spacecraft or lander.

DPTRAJ-ODP is available in two machine versions. The UNIVAC version (NPO-15586) is written in FORTRAN V, SFTRAN, and ASSEMBLER. (A processor is supplied for SFTRAN, a structured FORTRAN.) DPTRAJ and ODP have been implemented on a UNIVAC 1100-series computer. The VAX/VMS version (NPO-17201) is written in FORTRAN V, SFTRAN, PL/1 and ASSEMBLER. It was developed to run on all models of DEC VAX computers under VMS and has a central-memory requirement of 3.4 Mb. The UNIVAC version was last updated in 1980. The VAX/VMS version was developed in 1987.

This program was written by Daniel J. Alderson, Franklyn H. Brady, Peter J. Breckheimer, James K. Campbell, Carl S. Christensen, James B. Collier, John E. Ekelund, Jordan Ellis, Gene L. Goltz, Gerarld R. Hintz, Victor N. Legerton, Faith A. McCreary, Robert T. Mitchell, Neil A. Mottinger, Benjamin A. Moultrie, Theodore D. Moyer, Sheryl L. Rinker, Mark S. Ryne, L. Robert Stavert, Richard F. Sunseri, Tseng-Chan Michael Wang, and Peter J. Wolff of Caltech for **NASA's Jet Propulsion Laboratory**. *For further information, Circle 110 on the TSP Request Card.* NPO-17201

Mathematics and Information Sciences

Variable-Metric Algorithm for Constrained Optimization

A function is minimized subject to equality and inequality constraints.

The Variable Metric Algorithm for Constrained Optimization (VMACO) is a nonlinear computer program developed to calculate the least value of a function of *n* variables subject to general constraints (both equality and inequality). Generally, the first set of constraints is an equality (the target) and the remaining constraints are inequalities (boundaries). The VMACO program utilizes an iterative method in seeking the optimal solution. It can be "hooked" into a driver program (examples are provided), which can calculate the values for the real function, constraints, and their first-order partial derivatives with respect to the control variables.

It is assumed that the objective function is convex and unimodal. The user should be familiar enough with his or her simulation so that local maximums and minimums can be recognized.

The algorithm is based upon a variable-metric method presented by M. J. D. Powell and a quadratic programming method by R. Fletcher. This implementation requires more overhead in calculating each new control variable, but fewer iterations are required for convergence. In comparison with other algorithms, it has been found that VMACO handles test cases with constraints particularly well and that less execution time is necessary for convergence.

VMACO is written completely in ANSI Standard FORTRAN 77. The code is internally documented and modularly structured with rigid coding standards. The program requires approximately 26K of 8-bit bytes of central memory and was first released in 1988.

This program was written by James D. Frick of McDonnell Douglas Corp. for **Johnson Space Center**. *For further information, Circle 1 on the TSP Request Card.* MSC-21275

Mechanics

Piecewise-Linear Computation of Creep

An analogy is drawn between thermal and creep strains.

Ames Research Center, Moffett Field, California

The theory of elastic and inelastic stresses and strains in isotropic materials can be blended with finite-element computer programs to calculate residual stresses due to creep in structures. An analogy is drawn between thermal expansion and creep, enabling the use of the thermal-stress computational approach to calculate the creep stresses and strains. An overall transient solution is obtained by piecewise-linear iterations.

The theoretical basis is provided by Hooke's law for stresses and strains in an isotropic material, plus the expression of the total strain as the sum of elastic and inelastic components. The solutions of problems in inelasticity can be changed to those of problems in elasticity via a general analogy in which the distribution of strains in a body subject to a given set of body and surface forces with inelastic strain is the same as the distribution of strain in an identical body with no inelastic strain but with an additional set of body forces.

The inelastic component of strain is decomposed further into a component due to creep and a component due to thermal expansion. (Although thermal expansion can be reversed by a reversal in the increment of temperature, at a given fixed temperature for which a calculation is performed, the accumulated thermal expansion behaves mathematically as though it were an irreversible inelastic strain.) The difference between the total and inelastic strains is then substituted for the elastic strain in Hooke's law.

A representative computation (see figure) begins with the entry of data on the geometry, forces, temperatures, and properties of the materials, for use in calculating the elastic and thermal stresses on elements of the structure. The computed stresses in each element are inserted in the applicable creep law to determine whether they are sufficient to make that element creep. If the element is found to creep, then its creep strain during a specified interval is calculated on the basis of the creep law, which specifies the rate of creep as a function of the stress and temperature. The interval is the increment of time that is chosen to be short enough to enable the solution to converge to acceptably accurate values.

The creep strain in each creeping element is then converted to an equivalent fictitious component of thermal strain — preferably by adjusting the coefficient of thermal expansion. In the case of a transient problem, at this instant different temperatures and forces are submitted, and a new set of stresses in the elements is computed for comparison with the creep laws. Additional creep strains are compiled and converted to additional fictitious thermal expansions so that the cycle can be repeated for more increments of time. By this iterative process, the operating stresses and changes in operating stresses with time are identified.

The total residual stress caused by creep at the end of a given number of increments of time is computed from the cumulative creep strains of the individual elements. First, the structure is treated as being at a uniform temperature. Next, the coefficients of thermal expansion of the creeping elements are altered to simulate the cumulative creep strains previously computed for those elements. Finally, the altered coefficients are submitted as new inputs so that the residual creep stresses are calculated as though they were the result of elastic strains.

This work was done by Jerald Jenkins of **Ames Research Center**. *Further information may be found in NASA TM-86813 [N87-23995], "Inelastic Strain Analogy for Piecewise Linear Computation of Creep Residues in Built-Up Structures."*

Copies may be purchased [prepayment required] from the National Technical Information Service, Springfield, Virginia 22161, Telephone No. (703) 487-4650. Rush orders may be placed for an extra fee by calling (800) 336-4700.

ARC-12142

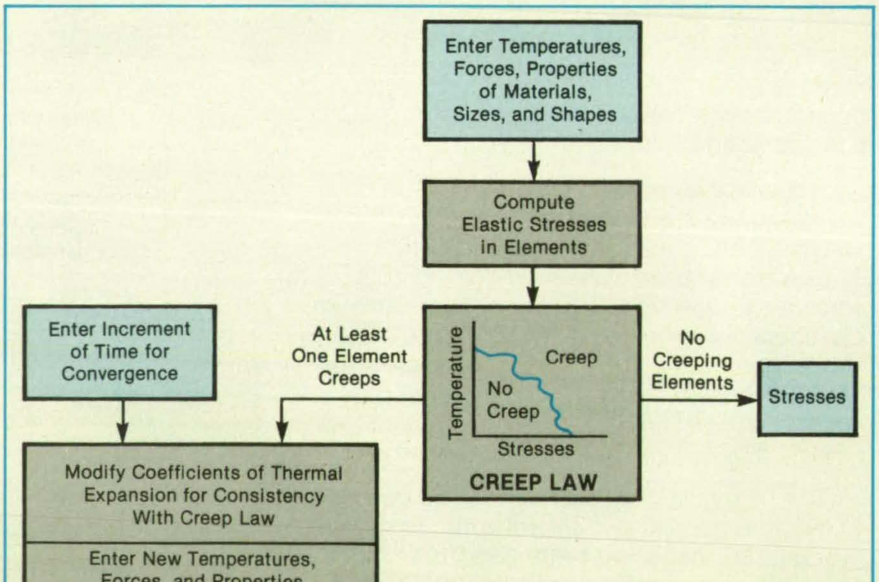

Creep Stresses in a structure are computed in an iterative process in which cumulative creep strains are treated as fictitious changes in coefficients of thermal expansion.

Never out of uniform.
GAF CARBONYL IRON POWDERS
GAF's Carbonyl Iron Powder particles are pherical in shape and, within any given roup, uniform in size distribution, from microns to 10 microns
The only ones that are domestically nanufactured, GAF's Carbonyl Iron Powders find ready and broad utility in he aerospace industry in coatings and dvanced composites. In addition, their vide range of uniform particle sizes, xcellent high frequency absorption, and lectromagnetic interference properties ecommend them for use in other aero- pace applications as well.
GAF's Carbonyl Iron Powders get along famously with plastic resins, and other metals & alloys, too, like tungsten, copper and bronze. Composites with improved properties are made more easily and economically, usually with no need for additional pre-processing.
If you think GAF's Carbonyl Iron Powders may fit into your plans, our Advanced Technology and Materials Group is available for developmental work on customers' aerospace applications.
All iron powders may look the same. But GAF Carbonyl Iron Powders are always in uniform.
See for yourself. For a free sample and literature, call or write: GAF Chemicals Corporation, Organometallics and Metals Group, 1361 Alps Road, Wayne, NJ 07470. (201) 628-3000.
©Copyright 1987 GAF Chemicals Corporation
GAF®
Where specialties are on the move
Circle Reader Action No. 404

Dynamic Delamination Buckling in Composite Laminates

A finite-element computer program performs a linear buckling analysis at each time step.

Lewis Research Center, Cleveland, Ohio

Under impact loading, composite laminates are subject to dynamic local delamination and buckling, with consequent loss of both stiffness and strength. A procedure for the mathematical modeling of dynamic delamination buckling and propagation of delamination, with plate bending elements and multipoint constraints, has been developed and incorporated into a finite-element computer program. The program predicts the time at which delamination buckling occurs, the shape of the dynamic-buckling mode, and the strain-energy-release rate due to the extension of the delamination crack. The method could be extended to handle such other defects as transply and edge cracks.

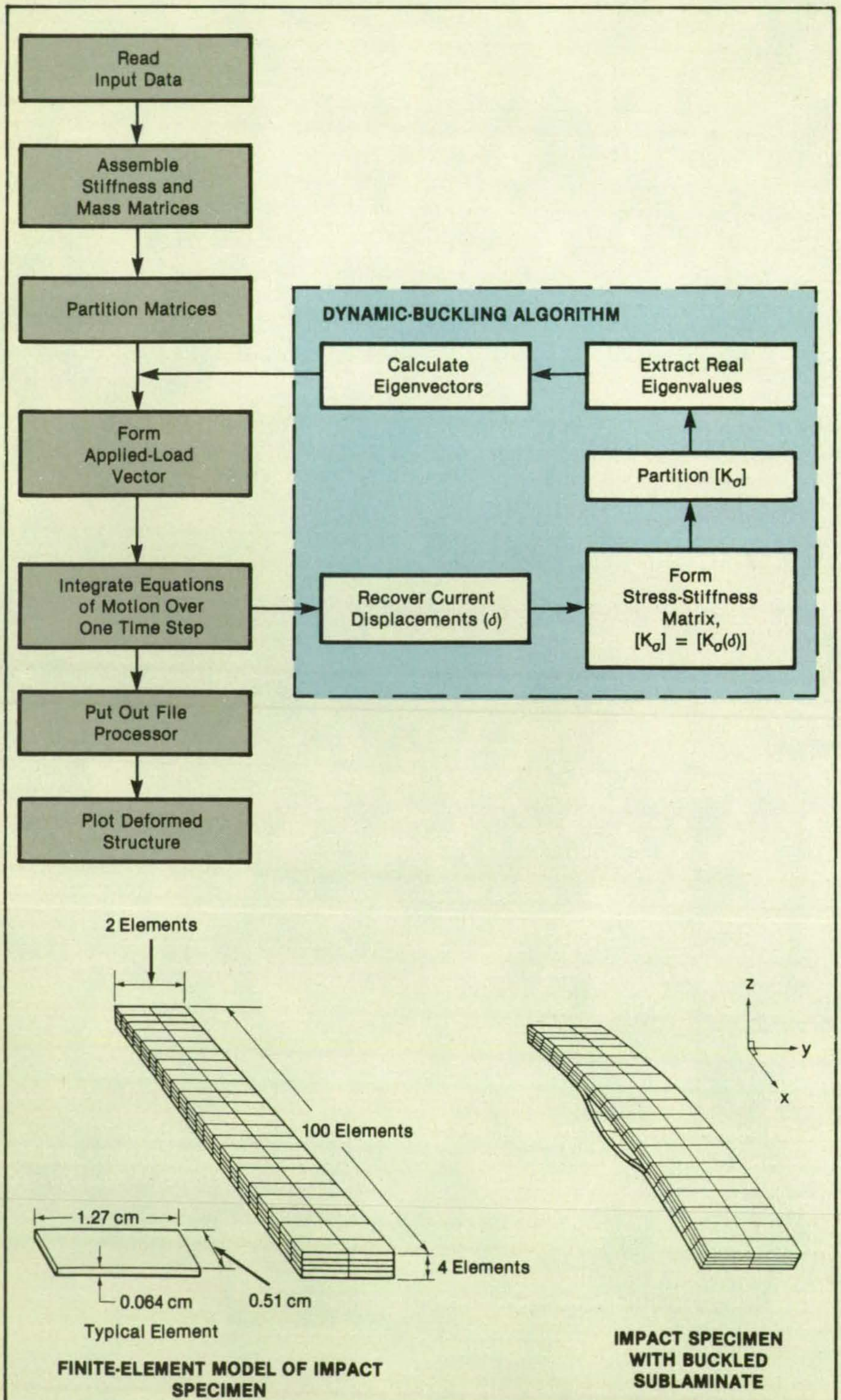

Figure 1. A **Dynamic-Buckling Algorithm** is added to a finite-element-analysis program to model dynamic local delamination and buckling in composite laminates subjected to impact loads.

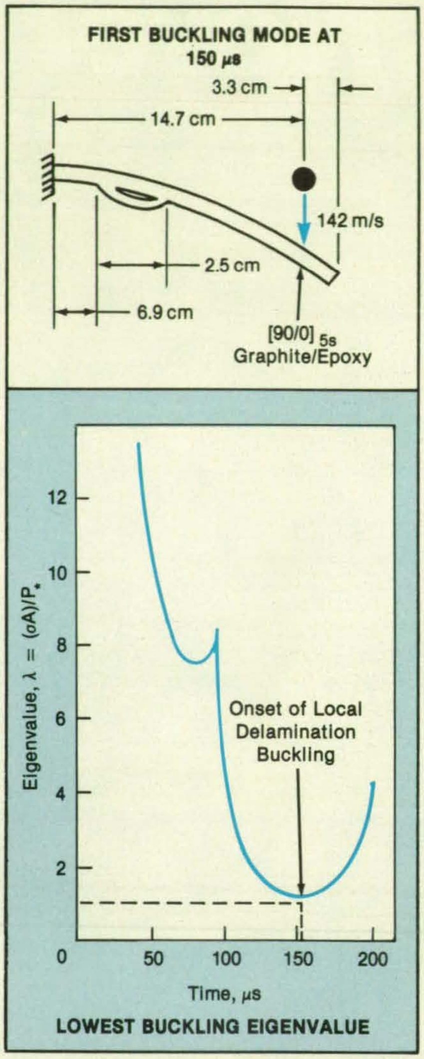

Figure 2. In a **Cantilevered Laminate Specimen** with an initial delamination, the lowest eigenvalue reached unity at 150 μs, indicating the onset of buckling.

The direct time-integration solution sequence in the finite-element program MSC/NASTRAN, Version 65A, is altered so that a linear buckling analysis is performed at each time step (see Figure 1). The buckling analysis requires the solution of the eigenvalue equation

$$[K] + \lambda[K_\sigma] \quad \{\phi\} = 0$$

where $[K]$ is the structural-stiffness matrix and $[K_\sigma]$ is the stress-stiffness matrix. Each scalar eigenvalue that satisfies this equation represents the dimensionless ratio

Permission of Margaret Truman Daniel

$\lambda = (\sigma A)/P_*$, where σ is the time-dependent compressive longitudinal stress in the delaminated sublaminate, A is the cross-sectional area of the sublaminate, and P_* is the critical compressive load that will make the sublaminate buckle. When such an eigenvalue falls to unity, buckling occurs in the mode, the shape of which is described by the corresponding eigenvector $\{\phi\}$.

The propagation of the initial delamination is modeled by removing, at the appropriate nodal points, the constraints that prevent the elements of neighboring plies from penetrating or separating from each other. This procedure increases slightly the total number of degrees of freedom while keeping the number of elements and the element mesh in the finite-element analysis constant as the delamination crack extends, but it greatly simplifies the simulation of the extension of the crack.

Numerical simulations of transverse impact loading of a unidirectional-laminate beam rigidly supported at both ends show that delaminations near the outer surface are susceptible to dynamic buckling and buckling-induced propagation. In the absence of reflections of flexural waves from the ends and/or the supports, transverse impact at a point near a delamination causes the delamination to propagate toward the point of impact, with little or no extension in the opposite direction.

The validity of the method has been tested experimentally by using it to predict buckling in a cantilevered specimen for which experimental data were available (see Figure 2). The calculated onset of delamination at approximately 150 μs after the beginning of impact is in reasonable agreement with data from high-speed photography, which showed that the buckling of the delamination and the initial extension of the crack started between two frames taken 125 and 187.5 μs after the beginning of the impact.

This work was done by Joseph E. Grady, Christos C. Chamis, and Robert A. Aiello of **Lewis Research Center**. *Further information may be found in NASA TM-100192 [N87-28611], "Dynamic Delamination Buckling in Composite Laminates Under Impact Loading: Computational Simulation."*

Copies may be purchased [prepayment required] from the National Technical Information Service, Springfield, Virginia 22161, Telephone No. (703) 487-4650. Rush orders may be placed for an extra fee by calling (800) 336-4700. The report is also available on microfiche at no charge. To obtain a microfiche copy, Circle 102 on the TSP Request Card.
LEW-14745

Capillary-Pumped Heat-Transfer Loop

A new system offers advantages of a heat pipe without its limitations.

Marshall Space Flight Center, Alabama

A new type of capillary-pumped heat-transfer loop primes itself at startup; it needs no external pumps for priming the working fluid. The new loop can remove substantial quantities of heat like that generated by people and equipment in rooms and vehicles. A demonstration unit removes heat loads as high as 2 kW. It ap-

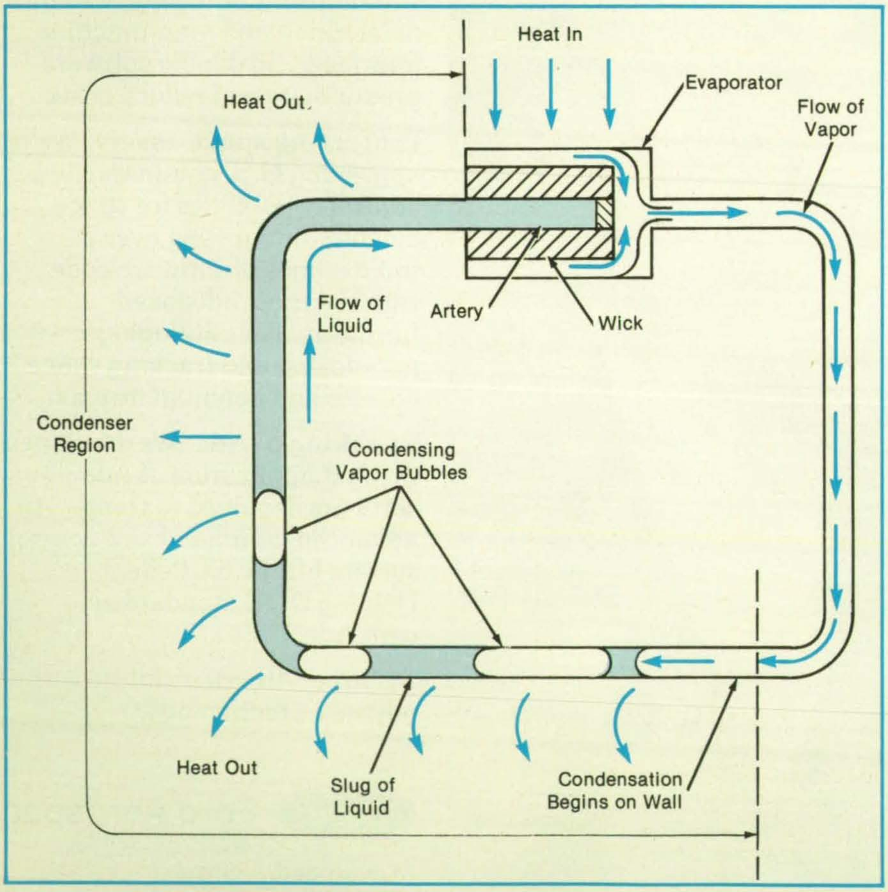

Figure 1. A **Capillary-Pumped Loop** creates a continuous path for its working fluid (water); both vapor and liquid move in the same direction. A key element in the operation of the loop is the formation of slugs of liquid, condensed from vapor and moved along the loop by vapor bubbles before and after it.

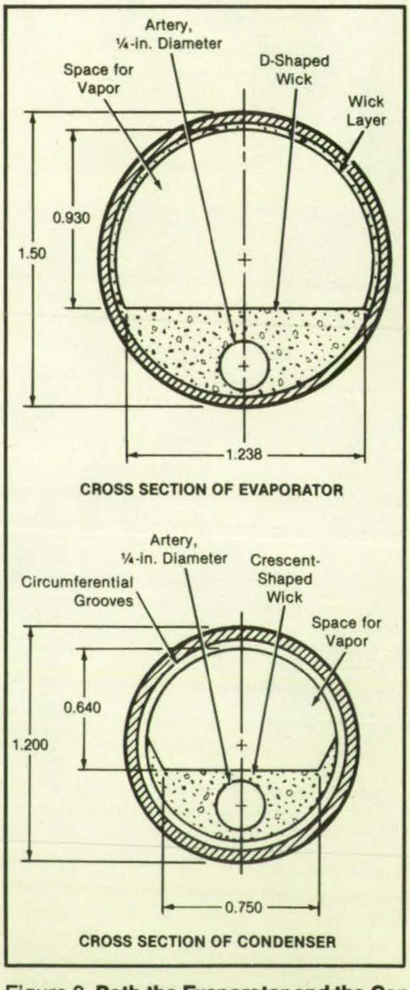

Figure 2. **Both the Evaporator and the Condenser** contain axial arteries that carry water. Heat entering the evaporator from the heat source provides the energy for the transport of fluid and heat. Dimensions are in inches.

pears feasible to enlarge the system to handle as much as 50 kW.

Unlike in a heat pipe, the liquid and vapor in a capillary loop do not flow in opposite directions in the same section of pipe but instead flow in the same direction around the loop. Furthermore, the wick occupies only the evaporator and condenser sections and not the full length of the tube as in a heat pipe (see Figure 1). The working fluid evaporates from the surface of the wick, which is heated by the load. In the new loop, the working fluid is water, and the wick and tubing are made of titanium.

The water vapor moves along the loop to a region of lower temperature, where it begins to condense. At first, the condensate forms a ring around the inside of the pipe and is dragged along the pipe by the flowing vapor. Eventually the mass of the condensate grows large enough so that surface tension forces the condensate to bridge the diameter of the pipe, forming a slug of liquid.

The slug behaves like a piston in a cylinder. The pressure of the vapor behind the slug pushes it along, and the partial vacuum of the condensing vapor before the slug pulls it along. Liquid pistons make it possible for capillary-pumped loops to carry large quantities of heat over long distances. The heat-transport distance is 1 m in the demonstration unit and is expected to be 10 m in a scaled-up unit.

A conventional capillary-pumped loop requires an external pump to feed working fluid to the evaporator when heat exchange is started. The new evaporator, however, is designed so that water never boils away from it completely. It always retains enough liquid water to start the heat-exchange cycle. It is fully passive, deriving its power from the heat load. It is also highly reliable because pumps and valves are eliminated.

The evaporator in the new unit consists of a thin-walled titanium tube, lined with a sintered powdered titanium wick at the top of its cross section and with a D-shaped block wick of the same material at its bottom (see Figure 2). Extending axially through the block wick is an artery for liquid water.

The condenser is a titanium tube with circumferential grooves to aid the transfer of heat from the vapor. A crescent-shaped block wick — also of sintered titanium — collects the condensate. An artery in the wick carries the condensed water to the tube that leads to the evaporator.

This work was done by Thermacore, Inc., for **Marshall Space Flight Center**. *For further information, Circle 57 on the TSP Request Card.* *MFS-27196*

Expansion Valve With Temperature-Sensitive Flow Regulation

A variable-area orifice adjusts the flow of cryogenic vapor.

John F. Kennedy Space Center, Florida

A Joule-Thomson expansion valve is designed so that particles or condensed contaminants in the vapor flowing through it are unlikely to clog its orifice. In addition, the new valve automatically adjusts the flow of the vapor; it allows a high initial flow for rapid cooling, but gradually reduces the flow as the operating temperature is reached. The flow can also be adjusted manually when necessary.

The valve was developed for the expansion of high-pressure vapors to condense them into low-pressure cryogenic liquids. The valve could be used, for example, to conserve helium coolant in a superconducting system by condensing the vapor boiling from a liquid-helium bath.

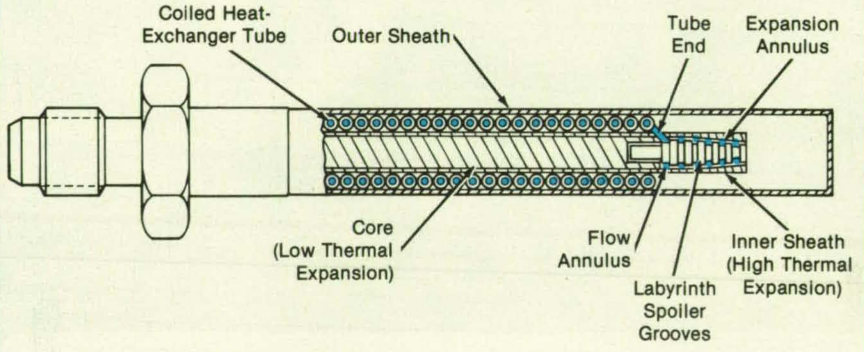

Cryogenic Vapor Flows Through a Coiled Tube and into an annulus, where it expands and condenses. In flowing through the tube, the vapor cools the supporting core and its sheath. Because the sheath contracts thermally more than the core does, the flow area of the annulus is gradually reduced.

In a conventional small Joule-Thomson nozzle, the apertures are so fine that they soon become blocked by condensed contaminants in the expanding medium. In the new valve, however, expansion takes place in an annulus rather than in a single circular hole (see figure). The annulus provides a relatively-large peripheral surface for a small cross-sectional flow area, so that complete clogging by particles is less likely than in the case of fine apertures. In addition, grooves in the annulus region serve as reservoirs for particles, further reducing the possibility of clogging.

The automatic flow adjustment of the new valve results from the carefully chosen coefficients of thermal expansion of the valve components. The core of the valve is made of glass-reinforced epoxy resin, which combines a low coefficient of expansion with a low thermal conductivity. Covering the core is a sheath of aluminum, which combines a high coefficient of expansion with a high thermal conductivity. The sheath tapers at the grooved tip of the core, forming the annulus. At startup, the cross-sectional area of the annulus is at a maximum, and the mass flow of the fluid is high. As the sheath and core are cooled by the medium, which flows around them through a coiled tube, the sheath contracts more than the core does, becoming both shorter and smaller in diameter. It thus reduces the cross-sectional area of the annulus and reduces the flow.

The valve is equipped with a locking micrometer with which the operator can manually vary the initial flow or make fine adjustments in the steady-state flow. This feature allows the same nozzle to be used over a range of flow rates and in a variety of applications.

This work was done by Graham Walker and Kelly Hedegard of General Pneumatics Corp. for **Kennedy Space Center**. *For further information, Circle 41 on the TSP Request Card.*

In accordance with Public Law 96-517, the contractor has elected to retain title to this invention. Inquiries concerning rights for the commercial use of this invention should be addressed to

General Pueumatics Corporation
7662 E. Gray Road, Suite 107
Scottsdale, AZ 85260

Refer to KSC-11372, volume and number of this NASA Tech Briefs *issue, and page number.*

Inframetrics infrared imaging: to see, to quantify, to understand.

ThermaGRAM® image of an automotive brake rotor.

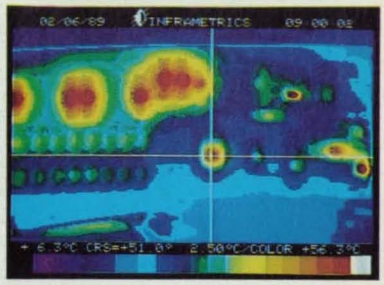

Model 600 provides spot temperatures of components on PC board. Line scan profiling, isotherm contouring and area measurement are all standard, without computer interface.


Model 600 on the lab bench...stalwart of sophisticated radiometers.

Whether you're looking for pressure leaks in an aircraft fuselage or fluid ingress in the flaps; electrical system hot spots or excessive bearing friction; delamination in composite structures or shorts in a multilayer printed circuit board...the infrared diagnostic technology of Inframetrics systems will quickly give you the answers you need.

Our concentration on *practical infrared imaging and temperature measurement* — the delivery of useful results, under real-world conditions, at reasonable prices — has made us a leader in infrared imaging radiometers, and producers of the widest variety of thermal imaging instruments in the world.

TV-compatible, compact and field-portable, Inframetrics Imaging Radiometers and Thermal Imagers provide real time imagery with excellent picture quality for the *highest total performance* commercially available today. Combine these capabilities with the most versatile image-processing system in the market; ThermaGRAM® performs histogram analysis, time vs. temperature studies, real time image analysis, and countless other functions.

Just consider the possibilities.

Inframetrics systems adapt to a wide variety of applications, including R&D, nondestructive testing, electronic diagnosis, quality control, facilities maintenance and medicine.


A complete system, cart-mounted, with optional VCR and Polaroid hard copy system, goes anywhere.

Model 445 high resolution thermal imager shows delamination in a composite panel. Ideal for qualitative analysis, nondestructive testing, security systems, more.

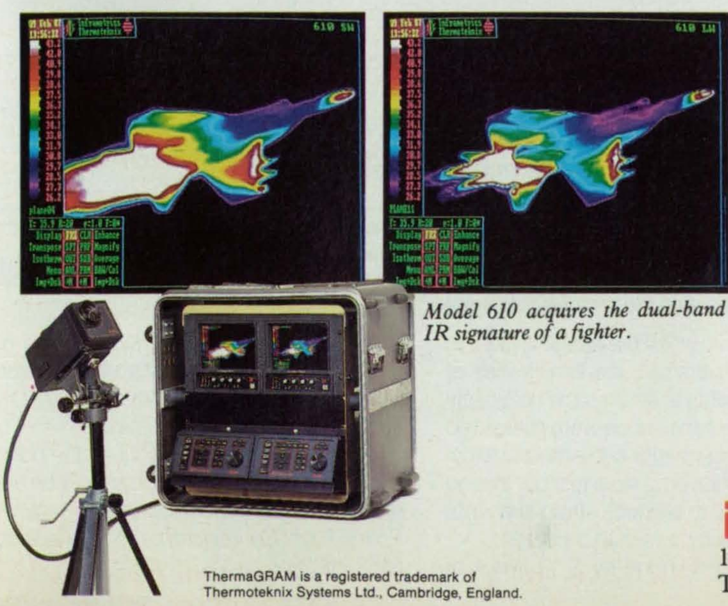
Model 610 acquires the dual-band IR signature of a fighter.

Inframetrics systems open the door to another engineering perspective on your problems. To learn more, tell us your application.

inframetrics The Infrared Specialists

16 Esquire Rd., No. Billerica MA 01862-2598 *Offices worldwide*
TEL 508-670-5555 • FAX 508-667-2702 • TWX 710-326-0659

Circle Reader Action No. 370

High-Temperature Strain-and-Temperature Gauge

A two-element gauge is used alternately in two different bridge circuits to measure both temperature and strain.

Marshall Space Flight Center, Alabama

A three-lead strain-and-temperature gauge of a type that has fallen into disuse in recent years has been developed for use at temperatures up to 750 °F (390 °C) on a fiber-reinforced carbon/carbon composite material that has a coefficient of thermal expansion of 0.8 ppm/°F (1.4 ppm/°C). Unlike most temperature-compensated gauges, the outputs of which show hysteresis, this gauge gives accurate results even during rapid heating and cooling cycles. Similar gauges of this type can be produced for materials with different coefficients of thermal expansion.

The total strain in a material includes mechanical strain due to stress plus apparent strain due to thermal expansion. To measure mechanical strain, it is necessary to compensate for the purely thermal component in the output of a strain gauge. This gauge comprises two wire sensing grids, the temperature coefficients of electrical resistance of which have opposite signs (see figure). The wires of the two grids are selected to have temperature coefficients of the proper magnitudes to provide changes of resistance with temperature that are equal in magnitude but opposite in sign when the gauge is bonded to the carbon/carbon or other substrate material. To measure strain, the two elements are connected in series and connected as one arm of a Wheatstone bridge, so that the strain components of the outputs of the two grids are added in the overall output signal while the components due to temperature cancel each other in the overall output. To measure temperature, the gauge is used as a three-terminal device forming half of a Wheatstone bridge: In this configuration, the temperature components are added together while the strain components cancel each other.

The elements of the gauge are made of Hitec K- (or equivalent) alloy wire. Annealed K-alloy wire, which has a high positive temperature coefficient of electrical resistance, is used for one element. K-alloy wire can be treated to produce a negative temperature coefficient of the desired magnitude for the other element. In this case, the negative element is treated so that it would be temperature-compensated if used along with a material that has a coefficient of thermal expansion of 6 ppm/°F (10.8 ppm/°C). This combination of alloys turns out to be closely temperature-compensated for use with the composite material of interest.

To minimize the component of output due to applied strain when the gauge is used to measure temperature, the sensitivities of the two elements to strain must be closely matched. The sensitivities were measured with the two elements cemented side-by-side on a cantilevered steel test bar loaded at the free end to produce strain and were found to differ by less than 1 percent.

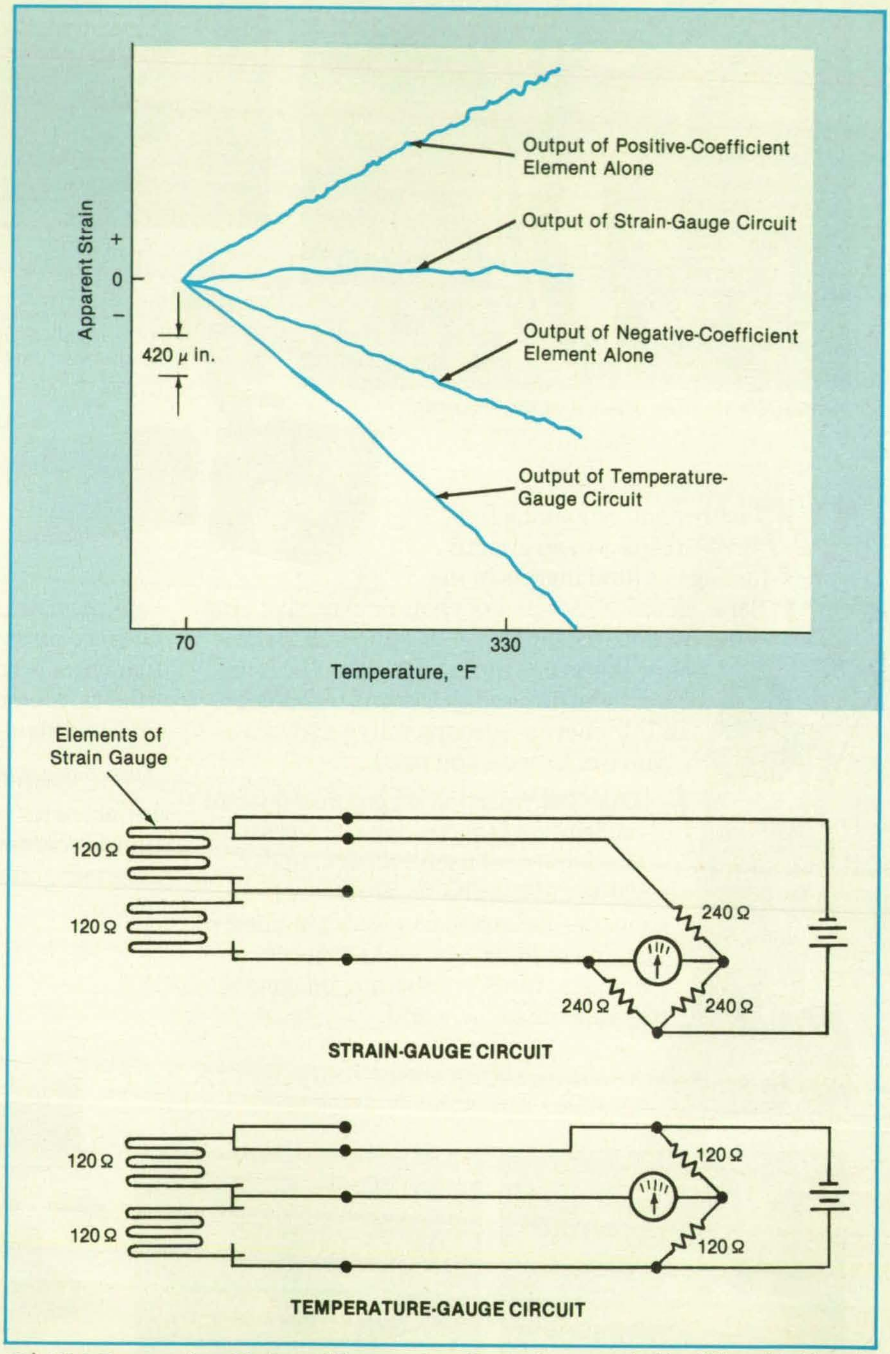

The **High-Temperature Strain-and-Temperature Gauge** is connected to different bridge circuits to measure strain and temperature. The graph shows the apparent-strain outputs of the individual elements, the net (temperature-compensated) strain output with the two elements in series, and the temperature signal.

This work was done by S. P. Wnuk of Hitec Products, Inc., and S. J. Lanius of Morton Thiokol, Inc., for **Marshall Space Flight Center**. *For further information, Circle 9 on the TSP Request Card.*

Inquiries concerning rights for the commercial use of this invention should be addressed to the Patent Counsel, Marshall Space Flight Center [see page 18]. Refer to MFS-28320.

THE CHALLENGE: "MACHINE HIGHLY COMPLEX AEROSPACE COMPONENTS WITH PRECISE REPEATABILITY. AND REDUCE COSTS SIGNIFICANTLY."

We were able to meet this challenge because at Howmet we work closely with our customer-partners. Our engineer-to-engineer approach allows us to take charge from concept through prototype to finished product and provide our customers with capabilities our competitors can't match.

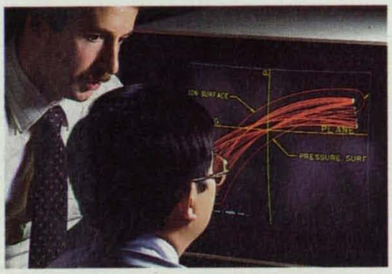

ECM equipment is integrated with customer CAD/CAM data.

GREATER DESIGN FREEDOM AND COST EFFECTIVENESS. At our New England Aircraft Products Division, in Farmington, CT, we produce airfoils up to 14″ in length by electrochemical machining (ECM). As a "stress-free" process, ECM permits thinner, more complex shapes which are otherwise extremely costly or impossible to manufacture. And our CAD/CAM technology permits your design to be duplicated precisely. With no final polishing required and a low scrap rate, manufacturing costs are reduced as much as 10%.

Howmet's Winsted Machining Center, in Winsted, CT, specializes in small to medium airfoils. Our state-of-the-art encapsulation system and CNC continuous dress creep feed grinders triple the removal rates while improving accuracy and throughput.

At Whitehall, MI, our Whitehall Machining Division specializes in medium to large airfoils and integral nozzles and rotors. We also run small lots and prototype work, offering fast turn time and low cost for special needs. Our creep feed grinders reduce machining time while increasing precision and flexibility.

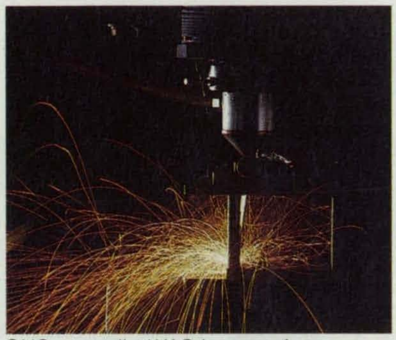

CNC-controlled YAG laser performs cutting, welding and drilling.

IMPOSSIBLE? CHALLENGE US. At Howmet, we employ the most advanced technologies to meet the strict requirements of our customer-partners. We will work closely with you, engineer to engineer, to

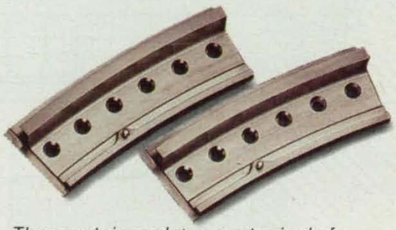

These retainer plates are typical of our precision-machined hardware.

bring your product cost-effectively from prototype work into production. For more information on our machining capabilities, write our Sales Department, Howmet Corporation, 475 Steamboat Road, Greenwich, CT 06836-1960. Or phone the Sales Manager at New England Aircraft Products Division, (203) 677-1376, Whitehall Machining Division, (616) 894-5686, or Winsted Machining Center, (203) 379-3314.

HOWMET CORPORATION

Partners. Challenge by Challenge.

New England Aircraft Products Division, Farmington, CT
Whitehall Machining Division, Whitehall, MI
Winsted Machining Center, Winsted, CT

ECM'd fan and compressor blades for P&W jet engines.

Circle Reader Action No. 335

Applying Thermal Gradients to Control Vibrations

Thermal actuators might be used to stabilize large structures.

NASA's Jet Propulsion Laboratory, Pasadena, California

Thermal gradients can be applied to a structure in a controlled way to help damp low-frequency vibrations, according to preliminary theoretical and experimental studies. Like mechanical actuators in prior experimental structural-vibration-damping systems, thermal actuators could be incorporated into structures as parts of feedback control systems that would automatically help to stabilize the structures. In some cases, active stabilization by differential heating might be preferable to pas-

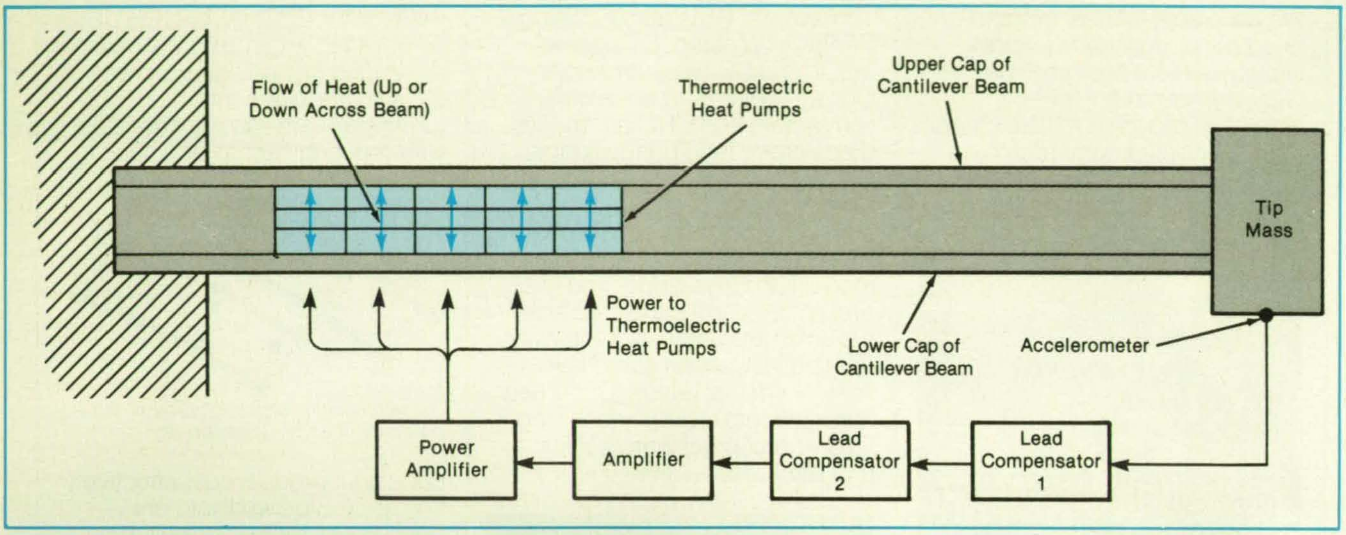

Responding to a Processed Signal From the Accelerometer, thermoelectric heat pumps apply thermal gradients that produce expansions and contractions in the upper and lower caps of the cantilever beam. These expansions and contractions partly counteract the vibrations sensed by the accelerometer, thus contributing to damping.

sive stabilization by damping or to active stabilization with suitably timed mechanical pulses.

The principle of dynamic stabilization via thermal gradients can be introduced via the example of a thermal damping phenomenon of a beam in bending vibration. As the beam deforms, the material on one side of the neutral axis is compressed and, therefore, heated slightly; the material on the other side of the neutral axis is subjected to tension and, therefore, cooled slightly. Thus, there arises a thermal gradient, which causes heat to flow from the compressed side to the tensed side. This flow of heat, which represents the conversion of mechanical to thermal energy, contributes to damping.

The new damping concept calls for the application of suitably timed and shaped thermal-gradient waveforms to generate expansions and contractions that counteract vibrations. In the system studied, the vibrating structure was a sandwich cantilever beam loaded with a mass at the end. Thermal gradients between the bottom and the top of the beam were generated by Peltier-effect thermoelectric heat pumps (see figure).

The vibrations of the beam were sensed by an accelerometer. The output of the accelerometer was fed through two lead compensators and two amplifiers, then applied to the thermoelectric heat pumps. The lead compensators and amplifiers acted as a control system that generated the proper amplitude and phase to compensate for both the natural vibrational frequency (about 2 Hz) of the loaded beam and the delays inherent in the thermal responses of the thermoelectric heat pumps and the beam. With the control system turned off, the damping ratio in the first vibrational mode was 0.81 percent. When the control system was turned on, the damping ratio increased to 7.4 percent.

This work was done by Donald L. Edberg of Caltech for **NASA's Jet Propulsion Laboratory**. *For further information, Circle 2 on the TSP Request Card. NPO-17067*

Books and Reports

These reports, studies, handbooks are available from NASA as Technical Support Packages (TSP's) when a Request Card number is cited; otherwise they are available from the National Technical Information Service.

Interaction of a Helicopter Blade With a Vortex

Measurements in a wind tunnel yield data for validation of computations.

A report describes an experimental investigation of the three-dimensional interaction of a helicopter rotor blade with a vortex like that generated by the preceeding rotor blade. The report provides theoretical aerodynamicists with data for validation of computer simulations of aerodynamic flow.

The investigation was carried out in a wind tunnel in which a vortex-generating blade was mounted vertically, and the blade under test was mounted horizontally downstream. A three-dimensional laser velocimeter measured the velocity field around the horizontal blade. Measurements of the velocity of circulation around the blade were used to calculate the spanwise distribution of lift on the blade. Mean flow velocities were measured over grids upstream of the blade. Variations of the strength and position of the vortex and of the angle of attack of the blade were examined.

The report describes the test configurations and instrumentation. It tabulates and discusses measured data. Finally, it describes and quantifies such sources of error as the effects of walls, deflections of the blade with changes in lift, unsteadiness in the position of the vortex, and instrumenta-

tion-related errors.

This work was done by Stephen Dunagan and Thomas Norman of **Ames Research Center**. *Further information may be found in NASA TM-100013 [N88-14962], "Lift Distribution and Velocity Field Measurements for a Three-Dimensional, Steady Blade/Vortex Interaction."*

Copies may be purchased [prepayment required] from the National Technical Information Service, Springfield, Virginia 22161, Telephone No. (703) 487-4650. Rush orders may be placed for an extra fee by calling (800) 336-4700.
ARC-12196

Predictive Attitude Maintenance for a Space Station

The peak angular-momentum-storage requirement is about half that of conventional reactive techniques.

A paper provides the mathematical basis for the predictive management of the angular momenta of control-moment gyroscopes (CMG's) to control the attitude of an orbiting space station. Numerical results are presented for pitch control of the proposed power-tower space station (the pitch axis is the dominant control problem for the tower). Based on prior orbit history and a mathematical model of the density of the atmosphere, predictions can be made of the requirements on the dumping and storage of angular momentum in relation to the current loading state of the CMG's and to acceptable attitude tolerances.

Numerical simulations indicate a potential for reduction in the peak angular-momentum-storage requirement of about half that of the previous reactive angular-momentum-management techniques based only on sensing present attitude errors and the present status of angular-momentum storage. These conclusions should be valid under all flight conditions since the test cases were run using the near-maximum atmospheric-density conditions of the 1971 Jacchia atmosphere model prediction for January 1, 1982, a date close to the 11-year peak of the solar cycle.

System dynamics are expressed and linearized in a manner appropriate to a large platform oriented along the local vertical or horizontal. With the simplified equations of motion, the pitch dynamics are decoupled from the other axes, but roll and yaw remain coupled. A deterministic optimal-control problem is posed with a quadratic performance index that includes, as variables, the torque loading of the space station, the CMG torque demand, and deviations of the attitude from a desired reference. These quantities are weighted with gain coefficients.

The problems of optimization of the uncoupled pitch and the roll and yaw lead to differential equations that predict the attitude. The pitch-attitude-control problem is described by a linear, constant-coefficient, fourth-order, differential equation. The coupled roll and yaw are described by a linear, constant-coefficient, eighth-order differential equation. Since both equations have only even derivatives in the homogeneous parts, the roots can be found by exact expressions.

A conceptual control-system design that includes predictive momentum management is presented in two block diagrams. The attitude predictions can be computed once per orbit. The attitude prediction includes an angular-momentum-desaturation term to prevent the unwanted large secular buildup of stored angular momentum in the future and to remove any angular momentum accrued on previous orbits as a result of unmodeled effects. A reaction control system based on thrustors would be used only for quick recovery from such large transient disturbances as those caused by docking vehicles.

This work was done by Philip D. Hattis of the Charles Stark Draper Laboratory, Inc., for **Johnson Space Center**. *To obtain a copy of the report, "Predictive Momentum Management for the Space Station," Circle 11 on the TSP Request Card.*
MSC-21216

Machinery

Hardward Techniques, and Processes

Books and Reports

Two-Pipe Heat-Transfer Loop

Liquid and vapor travel in separate tubes.

NASA's Jet Propulsion Laboratory, Pasadena, California

A device like a heat pipe transports heat over a long distance with negligible loss in temperature, though with considerably smaller total weight. The device uses no pumps or other mechanical means to move the working fluid: Instead it converts part of the available thermal energy to kinetic energy upon vaporization. The vapor carries the thermal energy in the form of latent heat of vaporization. Thus, the device can deliver thermal energy with a drop in temperature of only a fraction of a degree from the source to the sink.

Heat is delivered to an evaporator (see figure). There, the fluid evaporates from the surface of a porous structure. The surface tension of the liquid prevents the vapor from flowing into the porous structure, forcing the vapor down the vapor tube to a condenser. There, the fluid condenses on another porous structure that isolates the vapor from the liquid in the liquid tube. The liquid tube is exposed to thermal losses that cool the return fluid and assure a low vapor pressure in the return leg of the loop. Thus, the driving potential for the circulation of the working fluid is due to the temperature difference across the porous structure in the evaporator.

So that the working fluid will not condense in the insulated vapor tube as it flows from the heat source to the heat sink, the vapor is superheated and/or the vapor tube is traced with an electric heater to make up for any thermal losses from the vapor tube due to the limitations of the insulation. The amount of superheat and/or electric trace-heater power depends on the thermal loss from the vapor tube and the thermal power transfer.

This work was done by Robert Richter of Caltech for **NASA's Jet Propulsion Laboratory**. *For further information, Circle 13 on the TSP Request Card.*
NPO-17404

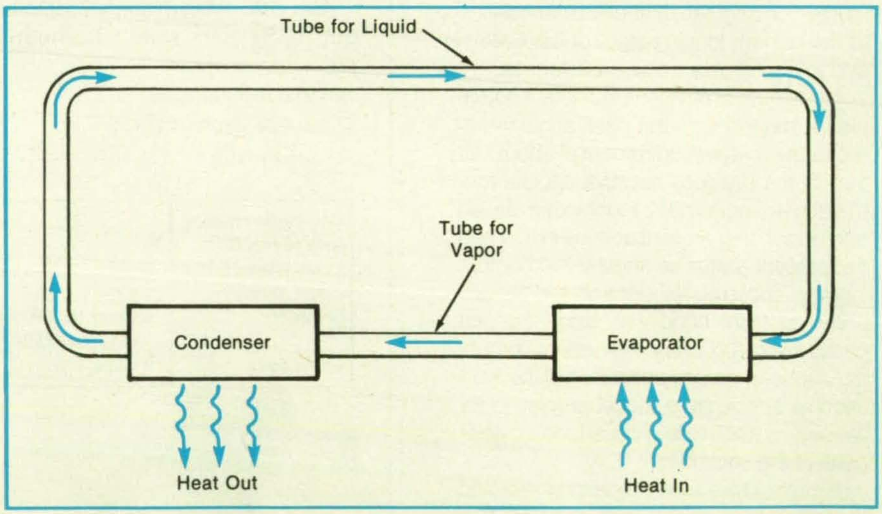

Liquid and Vapor Flow in Separate Pipes in this heat-transfer loop. A laboratory model that contained water as the working fluid was able to transfer 80 W of thermal power from the evaporator to the condenser.

Roller Bearings Survive Loss of Oil Supply

A ring holds a small emergency supply of oil.

Lewis Research Center, Cleveland, Ohio

A tapered roller bearing can operate for at least 30 min at speeds up to 11,000 r/min after its oil supply stops. The bearing was developed to enable such high-speed ma-

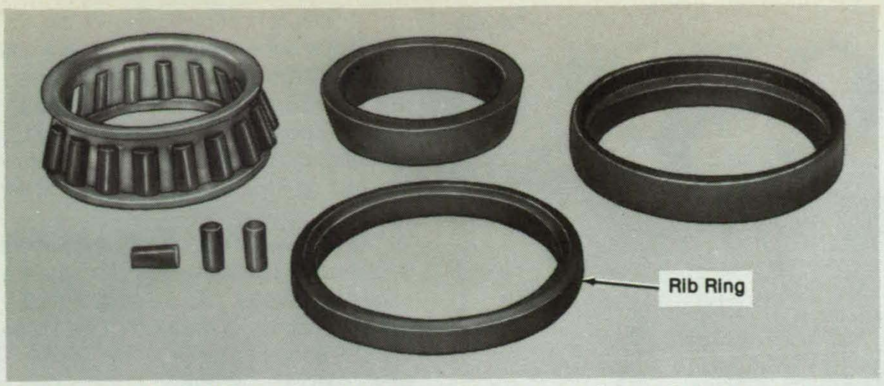

This **Bearing Was Still Operating** after 22 min without externally supplied oil at 12,000 r/min. The rib ring is made of porous high-speed steel.

chinery as a helicopter transmission to continue to operate safely when its oil pump fails.

The bearing cup includes a porous rib ring (see figure) that contains a residual oil supply to lubricate the rollers when the external oil supply is lost. The ring is made by sintering powdered metal, the pores of which hold the emergency oil. The residual oil impregnated into the ring bleeds out to the ends of the rollers by capillary action. The bleeding is initiated as the temperature of the bearing rises after the failure of the primary oil supply. The heating also squeezes oil out of the ring because the coefficient of thermal expansion of the oil exceeds that of the ring.

The critical aspects of the fabrication of the ring include the preparation of the metal powder and the final treatment of the surface. These operations determine the internal and surface porosity and, therefore, the amount of oil that can be stored and the rate at which it can be dispensed. After the ring has been compacted, sintered, and heat-treated, it is impregnated with oil. It is then ground to final shape, using a coolant to prevent retempering. To ensure that pores open into the interior of the bearing, the grinding smear that blocks the surface pores is removed by electroetching in an aqueous solution that contains perchloric acid.

Experimental bearings were evaluated at six speeds from 0.26 million to 2.4 million DN with a 65-mm-diameter tapered bearing. (DN is the product of the bearing diameter in millimeters and the angular speed in revolutions per minute.) The best results were obtained with porous rings made of CBS1000M steel at 75 percent of maximum density, which operated for the requisite half hour at speeds up to 0.72 million DN (11,000 r/min). At higher speeds, the bearings failed after decreasing intervals ranging from many minutes to a few seconds.

This work was done by G. E. Kreider and P. W. Lee of The Timken Co. for **Lewis Research Center**. *Further information may be found in NASA CR-180804 [N85-11135], "Improved Oil-Off Survivability of Tapered Roller Bearings."*

Copies may be purchased [prepayment required] from the National Technical Information Service, Springfield, Virginia 22161, Telephone No. (703) 487-4650. Rush orders may be placed for an extra fee by calling (800) 336-4700.
LEW-14749

Books and Reports

These reports, studies, handbooks are available from NASA as Technical Support Packages (TSP's) when a Request Card number is cited; otherwise they are available from the National Technical Information Service.

Zero-Gravity Fuel-Cell Product-Water Accumulator

Water is removed from the fuel cell by capillary action.

An assortment of documents describes a simple, passive system that removes water formed from the reaction of hydrogen and oxygen in a proton-exchange-membrane fuel cell. Designed for use in zero gravity, the system does not require any machinery or external source of power.

The system works by capillary action and differential pressure. Small wicks transport the product water from the oxygen sides of the cell membranes to a larger wick in contact with a filter (water-separating) plate. The filter plate retains the oxygen, and the small differential pressure of oxygen across this plate forces the water through the plate and into a channel.

From the channel, the water passes through a check valve into a spongelike sorbent material that occupies part of the volume of a detachable canister. As it absorbs water, this material expands into the remaining dry volume of the canister. A quick-disconnect flange at the end of the canister opposite the check valve facilitates the removal of the water for reuse. The water can also be discarded via a vacuum port at the end near the check valve.

To allow for expansion of the sorbent material, the pressure in the dry volume of

the canister is kept below that of the sorbent/water combination. The sorbent and canister can be sized to hold any convenient amount of water. As a preliminary guide to design, the capacity is chosen to be sufficient to hold the water accumulated during 8 h while operating at a power of 300 W.

This work was done by Thomas P. Barrera of **Johnson Space Center**. *To obtain a copy of the report, "Zero-Gravity Fuel Cell Water Storage Accumulator," Circle 112 on the TSP Request Card.*
MSC-21351

Simulator of Rain in Flowing Air

Drops are injected into slowly flowing air, which is then accelerated.

A report describes a relatively inexpensive apparatus that creates simulated precipitation from drizzle to heavy rain in flowing air. A small, positive-displacement pump and a water-injecting device are positioned at the low-airspeed end of a converging section of wind tunnel 10 in. (25 cm) in diameter. The drops injected by the array are entrained in the flow of air as it accelerates toward the narrower outlet, 15 in. (38.1 cm) downstream. The outlet is 5 in. (13 cm) in diameter.

This scheme makes it possible to furnish drops of fairly uniform size over a range of sizes in an airstream moving at a speed of 213 ft/s (65 m/s). Ordinarily, rains above the intensity of a drizzle are difficult to simulate because the high speed of slippage between the flowing air and the injected drops tends to shatter drops into smaller droplets corresponding to fogs or mists.

Nine injection tubes are fed by a common circular manifold. The water-injecting device is an array of nine hypodermic needles with an inside diameter of 0.009 in. (0.23 mm). The rate of waterflow is varied from 0.4 to 10.2 lb/h (0.05 to 1.2 g/s) to span the range from light to heavy precipitation.

The drops at the narrow (fast-flow) end of the section of wind tunnel are about 300 μm in diameter. This is more than twice the size of drops estimated from prior experimental results and correlations. However, it is smaller than the typical millimeter size of raindrops in heavy precipitation. Apparently, the apparatus produces smaller drops at a higher density than those of natural heavy rain.

This work was done by Richard M. Clayton, Young I. Cho, Parthasarathy Shakkottai, and Lloyd H. Back of Caltech for **NASA's Jet Propulsion Laboratory**. *To obtain a copy of the report, "Rain Simulation for High-Intensity Acoustic Nose Cavities," Circle 63 on the TSP Request Card.*
NPO-17237

Improving a Remote Manipulator

The latest parameters, tools, adaptations, and software are documented.

A set of three reports describes work on the Protoflight Manipulator Assembly (PFMA), a 2.4-meter remote manipulator with six degrees of freedom, counterbalanced for operation in Earth gravity. "Performance Characteristics of the Protoflight Manipulator Assembly" presents the parameters of the PFMA after a refurbishment of operating components. The document is intended to help simulation engineers understand the electromechanical responses of the manipulator arm. Data are furnished on dimensions, maximum joint travel, joint torques, mechanical backlash, voltages for releasing and resetting joint brakes, end-effector closure force, frequency response of each joint, rate scale factor for the control input to each joint, the position scale factor for the joint-angle-measuring sensors, and transient responses of the joints.

"End Effector and Task Board Development for the Protoflight Manipulator Assembly" describes special tools and adaptations that allow the PFMA to be used for servicing equipment. The tools include end-effector jaws for grasping and manipulating the equipment, an all-purpose end-effector mount that can accept special tools, and a device to connect and disconnect fluid couplings. A task board was modified by the addition of a rotating antenna, half of a fluid coupling, and a removable modular box and door. These additions enable the development of operation and simulation techniques.

"Modular Software Development for the Protoflight Manipulator Assembly" documents the interface and control software for the PFMA. It includes hierarchy charts, data-flow diagrams, a data dictionary, and logic flows, as well as a listing of the software. A section of the report details the operator choices and input requirements. It explains the prompts given to the operator by the program and the data needed to respond to the prompts. It also explains the layout of the data-base and automatic-sequence files.

This work was done by John W. Haslam, Jr., Nicholas Shields, Jr., Mary F. Fagg, and Ricardo C. Rodriguez of Essex Corp. for **Marshall Space Flight Center**. *For further information, Circle 94 on the TSP Request Card.*
MFS-27067

Fabrication Technology

Hardware Techniques, and Processes

Books and Reports

Robotic Tool for Tightening and Cutting

The tool can be used in the assembly of truss structures.

Lyndon B. Johnson Space Center, Houston, Texas

A robot end effector is designed for tightening tube couplers and for cutting tubes. Intended for use in building structures in space, the end effector can also be used as a hand tool for assembling truss structures for terrestrial buildings, tents, and oil rigs. It can also be used in place of a pipe wrench in plumbing work. The tool is operable by simple movements and thus can be manipulated by a technician wearing heavy protective clothing.

The tool reaches around an object, grasps it, locks in place around the object, and rotates the object (see figure). The tool can tighten or loosen a nut or collar in the middle of a tube, for example. The tool can also be fitted with a blade so that, when the tool rotates, it cuts into the tube.

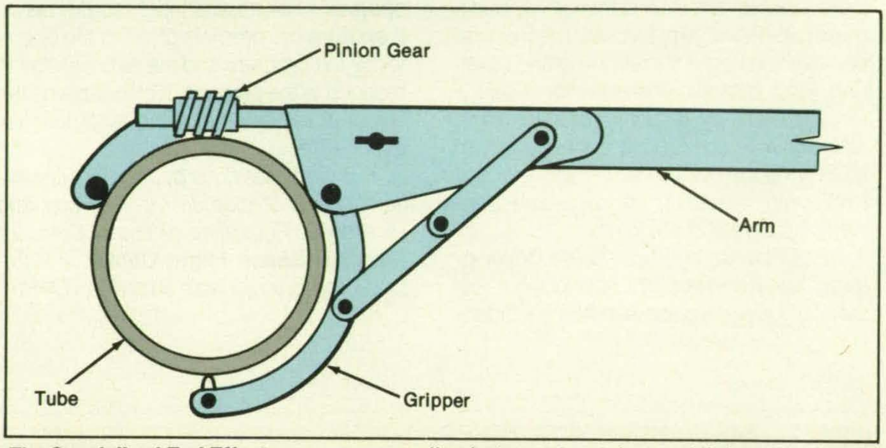

The **Specialized End Effector** grasps a coupling between two tubes and tightens it, thereby joining the tubes securely. The tool operates on the principle of a worm and pinion gear.

The tool can be used even if electrical power fails. In that case, the operator releases one of two head-attaching pins. A worm gear on the tool then acts as a pawl on a ratchet wheel, and the tool can be operated manually just like a ratchet wrench.

This work was done by Earl T. Cooney of McDonnell Douglas Corp. for **Johnson Space Center**. *For further information, Circle 14 on the TSP Request Card. MSC-21538*

Making Polymeric Microspheres

A combination of advanced techniques yields uniform particles for biomedical applications.

NASA's Jet Propulsion Laboratory, Pasadena, California

A process combines ink-jet and irradiation/freeze-polymerization techniques to make polymeric microspheres of uniform size in diameters from 100 to 400 μm. The microspheres can be used in chromatography, cell sorting, cell labeling, and the manufacture of pharmaceutical materials.

The liquid droplets are formed by a liquid-injection technique similar to that used in ink-jet printers. Liquid monomer flows through a nozzle vibrated by a piezoelectric transducer. The vibrations break the stream into droplets. The nozzle size, the flow rate, and the vibration frequency determine the droplet size and the size distribution, which can be kept within a narrow range.

The drops of liquid monomer are sprayed directly onto the surface of liquid nitrogen. The droplets freeze into an amorphous glassy phase, maintaining their spherical shape as they do so.

The frozen monomer particles, suspended in liquid nitrogen, are exposed to gamma radiation from cobalt-60. No significant polymerization occurs at the low temperature, but the particles store the free radicals created by the ionizing radiation. While the particles thaw slowly, polymerization by the radicals proceeds, and the particles solidify as spheres. The polymer molecules are only lightly cross-linked;

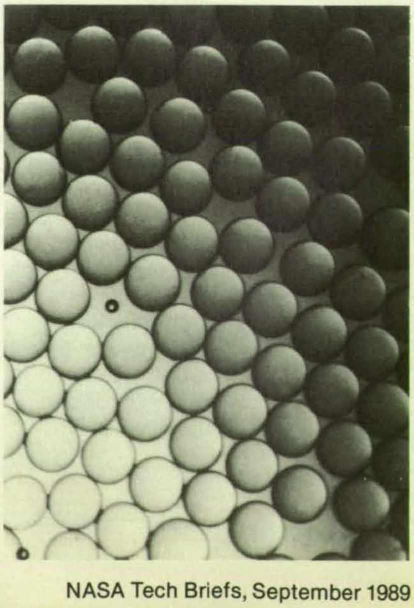

Microspheres of Polymeric Material have uniform size and shape after freezing, gamma irradiation, and slow thawing. The particles, shown here greatly magnified, are suspended in a solution of water and ethanol.

they can be further cross-linked by more gamma radiation, this time suspended in an aqueous solution at room temperature.

In a demonstration of the process, 2-hydroxyethylacrylate (HEMA) monomer was sprayed downward through an 80-μm-diameter orifice at a rate of 2.5 mL/min. A piezoelectric crystal vibrated the nozzle at 10 kHz. The resulting droplets had a diameter about twice that of the orifice. Their uniform size and formation rate was observed under stroboscopic light. The falling droplets passed through an electrode ring at 1.5 kV just below the nozzle. The ring charged the droplets so that they repelled each other as they fell instead of joining in larger globules.

The monomer HEMA droplets fell on the surface of liquid nitrogen in a bowl. The warm droplets boiled the liquid nitrogen as they impinged on it, creating a cushion of gas that supported the drops on the surface. Still charged, the floating droplets continued to repel each other and spread to the edge of the bowl where a corona discharge neutralized the droplet charge. The frozen droplets sank into the liquid-nitrogen pool.

The droplets were gently brushed into a smaller container of liquid nitrogen and exposed to gamma radiation at a rate of 0.1 Mrad/h for about 5 h. They were allowed to heat slowly at 0.2 °C/min to a temperature at which polymerization began. The resulting polyHEMA microspheres (see figure) had an average diameter of 180 μm. In some experiments, more than 95 percent of the monomer was converted to polymer.

Production rates of 10,000 spheres per second from a single nozzle are feasible. The process can be adapted to making hollow microspheres filled with gas or with biological and pharmaceutical materials.

This work was done by Won-Kyu Rhim, Michael T. Hyson, Sang-Kun Chung, Michael S. Colvin, and Manchium Chang of Caltech for **NASA's Jet Propulsion Laboratory**. *For further information, Circle 85 on the TSP Request Card.*

In accordance with Public Law 96-517, the contractor has elected to retain title to this invention. Inquiries concerning rights for its commercial use should be addressed to

Edward Ansell
Director of Patents and Licensing
Mail Stop 305-6
California Institute of Technology
1201 East California Boulevard
Pasadena, CA 91125

Refer to NPO-17023, volume and number of this NASA Tech Briefs *issue, and the page number.*

Spray Deflector for Water-Jet Machining

A cheap disk shields expensive parts from erosion.

Lewis Research Center, Cleveland, Ohio

A disk on a water-jet-machining nozzle protects the nozzle and parts behind it from erosion by deflected spray. The disk is part of the water-jet-machining unit. The water jet strikes the surface of the workpiece and rebounds toward the nozzle, impinging on the nozzle nut. The energetic water spray can wear away the nut and then attack the collet that holds the nozzle.

The disk consists of a stainless-steel backing with a neoprene facing that deflects the spray so that it does not reach the nut or other vital parts of the water-jet apparatus (see figure). Instead, the spray erodes the neoprene-rubber face of the disk. The disk is rotated to a new position from time to time to prolong its life by spreading the wear across its surface.

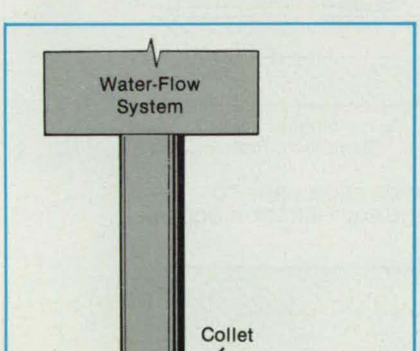

The **Deflector Disk** is a barrier between the erosive bounced jet and the nozzle nut.

This work was done by Michael A. Cawthon of **Lewis Research Center**. *No further documentation is available.*

Inquiries concerning rights for the commercial use of this invention should be addressed to the Patent Counsel, Lewis Research Center [see page 18]. Refer to LEW-14863

Compact Apparatus Grows Protein Crystals

A pair of syringes with ganged plungers produce crystals by hanging-drop method.

Marshall Space Flight Center, Alabama

A laboratory apparatus provides a delicately balanced combination of materials and chemical conditions for the growth of protein crystals. Intended for use on Earth and in the low gravitation of outer space, the apparatus and the technique for growth are based on the hanging-drop method for the crystallization of macromolecules.

The apparatus (see figure) includes a pair of syringes with ganged plungers. One syringe contains the protein solution; the other contains a precipitating-agent solution. The syringes intrude into a cavity lined with a porous reservoir material (for example, ultra-high-molecular-weight polyethylene) that is saturated with 1 mL or more of a similar precipitating-agent solution. Prior to activation, the ends of the syringes are plugged to prevent the transport of water vapor among the three solutions.

At the moment of activation, the plug is withdrawn, and then the plungers are moved to extrude the protein and precipitating-agent solutions from the syringes. The solutions mix and adhere to the joined tips of the syringes, forming a drop of 30 to 80 μL, in which the concentration of precipitant is lower than that in the reservoir material. Water begins to evaporate slowly from the drop. The water vapor is transported to and absorbed in the reservoir solution. This slow evaporation and transport continues until vapor-pressure equilibrium is reached.

As the concentrations of the protein and precipitating agent in the drop increase during evaporation, crystallization begins. Crystallization can start either before or at equilibrium. Crystallization can be hastened by local concentrations due to imperfect mixing of the two solutions, by impurities that act as nucleation sites, by a seed crystal, or by roughness on one or more of the surfaces in contact with the drop.

At the end of the time allotted for growth, protein crystals are suspended in the drop of mixed solution. To begin deactivation, the plungers are withdrawn to pull the solution and crystals back into the syringes. The plug is once again pushed against the tips of the syringes, sealing the solution and crystals inside. The solution and crystals are removed subsequently for further experimentation.

An alternative version of the crystal-growing technique involves a similar procedure, except that crystallization depends on the change in acidity or alkalinity of the drop. In this case, a volatile acid or alkaline solute (e.g., acetic acid or ammonia) is evaporated and transported instead of water.

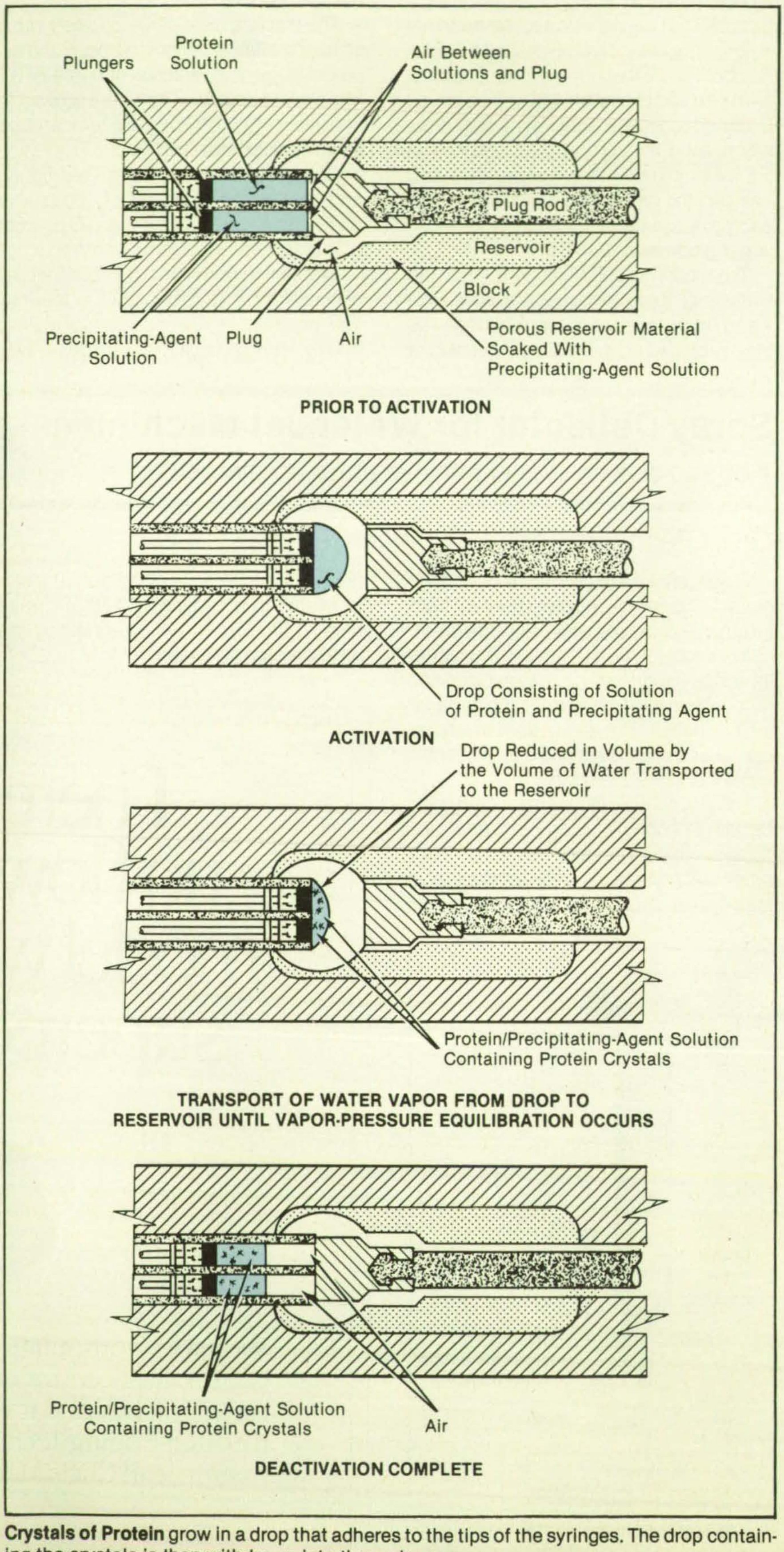

Crystals of Protein grow in a drop that adheres to the tips of the syringes. The drop containing the crystals is then withdrawn into the syringes.

This work was done by Charles E. Bugg, Lawrence J. DeLucas, Fred L. Suddath, Robert S. Snyder, Blair J. Herren, Daniel C. Carter, and Vaughn H. Yost of the University of Alabama for **Marshall Space Flight Center**. *For further information, Circle 163 on the TSP Request Card.*

Inquiries concerning rights for the commercial use of this invention should be addressed to the Patent Counsel, Marshall Space Flight Center *[see page 18]**.Refer to MFS-26088*

Making Jointless Dual-Diameter Tubes

Welds between sections that have different diameters are eliminated.

Marshall Space Flight Center, Alabama

A single tube can be made with an integral tapered transition section between straight sections of different diameters and wall thicknesses. The tube is made from a single piece; it contains no joints, welded or otherwise. It therefore is not prone to such weld defects as voids and need not be inspected for them.

The tube can be fabricated by either of two methods: drawing or reduction. In the drawing method, a straight tube is first drawn over a tapered mandrel to produce the tapered reduction in the thickness of the wall. The tube is then drawn through a series of segmented dies to reduce the diameter. The segments of a die (see figure) move together radially, under the action of a cam, as the tube passes through. The shape of the cam determines the shape of the taper in the diameter.

The inner surfaces of the die segments do not constitute a perfect cylinder until they are contracted together at the minimum diameter. To minimize out-of-roundness, the tube is rotated about its axis during drawing, and reduction in diameter by a single die is typically limited to 0.05 in. (1.3 mm). Because the tube can be annealed after any pass, it can be reduced to an extremely small diameter by several passes. The tapered section can be made as long as the dimensions of the drawbench will allow.

In the reduction method, the wall thickness and diameter are reduced in a single step by rolling the straight tube between grooved dies as it passes over a tapered mandrel. When a sufficient length of the narrower section has been produced at one end of the wider tube, the piece is removed from the rolling mill. The shape of the taper between the wide and narrow sections is determined on the inside by the shape of the mandrel and on the outside by the shape of the groove in the roller.

Because intermediate annealing is not possible in the single-step reduction method, the maximum reduction is determined by the working characteristics of the material. Usually, the smaller outside diameter cannot be less than 0.25 in. (6.4 mm). The length of the tapered section is limited by the diameter of the die rollers.

Both methods have been used to fabricate tubes of 316L corrosion-resistant stainless steel for use as a heat-exchanger coil. The wide end of the tube had an outside diameter of 0.5 in. (12.7 mm) with a wall, 0.032 in. (0.81 mm) thick, tapering to an outside diameter of 0.262 in. (6.7 mm) and a wall thickness of 0.026 in. (0.66 mm) over a transition section 10 in. (25.4 cm) long. A wide variety of wide and narrow tube sizes and taper lengths is possible, depending on the tube material and on the tapering method.

This work was done by Kathleen E. Kirkham of Rockwell International Corp. for **Marshall Space Flight Center**. *For further information, Circle 157 on the TSP Request Card.*
MFS-29004

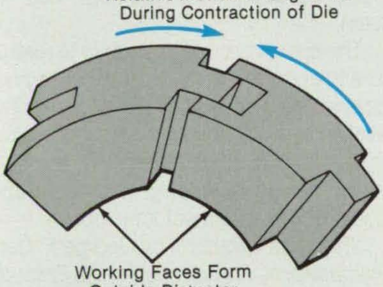

TWO ADJACENT SEGMENTS OF AN EIGHT-SEGMENT DRAWING DIE

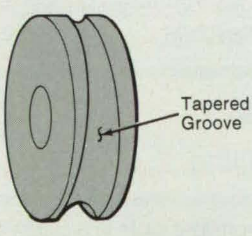

DIE ROLLER FOR REDUCTION METHOD

Alternative Methods of creating a taper between wider, thicker-walled and narrower, thinner-walled sections of tube employ contracting die segments, two of which are shown at left, or a tapered-groove roller (right). In either case, the tube is rotated around a tapered mandrel inside the tube to reduce the thickness of the wall.

Intelligent Welding Controller

A control system would adapt to changing design requirements and operating conditions.

Marshall Space Flight Center, Alabama

A proposed control system for gas/tungsten arc welding would require only that an operator specify such direct parameters of welds as widths and depths of penetration. From this information, the controller would drive a welding robot to produce welds that meet specifications. In contrast, the operator of a typical conventional welding controller must provide values of such indirect parameters as currents, voltages, and speeds and hope that they would yield welds that have the required geometries. The proposed control system would calculate the indirect parameters from the direct parameters.

The equipment and computer programs of the system would be divided into a controller domain and a supervisor domain (see figure). The controller domain would contain mainly components tightly bound to the welding process; for example, sensors and mathematical models. While welding is in progress, sensors would measure some of the direct parameters of the weld, while mathematical models would estimate the values of parameters that could not be measured. Comparators would produce error signals in the form of differences between the measured and estimated values of the direct parameters and the corresponding design values of parameters supplied by the user.

A multivariable controller would use the error signals to produce control signals, which would tend to reduce the errors. The number of input variables to the controller should exceed or equal the number of the output variables, which are control signals for the indirect parameters of the weld. These control signals would be fed simultaneously to the welding equipment and to a mathematical model that would simulate the dynamics of the weld puddle.

The portion of the system in the supervisor domain would adaptively tune the mathematical models, control algorithms, and other components in the controller domain, and would restructure the system when appropriate. In addition, it would maintain and update information on the welding process for later use, communicate with users, and perform other general tasks.

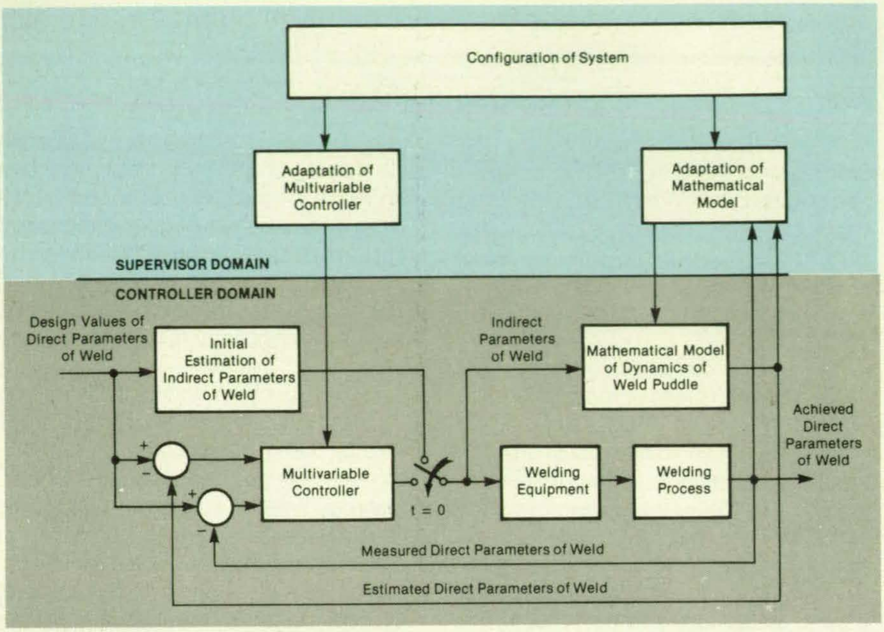

In the **Control System for a Robotic Welder**, components and functions intimately connected with the welding process would be assigned to the controller domain. More general functions would be assigned to the supervisor domain. The initial estimate of indirect parameters of the welding process would be applied to the system only at the beginning of a weld ($t = 0$); after the start of welding, outputs from the multivariable controller would take the place of the estimate.

Tuning (which would be done before welding operation) would be an iterative process in which the measured direct parameters would be compared to corresponding values of those parameters calculated by models, and the internal parameters of the models would be adjusted until the calculated and measured values would coincide. Because tuning would have to be carried out in a context of environmental conditions and other factors known only at a high level in the system, adaptation of the multivariable controller would be assigned to the supervisor domain.

The supervisor might choose to restructure the control system when welding conditions changed in such a way that another available model became more accurate than the one in use. Such restructuring would be done quickly so that welding could continue without interruption.

This work was done by George E. Cook, Ramaswamy Kumar, and Tanuja Prasad of Vanderbilt University and Kristinn Andersen and Robert J. Barnett of Mid-South Engineering, Inc., for **Marshall Space Flight Center**. *For further information, Circle 37 on the TSP Request Card.*
MFS-27195

Bonding Gauges to Carbon/Carbon Composites

Thermal-expansion properties are modified to prevent bonds from failing.

Marshall Space Flight Center, Alabama

A proposed transition layer would be deposited between a substrate and a strain or temperature gauge to be bonded to the substrate. The layer is intended particularly for gauges that must operate at temperatures above 600 °F (320 °C) and substrates like fiber-reinforced carbon/carbon composites, which are difficult to bond. The transition layer would reduce the stress caused by the difference between the thermal expansions of the gauge and substrate materials. Without the transition layer, the stress often weakens or breaks the bond.

The following process was proposed to deposit a transition layer on a carbon/carbon material that consists of graphitized rayon-fiber cloth in a glassy carbon matrix processed to 1,500 °C: The material is first cleaned in methanol and baked at 100 °C for 1 h to drive out hydrocarbons and unpyrolized phenolic resin. The surface on which the strain gauge is to be placed is cleaned by radio-frequency sputtering in argon. The sputtering removes a layer 50 Å thick and removes such contaminants as water vapor, oxide layers, and any

residual hydrocarbons.

A film of 80 percent nickel, 20 percent chromium 1,000 Å thick is deposited on the surface by radio-frequency sputtering in argon. Then a beam of argon ions is directed onto the surface at a kinetic energy of 90 keV to mix the nickel/chromium film and drive it into the substrate. The dose is 10^{17} ions/(cm)^2.

The surface is once again sputter-cleaned to a depth of 50 Å, and a nickel/chromium layer 5 μm thick is sputtered onto the surface as a protective layer for subsequent steps. The surface is masked so that only the gauge area is exposed, and the area is plasma-arc-sprayed with 80 percent nickel and 20 percent chromium to a thickness of 0.003 in. (0.076 mm). Next, a transition layer of half nickel/chromium, half aluminum oxide is plasma-arc-sprayed onto the surface. Finally, an insulating layer of aluminum oxide is rod-flame-sprayed onto the transition surface. The next step would be the attachment of the gauge.

This work was done by M. M. Lemcoe, for **Marshall Space Flight Center**, *A. H. Deutchman of Beam Alloy Corp., R. G. Brasfield of Morton Thiokol Corp., and D. E. Crawmer of Battelle Columbus Laboratories. For further information, Circle 132 on the TSP Request Card.*

Inquiries concerning rights for the commercial use of this invention should be addressed to the Patent Counsel, Marshall Space Flight Center [see page 18]. Refer to MFS-28315.

Making Large Composite Vessels Without Autoclaves

Differential thermal expansion provides the requisite pressure.

Marshall Space Flight Center, Alabama

A method for making a fiber-reinforced composite structure relies on heating and differential thermal expansion to provide the temperature and pressure necessary to develop full strength, without having to place the structure in a large, expensive autoclave. The method is suitable for such cylindrical structures as pressure vessels and tanks. It can be used for both resin-matrix (such as graphite-reinforced epoxy) and metal-matrix (such as graphite-reinforced aluminum) composites.

A layer of thermally expansive material such as aluminum surrounds a release layer on a mandrel (see figure). The uncured composite is wrapped tightly around the aluminum layer, separated from it by a thin layer of polytetrafluoroethylene or other nonsticking material so that the composite can later be easily released from the mandrel. A tight wrapping of graphite filaments surrounds the composite, separated from it by another layer of polytetrafluoroethylene.

As the assembly is heated, the aluminum expands about 22 times as much as the graphite-filament wrap does. Thus, the composite is squeezed between the aluminum and the graphite wrapping. For example, heating layers of aluminum, graphite/epoxy composite, and graphite wrap — each 0.25 in. (0.6 cm) thick on a mandrel 19 in. (48 cm) in diameter — through a temperature rise of 350 °F (194 °C) would create a pressure of about 790 lb/in.^{2} (5.5 MPa) in the composite layer. The pressure can be increased or decreased by increasing or decreasing the thickness of the expansion layer.

The assembly could be heated in an oven. Alternatively, if the structure is very large, electromagnetic induction from conductive coils around the assembly could heat the graphite-filament wrapping. Supplemental heating can be furnished by resistance elements within the mandrel.

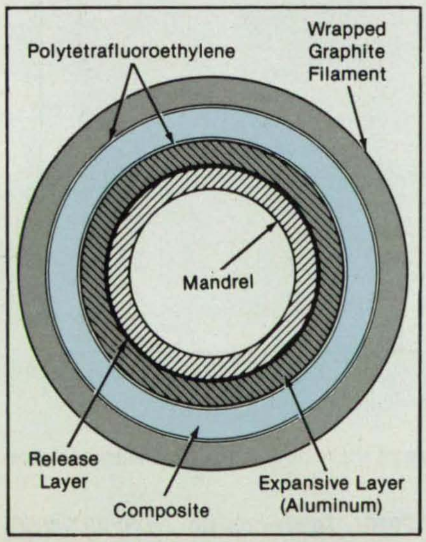

Layers of Differentially Expanding Material squeeze a fiber-reinforced composite between them when heated.

This work was done by W. A. Sigur of Martin Marietta Corp., for **Marshall Space Flight Center**. *For further information, Circle 104 on the TSP Request Card.*

Inquiries concerning rights for the commercial use of this invention should be addressed to the Patent Counsel, Marshall Space Flight Center [see page 18]. Refer to MFS-28390

Screen-Printed $YBa_2Cu_3O_{7-x}$ Films on Alumina

Superconducting films are made in a relatively simple process.

Lewis Research Center, Cleveland, Ohio

Thick films of $YBa_2Cu_3O_{7-x}$ superconductor have been deposited on highly-polished alumina substrates by screen printing. In addition to simplicity, the screen-printing technique offers the advantage that patterns for electronic and microwave circuits and devices can be printed directly, without additional etching steps.

The experiments on the screen-printing technique began with the preparation of the $YBa_2Cu_3O_{7-x}$ powder by solid-state reaction between Y_2O_3, $BaCO_3$ and CuO powders. The $YBa_2Cu_3O_{7-x}$ powder was then passed through a 500-mesh screen and mixed thoroughly with an organic vehicle to form a paste. The paste was then printed directly on the highly-pure alumina substrates through 325-mesh screens, some of which were stainless steel and some of which were silk.

The substrate-and-paste specimens were heated at 5 °C/min to various sintering temperatures from 900 to 1,000 °C, where they were held for various intervals from 5 min. to 4 h. The specimens were cooled at 3 °C/min to 450 °C, where they were annealed for 3 h. Finally, the specimens were cooled slowly to room temperature. The entire sintering-and-annealing process was carried out in flowing oxygen.

The thickness of the processed films ranged from ~30 to 50 μm. Those sintered at or above 980 °C were hard and adhered well to the substrates. The films were examined by x-ray diffraction to determine which solid-state phases were present. Microstructures were observed by optical and scanning electron microscopy. Electrical resistivities were measured in the standard four-probe configuration over a range of temperatures down to that of liquid helium (see figure).

The examinations and measurements showed that the properties of the films depend strongly on the sintering-and-annealing treatment. In terms of the adherence and superconducting-transition temperature of the films, the optimum annealing temperature and time were found to be 1,000°C and 15 min, respectively. Films with higher superconducting-transition temperatures but poorer adhesion were formed at 945 °C. Thus, there appears to be a need to increase adhesion at lower sintering temperatures.

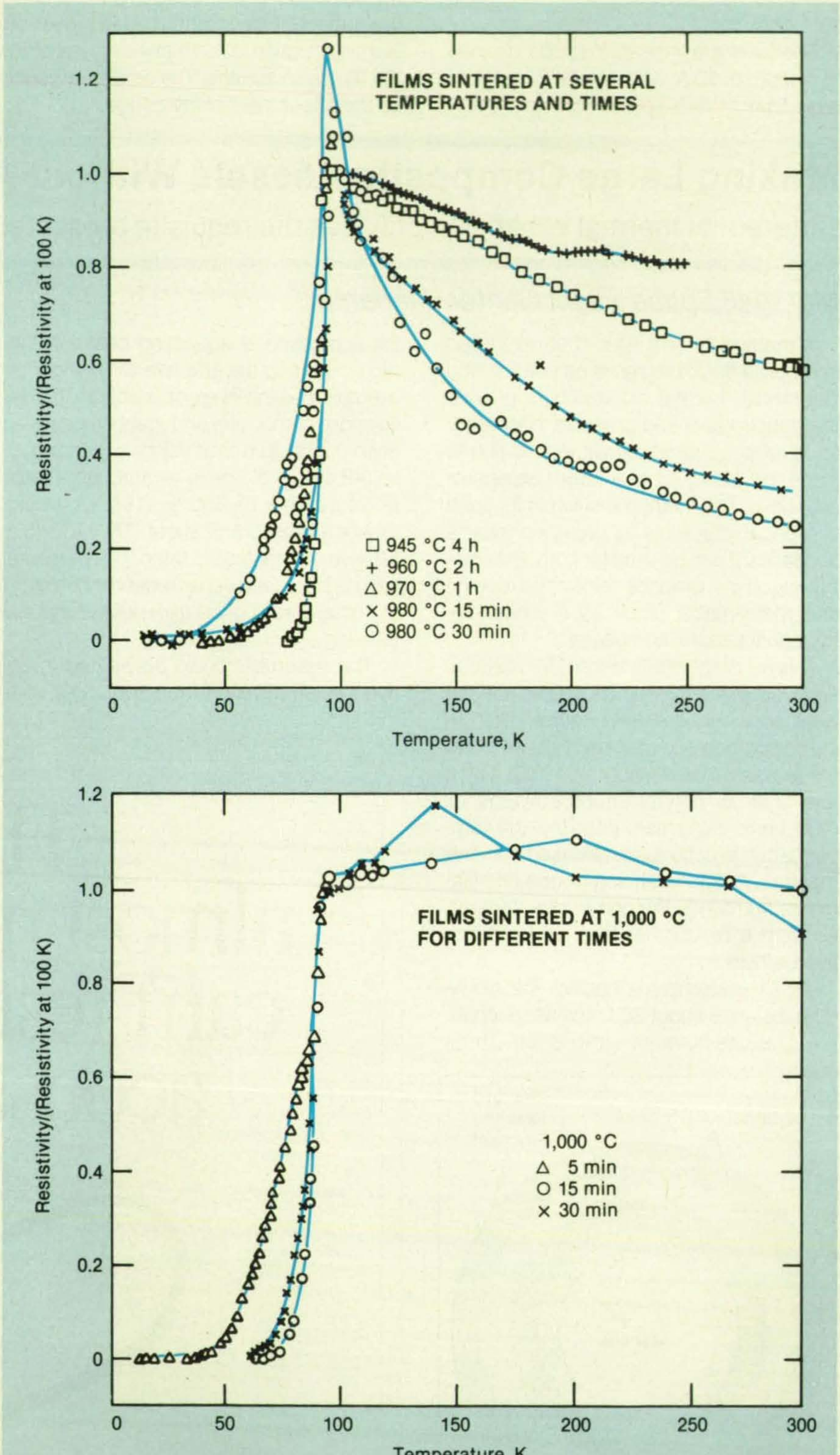

Plots of Normalized Resistivity Versus Temperature show the effects of annealing temperatures and times.

This work was done by Narottam P. Bansal and Rainee N. Simons of ***Lewis Research Center*** *and D. E. Farrell of Case Western Reserve University. Further information may be found in NASA TM-100860 [N88-22805], "Synthesis and Characterization of High-T_c Screen-Printed Y-Ba-Cu-O Films on Alumina."*

Copies may be purchased [prepayment required] from the National Technical Information Service, Springfield, Virginia 22161, Telephone No. (703) 487-4650. Rush orders may be placed for an extra fee by calling (800) 336-4700.
LEW-14829

Making Submicron $CoSi_2$ Structures on Silicon Substrates

Submicron epitaxial single-crystal lines have been fabricated by direct electron-beam exposure.

NASA's Jet Propulsion Laboratory, Pasadena, California

An experimental fabrication process makes submicron-sized structures of single-crystal metallic $CoSi_2$ on silicon substrates. When fully developed, the process may be used to make fine wires or dots that exhibit quantum confinement of charge carriers. The lateral dimensions of the structures will probably have to be tens of nanometers or less. Other potential applications include the use as electron-beam resists and fabrication of submicron gate electrodes in small field-effect transistors.

The process (see figure) begins with the deposition of a layer of amorphous (that is, noncrystalline) Co:Si (1:2) on the (111) surface of a silicon substrate at near room temperature. The stoichiometric ratio of the amorphous deposit is essential to formation at low temperature because it prevents the formation of intermediate silicide phases.

An electron beam is focused on the layer of amorphous Co:Si (1:2) and scanned across it as necessary to define the structure to be fabricated. In the area(s) struck by the electron beam, the amorphous Co:Si is crystallized, becoming single-crystal $CoSi_2$.

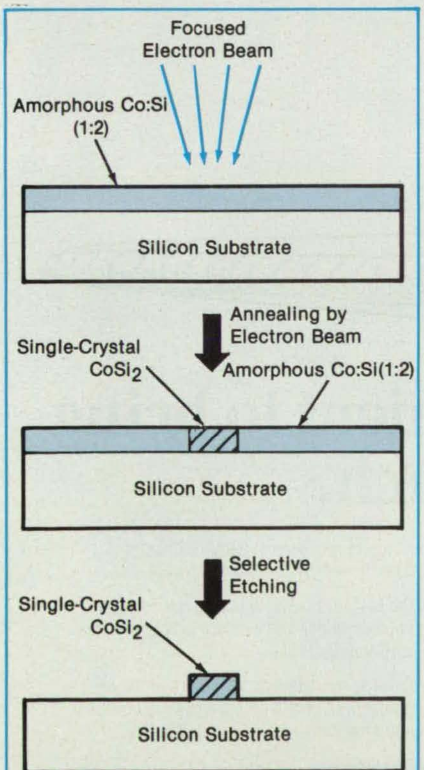

Amorphous Co:Si (1:2) Is Crystallized by an electron beam, becoming single-crystal $CoSi_2$. The remaining amorphous Co:Si is then preferentially etched away.

The remaining amorphous Co:Si is then removed selectively by a suitable etching technique. For example, a solution of $HF:H_2O$ (1:9) etches Co:Si (1:2) at a rate of about 3 Å/s, while it etches single-crystal $Co:Si_2$ much more slowly. This degree of selectivity is adequate for removal of the amorphous Co:Si without adversely affecting the surviving single-crystal $CoSi_2$.

The process was demonstrated by using a 300-keV, 10-μA electron beam from a transmission electron microscope to make single-crystal $CoSi_2$ lines 300 nm wide from a 10-nm-thick matrix of amorphous Co:Si on a silicon (111) substrate. The crystallized regions were sharply defined. The amorphous Co:Si remained unchanged only 10 nm away from the electron beam.

These results suggest that selective crystallization of $CoSi_2$ in an electron-beam lithography system should be possible. Allowing for the 8-nm width of the electron-beam spot and for a 10-nm-wide border on both sides, it should be possible to make structures that have lateral dimensions as small as 28 nm. In contrast, present electron-beam lithography with resist technology cannot produce features smaller than approximately 40 nm.

By the use of $CoSi_2$ structures as electron-beam resists, it may be possible to achieve dimensions smaller than those achievable by photoresist techniques. The patterned $CoSi_2$ could be used as a mask to etch the underlying material. Etching techniques that do not readily attack $CoSi_2$ would again be required. Techniques suitable for this purpose may include plasma etching in CF_4 and chemical etching in dilute $HF:H_2O$ or phosphoric acid.

This work was done by Simon K. W. Nieh, True-Lon Lin, and Robert W. Fathauer of Caltech for **NASA's Jet Propulsion Laboratory**. *For further information, Circle 10 on the TSP Request Card.*

This invention is owned by NASA, and a patent application has been filed. Inquiries concerning nonexclusive or exclusive license for its commercial development should be addressed to the Patent Counsel, NASA's Resident Office-JPL [see page 18]. Refer to NPO-17736

Glove Box for Hazardous Liquids

A conceptual box is designed for safe handling and cleaning.

Marshall Space Flight Center, Alabama

A proposed glove box (see figure) would enable a technician to handle hazardous liquids safely and to clean up quickly if a spill should occur. As in any glove box, the technician places hands and arms in gloves at a port to manipulate materials within the box.

Liquids in the box are contained in pouches (this feature is necessary if the box is to be used in zero gravity). To transfer liquid from one pouch to another, the technician inserts a syringe through a septum in a pouch, draws a precise volume of liquid into the syringe, inserts the syringe in the septum of another pouch, and expels the liquid.

To transfer the contents of a pouch to a waste-collection system, the technician inserts the quick-disconnect fitting at the end of a tube on the pouch into a quick-connect fitting on the wall of the box. The entire box can be vented to a vacuum to clean up a spill. When this is necessary, the operator makes use of a chamber in the glove port to prevent the gloves from rupturing under the vacuum and leaking outside air into the

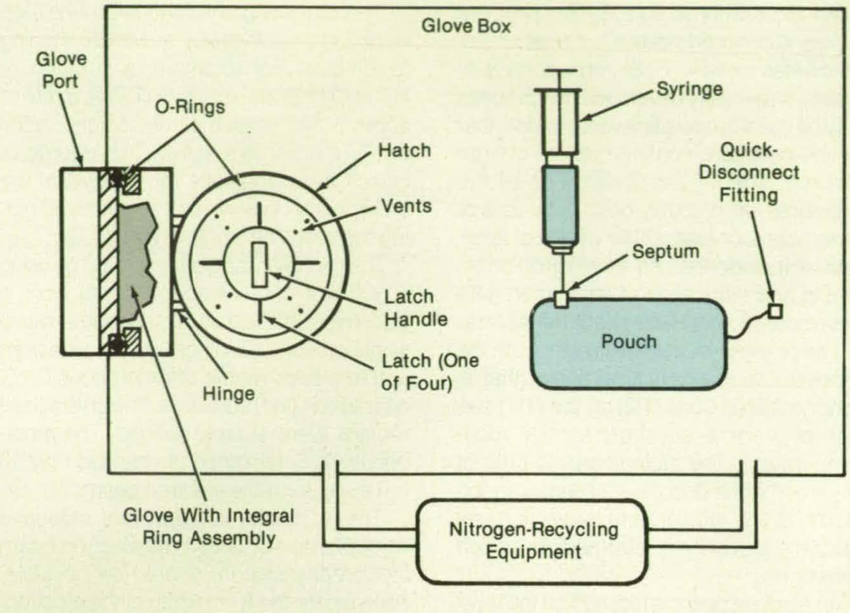

The **Glove Box** includes a hatch that seals off the glove ports so that the box can be vented and purged when necessary.

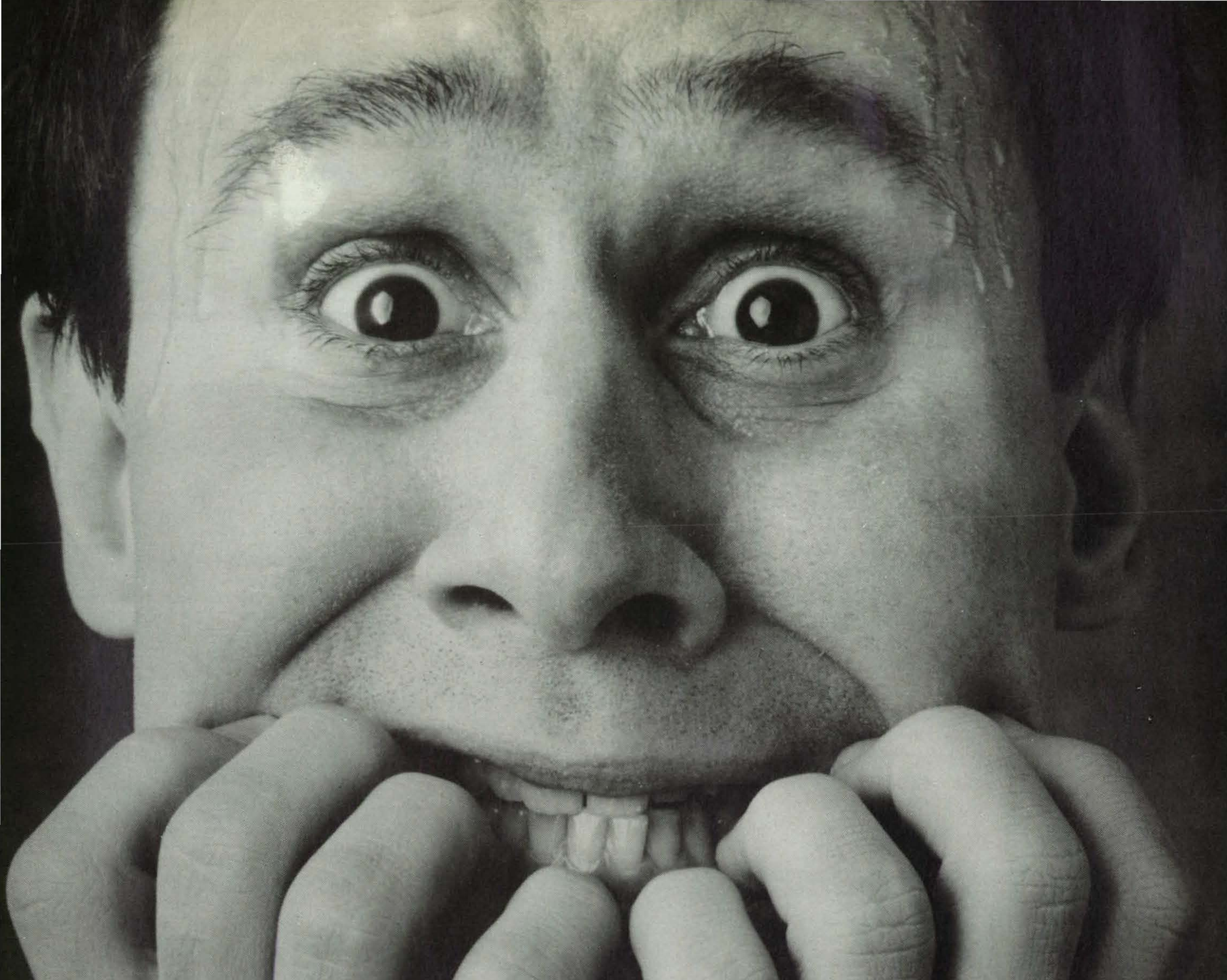

Sometimes overnight is absolutely, positively too late.

We're not knocking the other guys, but sometimes you need to get it there right away. The very same day. Today, not tomorrow.

With TWA's Next Flight Out® delivery service, you're in business.

Even as you read this, TWA planes are about to take off. We can make sure your small package is on the next flight out to any one of over 100 U.S. cities. And we'll deliver it door-to-door or airport-to-airport. Same day. Seven days a week.

We'll give you our money-back guarantee and Frequent Flight Bonus miles, too (exciting details when you call).

We also deliver next day to Europe and second day to the Middle East.

So for anything up to 70 pounds domestic and 50 pounds international, just call the 800 number. It's that easy. It's *not* that expensive. And most of all, it's fast —very, very fast.

1-800-638-7380

For information or immediate pick-up, ask for Agent 195.

Circle Reader Action No. 438

box. The operator simply closes a hatch inside the box to seal the glove port and withdraws hands and arms from the gloves, leaving the gloves in the glove chamber. The interior of the glove box can then be opened to the vacuum.

The gloves can be changed, if necessary, while the hatch is closed. The gloves are part of an integral ring-and-glove assembly. The ring seals to an O-ring in the glove port. A self-sealing plastic bag, attached to the outside of the glove port, is used to replace the gloves.

This work was done by R. N. Rossier and B. Bicknell of Martin Marietta Corp. for **Marshall Space Flight Center**. *No further documentation is available.*
MFS-28392

Healing Voids in Interconnections in Integrated Circuits

A seemingly harsh treatment fills voids (cracks) in aluminum conductors.

NASA's Jet Propulsion Laboratory, Pasadena, California

An unusual heat treatment heals voids (cracks) in aluminum interconnections on integrated circuits (IC's). The voids (cracks) have been attributed to such causes as mismatched thermal expansion and precipitation of silicon in the aluminum conductors during the processing of IC wafers and the packaging of IC chips. The treatment consists of heating an IC to a temperature between 200 °C and 400 °C, holding it at that temperature, and then plunging the IC immediately into liquid nitrogen.

Ordinarily, one would expect such a treatment to start voids (cracks) or make them longer. Indeed, the treatment was first tried in the effort to inflict further damage during a study of voiding (cracking) in aluminum interconnection in random-access-memory IC's. Researchers had hoped that further damage would lead to a capability to estimate growth kinetics. To their surprise, the treatment healed the interconnects (see figure).

In the new treatment, the high temperature is necessary but not the critical step and can range from 200 to 400 °C, which is speculated to depend on the temperature used to deposit aluminum in manufacture. A typical holding time at the evaluated temperature is 30 minutes. The critical step is the rapid cooling in liquid nitrogen.

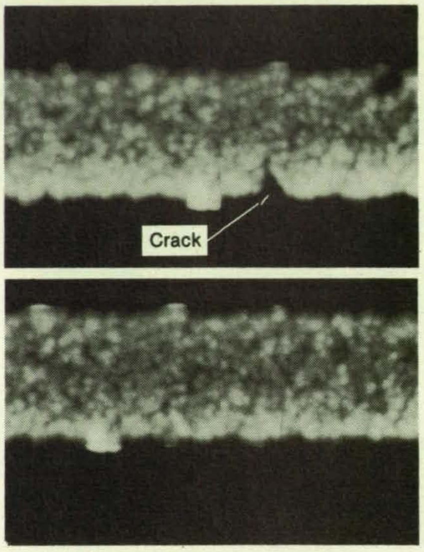

Two Voids (Cracks) can be observed on opposite sides of an aluminum interconnection. After the thermal treatment, the voids (cracks) have disappeared. The aluminum line is 7 μm wide. The pictures appear slightly fuzzy because the aluminum interconnection is being photographed through a glassivation layer that is on top of the aluminum.

This work was done by Edward F. Cuddihy, Russell A. Lawton, and Thomas Gavin of Caltech for **NASA's Jet Propulsion Laboratory**. *For further information, Circle 42 on the TSP Request Card.*

This invention is owned by NASA, and a patent application has been filed. Inquiries concerning nonexclusive or exclusive license for its commercial development should be addressed to the Patent Counsel, NASA's Resident Office-JPL [see page 18]. Refer to NPO-17678.

Arc-Light Reflector for Television Weld Monitoring

Light is spread more evenly over the image area.

Marshall Space Flight Center, Alabama

A conical, stainless-steel mirror attached to the end of a welding torch improves the distribution of light on the workpiece as its welding is monitored through the torch by television. An auxiliary light source is therefore not needed. Television monitoring not only protects the operators from the intense arc light but also facilitates automated welding.

In earlier versions of television weld monitoring, the extremely bright light of the welding arc closed down the camera aperture enough to lose the detail of the relatively dark surrounding region, particularly on overlays. The solution of this problem was to use auxiliary light sources to illuminate the area surrounding the arc. These sources were large, expensive, bright, quartz/halogen lights that did not work well.

The new conical mirror (see figure) on the other hand, reflects the already-available arc light onto the darker surrounding areas, providing the monitor with a clearer, more detailed image of the welding operation. Simple, small, and easy to install and remove, the mirror is relatively nonintrusive. For example, it does not interfere with the addition of filler wire.

This work was done by Stephen S. Gordon of Rockwell International Corp. for **Marshall Space Flight Center**. *No further documentation is available.*

This invention has been patented by NASA (U.S. Patent No. 4,633,060). Inquiries concerning nonexclusive or exclusive license for its commercial development should be addressed to the Patent Counsel, Marshall Space Flight Center [see page 18]. Refer to MFS-29134.

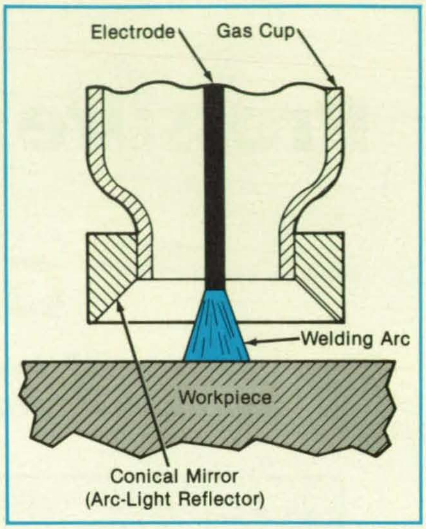

An **Arc-Light Reflector** directs light from the welding arc back onto the workpiece, enabling television monitoring of the welding operation and protecting the operator from the arc light.

Making Internal Molds of Long, Curved Tubes

Mold material is carried to an internal weld joint and removed after an impression is taken.

Marshall Space Flight Center, Alabama

A remotely operated device makes an impression mold of the interior surface of a tube at a weld joint. The mold provides an indication of the extent of the mismatch between the members at the joint. The device can be maneuvered to the weld to be inspected through a curved tube 3 in. (7.6 cm) in diameter by 50 in. (127 cm) long. It can readily be adapted to making molds to measure the depth of corrosion in boiler tubes or other pipes.

The device includes a V-notched head on the end of a set of hoses (see figure). The operator inserts the device in the tube and manipulates color-coded lines to guide it through the curves in the tube until the V-notch in the head engages a splitter rod at the weld joint. The operator inflates an airbag on the head to lock it in place. The operator then applies air pressure to an air cylinder that pushes a platen outward, forcing the molding material against the inner wall of the tube.

The operator releases the pressure in the cylinder and bag after the impression has been made. A retractor spring in the head draws the platen and molding material inward so that the device can be withdrawn. A steel cable acts as a redundant tether to ensure that all parts are extracted.

The V-notch can be indexed in 15° increments about the axis of the tube. This feature enables the taking of a series of impressions that cover all or a portion of the inner circumference of the tube.

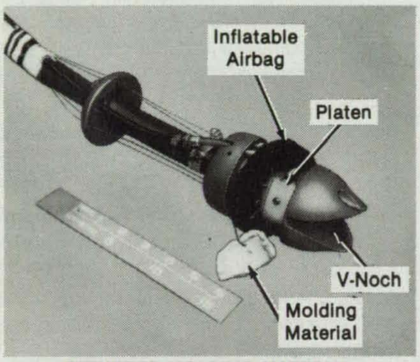

TETHERED MOLDING MATERIAL SEPARATED FROM HEAD TO SHOW PLATEN

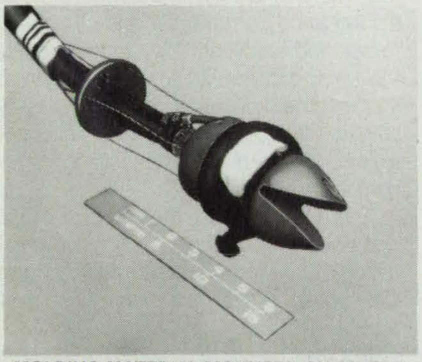

MOLDING MATERIAL MOUNTED ON PLATEN

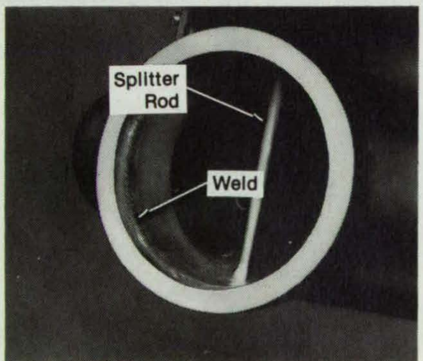

CUTAWAY VIEW OF TUBE SHOWING SPLITTER ROD AND WELD

When Pressurized, an Air Cylinder in the Head of the mold-making device forces the platen and mold material against the inner wall of the tube. The splitter rod, revealed in the cutaway tube, aids in the positioning of the V-notched head.

This work was done by Richard K. Burley of Rockwell International Corp. for **Marshall Space Flight Center**. *For further information, Circle 98 on the TSP Request Card. MFS-29435*

Lightweight, High-Current Welding Gun

A resistance welder delivers up to 4,000 A.

Marshall Space Flight Center, Alabama

A lightweight resistance-welding gun (see figure) delivers currents and weld forces ordinarily obtainable only from larger, heavier equipment. The hand-held gun supplies alternating or direct current over a range of 600 to 4,000 A and can apply forces from 40 to 60 lb (178 to 267 N) during welding.

The gun can be used to weld metal sheets in multilayered stacks. The high-current, high-force, short-duration heating minimizes cracking and produces welds that are large enough for critical structural applications.

The body of the gun is made of a nonmetallic material to keep its weight low. It is designed to be comfortable and convenient to use and enables the operator to adjust the welding current to suit the thickness of the weldment. The gun can be operated with a load cell instead of a miniature switch, to guard against misfiring or arc damage.

This work was done by Thomas F. Starck and Andrew D. Brennan of Rockwell International Corp. for **Marshall Space Flight Center**. *No further documentation is available.*

Inquiries concerning rights for the commercial use of this invention should be addressed to the Patent Counsel, Marshall Space Flight Center *[see page 18]**.Refer to MFS-29454.*

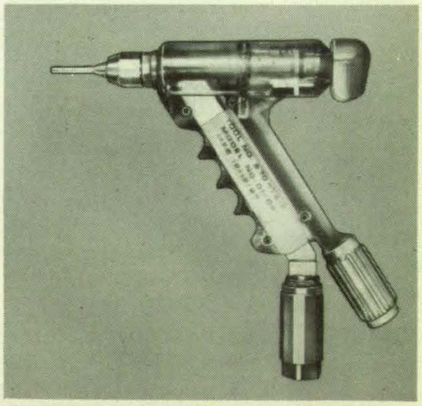

An Operator Can Maneuver This Welding Gun Easily and apply a large force to the weld joint with it.

Books and Reports

These reports, studies, handbooks are available from NASA as Technical Support Packages (TSP's) when a Request Card number is cited; otherwise they are available from the National Technical Information Service.

Variable-Polarity Plasma Arc Welding of Alloy 2219

Macrosegregation and characteristics of arcs are examined.

A report presents the results of a study of variable-polarity plasma arc (VPPA) welding of aluminum alloy 2219. The study consisted of two parts:

- An examination of the effects of microsegregation and transient weld stress on macrosegregation in the weld pool and
- Electrical characterization of the straight- and reverse-polarity portions of the arc cycle.

In VPPA welding, the polarity of the arc switches many times per second. The sputtering action of argon ions during reverse polarity disrupts the oxide film that normally forms on alloy 2219, thus improving the weldability of this uniquely weldable binary alloy of aluminum and copper.

The study led to the conclusion that alloy 2219 is weldable because large volumes of liquid are available during the latter stages of solidification. It also found that transient stresses cause exudation and flaws that are subsequently backfilled. These effects in turn cause macrosegregation, which manifests itself in radiographic contrast phenomena. Material enriched in copper was found at the surface of the weld, probably produced by sputtering and evaporation.

The study further showed that current in the arc falls during the reverse-polarity portion of the cycle, but voltage increases so much that greater power is often produced in the reverse part of the cycle than in the straight (forward-polarity) part. At any programmed current, the current in the straight-polarity portion of the cycle increases as the relative duration of the reverse-polarity portion is increased.

This work was done by Daniel W. Walsh of California Polytechnic State University and Arthur C. Nunes Jr., of **Marshall Space Flight Center**. *To obtain a copy of the report, "The Keyhole Region in VPPA Welds," Circle 108 on the TSP Request Card.*

Inquiries concerning rights for the commercial use of this invention should be addressed to the Patent Counsel, Marshall Space Flight Center [see page 18]. Refer to MFS-27223

Grinding Si_3N_4 Powder in Si_3N_4 Equipment

Three methods of grinding are compared.

Attrition milling in silicon nitride mills is a fast way of producing fine silicon nitride powders with minimum pickup of impurity, a report concludes. The report is based on a study of grinding silicon nitride powder in preparation for sintering it into a solid ceramic material.

Attrition, vibratory, and ball mills lined with reaction-bonded silicon nitride were tested. The rates of reduction of particle sizes and the changes in chemical compositions of the powders were measured so that the grinding efficiencies and the increases in impurity contents from wear of the mills and media could be evaluated for each technique.

The results showed that the attrition mill and the vibratory mill reduce the sizes of particles (measured by increases in surface area) at about the same rate — about eight times that of the ball mill. The amount of oxygen picked up by the particles increases with milling time. The cumulative increase in oxygen content as a function of the cumulative increase in particle surface area is about the same in ball and attrition milling but about six times as large in vibratory milling. Consequently, because of its high rate of reduction of particle size and low rate of absorption of oxygen, attrition milling is preferred.

Three milling fluids were tested: ethanol, heptane plus 3 volume percent ethanol, and n-butanol. In ball milling, butanol was found to cause more contamination with carbon than did the other fluids because it degraded a rubber cap on the mill. Butanol also caused slower reduction in the sizes of particles.

This work was done by Thomas P. Herbell, Marc R. Freedman, and James D. Kiser of **Lewis Research Center**. *Further information may be found in NASA TM-86864 (Revised) [N86-24839], "Particle Size Reduction of Si_3N_4 Powder with Si_3N_4 Milling Hardware."*

Copies may be purchased [prepayment required] from the National Technical Information Service, Springfield, Virginia 22161, Telephone No. (703) 487-4650. Rush orders may be placed for an extra fee by calling (800) 336-4700.
LEW-14821

Dynamic Transfers of Tasks Among Computers

An allocation scheme would give jobs to idle computers.

NASA's Jet Propulsion Laboratory, Pasadena, California

A distributed computer system consists of several computers with the same or different processing capabilities, connected together by a network. In such a distributed multicomputer system, there is a probability that one of the computer stations will be idle while another computer station will have more than one job waiting in the queue for service. We call this probability the imbalance probability. A high imbalance probability typically implies poor system performance. By reallocating queued jobs to idle or lightly loaded stations, a reduction in system response time can be expected. This technique is called load sharing and is one of the main focuses of this paper.

An ideal resource-sharing algorithm should have the following characteristics:

1. Dynamics: The load distribution can adapt to rapid system load changes.
2. Decentralized: Each processor determines, on its own, whether to process a job locally or send the job to some other station for processing. There is no need for a central dispatcher. Since the central dispatcher is not required, the problem of a single point of failure is eliminated.
3. Heterogeneous: The computer stations need not have the same processing power.

The proposed enhanced receiver-initiated dynamic algorithm (ERIDA) for resource sharing fulfills all the above criteria.

When a job finishes service and leaves a station in this new algorithm, the station checks the workload indicator by dividing the queue length by the service rate. If the workload indicator is below a certain low threshold level, the lightly loaded station initiates a search for the busiest station. If the workload indicator of the busiest station is above certain high threshold, a job from that busy station is transferred to the lightly loaded station. Thus, the ERIDA provides a method that balances the workload among hosts, resulting in an improvement in the response time and throughput performance of the total system.

The ERIDA adjusts dynamically to the traffic load of each station. When the workload indicator of every station is greater than a certain threshold level, the algorithm generates no overhead — an important advantage.

In a homogeneous 20-node system, service stations have the same service rates, and the arrival rates at each station are also assumed to be equal. The approximate ERIDA queueing model is validated by a GPSS/PC (general-purpose simulation system/personal computer) simulation. The comparison of results from the average response time generated by the approximate queueing model and the results from the simulation excercise are shown in the figure. This figure shows that the results from the approximate queueing models are very close to the simulation results.

Comparing the ERIDA to a non-achieveable centralized resource-sharing system (M/M/10), the figure shows that the ERIDA performance is worse than the centralized M/M/10 system. The inefficiency of the ERIDA can be illustrated by the following scenario: If one of the stations finishes the jobs in its queue and sees that all the other stations are not heavily loaded, this station will go to relinquish and remain idle until either another local job arrives or until wakeup timeout. This idle station will not be able to share the load with any other stations that become overloaded during its relinquish period. For this system configuration, we can conclude that a centralized resource-sharing scheme provides the best performance, since no job will wait if any station is idle. However, this centralized scheme is typically not practical for implementing on a distributed system.

In the same figure, the results of the ERIDA are compared against the case without load sharing, i.e., the case of multiple independent M/M/1 queues. The average response time is always improved

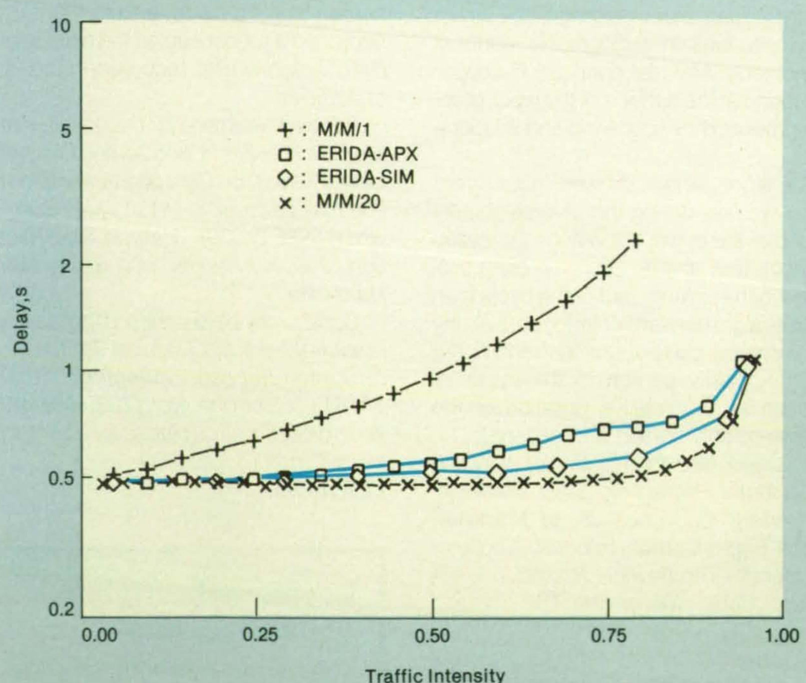

Average Response Time Comparison among ERIDA DIT (ERIDA-APX: □), ERIDA simulation (ERIDA-SIM: ◇), centralized (M/M/20: X) and an independent system (M/M/1: +), each operating in a 20-server homogeneous system.

when the ERIDA resource-sharing scheme is applied. Obviously, the independent M/M/1 queue system is inefficient, since there may be jobs queued up in front of one of the stations when the other one is idle.

This work was done by Howard T. Liu of Caltech and John A. Silvester of the University of Southern California for **NASA's Jet Propulsion Laboratory**. *For further information, Circle 47 on the TSP Request Card.*

This invention is owned by NASA, and a patent application has been filed. Inquiries concerning nonexclusive or exclusive license for its commercial development should be addressed to the Patent Counsel, NASA Resident Office-JPL [see page 18]. Refer to NPO-17197.

Network-Control Algorithm

Channels are allocated optimally to links in a multilink, multinode network.

NASA's Jet Propulsion Laboratory, Pasadena, California

An algorithm has been developed for the optimal routing of packets of data along the links of a multilink, multinode digital communication network. The algorithm is iterative and converges to a cost-optimal assignment that is independent of the initial assignment.

The network is assumed to have an arbitrary topology, in which each node is connected to several other nodes through full-duplex-multichannel links (see example figure). The problem is to determine the link route between originating and destination nodes and the number of channels for packet-switched traffic along the route that minimize the cost, subject to the constraints imposed by the maximum average allowable network delay.

To simplify the analysis, the cost of initial setup, the propagation delay on each link, and the processing delay at each node are neglected. The cost of using each half duplex link is assumed to be proportional to the number of channels used in that link: This assumption assures the convexity of the cost function, which in turn assures that the iterative optimization process leads to a global optimum.

The algorithm begins with the selection of an initial feasible flow vector, which characterizes the link route and the flow. The gradient of the cost function in the flow-vector space is then computed and used to find the shortest path. A flow-deviation subalgorithm is then used to find the next iteration of the feasible flow vector that minimizes the cost function. If the fraction of the user demand that satisfies this flow vector can be increased, it is increased, and the resulting cost function is evaluated. The foregoing steps are repeated until the decrements of the cost function at an iteration become arbitrarily small, indicating the attainment of the global optimum. The number of channels in each link is then assigned according to the resulting flow vector.

The algorithm depends in part on the assumption that the number of channels in a link can be treated as a continuous variable. This assumption may not be applicable where the number of channels is small, in which case integer programming can be used to determine the number of channels. The algorithm can also be modified to take account of different priorities among the packets belonging to different users by using different delay constraints or imposing additional penalties via the cost function.

This work was done by Hak-Wai Chan and Tsun-Yee Yan of Caltech for **NASA's Jet Propulsion Laboratory**. *For further information, Circle 125 on the TSP Request Card.*
NPO-17505

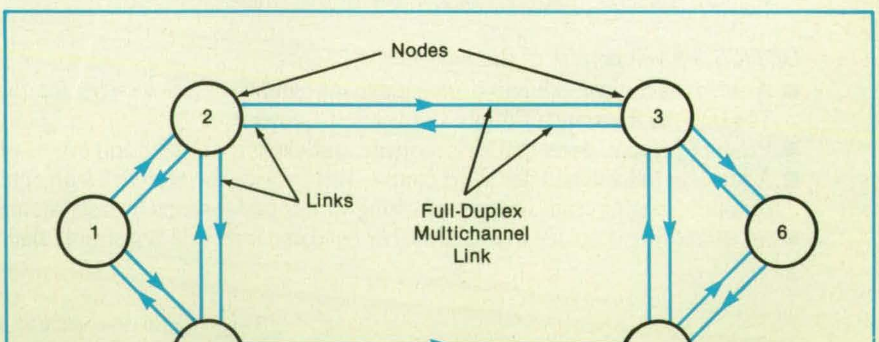

Each Node Is Connected to other nodes through links, each containing a number of two-way (one way at a time) channels. The algorithm assigns channels according to message traffic leaving and arriving at each node.

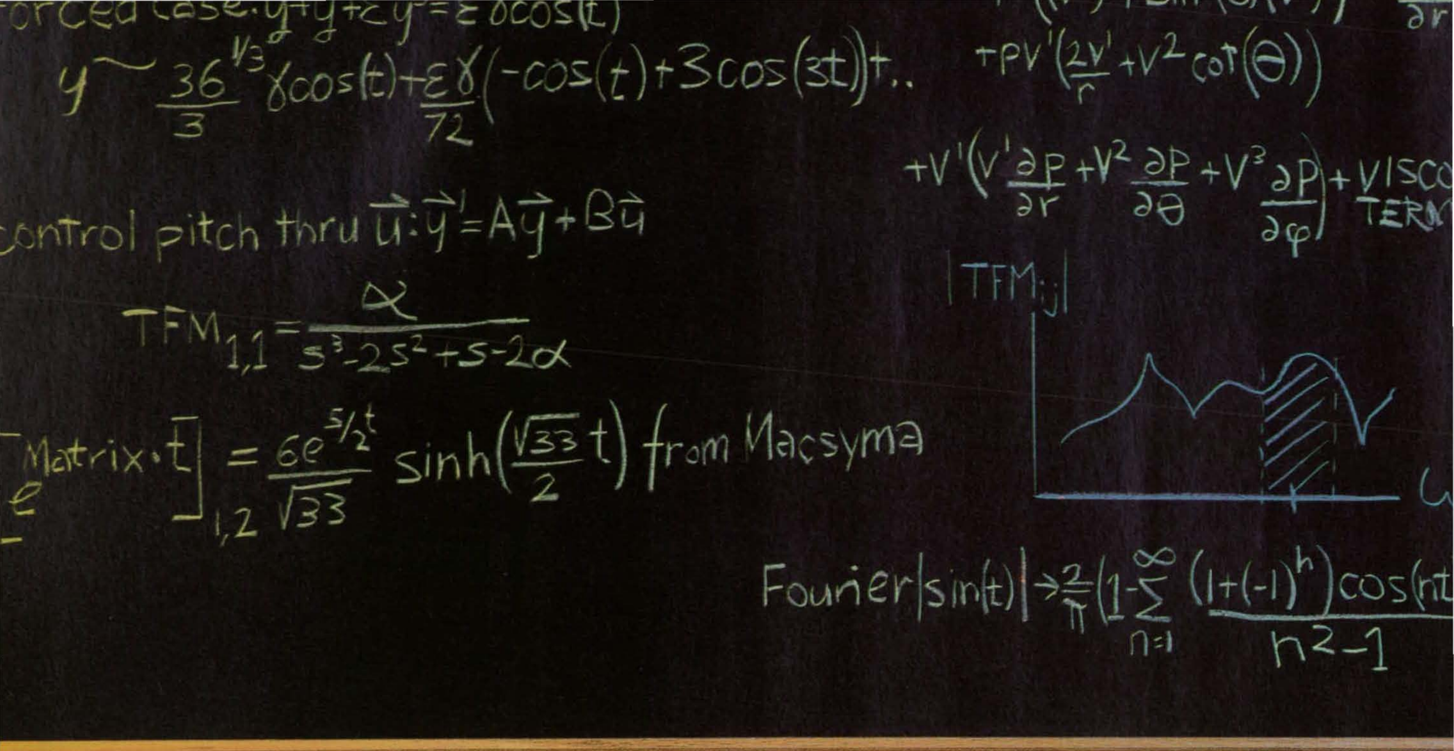

Macsyma®...

the most powerful math software in the world of mainframes, *now on PC's.*

Until now, if you wanted to combine symbolic and numerical analyses into a powerful approach to mathematical modeling, there was only one way to do it — MACSYMA and a *big* computer.

Now we've taken all the power, performance and productivity of MACSYMA and created a PC version, one that runs on any 386/DOS-based PC*.

So now you can perform complex symbolic, numerical, and graphical calculations automatically — in applications ranging from plasma physics to aeronautics, from economics to fluid mechanics and more — right at your desk. Such as differential and integral equations, Laplace and Fourier transforms, vector and tensor calculus. The same calculations that used to require mainframe performance.

There's one thing about MACSYMA that isn't complex — using it. In fact, using MACSYMA is so easy, you can get right to work using our On-line Help and Quick Reference Card — without even opening a book.

MACSYMA on a PC. As easy as π.
Call 1-800-MACSYMA (in Massachusetts, 617-221-1250).

Circle Reader Action No. 524

symbolics, Inc.

Computer Aided Mathematics Group
8 New England Executive Park East
Burlington, MA 01803 U.S.A.

* 100% IBM compatibles.

After centuries of practice, mankind perfects engineering calculations: MathCAD.

Announcing MathCAD 2.5: The Dawn of a New Age.

What the historians will call it, only time will tell.

Perhaps the Century of Speed, or the Era of Ease. But whatever the name, this is the age of MathCAD 2.5, the only math package that looks and works the way you think.

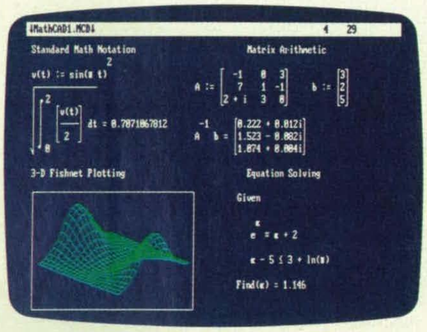

MathCAD 2.5 includes 3-D plotting, HPGL sketch import, and PostScript output.

MathCAD is far and away the best-selling math package in the world. Because it lets you perform engineering and scientific calculations in a way that's faster, more natural and less error-prone than the way you're doing them now—whether you're using a scratchpad, calculator, spreadsheet or program that you wrote yourself.

And now we've made the best even better. MathCAD 2.5 is a dramatically improved version that includes three-dimensional plotting, enhanced numerical analysis, and the ability to import HPGL files from most popular CAD programs, including AutoCAD.® And now you can print on PostScript® compatible printers.

And like before, MathCAD's live document interface™ lets you enter equations anywhere on the screen, add text to support your work, and graph the results. Then print your analysis in presentation-quality documents.

It has over 120 commonly used functions built right in, for handling equations and formulas, as well as exponentials, differentials, cubic splines, FFTs and matrices.

No matter what kind of math you do, MathCAD 2.5 has a solution for you. In fact, it's used by over 50,000 engineers and scientists, including electrical, industrial, and mechanical engineers, physicists, biologists, and economists.

But don't take our word for it; just ask the experts. PC Magazine recently described MathCAD as "everything you have ever dreamed of in a mathematical toolbox."

PC MAGAZINE EDITOR'S CHOICE
March 14, 1989 issue.
Best of '88
Best of '87

And for Macintosh® users, we present MathCAD 2.0, rewritten to take full advantage of the Macintosh interface. Entering operators and Greek letters into equations is pure simplicity!

Look for MathCAD 2.5 at your local software dealer, or give us a call. For more information, a free demo disk, or upgrade information,* dial 1-800-MATHCAD (in MA, 617-577-1017).

**If you purchased MathCAD 2.0 between 5/1/89 and 6/16/89, you can get a FREE upgrade to version 2.5 (otherwise, the upgrade cost is $99.00 until June 30, 1989; afterwards, the cost will be $149.00).*

MathCAD®

MathSoft, Inc. One Kendall Square, Cambridge, MA 02139

22

Available for IBM® compatibles and Macintosh computers. TM and ® signify manufacturer's trademark or manufacturer's registered trademark respectively. PE

Circle Reader Action No. 628

Using Inorganic Crystals To Grow Protein Crystals

Solid materials serve as nucleating agents.

NASA's Jet Propulsion Laboratory, Pasadena, California

Inorganic crystals can be used as nucleants or substrates for growing protein crystals. Inorganic crystals therefore promise to make the growth of protein crystals more easily controllable, more reliable, and more reproducible. Protein crystals can be induced by heterogeneous nucleation — and in some cases by epitaxy — to grow at lower supersaturations than are needed for spontaneous nucleation. Heterogeneous nucleation may make it possible to grow large, defect-free single crystals of protein more readily. Such protein crystals will benefit research in biochemistry and pharmacology.

A series of experiments tested the effects of 50 inorganic crystalline substrates on the growth of four proteins known to crystallize with exceptional reproducibility: chicken-egg lysozyme, jack-bean canavalin and concanavalin B, and beef-liver catalase. The inorganic nucleants were selected from a large collection of mineral and synthetic samples. They included alkaline earth fluorides, feldspars, zeolites, and micas, and compounds of transition-and heavy-metal ions.

The proteins differed widely in sensitivity to nucleants. Canavalin responded to at least 30 out of the 50 inorganic materials tested, while lysozyme nucleated quickly with only 9 nucleants and catalase with only 7. Usually the crystals nucleated by particles were of the same size, form, and quality as those of control crystals grown without the nucleants. However, anomalous forms were found: For example, lysozyme grew on magnesium oxide cleavages as spherulites but grew epitaxially on apophyllite as orthorhombic crystals (see figure).

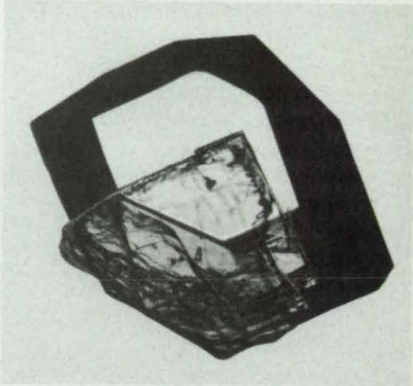

Epitaxial Growth of Lysozyme crystal on a cleavage of apophyllite.

This work was done by Paul J. Shlichta of Caltech and Alexander A. McPherson of the University of California for **NASA's Jet Propulsion Laboratory**. *For further information, Circle 75 on the TSP Request Card.*
NPO-17314

Books and Reports

These reports, studies, handbooks are available from NASA as Technical Support Packages (TSP's) when a Request Card number is cited; otherwise they are available from the National Technical Information Service.

Measuring Phytoplankton From Satellites

Present and future methods are examined.

A report reviews methods of calculating the concentration of phytoplankton from satellite measurements of the color of the ocean and using such calculations to estimate productivity of phytoplankton. Satellites have a unique ability to measure the quantity of phytoplankton quickly on a regional or ocean-basin scale. Satellite observations are the only way to obtain a comprehensive view of the ocean because they can give global coverage in 1 or 2 days. The information will aid in understanding the role of the ocean in the global carbon dioxide cycle.

As phytoplankton and their chlorophyll become more abundant, the color of the ocean shifts from blue to green. Color scanners aboard satellites detect this shift, providing the raw spectral data for use in calculations of concentration and productivity.

The report describes the Coastal Zone Color Scanner (CZCS), which was launched aboard the Nimbus 7 satellite and is the only instrument to date designed especially to measure the color of the ocean. The report discusses algorithms that correct the raw spectral data to remove the effects of backscattered sunlight and microscopic particles in the atmosphere. It discusses algorithms that take account of the absorption and scattering properties of water and of dissolved and suspended constituents, including sediments, phytoplankton, and products of the degradation of phytoplankton.

The report goes on to discuss ways of estimating rates of production of phytoplankton from measurements of concentration. The only method used thus far has been based on the correlation of satellite measurements with shipboard measurements or published values. Much-better estimates can be obtained if such factors as light and the supply of nutrients are taken into account. Mathematical models that include these factors as well as satellite data are undergoing development, as are satellite instruments that will provide the necessary data.

This work was done by C. O. Davis of Caltech for **NASA's Jet Propulsion Laboratory**. *To obtain a copy of the report, "Measuring Phytoplankton Biomass and Productivity From Space," Circle 69 on the TSP Request Card.* *NPO-17608*

New Literature

A new **PC data acquisition catalog** from Intelligent I/O, Tucson, AZ, covers plug-in carrier boards and modules, including a complete software library and all the necessary information to configure a cost-effective data acquisition system for PC/AT/XT, PS/2, and 386-type computers. Offered free of charge, the catalog features such new products as the IQ Workstation, a real-time data acquisition, test, measurement, and control system, and "SuperBoards," a family of small yet powerful single board products.
Circle Reader Action Number 702.

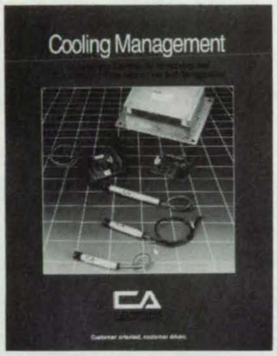

A free brochure from Cambridge Aeroflo Inc., Shirley, MA, describes the company's full line of **motor drivers, sensors, switches, and controls** for monitoring and regulating air flow, mass flow, and temperature. Product highlights include solid-state sensors and switches featuring glass bead thermistors that compensate for ambient temperature, air speed, altitude, relative humidity, and reversal in air flow.
Circle Reader Action Number 704.

Marketing Strategies International Inc., Mission Viejo, CA, has published a directory of more than 600 **resellers serving the CAE and computer graphics markets.** The directory includes software and hardware resellers, VARs, system houses and integrators, distributors, and consultants. It lists company name and address, phone number, products carried, and area of specialization.
Circle Reader Action Number 724.

A free booklet explains the Department of Defense **Computer-Aided Acquisition and Logistic Support (CALS) initiative,** which calls for a shared, on-line weapons system information database to replace the current paper-based system. Offered by Sun Microsystems Inc., Mountain View, CA, the booklet details the origin, goals, and key issues surrounding CALS, and suggests ways for government end-users and contractors to prepare for the initiative's impact.
Circle Reader Action Number 722.

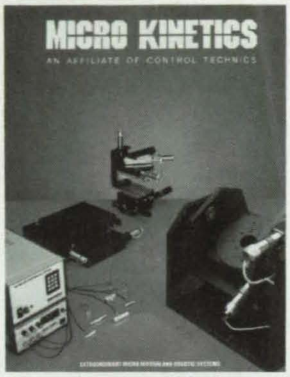

High-resolution **positioning components and systems** for the optical, defense, medical, and fiber optics industries are described in a new catalog from Micro Kinetics, Laguna Hills, CA. The 100-page publication features multi-axis table systems, drive master actuators, micrometers and ball screws, electronic controls, motors and drivers, precision translation tables, micropositioning systems, piezoelectric translators, and optical encoder gauges.
Circle Reader Action Number 706.

The Vantage™ Listing and Reference Manual features information on products compatible with the full line of **image processing subsystems** from Imaging Technology Inc., Woburn, MA. The publication lists software for image analysis and measurement, machine vision, medical imaging, and image compression and transmission, as well as hardware products such as video cameras, real-time disks, and display processors.
Circle Reader Action Number 728.

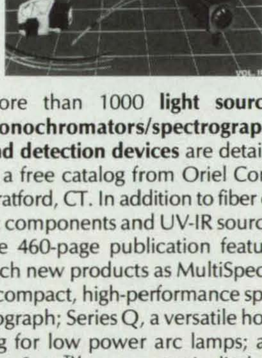

More than 1000 **light sources, monochromators/spectrographs, and detection devices** are detailed in a free catalog from Oriel Corp., Stratford, CT. In addition to fiber optic components and UV-IR sources, the 460-page publication features such new products as MultiSpec™, a compact, high-performance spectrograph; Series Q, a versatile housing for low power arc lamps; and InstaSpec™, an economic diode array detection system.
Circle Reader Action Number 708.

New on the Market

The Synco Chemical Corp., Bohemia, NY, is offering free sample tubes of Super Lube®, a synthetic, biodegradable **lubricant** that is safe for use on general manufacturing and food processing equipment. The product is impervious to water, grime, and extreme temperatures when used on anything that slides, swivels, rolls, or squeaks; on parts subject to rust, heat, cold, corrosion, or abrasive wear; or on surfaces that should be weatherproof or water-resistant. It provides lubrication from -45° to +450°F.
Circle Reader Action Number 774.

The UMIS-2000, a research tool for **characterizing surface materials,** including coatings and surface modified layers, is offered by Microscience Inc., Norwell, MA. A diamond indenter is forced into the surface under controlled load, and penetration displacement is recorded during the loading and unloading segments. Hardness and elastic modulus are derived without imaging the indent. The software system is IBM PC/AT compatible and provides instrument control, data acquisition and analysis, and file handling.
Circle Reader Action Number 772.

The LunaTrace **computer program** from American Imaging Services Inc., Carrollton, TX, enables designers to load optically scanned drawings or images directly into a CAD system, avoiding expensive and time-consuming manual conversion to CAD format. Designers can view, pan, zoom, plot, and convert images into intelligent CAD data using existing CAD software commands and equipment, including plotters. The menu-driven program requires 512 KB of memory and sells for $79.95.
Circle Reader Action Number 764.

Eastman Kodak Co., Rochester, NY, has added a **solid-state camera** with high resolution and RGB/NTSC compatibility to its still video product line. The CCD camera provides 330 TV lines of horizontal resolution in both NTSC and RGBoutput. Minimum illumination is 20 lux, using the optional f/1.4 12-72 mm zoom lens. It operates from 12V DC power and is supplied with an AC adapter.
Circle Reader Action Number 760.

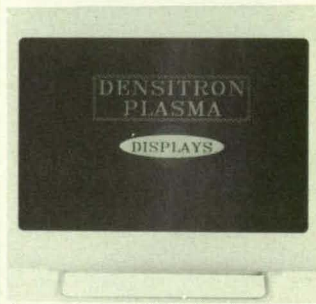

A new series of high brightness **AC plasma displays** has been introduced by Densitron Corp., Torrance, CA. The displays offer a typical contrast ratio of 20:1, 160 degree viewing angle, and 50,000 hours life with no reduction in pixel intensity. Select models feature grey scale capability; neon-orange pixels are available in 400 x 640 and 480 x 640 graphic formats.
Circle Reader Action Number 766.

The Model 3800-6 **computer tape cleaner** from Computer-Link Corp., Wilmington, MA, removes debris and loose oxide particles responsible for data error. After cleaning, the tape is evaluated for data handling capability. Operating with tape densities from 800 to 6250 bits per inch, the unit tests for such conditions as tape edge errors, multiple track errors, physical damage, and signal density errors. The user programs the test criteria and acceptable threshold for errors.
Circle Reader Action Number 762.

New on the Market

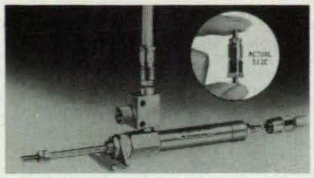

Miniature **quick-connect couplers** from Medo USA Inc., Wood Dale, IL, feature an automatic shut-off valve in the socket to eliminate leakage when the units are disconnected. Designed for air, gas, water, and chemical applications, the chrome-plated brass couplers are compatible with 3/32" or 1/8" soft tubes used in medical, pneumatic control, robotic, and scientific equipment, as well as machine tools.
Circle Reader Action Number 780.

Quad Design Technology Inc., Camarillo, CA, has introduced the Crosstalk Tool Kit (XTK), a **software package that predicts the effects of signal coupling,** or "crosstalk," on system performance early in the development of complex integrated circuits and printed circuit boards. XTK calculates the degree of coupling expected to occur between signals in high-density circuits, and it simulates the effects of this interference on signal waveforms in a circuit or a complete system. System developers can use this information to reduce signal noise and improve their designs. The software works with all logic families commonly used to build digital circuits, such as TTL, CMOS, and ECL.
Circle Reader Action Number 794.

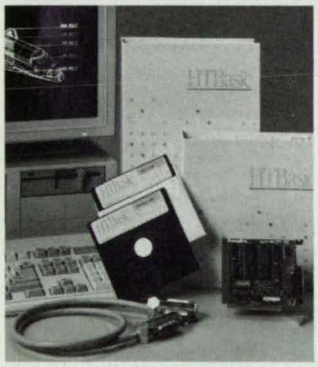

HTBasic, a new **software product** from TransEra Corp., Provo, UT, provides a simple method for developing and running HP BASIC programs on a PC. The software emulates the HP 9000 series 200/300 workstation BASIC. It supplies the entire language environment, including the unified path I/O system, graphic commands, full-screen edit mode, and interactive debugging commands. Also included are utility programs that transfer data files and ASCII programs between HP LIF format diskettes and MS-DOS disks.
Circle Reader Action Number 800.

RADEL®X **thermoplastic/carbon fiber prepregs** exhibit high damage tolerance, in-service capabilities of 325°F/wet, and quick and easy processing, according to the manufacturer — Amoco Performance Products Inc., Ridgefield, CT. The solvent-free systems offer unlimited shelf life with no change in mechanical properties. They can be processed by rapid fabrication methods such as filament winding and pultrusion, and come in a variety of forms, from 12-inch-wide unidirectional tape to commingled fabrics up to 60 inches wide.
Circle Reader Action Number 768.

The CGplot™ **software package** from Cerritos Computer Services Inc., Long Beach, CA, turns dot matrix and laser printers into color pen plotters by converting Hewlett-Packard Graphics Language (HP-GL) instructions into a format that can be used by most popular printers. The PC-based software is delivered with a graphics data spooler that allows the computer to be used for other purposes while simultaneously printing graphics. Priced at $395, CGplot requires 256 KB of memory and MS-DOS 3.0 or higher versions.
Circle Reader Action Number 758.

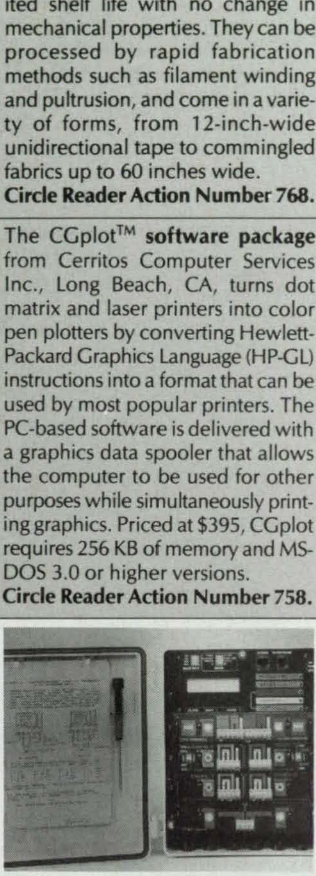

The OM220 **portable datalogger** from OMEGA Engineering Inc., Stamford, CT, will measure virtually any parameter and store it to internal memory, then download the data to a PC. Voltage, pressure, humidity, temperature, frequency, 4-20 mA loop, and pulse are all within its monitoring capabilities. Full OM220 control is directly implemented for RS232, RS485, and a modem.
Circle Reader Action Number 798.

Imagraph Corporation's new high-definition **frame grabber/display system** captures from both analog and digital sources and displays them in real time at sampling rates up to 40 MHz — far higher than other PC-AT based frame grabbers, according to the manufacturer. The HI*DEF™ system features a fully programmable capture system, with input black and white references, look-up tables for camera correction, capture resolution, sampling rate, and display resolution all independently software-selectable.
Circle Reader Action Number 790.

New on the Market

Data Retrieval Corp., Milwaukee, WI, has introduced TextBOOK Online Manuals, a new application for IBM and DEC systems that uses a free-form database to **manage large amounts of reference data and images online.** TextBOOK allows users to store, update, search, and retrieve information normally kept in paper or book form. It provides immediate access to updated text, thus avoiding data entry problems that accompany batch updates. Users can search and retrieve information by any word or phrase; a word index is generated automatically by the software.
Circle Reader Action Number 756.

Photometrics Ltd., Tucson, AZ, has introduced the Series 300 **CCD camera system** with 12-bit dynamic range. The camera features a 576 x 384 scientific-grade CCD imager and includes an intelligent controller with integrated frame store. Its detectivity is equal to an ASA rating in excess of 100,000, according to the manufacturer, and read noise is only 25 electrons per pixel. The system can serve as an independent data acquisition unit or can be connected to a host computer via an IEEE-488 interface.
Circle Reader Action Number 746.

A new line of **motorized positioning equipment** for laboratory and industrial applications has been introduced by Ealing Electro-Optics Inc., Holliston, MA. More than 50 standard stages are available with travel ranges of 25 mm to 1000 mm, positioning resolutions to 0.10, and speeds up to 250 mm/sec. In addition, Ealing is offering a microprocessor-based programmable controller that supports the combined operation of up to eight axes of stepper and DC servo motors. The controller features full front panel controls, 128 KB of memory, and both RS232 and IEEE-488 communication.
Circle Reader Action Number 754.

The **VGA Extender** allows the monitor and keyboard of a VGA-equipped PC/XT/AT or PS/2 to be placed up to 500 feet away from the system unit. Marketed by Communications Specialties Inc., Hauppauge, NY, the product consists of a transmitter and a remote receiver connected by a composite cable that combines the VGA and keyboard signals. Applications include security systems, desktop video systems, remote test and measurement devices, and office administrative processing systems.
Circle Reader Action Number 752.

The MDP-6E, an **image processing system** that integrates imaging, graphics, text, vector/array processing, and a high-resolution display, is offered by Computer Design and Applications, a subsidiary of Analogic Corp., Peabody, MA. The MDP-6E provides a SUN-compatible 1152 x 900 color frame buffer that enables the display of multiple images with separate Z mapping and X/Y zooming at over 10 million pixels/sec. The imaging subsystem is configured on three standard 6U size VME boards and is fully compatible with the SUN-3/E.
Circle Reader Action Number 750.

A new data acquisition, control, and analysis **software package for materials testing** has been introduced by Instron Corp., Canton, MA. The Series IX (Version 4.0) works with most MS-DOS compatible computers and supports a wide range of tension, compression, flexural, stress relaxation, peel, tear, and friction calculation and testing methods. The new version features an expandable database called LabVantage that enables materials testers to create SPC/SQC control charts, handle data from several instruments, and consolidate results.
Circle Reader Action Number 788.

Subject Index

Advertiser's Index

***RAC** stands for **Reader Action Card.** For further information on these advertisers, please circle the RAC number on the Reader Action Card elsewhere in this issue. This index has been compiled as a service to our readers and advertisers. Every precaution is taken to ensure its accuracy, but the publisher assumes no liability for errors or omissions.

NASA Tech Briefs, ISSN 0145-319X, USPS 750-070, copyright © 1989 in U.S., is published monthly by Associated Business Publications Co., Ltd. 41 E. 42nd St., New York, NY 10017-5391. The copyrighted information does not include the individual Tech Briefs which are supplied by NASA. Editorial, sales, production and circulation offices at 41 E. 42nd Street, New York, NY 10017-5391. Subscriptions for non-qualified subscribers in the U.S., Panama Canal Zone, and Puerto Rico, $75.00 for 1 year; $125.00 for 2 years; $200 for 3 years. Single copies $10.00. Remit by check, draft, postal or express orders. Other remittances at sender's risk. Address all communications for subscriptions or circulation to NASA Tech Briefs, 41 E. 42nd Street, New York, NY 10017-5391. Second-class postage paid at New York, NY and additional mailing offices.

POSTMASTER: please send address changes to NASA Tech Briefs, 41 E. 42nd Street, Suite 921, New York, NY 10017-5391.

U

V

W

Is your subscription about to expire?

Check the expire date. If it is less than 6 months now is the time to fill out a new qualification form so that there is enough time before your subscription expires.